A Guide to Supramolecular Assemblies in Polar Solutions

From Nanometre-Sized Cyclic Dimers to Large Vesicular Structures

Dissertation zur Erlangung
des naturwissenschaftlichen Doktorgrades
der Julius-Maximilians-Universität Würzburg

vorgelegt von
Thomas Helge Rehm
aus Würzburg

Würzburg 2008

Eingereicht am: 23.05.2008

bei der Fakultät für Chemie und Pharmazie

1. Gutachter: Prof. Dr. Carsten Schmuck

2. Gutachter: Prof. Dr. Frank Würthner

der Dissertation

1. Prüfer: Prof. Dr. Carsten Schmuck

2. Prüfer: Prof. Dr. Frank Würthner

3. Prüfer: Prof. Dr. Ingo Fischer

des Öffentlichen Promotionskolloquiums

Tag des Öffentlichen Promotionskolloquiums: 25.07.2008

Doktorurkunde ausgehändigt am:

Für meine Familie

“Ein Zögern überfiel uns, als ahnten wir, dass wir angekommen waren. Dass an dieser Stelle etwas anderes beginnen sollte. Wir drehten uns um und spähten unsicher in alle Richtungen.“

Populärmusik aus Vittula
Mikael Niemi

“Mama! Papa! Küche! ESSEN! JETZT!“

Julian

Danksagung

Die vorliegende Arbeit wurde in der Zeit von Juli 2004 bis Mai 2008 im Arbeitskreis von Herrn Prof. Dr. Carsten Schmuck am Institut für Organische Chemie der Julius-Maximilians-Universität Würzburg angefertigt.

Für das Gelingen dieser Arbeit bin ich folgenden Personen zu großem Dank verpflichtet:

… meinem Doktorvater **Herrn Prof. Dr. Carsten Schmuck** für die Möglichkeit, ein Thema bearbeiten zu dürfen, das sich durch seine große Vielseitigkeit und Neuartigkeit auszeichnet. Besonderer Dank gilt ihm, weil er es mir erlaubte und vor allem zutraute, meine eigenen Ideen und Projekte zu entwickeln und diese auch einzubringen. Seine Selbstverständlichkeit für außerplanmäßige Ereignisse erleichterte mir viele schwierige und anstrengende Passagen in der Zeit meiner Doktorarbeit.

… **Frau Dr. Franziska Gröhn**, **Frau Katja Klein** und **Herrn Frank Reinhold** am Max-Planck-Institut für Polymerforschung in Mainz für die vielen Lichtstreuungs- und Neutronenbeugungsexperimente, deren detaillierte Auswertung und sinngemäße Interpretation.
… **Herrn Dipl. Ing. Vladimir Stepanenko** und **Herrn Prof. Dr. Frank Würthner** für die zahlreichen AFM-Experimente und wichtigen Diskussionen über die erhaltenen Strukturdaten.
… **Herrn Dr. Xin Zhang**, **Herrn Prof. Dr. Frank Würthner** und **Herrn Prof. Dr. Georg Krohne** für die Möglichkeit zur Nutzung des Transmissionselektronenmikroskops.
Die Beiträge dieser Personen haben es erst möglich gemacht, eine Vorstellung und vor allem Beweise für den Aufbau meiner Strukturen zu erhalten. Besonderer Dank gilt all denen, die trotz ihres eigenen, engen Zeitplans immer eine Möglichkeit gefunden haben, meine Proben zu vermessen.

… **Herrn Dr. Sebastian Schlund** für die geduldige Beantwortung vieler Fragen, die sich mit dem Einsatz von MacroModel auf Linux ergaben. Weiterhin danke ich ihm auch für die durchgeführten DFT-Rechnungen einiger meiner Systeme.

… **Herrn Dr. Matthias Grüne** und **Elfriede Ruckdeschel** für alle DOSY-Experimente und die Beantwortung vieler Fragen, die sich im Zuge der Interpretation der NMR-Daten ergaben.
… **Herrn Dr. Michael Büchner** und **Fritz Dadrich** für die unterschiedlichsten massenspektrometrischen Untersuchungen und besonders für die geduldige Suche nach den gewünschten höheren Aggregaten meiner Systeme in der Gasphase. An dieser Suche haben sich weiterhin auch **Herr Dr. Mathias Schäfer** und **Frau Dipl. Chem. Miriam Drayss** (Institut für Organische Chemie, Universität zu Köln) sowie **Herr Dipl. Chem. Alexander Rang** und **Herr Prof. Dr. Christoph Schalley** (Institut für Chemie und Biochemie, Freie Universität Berlin) beteiligt.

… in besonderer Weise den Korrekturlesern meiner Doktorarbeit: **Herrn Dipl. Chem. Peter Wich**, meinem Bruder **Stephan** und meiner Frau **Stefanie**.

… den restlichen guten Geistern im Institut, die immer einen reibungslosen Arbeitsablauf ermöglicht haben. Besonders zu erwähnen ist dabei **Herr Dipl. Ing. (FH) Bernd Brunner**, der zu jeder Zeit die nötige Portion Geduld und Humor und für alle Probleme sowohl die richtigen Kabel als auch die passende Elektronik und Software zur Hand hatte. Weiterer Dank gilt **Herrn Markus Braun**, der auf seine unkomplizierte Weise alle technischen Probleme im und um das Labor lösen konnte.

… allen **Mitgliedern des AK Schmuck** für die lockere, lustige und musikalisch sehr abwechslungsreiche Zeit im und außerhalb des Labors; meinen ehemaligen F-Praktikanten (und jetzigen Kollegen) **Herrn Dipl. Chem. Karsten Klemm** und **Herrn Dipl. Chem. Tassilo Fenske** für die mühevolle Unterstützung bei der Umsetzung und Synthese etlicher Ideen.

… meinen langjährigen Schulfreunden **Volker**, **Martin**, **Christian** und **Gabriel** und natürlich der gesammelten Pfadfinderfraktion: **Matze** und **Simone**, **Tschäggsn**, **Peter**, **Conny**, **Birgit**, **Tine**, **Martin**, **der Ändi**, **Knorzi** und **Ursula**, **Tobi** und **Nina**, **Michi**, **Konsti** und dem ganze Rest, der es wert ist erwähnt zu werden, dies jedoch den Platz dieser Seite sprengen würde. Sie alle haben es geschafft, mich in den leider viel zu raren Momenten eines Kochabends oder Lagerfeuers geschickt von der Arbeit abzulenken.

… zuletzt und wohl am meisten meiner Familie für die ganzen Jahre, die sie mich schon durch mein Studium und nun auch durch meine Doktorarbeit getragen hat. Bei meinen Eltern bedanke ich mich besonders für die finanzielle und moralische Unterstützung, bei meinen Geschwistern **Stephan** und **Susanne** dafür, dass sie immer an meiner Seite standen. Meiner lieben Frau **Stefanie** danke ich von tiefstem Herzen, dass sie in allen Phasen dieser Arbeit immer eine behütende Hand über mich hatte. Unserem wundervollen Sohn **Julian** danke ich zum Schluss für seine einzigartige und einfache Art mir zu zeigen, welcher Weg der richtige ist.

A Guide to Supramolecular Assemblies in Polar Solutions

From Nanometre-Sized Cyclic Dimers to Large Vesicular Structures

Table of contents

1 Introduction

1.1 Supramolecular chemistry

The term *supramolecular* describes the chemical condition of matter which emanates from the creation of higher ordered structures based on molecular subunits. Different kinds of non-covalent interactions like hydrogen bonding, π-π stacking, ion pairing or hydrophobic interactions are used to build self-assembled systems from at least two, but mostly more monomers.[1] Depending on the strength of the non-covalent interactions and the given structure of the individual subunit tailor-made supramolecular systems can be created. Via the process of self-assembly both physical and chemical properties of the supramolecule differ widely compared to the features of the subunit.[2] Therefore selective modifications of the subunit give rise to programmable superstructures which could be used for specific transport, catalysis or recognition for example. Supramolecular chemistry provides concepts and tools of high impact for the synthesis, analysis and reactivity of chemical systems beyond the single molecule.[3]

1.2 Defined supramolecular structures with tailor-made properties

Since the rise of supramolecular chemistry in the last century scientists examined the characteristics of non-covalent interactions to a great extent. Over the years they were able to differentiate clearly between covalently and non-covalently bound systems. Not only the properties of the new structures themselves were fascinating but also the possibility for a direct external control of these properties. Depending on the type of non-covalent interaction the manipulation of the subunits by external stimuli like temperature, pH value or polarity of the solvent can initiate the self-assembly process or prevent it. Once self-assembled the striking properties of the supramolecule emerge and can be examined or used for new applications.

As a fascinating example *Stupp et al.* introduced synthetic peptide amphiphiles (PA) which use hydrophobic interactions, here a hydrophobic collapse, in order to form fibres of a length up to one micrometer in water.[4] Further addition of heparin yields in a PA-heparin complex (Figure 1.1C) which promotes in vivo the growth of blood vessels after addition of angiogenic growth factors. First tests in a mouse model showed extensive neovascularisation (Figure 1.1A), whereas in the control experiment with collagen, heparin and growth factors but without the peptide only a minor neovascularisation occurred (Figure 1.1B). This example illustrates the power of supramolecular chemistry in an outstanding way: a molecule as small as the above mentioned peptide self-assembles into a structure far larger than itself and initiates, in combination with natural additives, the growth of living tissue. Nature uses this principle widely. In case of osteogenesis,

the bone development, specific proteins (collagenous fibres and ground substances) are generated by osteoblasts. Upon mineralisation of the organic matrix with hydroxyl apatite as inorganic material new bone tissue is developed. Also the tobacco mosaic virus is a most prominent example for a very efficient self-assembly of small molecules leading to a highly complex structure.

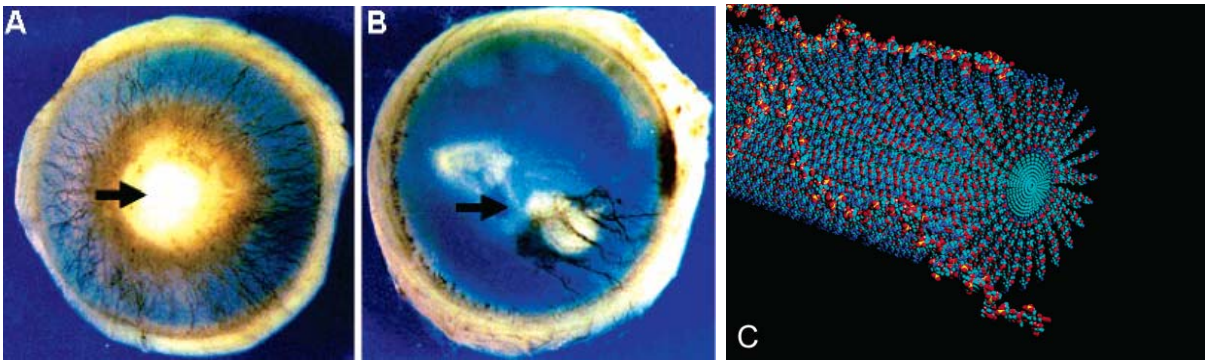

Fig. 1.1 *First applications in regenerative medicine: a complex of a peptide amphiphile fibre and heparin serves as a template for the growth of blood vessels; reprinted in part with permission from Nano Lett.* ***2006****, 6, 2086-2090. Copyright (2006) American Chemical Society.*

Fujita et al. introduced several types of supramolecular structures based on metal-ligand interactions between palladium metal centres and nitrogen-containing heterocyclic ligands as another approach in supramolecular chemistry. Starting with a molecular square, based on the self-assembly of $[enPd(II)]^{2+}$ units with 4,4´-bipyridine as a more or less simple ligand, the introduction and combination of more complex, multi-dentate ligands lead to prisms, nanotubes or spheres.[5] In his work *Fujita* uses three concepts of supramolecular chemistry: 1) metal-ligand interactions for strong binding between the subunits; 2) tailor-made ligands with a defined geometry for the construction of well-defined structures; 3) the use of the hydrophobic cavity inside the supramolecule. Beside the aesthetic account of these systems also the practical sense for science is of high impact. Recently, *Fujita et al.* could show that inside a self-assembled coordination cage *Diels-Alder* reactions between anthracene and phthalimides proceed with an unusual regioselectivity.[6] Due to the limited space inside the cage the reactants approach themselves in a different manner (Figure 1.2A) compared to a reaction in a similar bowl-shaped host or in free solution (Figure 1.2B). The constrained arrangement inside the cage promotes the reaction of an external ring of the anthracene with the phthalimide yielding the 1,4-*Diels-Alder* product. This experiment shows clearly that the application of supramolecular catalysts in organic synthesis opens the door for products which are rarely available via conventional routes.

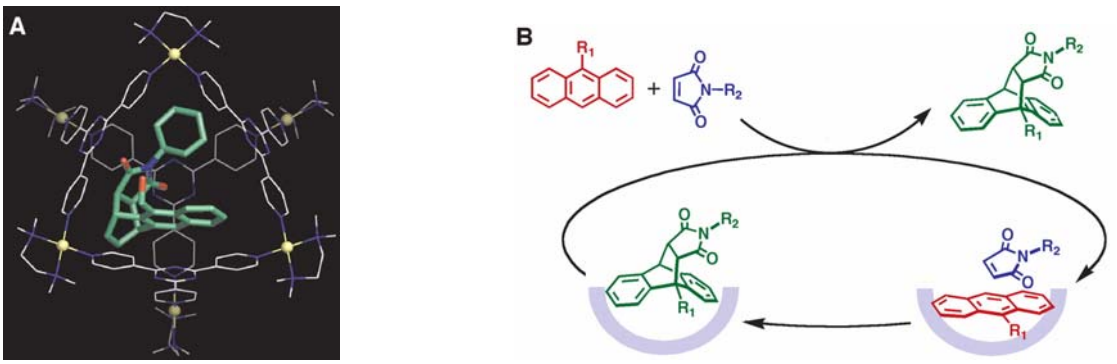

Fig. 1.2 *Different reaction paths due to the restricted space inside a supramolecular catalyst: A) the coordination cage leads to the 1,4-Diels-Alder product; B) the bowl-shaped host yields in the 9,10-Diels-Alder product; from Science* ***2006****, 312, 251-254. Reprinted with permission from AAAS.*

As a last example an extraordinary feature of self-assembled systems should be mentioned. Although supramolecular interactions are by far not as strong as covalent bonds they do have one major advantage: the reversible nature of their formation. In other words self-assembled structures have the possibility of self-healing. Often the formation of conventional polymers, for example, is kinetically controlled. Due to this fact the resulting material can contain defects which are permanently trapped in the covalent structure. Self-assembled materials instead can rearrange under appropriate conditions, so that most of the defects in the supramolecule can be removed on the way to the thermodynamic minimum.[7] In 1997 *Meijer et al.* introduced a quadruple hydrogen bonding unit based on ureidopyrimidones, which he used to demonstrate the outstanding feature of self-healing polymers.[8] In one case scratched coatings based on supramolecular polymers underwent self-healing by rising the temperature up to 140 °C. The external stimulus disrupted the supramolecular polymerization so that the monomers could rearrange. By cooling the sample to room temperature the self-assembly process was initiated again and the coating showed no more defects.

The three different examples mentioned above with relevance to regenerative medicine, chemical synthesis and material science all rely on the principles of supramolecular chemistry: tailor-made molecules self-assemble via non-covalent interactions to higher ordered structures with new and fascinating properties. The topic of this PhD thesis is based on the concepts of supramolecular chemistry. The following chapters will describe the application of guanidiniocarbonylpyrrole carboxylate zwitterions as a new self-complementary binding motive in supramolecular material science. Its self-assembly allows the formation of supramolecular architectures in polar solutions and represents an important alternative to well known binding mo-

tives.[9] Beside the analysis of supramolecular systems also new developments and concepts for defined supramolecular structures will be introduced.

1 J. Steed, J. Atwood, *Supramolecular Chemistry*, **2000**, Wiley & Sons, Chichester.

2 a) F. Vögtle, *Supramolekulare Chemie*, **1992**, Teubner Verlag, Stuttgart; b) K. Ariga, T. Kunitake, *Supramolecular Chemistry – Fundamentals and Applications*, **2006**, Springer Verlag, Berlin.

3 a) J.-M. Lehn, *Supramolecular Chemistry. Concepts and Perspectives*, **1998**, Wiley-VCH, Weinheim; b) H.-J-Schneider, A. Yatsimirsky, *Principles and Methods in Supramolecular Chemistry*, **2000**, Wiley & Sons, Chichester.

4 K. Rajangam, H. Behanna, M. Hui, X. Han, J. Hulvat, J. W. Lomasney, S. Stupp, *Nano Lett.* **2006**, *6*, 2086-2090.

5 K. Fujita, M. Tominaga, A. Hori, B. Therrien, *Acc. Chem. Res.* **2005**, *38*, 371-380.

6 M. Yoshizawa, M. Tamura, M., Fujita, *Science* **2006**, *312*, 251-254.

7 A. Bosman, R. Sijbesma, E. Meijer, *Materials Today* **2004**, *7*, 34-39.

8 a) R. Sijbesma, F. Beijer, L. Brunsveld, B. Folmer, J. Hirschberg, R. Lange, J. Lowe, E. Meijer, *Science* **1997**, *278*, 1601-1604; b) L. Brunsveld, B. Folmer, E. Meijer, R. Sijbesma, *Chem. Rev.* **2001**, *101*, 4071-4091.

9 a) C. Schmuck, W. Wienand, *J. Am. Chem. Soc.* **2003**, *125*, 452-459; b) C. Schmuck, *Coord. Chem. Rev.* **2006**, *205*, 3053-3067; c) Th. Rehm, C. Schmuck, *Chem. Commun.* **2008**, 801-813.

2 Projects and concepts

In 1999 *Schmuck* introduced the guanidiniocarbonylpyrrole carboxylate zwitterion **2.1** as a versatile building block for supramolecular structures.[1] In contrast to already known, self-complementary building blocks, which are nearly all based on pure hydrogen bonding, this new binding motive uses the combination of a multiple hydrogen bonding array *together* with ion pair formation (Figure 2.1). Both supramolecular interactions are required hand in hand in order to design a building block which dimerizes not only in polar organic solvents like DMSO, but also in water.[2] A more detailed view on this building block with its advanced features will be given in chapter 3.

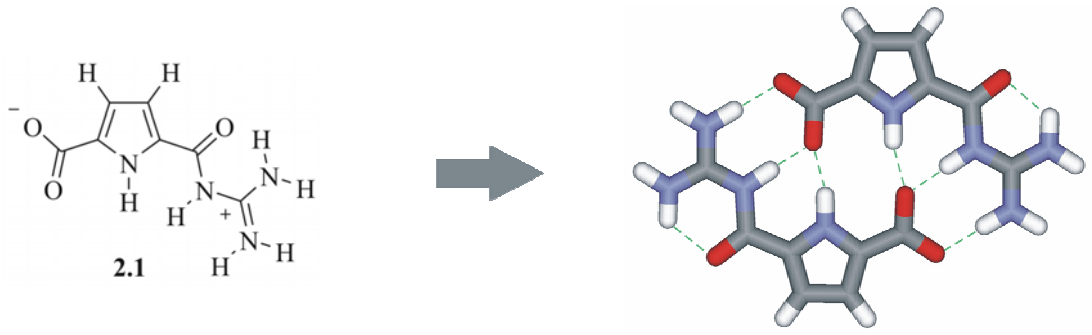

Fig. 2.1 *Guanidiniocarbonylpyrrole carboxylate zwitterion: strong dimerization via the combination of hydrogen bonds with ionic interactions (hydrogen bonds are shown in green).*

By now several derivatives based on the original building block are available. Beside the introduction of solubility enhancing groups, the introduction of linker moieties, like ω-amino acids for example, are very useful for the synthesis of multivalent building blocks. The first part of this thesis is based on this idea. It discusses the self-assembly of four monomers which are all capable of multiple ion pairing (bis- or triple-zwitterions). The second part describes a new idea of enhancing the primal building block. The introduction of α-amino acids separates the carboxylate from the pyrrole core and leads to a greater flexibility within the monomer. This new degree of freedom results in a dramatic change of the self-assembly. The last part of this work presents concepts for the synthesis of supramolecular boxes, cages and new zwitterionic binding motives.

In order to understand the self-assembly process of such building blocks several analytical methods were applied. Beside the standard techniques (^{1}H-, ^{13}C-NMR spectroscopy, mass spectrometry, FTIR spectroscopy), also atomic force microscopy, transmission electron microscopy, dynamic light scattering and small angle neutron scattering were used in collaboration with external partners to study the dimension and the interior of the supramolecular structures. Furthermore

DOSY NMR experiments provide information about the size of the monomers, dimers or oligomers. Beside these investigations theoretical methods based on molecular modelling were also applied.

2.1 From nanometre-sized cyclic dimers to large supramolecular structures

As mentioned above the connection of several zwitterions within one monomer is possible via the introduction of ω-amino acids into the original building block. Depending on the characteristics of the spacer (length, functional groups, rigidity) monomers with different properties can be obtained. Figure 2.2 shows two monomers from earlier work[3] (**2.2**, **2.3**) as well as one new monomer (**2.4**). Initially, they were designed to build supramolecular polymers, but surprisingly the influence of the spacer was so profound that the structures of the resulting supramolecules could be controlled by the variation of the linker properties (length, functional groups).

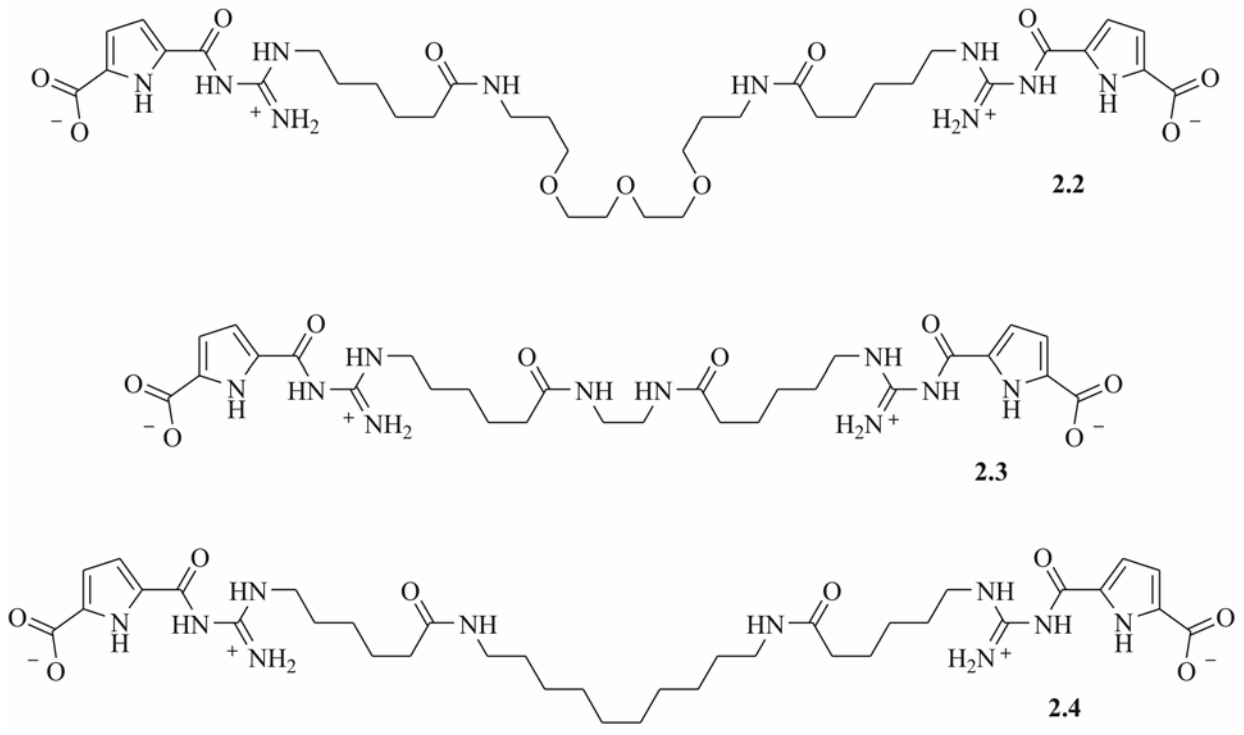

Fig. 2.2 *Bis-zwitterionic monomers with different types of spacers: long and hydrophilic (**2.2**), short and hydrophobic (**2.3**) or long and hydrophobic (**2.4**).*

In addition to the above mentioned bis-zwitterionic monomers the triple-zwitterionic building block **2.5** was of interest due to the possible formation of supramolecular networks (Figure 2.3). These four multiple bonding molecules are introduced in order to demonstrate the formation of supramolecular structures with different modes of self-assembly depending on the length and

functionality of the linker. In chapter 4 the results of these studies will be presented in more detail.

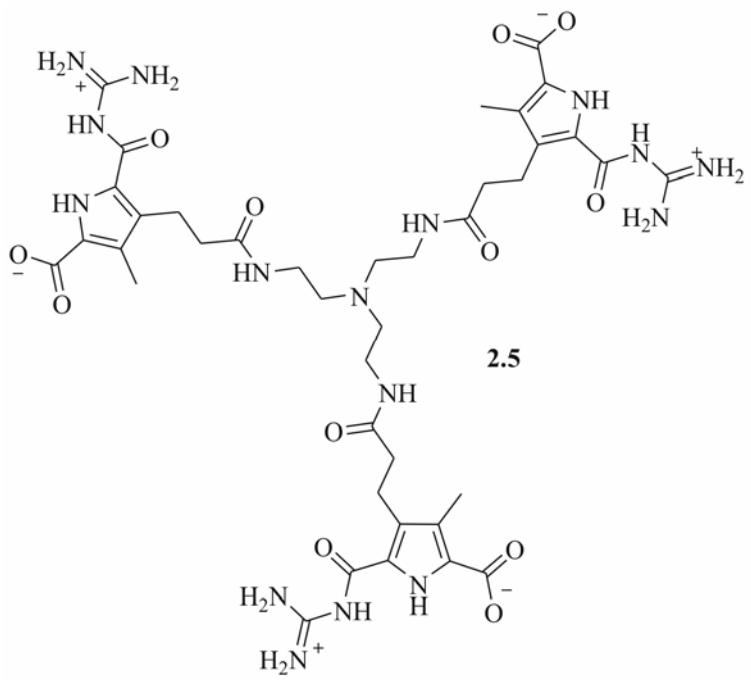

Fig. 2.3 *The triple-zwitterionic monomer* ***2.5*** *as a starting point for network-like structures.*

2.2 Changing the binding mode: vesicles from *α*-amino acid derived zwitterions

The influence of the distance between the carboxylate and the guanidiniocarbonylpyrrole on the self-assembly process has been investigated in earlier work.[4] By the introduction of flexible linkers between carboxylate and binding site five derivatives with distance-dependent association properties were synthesized. The zwitterion with the shortest linker showed extensive oligomerization as proved by NMR dilution and ESI-MS experiments. Due to the limited solubility a detailed analysis of the larger oligomers was not possible. Now the idea was to substitute the shortest linker (glycine) by *α*-amino acids which contain side chains as another structural element (like a methyl group in *L*-alanine). This resulted in new systems with a behaviour that was in total contrast to the so far known flexible zwitterions. In order to get a deeper insight into the impact of the amino acid side chain three other zwitterions based on *L*-serine, *L*-phenylalanine and *L*-tyrosine were also synthesized and examined (Figure 2.4).

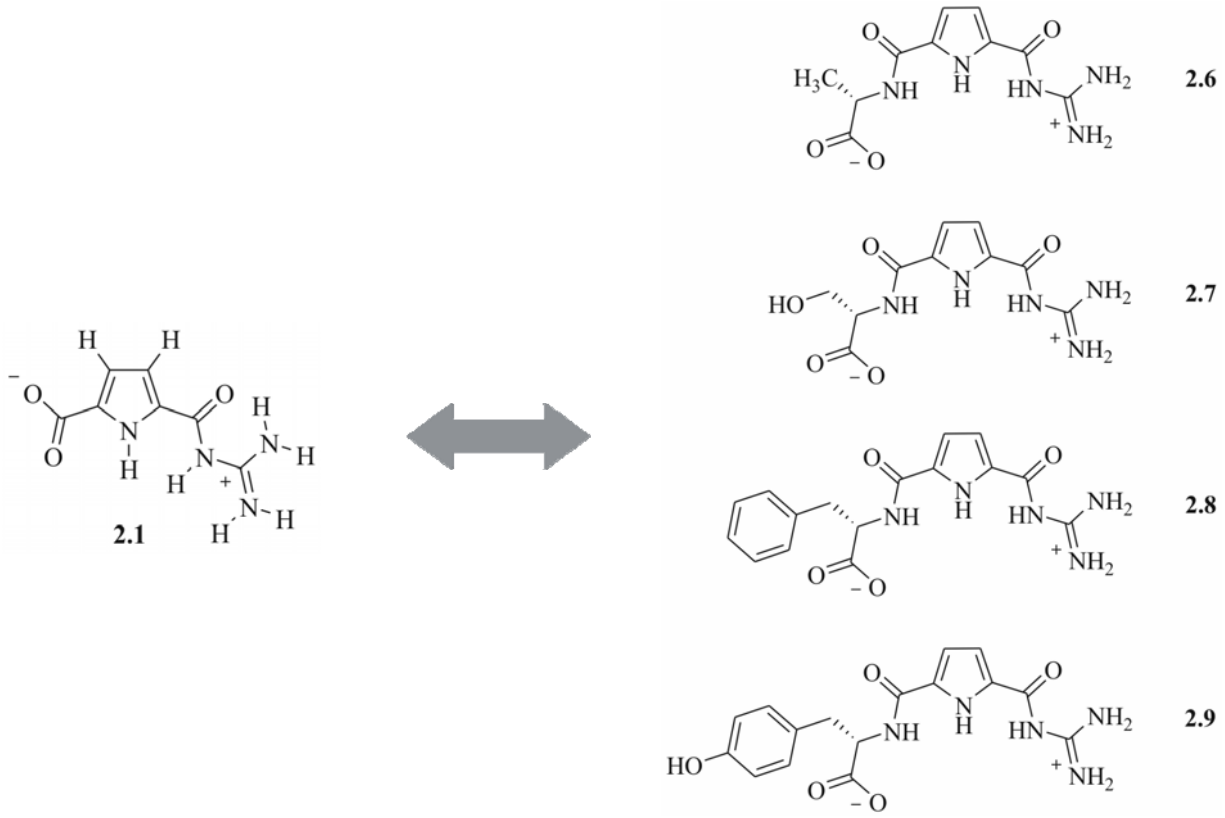

Fig. 2.4 *Increased flexibility and functionalization of the primal building block via the introduction of α-amino acids.*

2.3 Concepts for the syntheses of boxes, cages and new zwitterions

In the last part of this thesis the synthesis of more defined supramolecular structures is discussed. Whereas nearly all of the above mentioned systems represent the self-assembled products of an undefined number of monomers the concepts for these new *stoichiometric* structures are based on dimerizing monomers resulting in well-defined boxes or cages. In order to achieve this desired type of self-assembly the rigidity of the monomers has to be increased by the introduction of semi-flexible linkers. For example, Figure 2.5A shows a calculated dimer with a box-like structure based on the programmed self-assembly of a semi-flexible bis-zwitterion. Again a specific linker is important in order to connect the building blocks in the desired mode. For this reason the synthesis of the multi-purpose compound **2.10** was developed which is used for further linkage with different rigid linkers (Figure 2.5B).

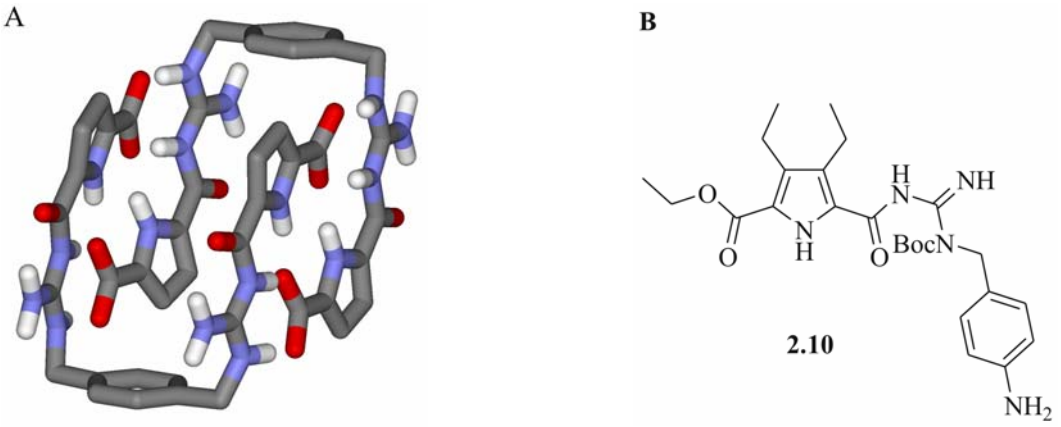

Fig. 2.5 *A) Stoichiometric self-assembly leads to defined supramolecular structures (unpolar hydrogens are omitted for clarity); B) fully protected multi-purpose zwitterion* ***2.10*** *for linkage with rigid spacers.*

Further development of the original zwitterion was also a point of interest. Although there is already a water-soluble derivative based on triethylene glycol chains in the periphery of the pyrrole core, the introduction of amines close to the core might have one more advantage besides better solubility in water (Figure 2.6A). Several gas phase experiments with the above mentioned flexible zwitterions were hindered due to the inefficient ionisation of the self-assembled structures.[5] Via the introduction of an additional charge in form of an ammonium group the compound does not have to be ionizised anymore, which should result in an increased signal intensity in the gas phase experiments.

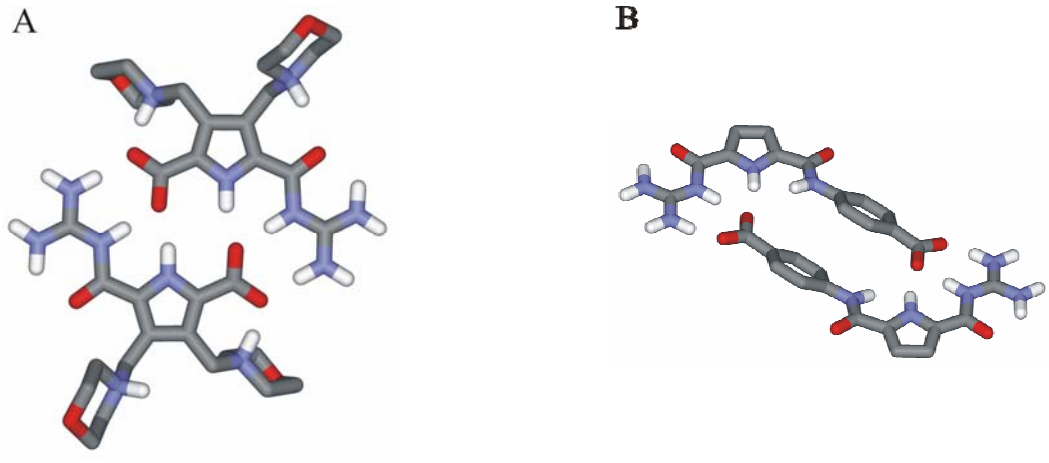

Fig. 2.6 *A) Nitrogen containing aliphatic substituents at the pyrrole periphery increase the solubility in water via protonation; B) additional π-stacking enhances the dimerization properties of the primal zwitterion (unpolar hydrogens are omitted for clarity).*

The second modification of the primal zwitterion is presented by the introduction of another type of supramolecular interaction (Figure 2.6B). Beside hydrogen bonding and ionic interactions the

possibility of π-stacking should increase the association strength, particularly in polar solvents. A simple motive capable of π-stacking is *p*-amino benzoic acid. Introduction of this amino acid results again in separation of the binding partners as mentioned for the α-amino acid derived zwitterions. However, the rigidity of the benzene core prevents the intramolecular interaction between carboxylate and the guanidinio group which should therefore promote the intermolecular dimerization.

The aim of the third part of this thesis is the synthesis of the fully-protected precursors of these molecules. During the course of this thesis the deprotection and examination of the resulting zwitterionic structures was not possible anymore, but is a definitive object for future work.

---

1 C. Schmuck, *Eur. J. Org. Chem.* **1999**, 2397-2403.
2 C. Schmuck, W. Wienand, *J. Am. Chem. Soc.* **2006**, *125*, 452-459.
3 Th. Rehm, Diploma thesis, University of Würzburg, **2004**.
4 C. Schmuck, Th. Rehm, L. Geiger, M. Schäfer, *J. Org. Chem.* **2007**, *72*, 6162-6170.
5 M. Schäfer, C. Schmuck, L. Geiger, M. Chalmers, C. Hendrickson, A. Marshall, *Int. J. Mass. Spec.* **2004**, *237*, 33-45.

3 State of the art

This chapter is arranged into four sections. The first section will shortly review the most common possibilities of self-assembly. Selective examples will demonstrate the principles behind the respective supramolecular interaction, also discussing their benefits and drawbacks. The second section will present guanidiniocarbonylpyrrole carboxylate zwitterions and their self-assembly in more detail. Beside the development of the building block also the importance of each structural unit will be described. The third section will give an introduction into vesicle formation. Here, selected examples will be discussed which represent both the classical, e.g. block copolymers, and non-classical vesicle forming molecules, e.g. by functional interactions. The last section will give a short overview of the analytical methods which were used to examine the supramolecules.

3.1 Self-assembly based on various supramolecular interactions

As one of the most widely examined non-covalent interactions hydrogen bonds are used often in supramolecular chemistry.[1] The most prominent example in Nature is the use of multiple hydrogen bonding arrays in DNA for information storage. Well-defined subunits in terms of the nucleobases adenine, thymine, cytosine and guanine encode genetic information depending on their sequence within the single strand. Securing this data takes place by dimerization of two complementary strands resulting in one double helix. The required complementarity between the strands is based on the sequence of the nucleobases and their hydrogen bonding pattern. In case of natural DNA only two nucleobase combinations are possible: adenine **3.1** with thymine **3.2** (Figure 3.1A) and cytosine **3.3** with guanine **3.4** (Figure 3.1B).[2]

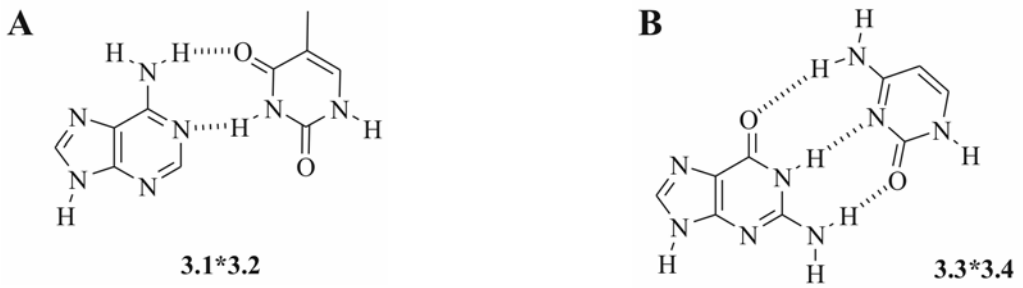

Fig. 3.1 *Hydrogen donor-acceptor sequence specific dimerization of nucleobases: A) adenine – thymine; B) cytosine – guanine.*

Discrimination between the binding motives is defined by the number and sequence of hydrogen bond donors (D) and hydrogen bond acceptors (A). Adenine and thymine represent a AD bonding pattern, whereas cytosine shows an AAD and guanine a DDA sequence.

Based on this idea numerous examples of artificial hydrogen bonding motives are available nowadays. The already mentioned binding motive of *Meijer* based on ureidopyrimidones gained exceptional importance (Figure 3.2A).[3] Four hydrogen bonds interact in a self-complementary manner whereas the angles between D – H ··· A have an ideal value of 180 ° resulting in maximum bond strength. Beside the perfect structure of the subunit the unusual high association constant of $K_{ass} > 10^7$ M^{-1} in chloroform emanates also from the reduction of secondary repulsive interactions. In comparison to the ADAD bonding array based on triazine (Figure 3.2B) four out of six repulsive interactions are eliminated due to the rearrangement of the donor and acceptor sequence.[4] Following this principle *Jørgensen* recommended a quadruple binding motive with AAAA and DDDD binding sites. Due to the complete elimination of secondary repulsive interactions the association strength should increase once more. Unfortunately, this binding motive is no longer self-complementary allowing only heteroassociation of different molecules. Therefore the AADD sequence represents the most stable self-complementary binding motive.[5]

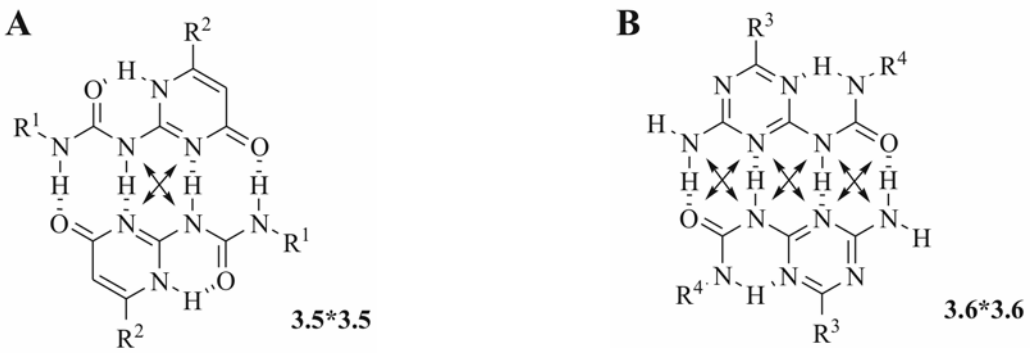

Fig. 3.2 *Quadruple hydrogen bonding arrays: ureidopyrimidone based AADD sequence with two repulsive interactions (A) versus triazine based ADAD sequence with six repulsive interactions (B).*

Following the *Gulliver Principle* the increase of hydrogen bonds used for dimerization should also increase the association strength.[6] Therefore, *Krische et al.* introduced duplex oligomers based on oligo(aminotriazines).[7] The tape-like trimer **3.7** with ten hydrogen bonds has an association constant of $K_{ass} = 6.9 \cdot 10^8$ M^{-1} in chloroform (Figure 3.3). Surprisingly the extension of the binding pattern to fourteen hydrogen bonds resulted in a very low association constant of $K_{ass} = 1.1 \cdot 10^3$ M^{-1} in chloroform. Although four more hydrogen bonds were involved in the self-assembly process no stronger association takes place. Most likely the internal structure of the largest tape is the reason for the impaired association. The extension of the binding motive resulted also in an increased flexibility of the whole monomeric structure so that two processes compete with each other: self-folding versus dimerization. In conclusion not only the number

and sequence of hydrogen bonds is important for the strength of the self-assembly process, but also the internal structure of the bonding array. This important point will be discussed in detail in chapter 3.2.

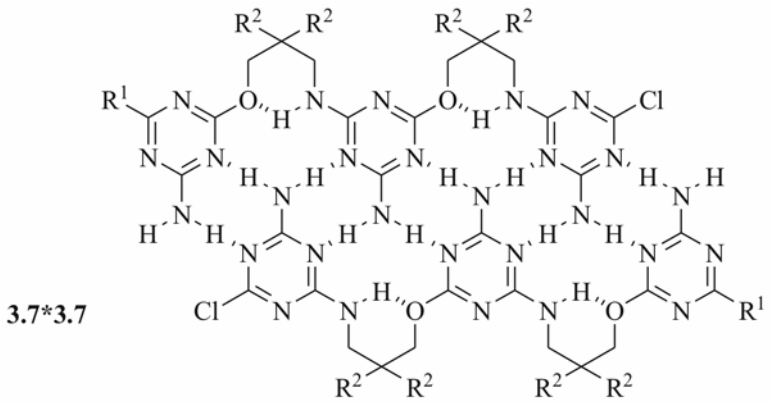

Fig. 3.3 *Extending the number of hydrogen bonds increases the association strength to a certain limit.*

Beside their striking advantages of specificity and directionality hydrogen bonds have one main disadvantage. All above mentioned examples require relatively unpolar solvents like chloroform. The addition of small amounts of polar or protic solvents like methanol, DMSO and water prevents any self-assembly processes based on pure hydrogen bonding.[8]

In order to avoid this restriction even stronger non-covalent interactions have to be exploited. One possibility is the application of metal-ligand interactions. As the strength of coordination bonds between metal cations and organic ligands can easily approach the stability of covalent bonds the use of metal-ligand interactions is not limited to organic solvents. Due to the incorporated charges of the metal centres also water solubility is possible. Beside *Fujitas* well-defined nanostructures[9] also oligomeric and polymeric architectures are possible. Recently *Würthner et al.* presented the results of the coordination of terpyridine enhanced perylene diimides with Zn^{2+} ions (Figure 3.4).[10] The variation of the metal ion concentration controls the degree of oligomerization. All stages of complexation from the metalfree monomer over the polymer to the fully complexed monomer were studied by DOSY NMR. By addition of one equivalent of Zn^{2+} ions the diffusion coefficient declined one order of magnitude from $\log D = -9.45$ m^2 s^{-2} to $\log D = -10.45$ m^2 s^{-2} compared to the uncomplexed monomer. This clearly indicates the formation of large oligomers which were also analysed by AFM. Rod like filaments with a length of *ca*. 50 ± 5 nm were observed, representing 15 monomeric units with an approximated length of 3 nm.

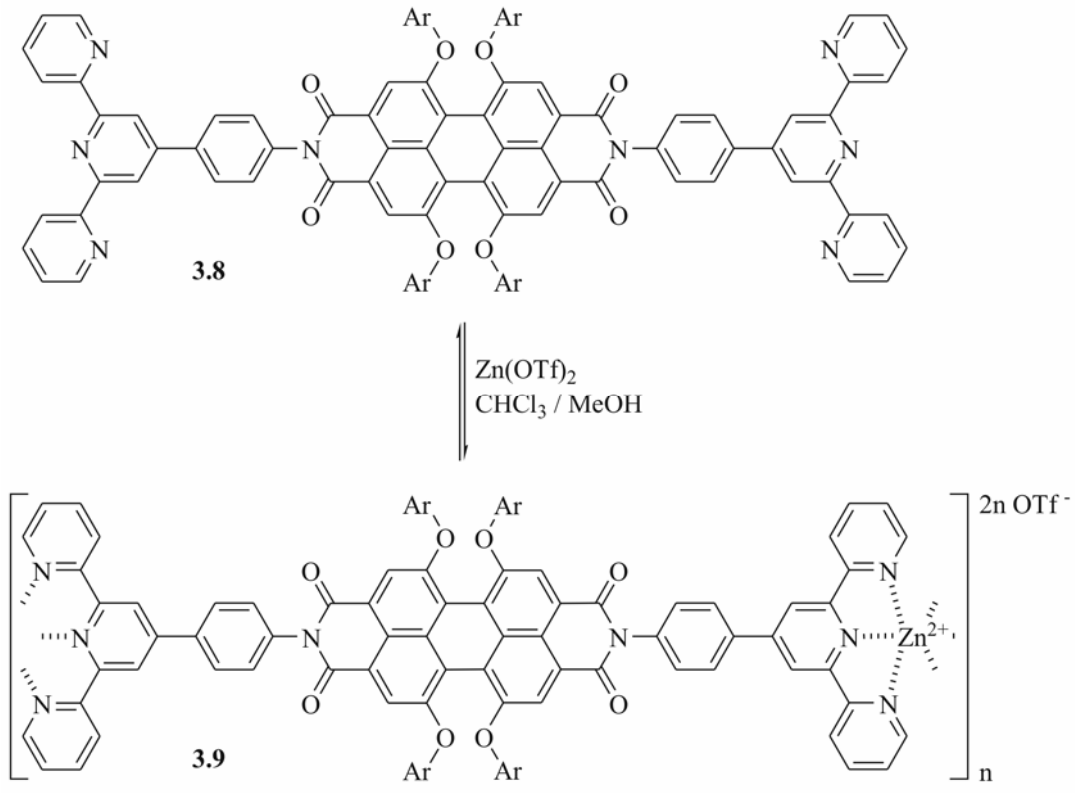

Fig. 3.4 *Metal directed self-assembly of terpyridine functionalized perylene diimides.*

Although metal-ligand interactions are an advanced alternative to pure hydrogen bonding for supramolecular structures in polar solvents, they do also have certain disadvantages. First, transition metals are quite expensive and in economical sense hamper any wide-spread potential application. Also, transition metals often possess a certain toxicity resulting in environmental and health problems. Finally, metal-ligand interactions only allow for heteroassocitions. This means that both metal ion and ligand have to be present in the correct ratio. A deviation from the ideal ratio can lead to the disruption of the desired structure. However, this behaviour can also be used for an external control of the supramolecular system (Figure 3.5).

Fig. 3.5 *Metal ion concentration as external control for the degree of polymerization.*

Another possibility to provoke self-assembly in polar solvents is the use of hydrophobic and aromatic stacking interactions. *Iverson et al.* developed self-folding molecules based on aromatic interactions between electron rich 1,5-dialkoxynaphthlenes (DAN) and electron poor 1,4,5,8-naphthalene-tetracarboxylic diimides (NDI).[11] These so called "aedamers" can be obtained by

covalent oligomerization of both DAN and NDI with solubility enhancing linkers like aspartic acid (Figure 3.6). Isothermal titration calorimetry (ITC) was used in order to investigate the self-assembly process in water. An oligomer with four aromatic units interacts with a complementary oligomer resulting in an association constant of $K_{ass} = 3.5 \cdot 10^5\ M^{-1}$.

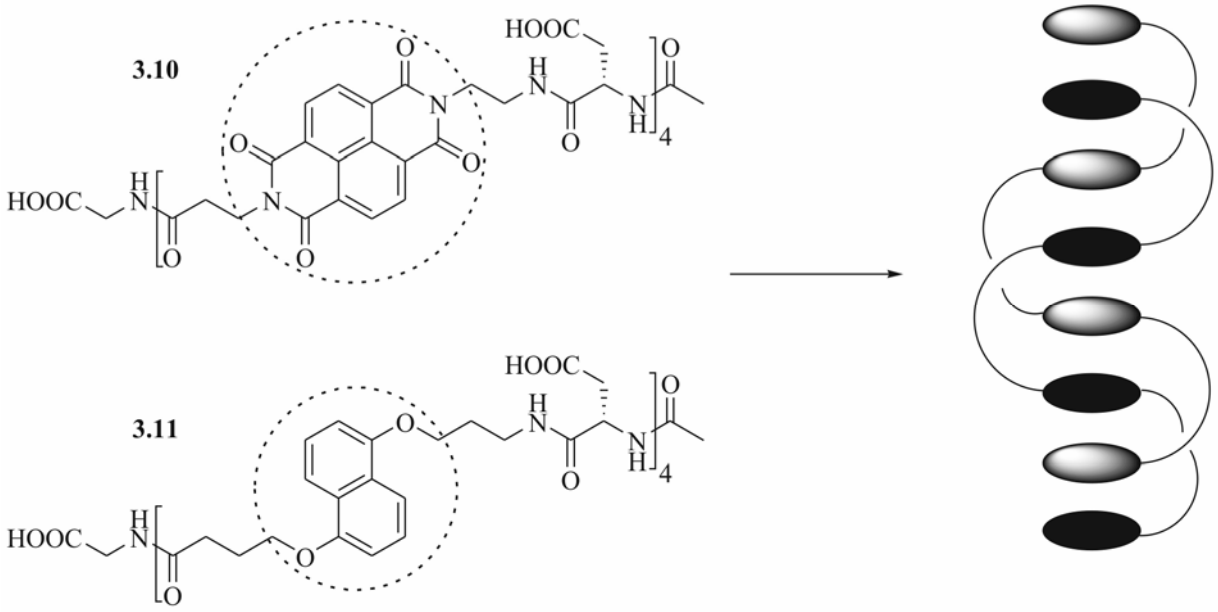

Fig. 3.6 *Hetero-duplex formation promoted by aromatic stacking interactions in water.*

Unfortunately, the synthesis of the monomers is often difficult. The linkers for example have to accomplish two functions. First, as it is the principle behind this interaction, the hydrophobicity also requires additional solubility enhancing groups like the aspartic acids. They have to be included into the linkers. Secondly, the linkers must have a certain length in order to allow the intercalation of one DAN unit between two NDI units, for example. This defined length plays an important role in another point: as it is known from ITC experiments the whole self-assembly process is enthalpy driven, but entropically unfavoured. The large negative entropy contribution most likely stems from the loss in flexibility of the linkers upon association. Only with the ideal linker length the association process can be optimized.

In addition to the metal-ligand interactions, hydrophobic and aromatic stacking interactions ion pair formation is also an important method for the self-assembly in polar solvents. Two different types of ion pairs can be used: point charges like ammonium groups or hydrogen bond directed charges like amidinium groups as examples for cationic binding sites. Both types are stronger than hydrogen bonds but weaker than coordination bonds. Due to this fact simple electrostatic interactions between two complementary charges are most often not strong enough for self-assembly in polar solvents. However, external conditions like hydrophobic shielding or the use

of less polar solvents like acetonitrile can improve the association. Nevertheless, the application of the first type of ion pairs is rather improper for self-assembly, at least between two small molecules.[12] For the latter type most often amidinium, guanidinium and carboxylate ions are used.[13] In order to prevent the handicap of weak binding between single ion pairs the *Gulliver Principle* is applied again. By combination of several ionic interactions strong association can also take place in polar, organic solvents or even water. As an example *Yashima et al.* created artificial double helices based on ion pair formation (Figure 3.7).[14] Circular dichroism measurements both in chloroform and DMSO proved the formation of stable helices. ^{1}H-NMR experiments gave also comparable results. Only 40 % of the double helices underwent dissociation in pure DMSO as highly competing solvent during ion pair and hydrogen bond formation.

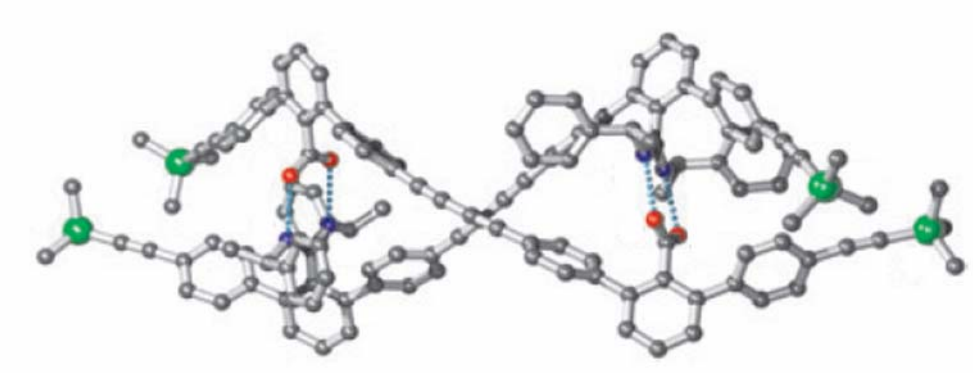

Fig. 3.7 *Crystal structure of an artificial double helix based on ion pair formation between amidinium (blue) and carboxylate groups (red) (the silicon atom from the trimethylsilyl group is highlighted in green); Y. Tanaka, H. Katagiri, Y. Forushu, E. Yashima: "A Modular Strategy to Artificial Double Helices", Angew. Chem. Int. Ed.* ***2006****, 44, 3867-3870. Copyright Wiley-VCH Verlag GmbH & Co. KGaA. Reproduced with permission.*

As both binding partners are sensitive to pH changes external control of the self-assembly process is possible by addition of acid or base. With this combination of interactions a method is at hand which provides well-defined self-assembly in polar solvents: strong binding with simple, but efficient external control. Although the combination of many ion pairs within one monomer, as claimed by the *Gulliver Principle*, is an impressive method the idea of improving a single ion pair has to be reconsidered also.

3.2 Guanidiniocarbonylpyrrole carboxylate zwitterions – self-complementary building blocks for supramolecular structures in polar solvents

Schmuck introduced guanidiniocarbonylpyrrole carboxylate zwitterions as multi-purpose building blocks in supramolecular chemistry.[15] The ability of strong self-assembly in polar solvents

between a carboxylate group and a guanidiniocarbonylpyrrole function is based on several concepts referring to the chemical behaviour of the zwitterion and its structure: 1) introduction of further hydrogen bonds for multi-dentate binding; 2) increasing the acidity of the guanidinium cation in order to promote stronger hydrogen bonds; 3) self-complementarity by introduction of both binding partners in one molecule; 4) rigidity in order to prevent intramolecular interactions between the carboxylate anion and the guanidinium cation.

Comparing the ion pair formation of three different guanidinium ions with pyrrole carboxylate **3.12** in 40 % water in DMSO shows a clear trend according to the first two points (Figure 3.8). The combination of the parent guanidinium ion **3.13** with the carboxylate (Figure 3.8A) does not lead to any ion pair formation whereas the acyl guanidinium **3.14** cation forms an ion pair with K_{ass} = 150 M^{-1} (Figure 3.8B). Another significant increase in the association strength arises from the introduction of one more hydrogen bond donor and acceptor in **3.15** resulting in an association constant of $K_{ass} = 4.1 \cdot 10^3$ M^{-1} (Figure 3.8C). Due to the already achieved binding strength the association constant for **3.15*3.12** measured in pure DMSO could only be estimated to be in the order of $K_{ass} \geq 10^5$ M^{-1}.[16]

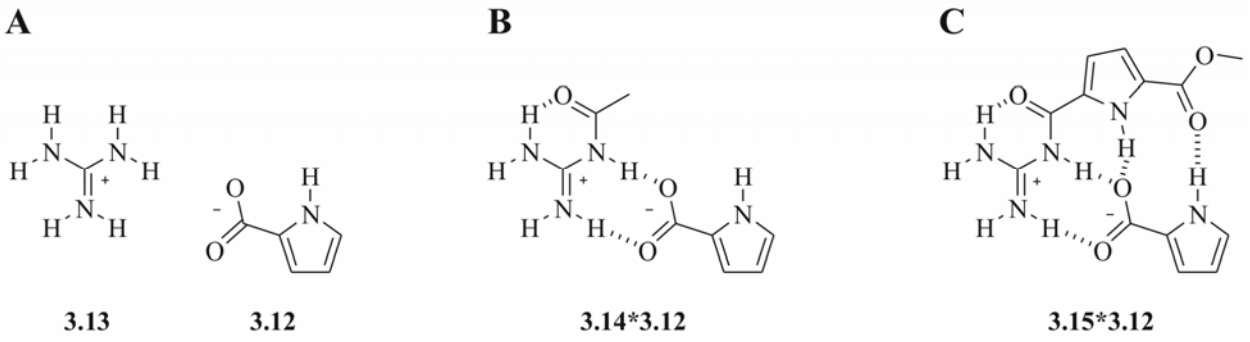

Fig. 3.8 *Improving guanidinium cations: from a simple bi-dentate binding cation to an acylated multi-dentate binding cation.*

Beside the increase of the number of hydrogen bonds also the acylation of the cation plays an important role for the strong association. Arginine as natural analogue has a pK_a value of 13.5 whereas the guanidiniocarbonyl pyrrole cation has a pK_a of about 6-7.[17] Thus the increased acidity of the latter cation results in stronger hydrogen bonds[18] as demonstrated in the systematical study mentioned above.

The last two concepts in terms of self-complementarity and rigidity lead to several advantages, not only for the synthesis of subsequent monomers but also for the overall stability of the self-assembled dimer. First of all it is far easier to introduce one complete building block, which is self-complementary compared to the separate introduction of both binding partners, which re-

sults in heteroassociation. The latter point clearly depends on the structure of the linker between the guanidiniocarbonyl function and the carboxylate group. A flexible linker provides the opportunity of intramolecular interaction.[19a] This point was recently discussed by the examination of five flexible zwitterions (Figure 3.9A). We were able to show that in general any intramolecular interaction weakens the intermolecular self-assembly as depicted in Figure 3.9B.[b]

A B

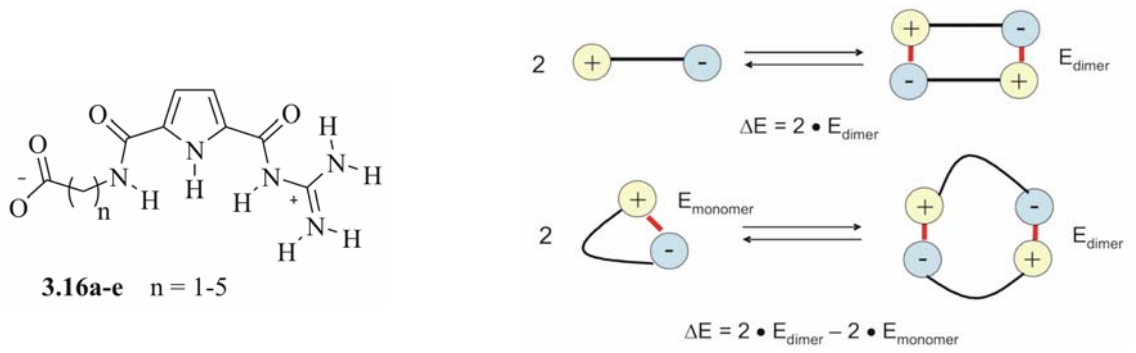

Fig. 3.9 *Flexible zwitterions as probe for the influence of intramolecular interactions on intermolecular self-assembly; reprinted with permission from J. Org. Chem.* ***2008****, 72, 6162-6170. Copyright (2008) American Chemical Society.*

The use of pyrrole as linking core is the perfect choice in this case. Beside its rigidity pyrrole also contains a polar NH group, which represents a hydrogen bond donor. Pyrrole has a pK_a value of about 23 in DMSO which is comparable with a simple alcohol.[20] Electron withdrawing substituents introduced in position 2 and 5 of the pyrrole finally increase the acidity of the aromatic core, which strengthens its hydrogen bond donor ability.

In conclusion the conceptual design of guanidiniocarbonylpyrrole carboxylate zwitterions based on improved ion pair formation, self-complementarity and rigidity results in the most stable supramolecular dimer only based on electrostatic interactions known so far (Figure 3.10). Beside its outstanding self-association properties in polar solvents (K_{ass} = 170 M^{-1} in pure water) the possibility of external control is given as well.[21] Addition of acid or base leads either to the cationic or to the anionic form of the building block. In both forms efficient dimerization can not take place, which results in the disruption of the supramolecular structure. Adjusting the pH to a value of *ca*. 6 the zwitterionic state is stable again, which initiates the self-assembly process.

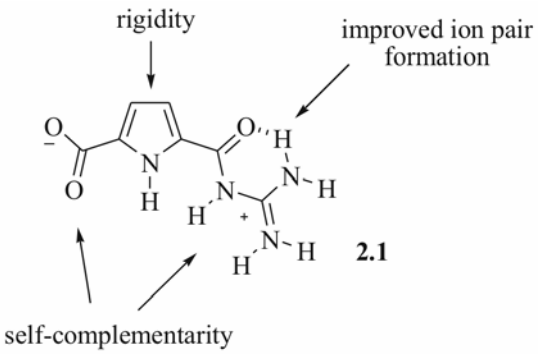

Fig. 3.10 *Conceptual design of the zwitterionic building block* ***2.1****.*

Meanwhile theoretical results describe the self-assembly of different derivatives of the primal zwitterion. Computational examinations on B3LYP level by *Schlund et al.* gave a deeper insight into the contribution of individual non-covalent interactions.[22] Beside the zwitterions with furan and cyclopentadiene core also the substitution of the guanidinium function was a point of interest. Two derivatives with amidinium groups were calculated as well as one neutral analogue based on aminopyridine (Figure 3.11). These systems were used either to switch-off individual hydrogen bonds and charges or to introduce repulsive interactions.

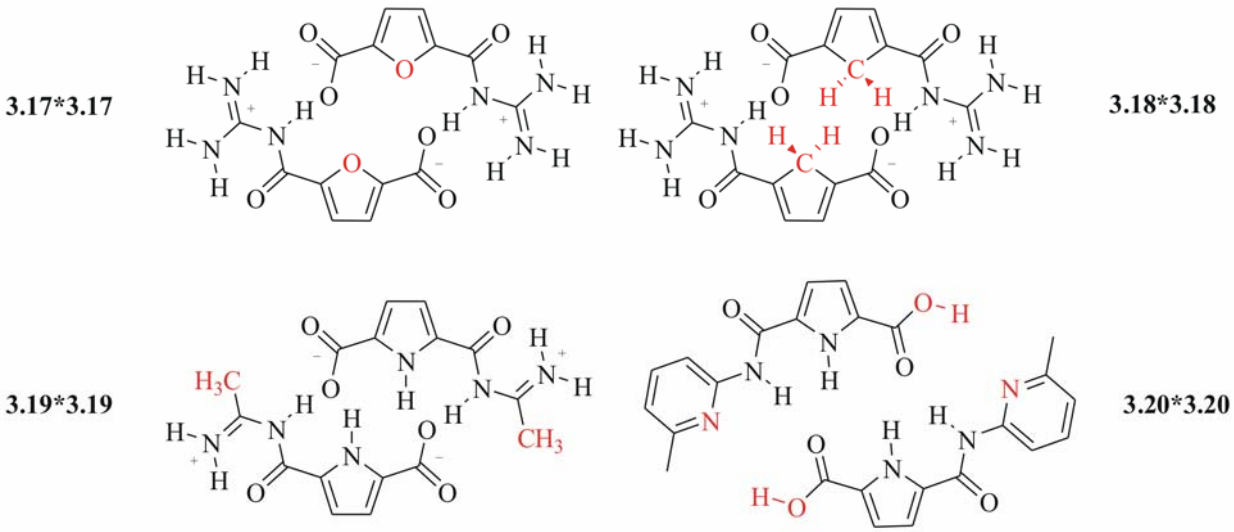

Fig. 3.11 *Selective elimination or modification of non-covalent interactions identifies their individual contribution to the self-assembly process (modified binding patterns are marked in red).*

In conclusion *Schlund* was able to prove that on one hand charge interactions within ionic hydrogen binding arrays are significantly more stable than simple point charges. On the other hand the introduction of neutral hydrogen bonds further promote the dimerization, but not as efficient as the charge interactions. Moreover repulsive interactions lead to a significant destabilization of the dimer.

Experimentally the neutral analogue **3.20** was the first one examined in great detail in order to achieve information about the contribution of the ionic interaction. As already explained binding motives based on pure hydrogen bonding are not able to self-assemble in polar solvents. Comparing ^{1}H-NMR dilution experiments of the neutral analogue gave an association constant of $K_{ass} > 10^4$ M^{-1} in pure chloroform whereas the addition of only 0.5 % DMSO resulted in a massive decrease of K_{ass} to a value of 330 M^{-1}. In pure DMSO no more dimers could be detected. This clearly shows that ionic interactions are absolutely necessary for the dimerization in polar, protic solvents. Although first experiments with the furan, pyridine and benzene zwitterions give better results in contrast to the neutral analogue, one thing is similar for all of them: they are by far not as stable as the primal pyrrole dimer. In the case of furan and pyridine this can be easily explained by the repulsive interactions between the free electron pairs of the ring heteroatoms and the carboxylate group.[23] In contrast to this the benzene zwitterion has no heteroatom which destabilizes the dimerization by repulsive interactions, but the aromatic CH, which substitutes the nitrogen of pyridine, is not a hydrogen bond donor (Figure 3.12). Due to this fact a attractive interaction with the carboxylate is not possible. Another reason for the hindered dimerization of the benzene zwitterion is the different geometry of the six-membered ring compared to the five-membered pyrrole ring. Due to steric interactions between the central aromatic CH and the guanidinioamide NH the whole molecule is slightly distorted leading to a non-planar structure in the dimer. This geometry prevents an efficient interaction between the binding partners leading to a low association constant.[24]

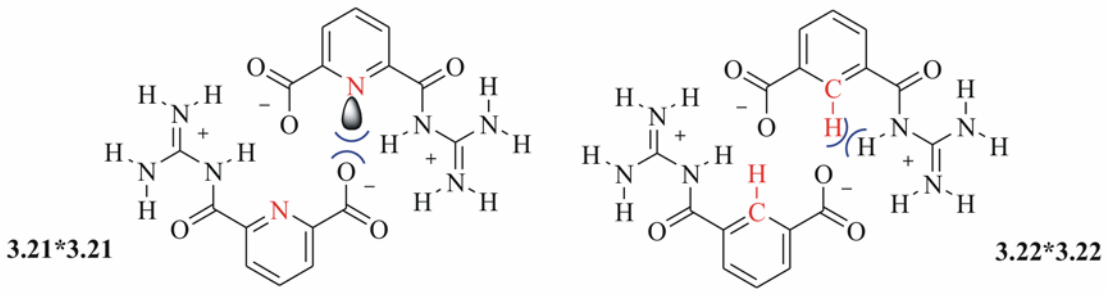

Fig. 3.12 *Structural restrictions based on repulsive electrostatic or steric interactions prevent efficient dimerization.*

In conclusion up to now guanidiniocarbonylpyrrole carboxylate zwitterions are the most efficient self-complementary binding motives for self-assembly in polar solvents based only on electrostatic interactions. Both theoretical and experimental examinations demonstrate the crossover of conceptual design to real application.

3.3 Vesicle forming molecules

This section will describe the formation of supramolecular structures of defined spherical shape. Vesicles, hollow spheres filled with solvent, result from the self-assembly of tailor-made monomers of individual size and functionalization. One has to distinguish between the classical vesicle forming molecules like amphiphipilic phospholipids or block-copolymers and the non-classical vesicle forming molecules like small peptides or functionalized aromatic compounds. In this section some selected examples of both classes will be presented to show the different possibilities for the formation of well-defined vesicles.

3.3.1 Classical vesicle formation

The classical way to form vesicles is based on Nature. Cell membranes are formed by glycerophospholipids. Here, the polar head group contains a glycerol molecule which bears one phosphate ester at a carbon atom and two long fatty acids at the remaining carbon atoms. Additionally, the head group can be derivatised by an esterification of the phosphate group with different molecules like choline, serine of inositol. The resulting molecules are the most common glycerophospholipids in biological membranes.[25] Figure 3.13 shows the structure of phosphatidylcholine and the schematical formation of a vesicle in an aqueous medium.

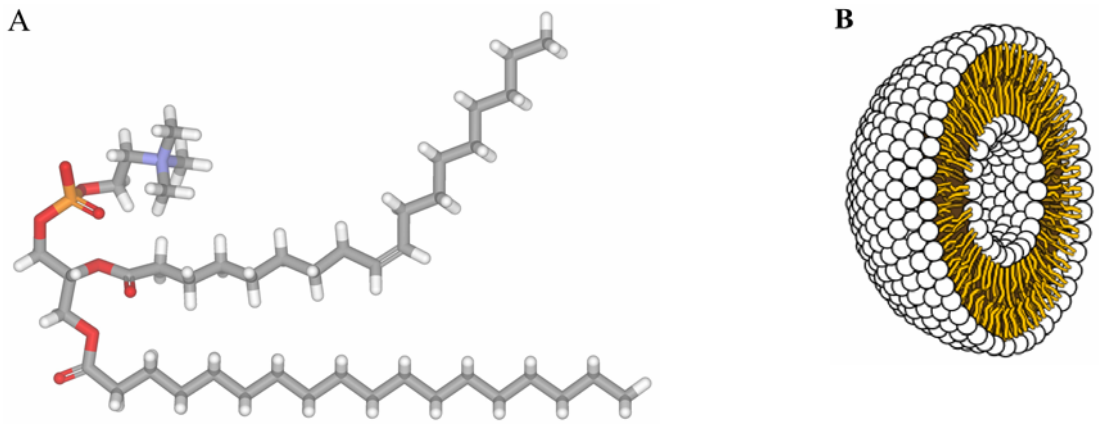

Fig. 3.13 *A) Phosphatidylcholine as a natural amphiphile for vesicle formation; B) minimization of unfavourable interactions between the unpolar alkyl chains and the aqueous environment leads to the formation of vesicles based on bilayer membranes (picture taken from reference 26).*

Lipid bilayers represent very stable structures based on two strong non-covalent interactions. First, hydrophobic forces of the alkyl chains form an environment that efficiently excludes water. Second, the charged head groups are in close contact to the aqueous solution and are the interface to the lipids. This combination leads to a bilayer structure in which the hydrophobic part of

the membrane is shielded against the aqueous medium by the polar head groups. On one hand the membranes are very flexible due to the flexible monomers, on the other hand they are very stable due to the strong interactions between the monomers. These vesicles are termed *liposomes* and their bilayer conformation represents the basic lipid structure of all biological membranes.

Synthetic vesicle forming molecules are based on the same principles found in the amphiphilic glycerophospholipids. The combination of hydrophobic and hydrophilic blocks in a copolymer leads also to the formation of hollow spheres. One advantage of these synthetic monomers is the possibility to combine a large number of different polymer blocks. According to the size and chemical functionalization of each block vesicles of varying dimension and quality are formed.[27] Beside the amphipihlic character of the copolymer also the molecular architecture of each block is important for the vesicle formation. Not only chain-like polymers, but also rod-like[28] or dendritic polymer blocks[29] of different size are used. In addition to this structural characteristic also the combination of three or four blocks within one monomer is possible yielding an even greater number of combinations.[30] In conclusion, tailor-made vesicles can be formed via the self-assembly of synthetical block copolymers whereas each polymer block is able to control the character of the resulting supramolecular structure.

Biologically inspired polymers like polypeptides can be also used as part of a block copolymer. In 2005 *Deming et al.* presented the self-assembly of a charged block copolypeptide which forms stable vesicular structures.[31] Here, a series of poly(*L*-lysine)-*b*-poly(*L*-leucine) block copolymers were prepared with a range of 20 to 80 *L*-Lys (*K*) residues and 10 to 30 *L*-Leu (*L*) residues. For example, the block copolypeptide sample $K_{60}L_{20}$ gave vesicles with a mean diameter of 960 nm. Interestingly, only samples with a helical conformation in the hydrophobic segment were able to form stable vesicles. Therefore a statistically racemic hydrophilic segment was combined with short (10 *L* residues), middle (20 *L* residues) and long (30 *L* residues) hydrophobic blocks. The first combination with the short *L*-Leu segment formed only micellar aggregates of *ca*. 25 nm in diameter whereas the other block copolymers formed vesicles with diameters of 1040 nm (middle) and 15 μm (long). The helix formation was proved by circular dichroism analysis and showed that only 10 % of the short *L*-Leu segment has a helical conformation. In the case of the middle and the long *L*-Leu segments 55 % and 90 % of the appropriate domains exist in the helical conformation, respectively. Figure 3.14 shows the proposed mode of self-assembly of the $K_{60}L_{20}$ into vesicles. In order to test the integrity of the vesicles Texas Red labeled dextran was encapsulated during the vesicle formation. Still after five days no dextran could be detected outside the vesicles. In conclusion, these polypeptide based block copolymers self-assemble into

large vesicles which are able to efficiently trap solutes and make them promising biomimetic encapsulants.

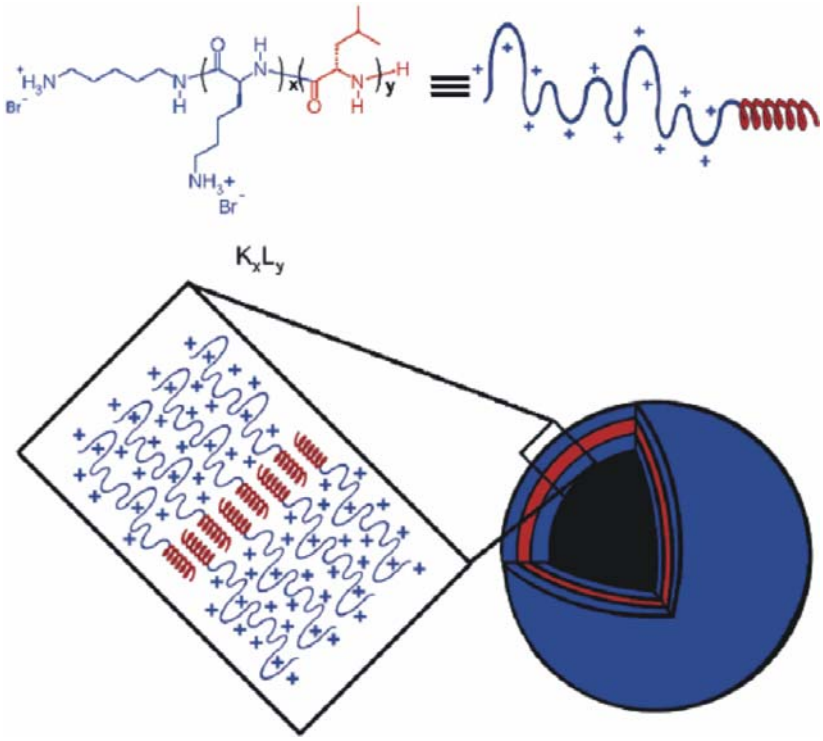

Fig. 3.14 *Self-assembly of $K_{60}L_{20}$ into vesicles: helical hydrophobic segments (red) form the inner shell of the vesicle membrane; the hydrophilic L-Lys segments (blue) are at the interface to the aqueous environment; reprinted with permission from J. Am. Chem. Soc.* ***2005****, 127, 12423-12428. Copyright (2005) American Chemical Society.*

Wegner et al. presented in 2005 the combination of two monodendrons based on poly(benzyl ether) (PBE) and poly(methallyl dichloride) (PMDC) as an example for a dendrimeric block co-polymer architecture.[32] Computational simulations show that the codendrimeric monomer has on one side a shape of a cone (PBE) and on the other side a shape of a ball (PMDC). This molecular architecture is very different in comparison to the linear polymer blocks with regard to the stability and flexibility of the monomer. First experiments were performed by diluting the codendrimer in pure THF and subsequent addition of diisopropylether (DIE) which is a nonsolvent for the poly(benzylether) dendron. Reaching a solvent ratio of 1:1 the solution was dropped onto a freshly cleaved mica surface in order to investigate the self-assembled structures via AFM. Here, spherical aggregates with a mean diameter of 150 nm were found which had a height in the range of 4-8 nm. Additionally, DLS experiments confirmed the formation of spherical structures in a THF/DIE solvent mixture (1:1) with a hydrodynamic radius of r_H = 46 nm. The larger vesicle diameter obtained from AFM is the result of the vesicle deformation upon the interaction with

the mica surface. TEM experiments also confirmed the dimension of the vesicles and provided additional information about the rigidity of the spherical aggregates. Figure 3.15A shows a TEM image of spherical plates with constant electron contrast which is typical for soft or rubber-like vesicles. In contrast to hard vesicles the collapsed soft vesicles have a nearly constant thickness from the periphery to the centre of the particle resulting in a constant electron contrast as seen in the TEM images. Figure 3.15B shows the suggested mode of vesicle formation (*d*). As result of the special molecular architecture (*a*) an interdigitated layer model is suggested which leads to a dense packing and low interfacial free energy (*b* and *c*). A bilayer formation as depicted in (*e*) would result in many holes within the membrane. In conclusion, codendrimeric architectures also offer the possibility of vesicle formation. The different solubility of each dendron block in THF/DIE mixtures is the driving force for formation of vesicles. Due to the defined structure of the codendrimer the vesicle membrane is less thick than the membranes formed by linear-linear block copolymers with the same molecular weight.

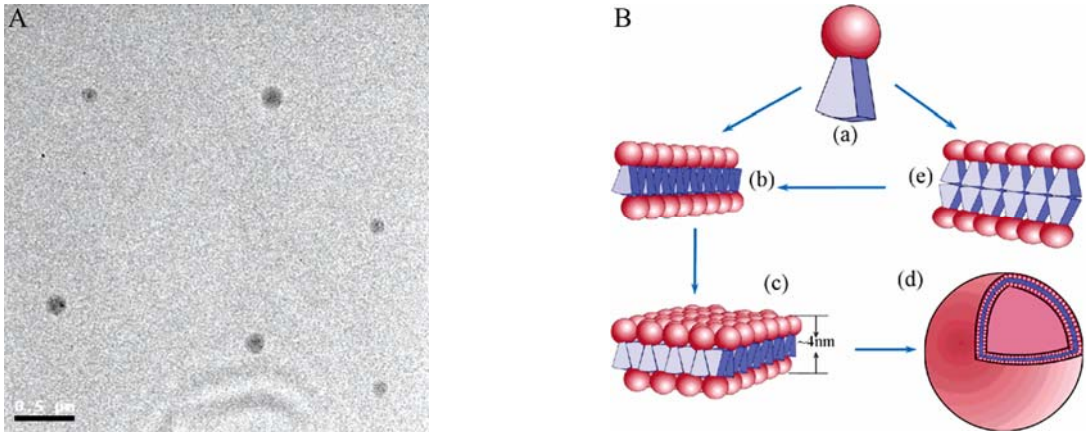

Fig. 3.15 *A) TEM image of the soft vesicles showing a constant electron contrast (the black bar corresponds to 500 nm); B) suggested mode of self-assembly of the discussed codendrimer; reprinted with permission from J. Am. Chem. Soc.* ***2005****, 127, 15107-15111. Copyright (2005) American Chemical Society.*

Synthetical block copolymers are one of the most often used compound class for the defined formation of vesicles. With increasing knowledge in supramolecular chemistry the application of other well-defined monomers was considered to build large vesicular structures with tailor-made properties. Hence, the next section discusses some selected examples which use non-classical vesicle forming molecules as monomers.

3.3.2 Non-classical vesicle formation by functional interactions and complementarity

In contrast to the classical head-group surfactants and phospholipids a rather small number of synthetic molecules is known which efficiently self-assemble into vesicles. One group comprises

functionalized calixarens,[33] cyclodextrines,[34] cryptands[35] or cucurbit[6]urils.[36] All members of this group have a built-in curvature that promotes vesicle formation. Shape-persistent macrocycles[37] or π-conjugated oligomers[38] represent another group of non-classical vesicle forming molecules. Although these monomers do not come up with a vesicle promoting preorganization within the molecular architecture they are certainly able to form well-defined vesicular structures by extensive aromatic interactions. A third group represents the use of small peptides. Recently *Matsuura et al.* adopted a self-assembly process from Nature in order to design nanospheres with a narrow size-distribution.[39] Hydrogen bonding mediated, antiparallel β-sheet formation is an efficient method to create self-assembled structures of various kinds. The idea here was to connect three β-sheet-forming peptides (FKFEFKFE) with a C_3-symmetric core molecule. Due to the constrained geometry of the core only intermolecular self-assembly is possible (Figure 3.16). First circular dichroism and FT-IR experiments in aqueous HCl (24 μM, pH 3.3) provided data, which are characteristic for anti-parallel β-sheet formation.

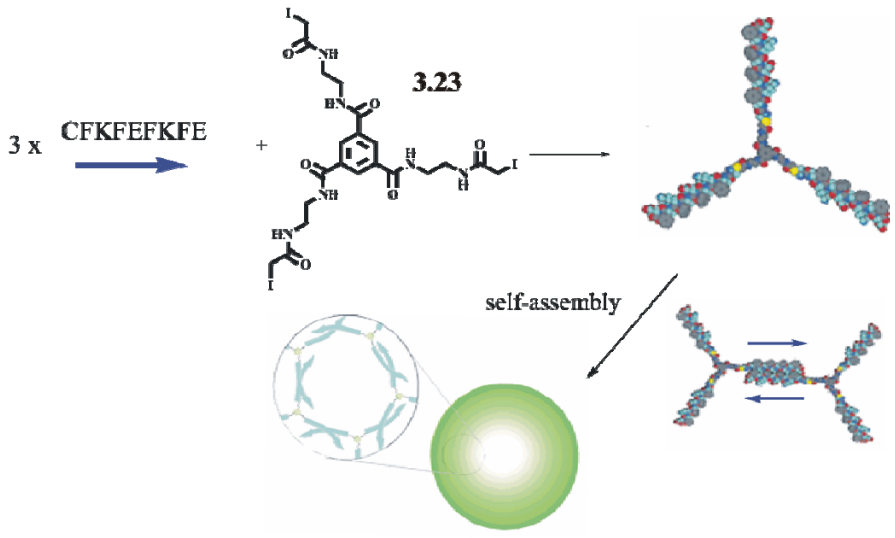

Fig. 3.16 *Hydrogen bonding mediated β-sheet formation as functional interaction for efficient vesicle design; reprinted with permission from J. Am. Chem. Soc.* ***2005****, 127, 10148-10149. Copyright (2005) American Chemical Society.*

Further investigations concerning the dimension and structure of the supramolecule were performed. Both AFM and DLS experiments exclusively showed only the presence of spherical nanostructures with a mean diameter of *ca*. 19 nm (DLS) and a height of about 2.3 nm (AFM). Comparing AFM measurements of the pure peptide afforded fibrils with a width of *ca*. 40 nm and a height of *ca*. 1 nm. Comparing both heights suggests the formation of vesicular structures whereas the doubled height in the AFM pictures results from the lamination of the vesicle walls. SEM experiments also showed concave like structures which are most likely formed by the col-

lapse of the parent vesicular structure. In conclusion all experimental data prove the existence of vesicles based on the self-assembly of β-sheets.

A quite similar concept was published by *Gazit et al.*[40] Instead of hydrogen bonding they use aromatic stacking interactions in order to self-assemble a tripodal dipeptide based on tryptophan as binding motive. The resulting vesicles have a mean diameter of *ca.* 1 μm as observed by SEM experiments (Figure 3.17).

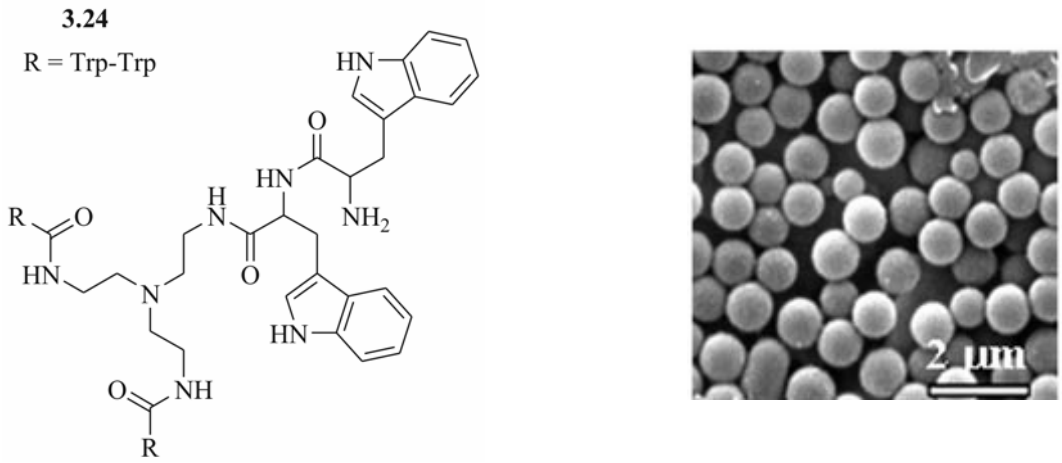

Fig. 3.17 *Aromatic stacking interactions between tripodal ditryptophan peptides result in vesicles formation; S. Gosh, M. Reches, E. Gazit, S. Verma: "Bioinspired Design of Nanocages by Self-Assembling Triskelion Peptide Elements", Angew. Chem. Int. Ed.* ***2007****, 46, 2002-2004. Copyright Wiley-VCH Verlag GmbH & Co. KGaA. Reproduced with permission.*

Beside the efficient self-assembly this building block has another interesting property. By protonation of the free amino functions repulsive electrostatic interactions degrade the supramolecular structure. Assuming that these vesicles are able to encapsulate drugs for example, the free amino functions serve as embedded trigger for selective release of the vesicles' load.

Another example describes the combination of both hydrogen bonding and aromatic stacking interaction in order to design vesicles in a two-step procedure. In the first step *Jiang et al.* attached *Frechet*-type dendrons of second and third generation with a carboxyl group to a polymer main chain based on *poly*-(4-vinylpyridine) (PVP).[41] The formation of hydrogen bonds between the carboxyl and the pyridyl groups was proved by ^{13}C-NMR experiments. A pure solution of the dendrons resulted in self-association of two carboxyl groups leading to a signal at 171 ppm. After addition of the pyridine containing polymer this signal disappeared completely whereas another signal arose at 169 ppm indicating the formation of the desired hydrogen bonds between the dendrons and the polymer chain. These so called hydrogen-bonded dendronized polymers (HB denpols) self-assemble in a second step into vesicular structures promoted by ultrasonic

treatment. This second process is affected by the benzyl groups of the dendrons. Efficient aromatic stacking interactions between the sector-type dendrons lead to a layer-by-layer membrane structure of the vesicle as it is shown schematically in Figure 3.18. In this example an average number of ten dendrons is attached to one polymer chain. This loading results in self-assembled vesicles with a mean diameter of about 282 nm as evidenced by DLS and TEM.

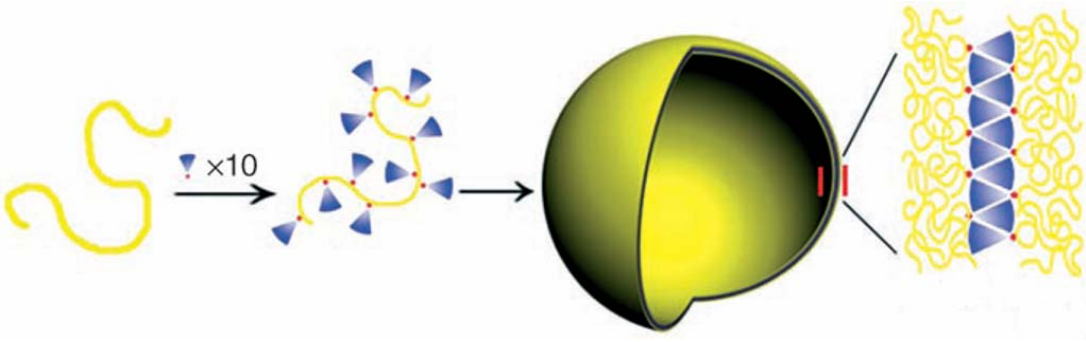

Fig. 3.18 *Stepwise self-assembly results in vesicles with layer-by-layer membrane structure (PVP/dendron/PVP); D. Xie, M. Jiang, G. Zhang, D. Chen: "Hydrogen-Bonded Dendronized Polymers and Their Self-Assembly in Solution", Chem. Eur. J.* ***2007****, 13, 3346-3353. Copyright Wiley-VCH Verlag GmbH & Co. KGaA. Reproduced with permission.*

Interestingly, the TEM images did not show a change in contrast intensity from the centre to the periphery of the particle. This would assume a solid sphere and not a hollow vesicle as expected. But a closer look at the AFM images indicates the collapse of the parent vesicles as the observed particles have just a height of about 9 nm, which is far smaller than the mean diameter of the particles observed by DLS. The absent variation in the contrast of the TEM images arises therefore from the homogenous two-layered structure of the collapsed vesicle (Figure 3.19).

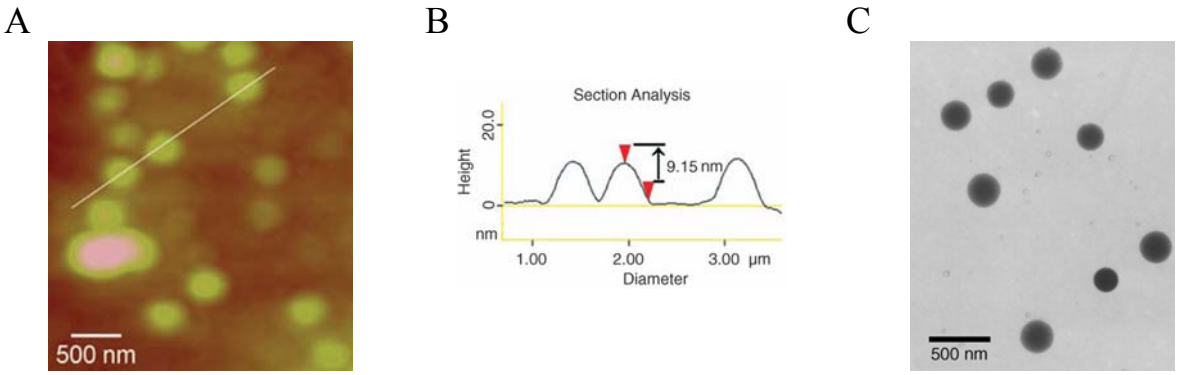

Fig. 3.19 *A) Height AFM image of vesicles based on hydrogen-bonded dendronized polymers; B) particle-height analysis of representative particles; C) TEM images of collapsed vesicles without darkening contrast; D. Xie, M. Jiang, G. Zhang, D. Chen: "Hydrogen-Bonded Dendronized Polymers and Their Self-Assembly in Solution", Chem. Eur. J.* ***2007****, 13, 3346-3353. Copyright Wiley-VCH Verlag GmbH & Co. KGaA. Reproduced with permission.*

One interesting feature of this vesicle formation is the possibility to increase the loading of the polymer chain. For example the combination of 23 dendrons attached to one polymer chain results in smaller vesicles (134 nm), but thicker membranes (30-40 nm). The increased membrane consists most likely of several alternating dendron and PVP layers. The enhanced stability could be proved by TEM experiments as the images show a clear contrast between the centre and the periphery of the observed particles. With this concept it is possible to design vesicles of different softness by adjusting the loading of the polymer chain with the second building block.

Whereas the former example represents a vesicle formation with diameter-dependent membrane thickness the combination of wedge- and dumbbell-shaped monomers offers the possibility of direct diameter control without changing the membrane thickness. Just recently *Würthner et al.* introduced asymmetric perylene diimides with different substituents in the imide positions leading to amphiphilic building blocks (Figure 3.20).[42] Mixtures with varying ratios of both components gave bilayer vesicles of well-defined diameter.

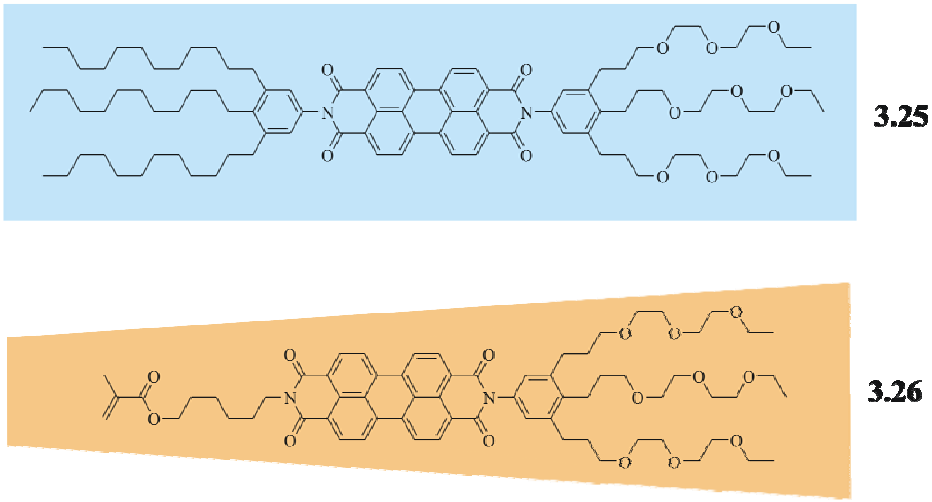

Fig. 3.20 *Dumbbell- and wedge-shaped perylene diimdes as co-self-assembling monomers for morphology controlled vesicle formation.*

For example a mixture of dumbbell-shaped and wedge-shaped monomers in a ratio of 1:8 yielded vesicles with a mean diameter of 94 nm. A ratio of 1:4 enlarges the diameter to a value of 133 nm (Figure 3.21A). In contrast, a blank sample of pure wedge-shaped monomer produces micelles with a diameter of *ca*. 5 nm (Figure 3.21B) whereas the self-assembly of pure symmetric dumbbell-shaped monomers results in rod-like aggregates with a diameter of *ca*. 4 nm (Figure 3.21C). In conclusion this method provides efficient vesicle formation with morphology control. Adjusting the ratio between both building blocks has direct influence on the vesicle curvature and therefore the diameter.

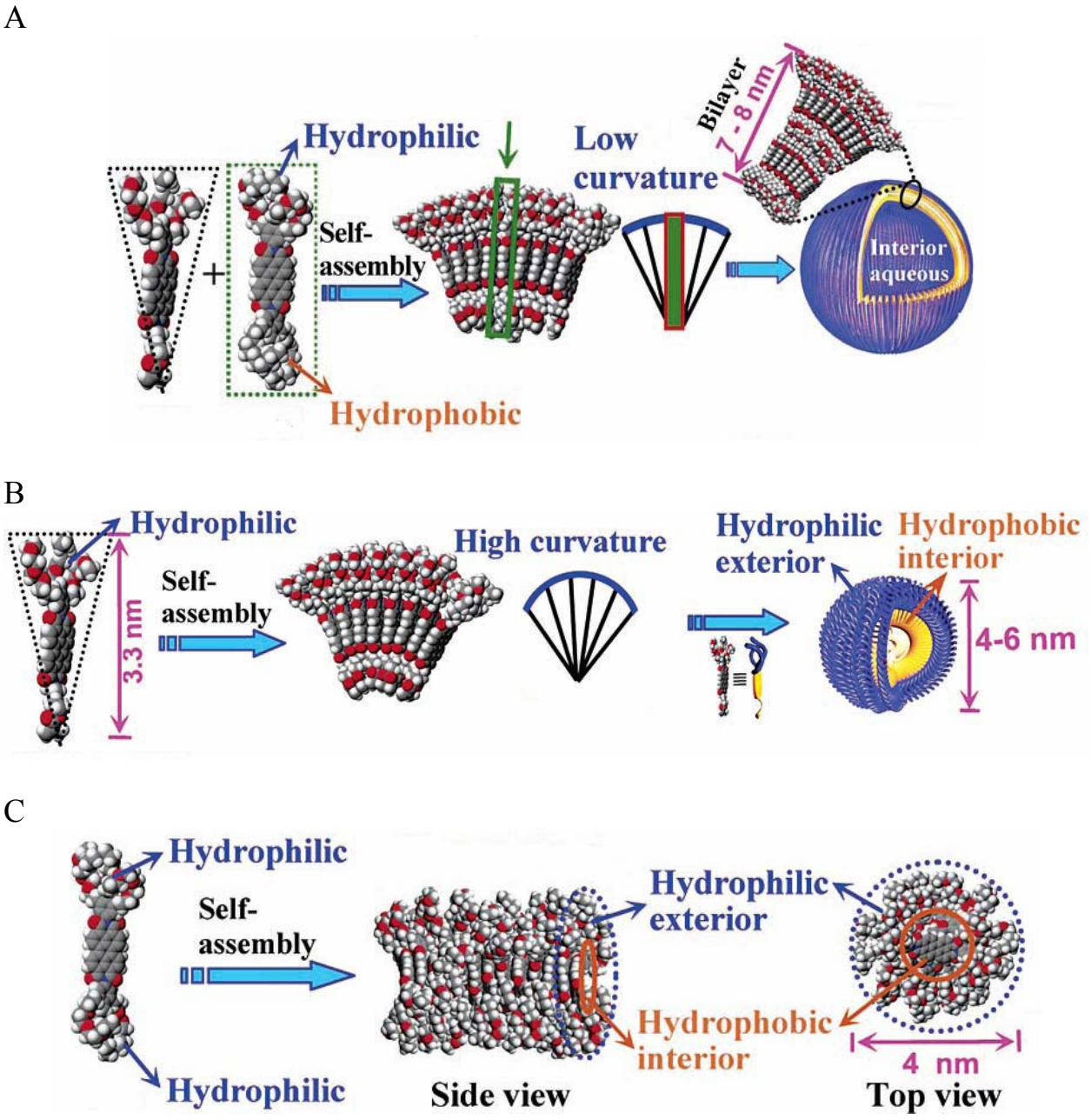

Fig. 3.21 *Morphology control: Vesicle formation by co-self-assembly (A); micelles or rod-like aggregates via self-assembly of pure wedge-shaped monomers (B) or pure dumbbell-shaped building blocks (C); reprinted in part with permission from J. Am. Chem. Soc.* ***2007****, 129, 4886-4887. Copyright (2007) American Chemical Society.*

But another property of this system should also be mentioned. As every supramolecular process can be described as an equilibrium reaction between the monomers and the supramolecule, size and structure can vary due to an external influence like temperature or solvent polarity. In order to make a snapshot of the supramolecule in a defined state the desired structure has to be removed from the equilibrium reaction. In case of these vesicles photopolymerization was used in order to connect the self-assembled monomers covalently. For this reason the wedge-shaped

monomer has a polymerizable unit in terms of a double bond at the end of the single stranded substituent. UV irradiation at 350 nm initiates the polymerization yielding shape-persistent vesicles (Figure 3.22). As proof any addition of dumbbell-shaped monomer showed no further variation in size and structure of the polymerized vesicles.

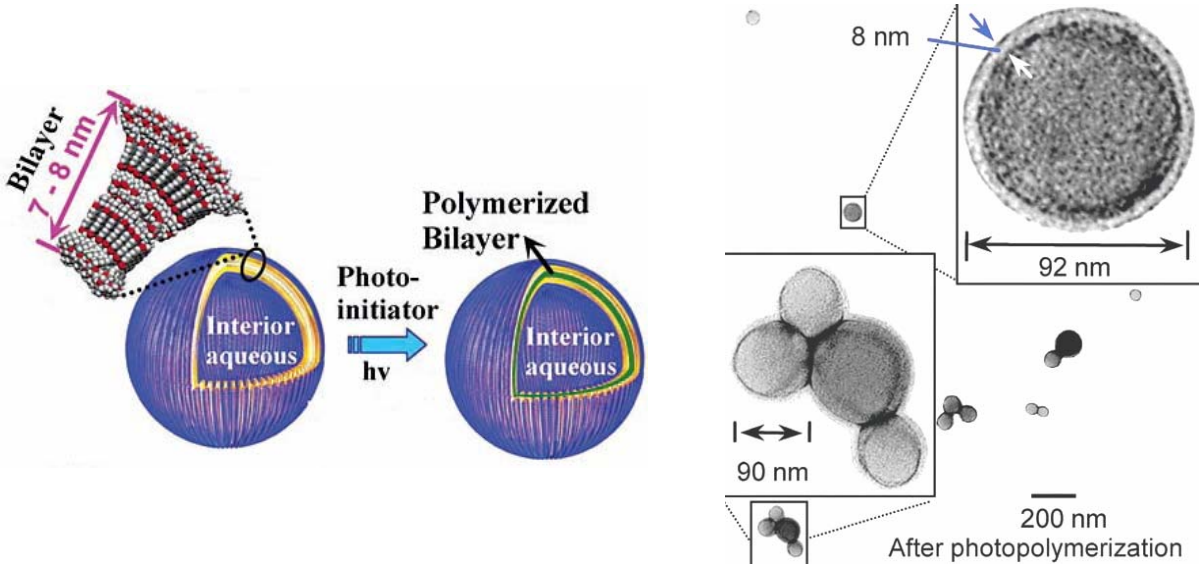

Fig. 3.22 *Covalent steeling via photopolymerization results in shape-persistent vesicles; reprinted in part with permission from J. Am. Chem. Soc.* ***2007****, 129, 4886-4887. Copyright (2007) American Chemical Society.*

The last example describes the use of small dipeptides as vesicle forming monomers. *Görbitz* first found that small dipeptides can self-assemble into well-defined structures like nanotubes.[43] *Gazit et al.* used this principle and introduced the core recognition motive of *β*-amyloid, the diphenylalanine structural motive, as nanotube forming monomer in zwitterionic state.[44] By diluting an aqueous solution of these nanotubes with water *Shelnutt et al.* could also observe the formation of vesicles in addition to the nanotubes.[45] Using the same principle together with a cationic dipeptide (H-Phe-Phe-NH_2·HCl) *Li et al.* introduced positively charged nanotubes at a physiological pH value of 7.2. Upon dilution with water the cationic dipeptide nanotubes rearrange into vesicles with a diameter of 100 nm as revealed by AFM experiments.[46] Most likely this reassembly process is the result of electrostatic repulsion instead of a different binding mode of hydrogen bonds or aromatic stacking interactions. The resulting vesicles were used for the DNA transfer into cells due to a strong ionic interaction between the positively charged vesicle membrane and the negatively charged DNA backbone (Figure 3.23).

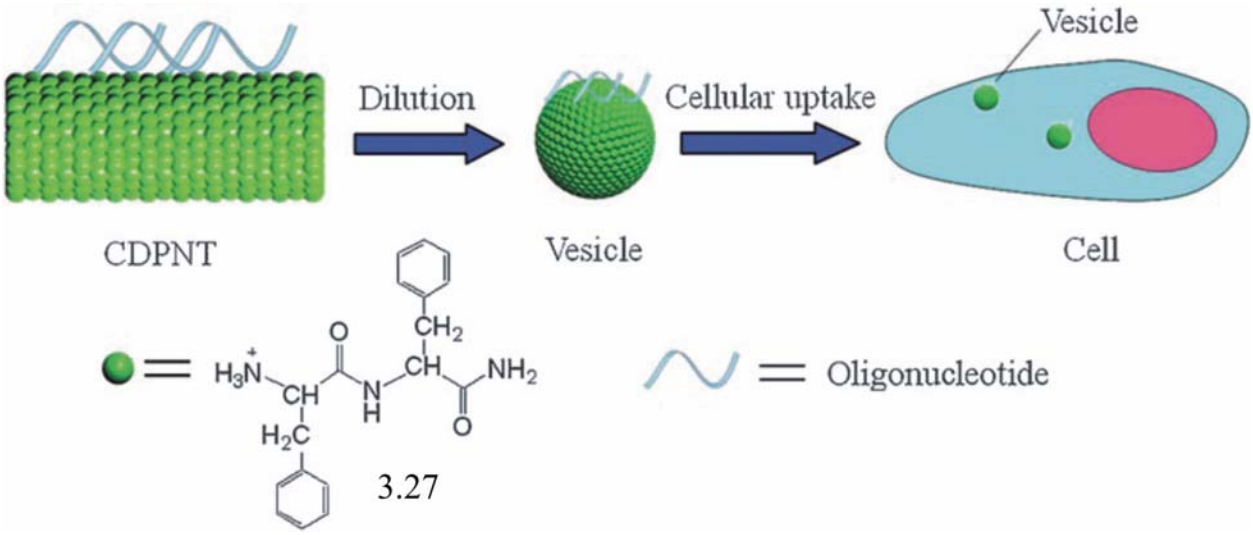

Fig. 3.23 *Self-assembled nanotubes rearrange to vesicles upon dilution in water; X. Yan, Q. He, K. Wang, L. Duan, Y. Cui, J. Li: "Transition of Cationic Dipeptide Nanotubes into Vesicles and Oligonucleotide Delivery", Angew. Chem. Int. Ed.* ***2007****, 46, 2431-2434. Copyright Wiley-VCH Verlag GmbH & Co. KGaA. Reproduced with permission.*

In conclusion several concepts are available, which all lead to well-defined vesicular structures. The interactions used for vesicle formation range from hydrogen bonding over aromatic stacking to hydrophobic interactions or combinations of them. Depending on the method, morphology control can be applied in order to generate structures with a narrow size distribution. Also the stability of the vesicles can be improved by controlling the thickness of the membrane. Beside the tailor-made design of the vesicles also prospective applications are a point of interest. Embedded triggers can be used to release selectively the load of the vesicle by disruption of the supramolecular structure. In contrast to this the reinforcement of the supramolecule is also possible instead of its destruction. Polymerizable functions like double bonds can be introduced to covalently entrap the self-assembled structure. Also biological applications are known since charged vesicles can be used as molecular transporters for DNA. Hence vesicles represent a perfect example for supramolecular chemistry: tailor-made monomers self-assemble into the desired supramolecules with defined properties.

3.4 Theoretical background of the analytical methods

Beside the standard analytical methods like ^{1}H-/^{13}C- NMR spectroscopy, FT-IR spectroscopy and high-resolution mass spectrometry also more special methods were applied. DOSY NMR and DLS provide information about the dimension of supramolecular assemblies in solution whereas SANS gives more detailed information about the internal structure of large su-

pramolecules. AFM and TEM are used to visualize and measure the self-assemblies as snapshots of particles taken out of the solution and fixed on a surface.

3.4.1 Diffusion ordered spectroscopy NMR[47] (DOSY NMR)

In solution molecules have two different types of mobility: rotational and translational motion. The latter describes the movement of the molecule depending on its shape and size as well as the viscosity of the solvent and the temperature of the sample. The DOSY NMR technique is a very efficient method to determine this mode of motion which is also known as *Brownian* motion or self-diffusion. Due to the non-invasive measurement under equilibrium conditions DOSY NMR is a powerful tool for the examination of supramolecular assemblies. As this method plots the translational diffusion coefficient *D* against the relative shift of the protons a clear assignment of the structural information on the appropriate diffusion coefficient is possible. Hence complex mixtures of several compounds can be separated in the form of a "virtual" HPLC.

The relation between the diffusion coefficient *D* and the size of a spherical molecule in terms of its radius is described by the *Stokes-Einstein* equation:

$$D = \frac{k_B \cdot T}{f_0} = \frac{k_B \cdot T}{6\pi \cdot \eta \cdot r_{sph}} \qquad \text{(Eq. 3.1)}$$

where k_B is the *Boltzmann* constant, T the absolute temperature, f_0 the friction coefficient of a spherical object, η the viscosity of the solvent and r_{sph} the hydrodynamic radius. Two important things have to be pointed out. In order to compare two DOSY NMR experiments both temperature and viscosity must be stable. Due to temperature fluctuations convections inside the sample lead to non-random movements of the particles. Beside this also the direct influence of the temperature on the viscosity can lead to errors in the interpretation of the results.

A method very often used for the analysis of diffusion processes is based on the pulsed gradient spin echo experiment (PGSE). This method results in the spatial labelling of the molecules by applying a magnetic gradient along the *z*-axis of the spectrometer. This means that every molecule is marked according to its actual place within the sample tube. Within a certain time frame Δ the molecules change their position due to their capability of translatory self-diffusion. After that a second magnetic field gradient is applied in order to resolve the new position of the molecules in the sample tube. The resulting spin echo signal intensity I is attenuated compared to the starting signal intensity I_0, depending on the diffusion time Δ as well as the parameters of the magnetic field gradient (g = gradient strength, δ = gradient length):

$$I = I_0 \cdot e^{-D \cdot \gamma^2 \cdot g^2 \cdot \delta^2 \cdot \left(\Delta - \frac{\delta}{3}\right)} = I_0 \cdot e^{-D \cdot g^2 \cdot const} \qquad \text{(Eq. 3.2)}$$

where γ is the gyromagnetic ratio of the observed nucleus. In the DOSY experiment all parameters are kept constant except the gradient strength g. The signal intensity I is measured repeatedly and plotted against the varying gradient strength g which results in a *Gauss* curve. By curve fitting the diffusion coefficient D is obtained as the gradient of the curve. In Figure 3.24 the resulting *Gauss* curve for tetramethylsilane (TMS) in a DMSO-d_6/D_2O mixture (4:1) is depicted. TMS is not only used as shifting reference, but also as diffusion reference. As DOSY experiments are often used to investigate samples with different concentrations one has to account that the viscosity of the solvent also changes with the concentration of the solute. In order to follow and control this change TMS is used as inert probe (no hydrogen bonding, no dipole character) with known hydrodynamic radius.

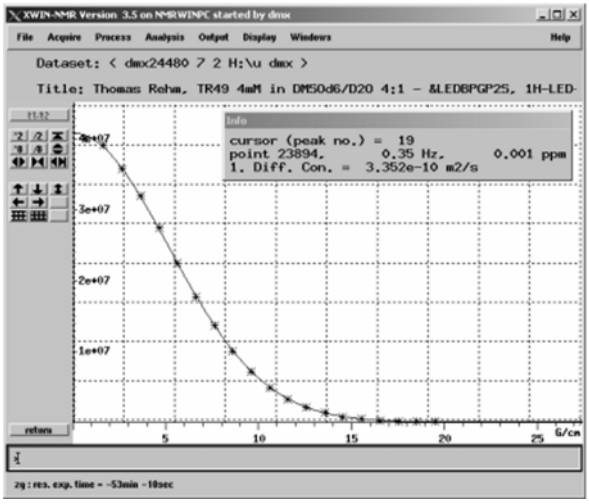

Fig. 3.24 *Tetramethylsilane (TMS) is used as an internal standard for both shifting and diffussion.*

As equation 3.1 considers only spherical molecules non-spherical compounds like ellipsodial molecular objects are described via the radius of a hydrodynamically equivalent sphere. By introduction of a shape factor P into the friction coefficient the molecular dimensions of the ellipsoid can be obtained also from the diffusion coefficient D. The shape factor P is defined as ratio between the semimajor to the semiminor axis of the ellipsoid, with P always greater than one. The enhanced equation of the friction coefficient is therefore:

$$f = f_0 \cdot \left(\frac{P^{-\frac{1}{3}} \cdot \left(P^2 - 1\right)^{\frac{1}{2}}}{\ln\left[P + \left(P^2 - 1\right)\right]^{\frac{1}{2}}} \right) \qquad \text{(Eq. 3.3)}$$

As the shape factor *P* has two parameters (both axes of the ellipsoid) with unknown values one of them must be derived from another source like x-ray crystallography or molecular modelling. With this model also the dimension of non-spherical molecules can be measured.
Due to the fact that this method is based on NMR technique the observation of supramolecular structures is limited to self-assembled particles with a rather small amount of monomers. If, for example, the number of building blocks becomes too large signal broadening leads to improper NMR spectra due to signal overlap or weak signal intensity. In order to get information about the dimension of supramolecular structures built up from hundreds of monomers other techniques have to be applied.

3.4.2 Dynamic light scattering[48] (DLS)

Any light scattering method is based on the stimulation of matter by radiation. In the case of dynamic light scattering laser light (with a certain wavelength beyond the absorption range of the analyte) interacts with particles, which are dissolved in an appropriate solvent. The interaction of the electric component of the radiation with the particle in terms of the electrons results in induced dipoles which oscillate with the same frequency as the applied laser light, i.e. the scattered light is coherent. Hence one important experimental condition has to be fulfilled: the wavelength of the applied laser light has to be larger than the size of the particles. Typically the particle diameter should be a tenth of the wavelength of the used light. On that condition all induced dipoles are in phase. Therefore the total dipole moment represents the whole particle. In case of a too small wavelength dipoles of varying strength and direction will be induced. This leads to a segmentation of the particle according to each induced dipoles. The total dipole moment does not represent the whole particle any longer (Figure 3.25). Other techniques like neutron or x-ray scattering benefit from this spatially separated stimulation. They are used to interpret the internal structure of such particles. However, this method will be discussed later in section 3.4.3. In conclusion dynamic light scattering is able to detect and examine particles which consist of hundreds or thousands of monomers. In this case the information of the particle size is not transferred by the mean signal of single monomers but by the total dipole moment of one particle. This is in clear contrast to the DOSY NMR technique.

Fig. 3.25 *Influence of the laser light wavelength on the induction of dipoles inside the particle: short wavelengths lead to unwished segmentation of the particle.*

As dynamic light scattering is a technique for the measurement of the translational motion of particles in solution the experimental conditions have to be similar to the DOSY NMR experiments. Beside both stable temperature and viscosity of the sample one has to take into account that laser light introduces energy from the outside into the sample. Therefore the wavelength and the intensity of the laser should be well adjusted in order to prevent any photochemical reactions or conformation changes of the particles.

In DLS experiments the diffusion coefficient is extracted from the intensity fluctuations of the scattered light depending on the time. Within a small sample volume and in the microsecond time range the scattered light of particles is detected. The intensity fluctuations result from the self-diffusion of particles which causes incidental agglomeration and variation in the number of particles in the scattering volume. Figure 3.26 shows the important correlation: large particles cause a rather slow change of intensity, whereas small particles lead to a quick intensity change.

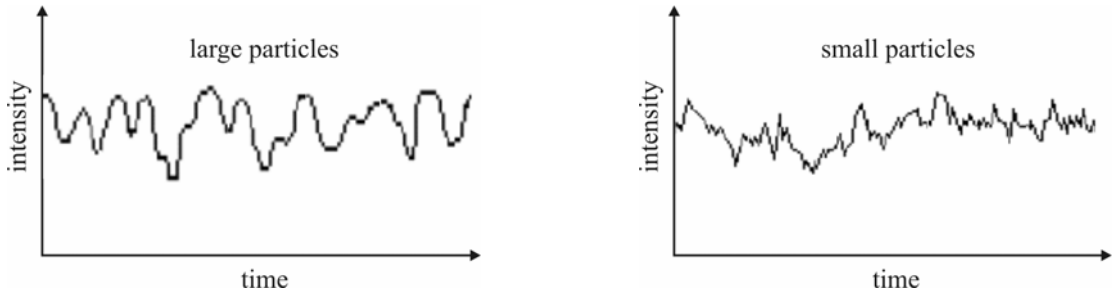

Fig. 3.26 *Different speed of intensity fluctuations as a result of the particle size and shape.*

Both time and intensity fluctuations are used to measure the diffusion coefficient by means of an autocorrelation function. This function describes the correlation of the scattered light intensity at a given time t with the intensity at the advanced time $t + \delta t$.

$$G(\delta t) = \langle I(t) I(t + \delta t) \rangle \qquad \text{(Eq. 3.4)}$$

In case of a static solution with particles which do not self-diffuse the intensity will be always the same, because there is no variation in the number of particles in the scattering volume. But

due to the random movement of the particles in a real solution the correlation between the starting intensity and the intensity at any time later will decrease until at $t = \infty$ no correlation will take place any more. This autocorrelation function G is an exponential decaying function of the time delay δt. It is described in the following equation for monodisperse systems, i.e. solutions containing just particles of one size:

$$G(\delta t) = A\left(1 + B \cdot e^{-2 \cdot D \cdot q^2 \cdot \delta t}\right) \quad \text{(Eq. 3.5)}$$

$$\text{with } q = \frac{4 \cdot \pi \cdot \eta}{\lambda} \cdot \sin\frac{\theta}{2} \quad \text{(Eq. 3.6)}$$

where A is the baseline and B the intercept of the correlation function, D the diffusion coefficient, η the refraction index of the solvent, λ the wavelength of the laser and θ the scattering angle. For polydisperse systems the exponential decays of all particle sizes have to be added and included into the auto correlation function. Various algorithms can be used to extract size information from the autocorrelation function. One approach is the *cumulant* analysis. It fits a single exponential to the auto correlation function and obtains the mean size of all particles and an estimate of the width of the distribution. The second approach is the *CONTIN* algorithm. By fitting a multiple exponential to the autocorrelation function information is obtained according to the distribution of particle sizes. Beside this also the number of particles belonging to one size class can be obtained. Therefore a more realistic view can be given on the size and distribution of particles in a polydisperse solution. In conclusion DLS has the true advantage to examine the dimension of particles which have self-assembled from a large number of monomers. This is in clear contrast to the DOSY NMR technique. But, in order to investigate the internal structure of the supramolecules, a method has to be applied which can discriminate unequal regions within the self-assembled structure.

3.4.3 Small angle neutron scattering[49] (SANS)

Beside the pure dimension also the interior and the shape of the observed particles is an important point. In order to get an insight into the constitution of the supramolecule the probe has to enter the supramolecule. But the probe also has to be able to discriminate individual parts of the particle. The latter one can be achieved by reduction of the wavelength as already discussed in the former section. The first point is given by the application of another radiation source in terms of neutrons. As neutrons have no charge they do not interact with the electron shell of atoms but with the nuclei. Beside their ability of high penetration neutron radiation is able to differentiate the atoms within one sample. In case of x-ray scattering for instance the scattering cross-section

increases in direct proportion with the increasing atomic number and the number of electrons, respectively. However, the interaction between neutrons and atoms varies irregularly with the atomic number. Hydrogen (^{1}H) has a neutron scattering cross-section *s* of 1.75 barn which is nearly the same as that of manganese. In contrast to this the hydrogen isotope deuterium (^{2}H) has a value of *s* = 5.6 barn (1 barn = 10^{-24} cm^2). Beside this efficient discrimination neutron scattering permits the detection of hydrogen atoms in contrast to x-ray scattering. This is a very important point for the measurement of biological samples. On the other side neutron scattering has several more advantages. As the wavelength of neutron radiation can be also adjusted in the range of x-rays the energy of these neutrons is several orders of magnitude lower than the energy of x-rays with the same wavelength. Whereas the energy *E* and the wavelength λ of the electromagnetic radiation are associated by the *Planck*'s equation

$$E = \frac{h \cdot c}{\lambda} \qquad \text{(Eq. 3.7)}$$

with *h* as *Planck*'s constant and *c* as light speed in the vacuum, the energy of a neutron is given by its kinetic energy E_n due to its finite mass m_n:

$$E_n = \frac{h^2}{2 \cdot m_n \cdot \lambda^2} = \frac{m_n \cdot \nu^2}{2} \qquad \text{(Eq. 3.8)}$$

with ν as the velocity of the neutron and λ as its wavelength. Due to this fact the energy of the neutrons can be adjusted by velocity moderators like graphite which are located between the neutron source and the sample. For example, a thermal neutron with a wavelength of 0.15 nm has the energy of *ca*. 36 meV, whereas x-ray photons with the same wavelength have the energy of *ca*. 8 keV. With a value of *ca*. 4 eV for the bond energy of a C-C bond one can estimate the destructive power of x-rays to biological samples. In conclusion neutron scattering is an efficient method for the analysis of the interior structure of the observed particle. Beside the high penetration ability also the use of thermal neutrons leads to a non-destructive examination of the sample. In any SANS experiment a neutron beam is directed at a sample of which only a small volume *V* is highlighted. The scattered radiation is collected by a detector of defined size *dx·dy*, distance *L* to the sample and scattering angle θ. The intensity of the scattered radiation can be described by the following equation:

$$I(\lambda, \theta) = I_0(\lambda) \cdot (\Delta \cdot \Omega) \cdot \eta(\lambda) \cdot T \cdot V \cdot \frac{\partial \sigma}{\partial \Omega}(Q) \qquad \text{(Eq. 3.9)}$$

where $I_0(\lambda)$ is the initial radiation intensity, $\Delta \cdot \Omega$ a solid angle element described by $dx \cdot dy / L^2$, $\eta(\lambda)$ the detector efficiency, *T* the sample transmission and $(\partial\sigma/\partial\Omega)(Q)$ the differential cross-section. The first three terms depend on the technical quality of the SANS setup whereas only the last

three terms of equation 3.9 are sample dependent. The most important term is the last one since it contains information about the particles. The differential cross-section can be described by the following equation:

$$\frac{\partial\sigma}{\partial\Omega}(Q) = N_p \cdot V_p^2 \cdot (\Delta\cdot\delta)^2 \cdot P(Q)\cdot S(Q) + B \qquad \text{(Eq. 3.10)}$$

where σ is the cross section, Ω the solid angle, N_p the number concentration of scattering particles, V_p the volume of one scattering particle, $(\Delta\cdot\delta)^2$ the contrast, $P(Q)$ the form factor, $S(Q)$ the structure factor, Q the scattering vector and B the background signal. The scattering vector Q represents the difference of the initial and the scattered neutron beam in terms of vectors. The form factor $P(Q)$ describes how the differential cross-section is modulated by interferences resulting from scattered radiation within one scattering body. This term is very important due to the information about the shape of the particle. A general description is given by the *Van de Hulst* equation which introduces shape parameters for different kinds of topologies like spheres, cylinders or rods. The structure factor $S(Q)$ describes the degree of local order in the sample. It is based on the interference of the scattered radiation of every scattering body within the sample volume V. In conclusion the extraction of the data from the scattered radiation leads to a detailed specification of the observed particles in terms of shape and degree of order within the sample.
With these analytical methods (DOSY NMR, DLS and SANS) it is possible to examine supramolecular structures in solution. Beside the dimension of the supramolecules also the internal structure can be investigated in high detail in order to get a deeper insight into the self-assembly process of the respective system. Hence, beside the investigation in solution also the self-assembly on a solid substrate is a point of interest. The next two sections will give a short introduction in commonly used techniques (AFM, TEM) which are able to examine structures on a solid substrate on the nanometer scale.

3.4.4 Atomic force microscopy[50] (AFM)

Beside the above mentioned methods which provide information about the dimension and the internal structure of the supramolecular assemblies in solution, also the self-assembly on a solid substrate is an important point of interest. Due to its high resolution under convenient conditions AFM is often used to generate a three-dimensional map of deposited self-assembled structures on a flat surface. The idea behind this technique is based on the interaction between the surface with the deposited substance and a sharp tip which is attached to a cantilever. The force between the tip and the surface is very small, mostly less than 10^{-9} N. Hence, a direct measurement of such a small force is not really easy to perform. Due to this fact indirect measurement is the

method of choice. The deviation of the cantilever resulting from the interaction with the surface is sensed with a laser. A mirrored surface on the back side of the cantilever reflects the laser beam onto a position-sensitive detector. Therefore small deflexions of the cantilever result in an exact signal at the detector. The assembly of the detector data with the computer-controlled motion of either the tip or the surface results in a three-dimensional map of the observed surface (Figure 3.27). Three different scanning modes are possible: In the contact mode the tip slightly touches the surface whereas repulsive forces lead to the deviation of the cantilever. In the non-contact mode the tip does not touch the surface. The cantilever is deflected by attractive interaction with the surface. The third type is the tapping mode. Whereas non-contact and contact mode result either in low resolution due to weak interacting forces or in sample damage the tapping mode represents the best results. In this method the cantilever oscillates vertically with a frequency of 50 – 500 kHz. As the oscillating cantilever periodically contacts the surface the resulting cantilever oscillation is reduced due to loss of energy caused by the interaction with the surface. The reduced oscillation is therefore used to identify the surface features.

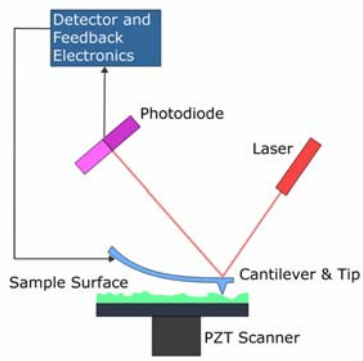

Fig. 3.27 *Schematic illustration of the AFM principle: tip-surface interactions lead to the deflection of the cantilever resulting in a three-dimensional map (picture taken from reference 51).*

Due to the high frequency used for tapping mode the tip makes the surface viscoelastic in case of contact, i.e. the surface gets stiff and can not be damaged anymore. Also shear forces, a known problem from contact mode resulting in surface damage, are not occurring as the applied force is always vertical. Tapping mode is also the method of choice for measurements in fluids. In this case not only the cantilever is oscillating but also the entire fluid cell. But the principle remains the same: with contact to the surface the oscillation is reduced resulting in a spatially assigned signal. In conclusion AFM can be used for size measurements on the nano scale. Beside the examination of synthetic samples for material science also biological systems like cells or DNA can be measured and visualized.

3.4.5 Transmission electron microscopy[52] (TEM)

The resolution of every microscope is depending on the wavelength of the applied radiation. *Abbe* defined in the following equation the dependency between the maximum resolution and the wavelength of the applied radiation:

$$d = \frac{\lambda}{2 \cdot n \cdot \sin \alpha} \qquad \text{(Eq. 3.11)}$$

where d is the minimum distance between two separately observable objects, λ the wavelength of the applied radiation, n the refraction index of the medium and α the half aperture angle of the lens. In case of a light microscope the resolution is limited to the minimum wavelength of λ = 400 nm. With a maximum aperture angle of 70 ° and a refraction index for air of about 1 objects smaller than d = 213 nm can not be measured anymore. So the idea is to decrease the wavelength λ in order to increase the resolution. The use of elementary particles (electrons) as radiation source is the best way to decrease the wavelength by several orders of magnitude. *De Broglie* postulated the wave-particle dualism describing the dependency between the impulse p of a particle and its wavelength λ:

$$\lambda = \frac{h}{p} \qquad \text{(Eq. 3.12)}$$

where h is *Planck*'s constant. The impulse p_e of an electron which undergoes the acceleration voltage U_a can be described by the following equation:

$$p_e = \sqrt{2 \cdot m_0 \cdot e \cdot U_a \cdot \left(1 + \frac{e \cdot U_a}{2 \cdot m_0 \cdot c^2}\right)} \qquad \text{(Eq. 3.13)}$$

where m_0 is the rest mass of an electron, e the elementary charge and c the light speed in vacuum. Combining the equations 3.12 and 3.13 results in the following "rule of thumb":

$$\lambda[\text{nm}] = \sqrt{\frac{1.5}{U_a[\text{V}]}} \qquad \text{(Eq. 3.14)}$$

Now, in case of a standard transmission electron microscope with an acceleration voltage U_a of about 80,000 Volt the resulting wavelength λ is about $4.3 \cdot 10^{-3}$ nm. This wavelength leads to a theoretical resolution of 0.21 nm. But, unfortunately, due to several errors like spherical and chromatic aberrations the practical resolution is not limited by the wavelength of the electrons, but by the quality of the electromagnetic lenses and electrical equipment (Figure 3.28). Lenses with errors due to spherical aberrations provide an inhomogeneous electron beam where the outer electrons are more deflected than the interior ones. In other words the electrons can not be focused in one point anymore. This leads to blurred images of the samples. The second error

results from a moderate control of the electron source. If the acceleration voltage is not kept constant the emitted electrons have different wavelengths as described by equation 3.14. Since every lens has a different refractive index for every wavelength polychrome radiation can not be focused in one point. This leads also to rather blurred images.

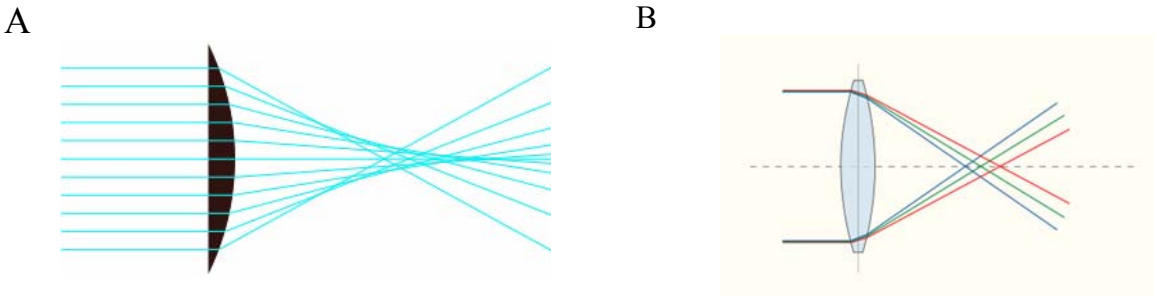

Fig. 3.28 *A) Spherical aberration due to different deflection of the electrons from the centre and the periphery of the lens; B) chromatic aberration through polychrome radiation (pictures taken from reference 53).*

The main principle of sample imaging by transmission electron microscopy is based on the scattering of the electrons by the atoms of the sample. There are two different types of scattering that can occur: A) inelastic scattering by weak interaction of the electron beam with the electron shell of the sample atoms and B) elastic scattering by strong interaction of the electron beam with the atomic nuclei. In the first case the scattering intensity is rather weak, but the electrons lose energy leading to a different wavelength compared to the initial electron wavelength. Due to this chromatic aberration the weakly deviated electrons are no longer in the focal plane of the initial electron beam. This leads to a black and white contrast differential, which images the sample on a large scale. In the second case the electrons are scattered far stronger but keep their energy and wavelength respectively. As a result of the large scattering angle these electrons can be absorbed by the aperture stop without abatement of the unscattered electron beam. Due to the loss of these electrons again a contrast differential is produced which displays the sample magnified. Both scattering types contribute to the sample imaging depending on the properties of the sample. One important point is the chemical composition of the sample. Biological samples consist of hydrogen, carbon, nitrogen and oxygen and thus have a rather poor contrast, i.e. they are electron transparent as all samples based on atoms with low atomic number. In contrast to this inorganic materials with heavy atoms lead to strong scattering of the electron beam. Therefore staining techniques have been developed in order to enhance the contrast of biological samples. An aqueous solution of uranyl acetate is a commonly used negative-staining reagent. The salt solution surrounds the biological sample at which upon drying a thin crystalline uranyl acetate film

forms. Due to the high scattering ability of the uranyl cation the electron beam only permeates the sample resulting in a strong contrast between the inorganic salt film and the organic sample. This technique produces images of inverted contrast (negative-staining) because the sample is not the active scattering compound but the uranyl acetate. In conclusion transmission electron microscopy can enhance the resolution to the sub-nano scale. High resolution TEM is nowadays able to differentiate between atoms with distances as short as some ten picometers (1 nm = 1000 pm). With this technique not only the dimension of the observed object can be determined but also the surface structure can be examined.

1 J. Steed, D. Turner, K. Wallace, *Core Concepts in Supramolecular Chemistry and Nanochemistry*, **2007**, Wiley & Sons, Chichester.

2 J. Berg, J. Tymoczko, L. Stryer, *Biochemistry. International Edition*, **2006**, Palgrave MacMillan, New York.

3 R. P. Sijbesma, F. H. Beijer, L. Brunsveld, B. J. B. Folmer, J. H. K. K. Hirschberg, R. F. M. Lange, J. K. L. Lowe, E. W. Meijer, *Science* **1997**, *278*, 1601-1604.

4 F. Beijer, H. Kooijman, A. Spek, R. Sijbesma, E. Meijer, *Angew. Chem. Int. Ed.* **1998**, *37*, 75-78.

5 a) W. Jørgensen, J. Pranata, *J. Am. Chem. Soc.* **1990**, *112*, 2008-2010; b) J. Pranata, S. Wierschke, W. Jørgensen, *J. Am. Chem. Soc.* **1991**, *113*, 2810-2819; c) W. Jørgensen, D. Severance, *J. Am. Chem. Soc.* **1991**, *113*, 209-216.

6 For some recent examples of multiple H-bonded assemblies see: a) S. Djurdjevic, D. Leigh, H. McNab, S. Parsons, G. Teobaldi, F. Zerbetto, *J. Am. Chem. Soc.* **2007**, *129*, 476-477; b) B. Gong, *Polym. Int.* **2007**, *56*, 436-434; S. Li, D. Xie, B. Gong, H. Guo, *Chem. Phys. Lett.* **2005**, *410*, 264-268; c) Y. Yang, Z.-Y. Yang, Y.-P. Yi, J.-F. Xiang, C.-F. Chen, L.-J. Wan, Z.-G. Shuai, *J. Org. Chem.* **2007**, *72*, 4936-4946; d) P. Baruah, R. Gonnade, U. Phalgune, G. Sanjayan, *J. Org. Chem.* **2005**, *70*, 6461-6467; e) P. Prabhakaran, V. Puranik, G. Sanjayan, *J. Org. Chem.* **2005**, *70*, 10067-10072.

7 E. Archer, M. Krische, *J. Am. Chem. Soc.* **2002**, *40*, 5074-5083.

8 a) D. Williams, M. Westwell, *Chem. Soc. Rev.* **1998**, *27*, 57-64; b) A. Davis, R. Wareham, *Angew. Chem.* **1999**, *38*, 2978-2996.

9 K. Fujita, M. Tominaga, A. Hori, B. Therrien, *Acc. Chem. Res.* **2005**, *38*, 371-380.

10 R. Dobrawa, M. Lysetska, P. Ballester, M. Grüne, F. Würthner, *Macromolecules* **2005**, *38*, 1315-1325.

11 a) A. Zych, B. Iverson, *J. Am. Chem. Soc.* **2000**, *122*, 8898-8909; b) G. Gabriel, B. Iverson, *J. Am. Chem. Soc.* **2002**, *124*, 15174-15175.

12 In contrast to Coulomb interactions between two point charges which are non-directional, charge interactions with organic molecules such as guanidinium cations are directional. This can be due to the formation of H-bond enforced ion pairs and/or the anisotropic solvation of such ions: P. Mason, G. Neilson, J. Enderby, M.-L. Saboungi, C. Dempsey, A. MacKerell, Jr., J. Brady, *J. Am. Chem. Soc.* **2004**, *126*, 11462-11470.

13 For comprehensive reviews of anion recognition by organic cations see the following: a) K. Schug, W. Lindler, *Chem. Rev.* **2005**, *105*, 67-114; b) R. Houk, S. Tobey, E. Anslyn, *Top. Curr. Chem.* **2005**, *255*, 199-229; c) P. Blondeau, M. Segura, R. Perez-Fernandez, J. de Mendoza, *Chem. Soc. Rev.* **2007**, *36*, 198-210; d) F. Schmidtchen, M. Berger, *Chem. Rev.* **1997**, *97*, 1609-1646.

14 Y. Tanaka, H. Katagiri, Y. Furusho, E. Yashima, *Angew. Chem. Int. Ed.* **2005**, *44*, 3867-3870.

15 C. Schmuck, *Coord. Chem. Rev.* **2006**, *205*, 3053-3067.

16 C. Schmuck, *Eur. J. Org. Chem.* **1999**, 2397-2403.

17 a) C. Schmuck, *Chem. Eur. J.* **2000**, *6*, 709-718; b) B. Storey, W. Sullivan, C. Moyer, *J. Org. Chem.* **1964**, *29*, 3118-3120.

18 a) Y. Zheng, R. Ornstein, *J. Am. Chem. Soc.* **1996**, *118*, 11237-11243; b) B. Dietrich, D. Fyles, T. Fyles, J.-M. Lehn, *Helv. Chim. Acta.* **1979**, *62*, 2763-2787.

19 a) S. Schlund, C. Schmuck, B. Engels *Chem. Eur. J.* **2007,** *13*, 6644-6653; b) C. Schmuck, Th. Rehm, L. Geiger, M. Schäfer, *J. Org. Chem.* **2007**, *72*, 6162-6170,

20 F. Bordwell, G. Drucker, H. Fried, *J. Org. Chem.* **1981**, *46*, 632-635.

21 C. Schmuck, W. Wienand, *J. Am. Chem. Soc.* **2003**, *125*, 452-459.

22 S. Schlund, C. Schmuck, B. Engels, *J. Am. Chem. Soc.* **2005**, 127, 11115-11124.

23 a) C. Schmuck, U. Machon, *Chem. Eur. J.* **2005**, *11*, 1109-1118; b) C. Schmuck, U. Machon, *Eur. J. Org. Chem.* **2006**, 4385-4392.

24 C. Rether, Diploma thesis, University of Würzburg, **2006**.

25 Th. Devlin (Editor), *Textbook of Biochemistry with clinical correlations Fifth Edition*, **2002**, Wiley-Liss, New York.

26 Article: *Lipid Bilayers*. In: *Wikipedia, the free enzyclopedia*, 05.02.2008, URL: http://en.wikipedia.org/wiki/Image:Phospholipids_aqueous_solution_structures.svg.

27 a) B. Discher, D. Hammer, F. Bates, D. Discher, *Curr. Opin. Colloid Interface Sci.* **2000**, *5*, 125-131; b) S. Burk, H. Shen, A. Eisenberg, *Macromol. Symp.* **2001**, *175*, 273-284; c) D. Discher, A. Eisenberg, *Science*, **2002**, *297*, 967-973; d) M. Antonietti, S. Förster, *Adv. Mater.* **2003**, *15*, 1323-1333; e) P. Soo, A. Eisenberg, *J. Polym. Sci., Part B: Polym. Phys.* **2004**, *42*, 923-938.

28 a) S. Jenekhe, X. Chen, *Science*, **1999**, 372-375; b) X. Chen, S. Jenekhe, *Macromolecules*, **2000**, *33*, 4610-4612.

29 a) C. Hawker, J. Frechet, *J. Am. Chem. Soc.* **1992**, *114*, 8405-8413; b) K. Aoi, K. Itoh, M. Okada, *Macromolecules*, **1997**, *30*, 8072-8074; c) J.-F. Nierengarten, J.-F. Eckert, Y. Rio, M. del Pilar Carreon, J.-L. Gallani, D. Guillon, *J. Am. Chem. Soc.* **2001**, *123*, 9743-9748.

30 J.-F. Gohy, N. Willet, S. Varshney, J.-X. Zhang, R. Jérôme, *Angew. Chem. Int. Ed.* **2001**, *40*, 3214-3216.

31 E. Holowka, D. Pochan, T. Deming, *J. Am. Chem. Soc.* **2005**, *127*, 12423-12428.

32 M. Yang, W. Wang, F. Yuan, X. Zhang, J. Li, F. Liang, B. He, B. Minch, G. Wegner, *J. Am. Chem. Soc.* **2005**, *127*, 15107-15111.

33 a) M. Lee, S.-J. Lee, L.-H. Jiang, *J. Am. Chem. Soc.* **2004**, *126*, 12724-12725; b) Y. Tanaka, M. Miyachi, Y. Kobuke, *Angew. Chem. Int. Ed.* **1999**, *38*, 504-506.

34 a) B. Ravoo, R. Darcy, *Angew. Chem. Int. Ed.* **2000**, *39*, 4324-4326; b) B. Jing, X. Chen, X. Wang, C. Yang, Y. Xie, H. Qiu, *Chem. Eur. J.* **2007**, *13*, 9137-9142.

35 a) P. Ghosh, T. Khan, P. Bharadwaj, *Chem. Commun.* **1996**, 189-190; b) P. Bandyopadhyay and P. Bharadwaj, *Langmuir*, **1998**, *14,* 7537-7538.

36 a) H.-K. Lee, K. Park, Y. Jeon, D. Kim, D. Oh, H. Kim, C. Park, K. Kim, *J. Am. Chem Soc.* **2005**, *127*, 5006-5007; b) Y. Jeon, P. Bharadwaj, S. Choi, J. Lee, K. Kim, *Angew. Chem. Int. Ed.* **2002**, *41*, 4474-4476.

37 S. Seo, J. Chang, G. Tew, *Angew. Chem. Int. Ed.* **2006**, *45*, 7526-7530.

38 a) L. Jiang, R. Hughes, D. Sasaki, *Chem. Commun.* **2004**, 1028-1029; b) I. Shklyarevskiy, P. Jonkheijm, P. Christianen, A. Schenning, E. Meijer, O. Henze, A. Kilbinger, W. Feast, A. Del Guerzo, J.-P. Desvergne, J. Maan, *J. Am. Chem. Soc.* **2005**, *127*, 1112-1113; c) F. Hoeben, I. Shklyarevskiy, M. Pouderoijen, H. Engelkamp, A. Schenning, P. Christianen, J. Maan, E. Meijer, *Angew. Chem. Int. Ed.* **2006**, *45*, 1232-1236.

39 K. Matsuura, K. Murasato, N. Kimizuka, *J. Am. Chem. Soc.* **2005**, *127*, 10148-10149.

40 S. Ghosh, M. Reches, E. Gazit, S. Verma, *Angew. Chem. Int. Ed.* **2007**, *46*, 2002-2004.

41 D. Xie, M. Jiang, G. Zhang, D. Chen, *Chem. Eur. J.* **2007**, *13*, 3346-3353.

42 X. Zhang, Z. Chen, F. Würthner, *J. Am. Chem. Soc.* **2007**, *129*, 4886-4887.

43 C. Görbitz, *Chem. Eur. J.* **2001**, *7*, 5153-5159.

44 a) M. Reches, E. Gazit, *Science* **2003**, *300*, 625-627; b) M. Reches, E. Gazit, *Nano Lett.* **2004**, *4*, 581-585; c) L. Adler-Abramovich, M. Reches, V. Sedman, S. Allen, S. Tendler, E. Gazit, *Langmuir* **2006**, *22*, 1313-1320.

45 Y. Song, S. Challa, C. Medforth, Y. Qiu, R. Watt, D. Pena, J. Miller, F. van Swol, J. Shelnutt, *Chem. Commun.* **2004**, 1044-1045.

46 X. Yan, Q. He, K. Wang, L. Duan, Y. Cui, J. Li, *Angew. Chem. Int. Ed.* **2007**, *46*, 2431-2434.

47 a) G. Morris*, Encyclopedia of Nucl. Magn. Reson.* **2002**, *9*, 35-44; b) E. Cabrita, S. Berger, *Magn. Reson. Chem.* **2001**, *39*, S142-S148; c) C. Johnson Jr., *Progr. Nuc. Magn. Reson. Spect.* **1999**, *34,* 203-256; d) Y. Cohen, L. Avram, L. Frish, *Angew. Chem. Int. Ed.* **2005**, *44*, 520-554; e) L. Allouche, A. Marquis, J.-M. Lehn, *Chem. Eur. J.* **2006**, *12*, 7520-7525.

48 a) A. Fröba, A. Leipertz, *Diffusion Fundamentals 2*, **2005**, 63.1-63.25; b) N. Santos, M. Castanho, *Biophysical Journal*, **1996**, *71*, 1641-1646; c) M. Lechner, K. Gehrke, E. Nordmeier, *Makromolekulare Chemie*, **2003**, Birkhäuser Verlag; d) Malvern Instruments Ltd. *Dynamic Light Scattering: An Introduction in 30 Minutes*, http://www.malvern.co.uk/common/downloads/campaign/MRK656-01.pdf, (13.11.2007).

49 S. King, *Small-angle Neutron Scattering* in: *Modern Techniques for Polymer Characterisation* (Eds.: R. Pethrick, J. Davidson), **2003**, Wiley & Sons, Chichester.

50 a) G. Binnig, H. Rohrer, *Rev. Mod. Phys.* **1999**, *71*, S324-S330; b) F. Giessibl, *Materials Today* **2005**, 32-41; c) P. Samori, *Chem. Soc. Rev.* **2005**, *34*, 551-561; d) H.-Q. Li, D. Thomas, *Atomic Force Microscopy* (http://www.chembio.uoguelph.ca/educmat/chm729/afm/firstpag.htm), (13.11.2007).

51 Article: *Atomic Force Microscopy*. In: *Wikipedia, the free enzyclopedia*, 13.11.2007, URL: http://en.wikipedia.org/wiki/Image:Atomic_force_microscope_block_diagram.png.
a) S. Flegler, J. Heckmann Jr., K. Klomparens, *Elektronenmikroskopie,* **1995**, Spektrum Akademischer Verlag GmbH; b) Professur für Physikalische Messtechnik, TU Dresden, http://tu-dresden.de/die_tu_dresden/fakultaeten/Fakultaet_mathematik_und_naturwissenschaften/fachrichtung_physik/isp/tbg/lehre/TEM.pdf, (13.11.2007).

53 a) Article: *Spherical aberration*. In: *Wikipedia, the free enzyclopedia*, 13.11.2007, URL: http://en.wikipedia.org/wiki/Image:Spherical_aberration_2.svg; b) Article: *Chromatic aberration*. In: *Wikipedia, the free enzyclopedia*, 13.11.2007, URL: http://en.wikipedia.org/wiki/Image:Lens6a.svg.

4 Results and discussion

4.1 Supramolecular architectures based on the self-assembly of bis- or triple-zwitterions

In this section the main focus will be on the self-assembly of zwitterions, which are all connected covalently by different spacers. Four examples will be presented, which differ in length, shape and chemical structure of the spacer. Every example shows special and well-defined characteristics with respect to the incorporated linker. With the efficient control of the self-assembly mode by the variation of the spacer, programmable monomers are at hand.

4.1.1 Discrete nanometre-sized cyclic dimers via the self-assembly of a bis-zwitterion with a flexible hydrophilic spacer[1]

The basic idea of this project was to synthesize a monomer for supramolecular polymers which can gel polar organic solvents or even water. With this intention 1,13-diamino-4,7,10-trioxatridecane was used in **2.2** as a long and hydrophilic spacer in order to connect two zwitterions (Figure 4.1).

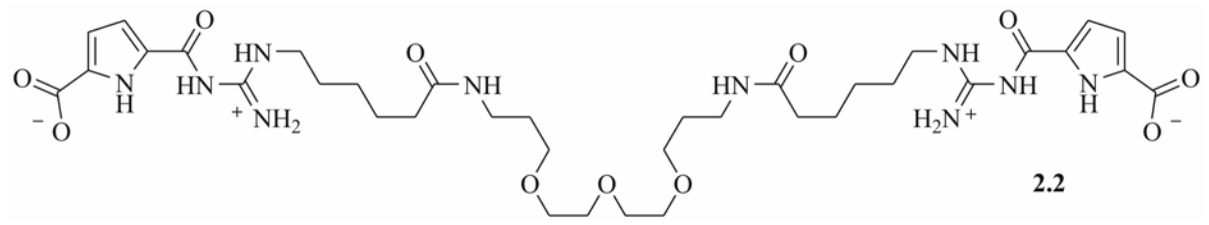

Fig. 4.1 *Bis-zwitterion **2.2** with a long and hydrophilic spacer.*

Since the general synthesis (*Triflate route*) of this compound class has been developed earlier in former work[2] only a short overview will be given here (Figure 4.2). First, via activation of the guanidino group by triflic anhydride[3], 6-amino caproic acid methyl ester **4.1** was attached to the pyrrole benzyl ester **4.2**. After hydrolysis of the methyl ester group in **4.3** the resulting free acid **4.4** was reacted with the spacer **4.5** using PyBOP as coupling reagent. Deprotection of **4.6** first with hydrogen and Pd on charcoal and then with trifluoroacetic acid provided, after pH adjustment to a value of 6, the flexible bis-zwitterion **2.2**. Since the deprotection with TFA and the pH adjustment with sodium hydroxide solution resulted in the corresponding salt as a byproduct ($Na^+CF_3COO^-$) a further washing step of the crude product had to be carried out. Otherwise both cation and anion of this salt could interfere with an efficient dimerization of the guanidiniocar-

bonylpyrrole zwitterions. Therefore refluxing the crude bis-zwitterion in a water/dioxane mixture (1:1) gave the salt-free product.

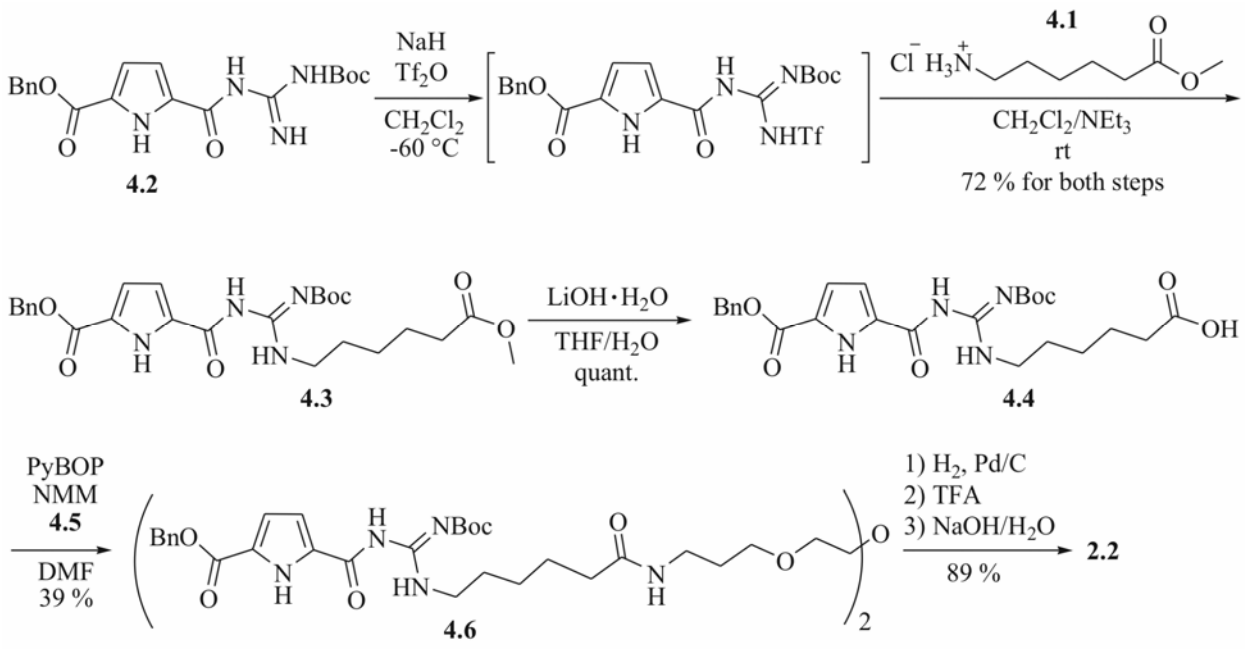

Fig. 4.2 *Synthesis of the bis-zwitterion **2.2** via the Triflate route.*

First investigations of the self-assembling properties of **2.2** were done by NMR studies.[4] As it is already well known for the binding motive used that the ^{1}H-NMR spectrum shows very characteristic signals for all NH protons which are involved in the dimerization of the zwitterions. In case of **2.2** as a new derivative of the primal zwitterion the dimerization had to be confirmed again in order to exclude any negative influence of the spacer on the dimerization.

Figure 4.3A represents the ^{1}H-NMR spectrum of the self-assembled primal zwitterion and the corresponding signals for all NH protons.[5] Comparing the ^{1}H-NMR spectrum of **2.2** (1 mM in DMSO-d_6) in Figure 4.3B with the signals of the primal zwitterion demonstrates two important results: 1) full dimerization of the alkylated binding motive at low concentrations; 2) splitting of the guanidinio NH protons into three instead of two signals since the protons are no longer equal. The assignment of the proton *e* was possible by comparison with the ^{1}H-NMR spectrum of the fully protected precursor of **2.2**. With a small shift of just $\Delta\delta$ = 0.02 ppm it is quite certain that in both compounds this proton *e* undergoes intramolecular hydrogen bonding to the amide oxygen and does not participate in the dimerization.

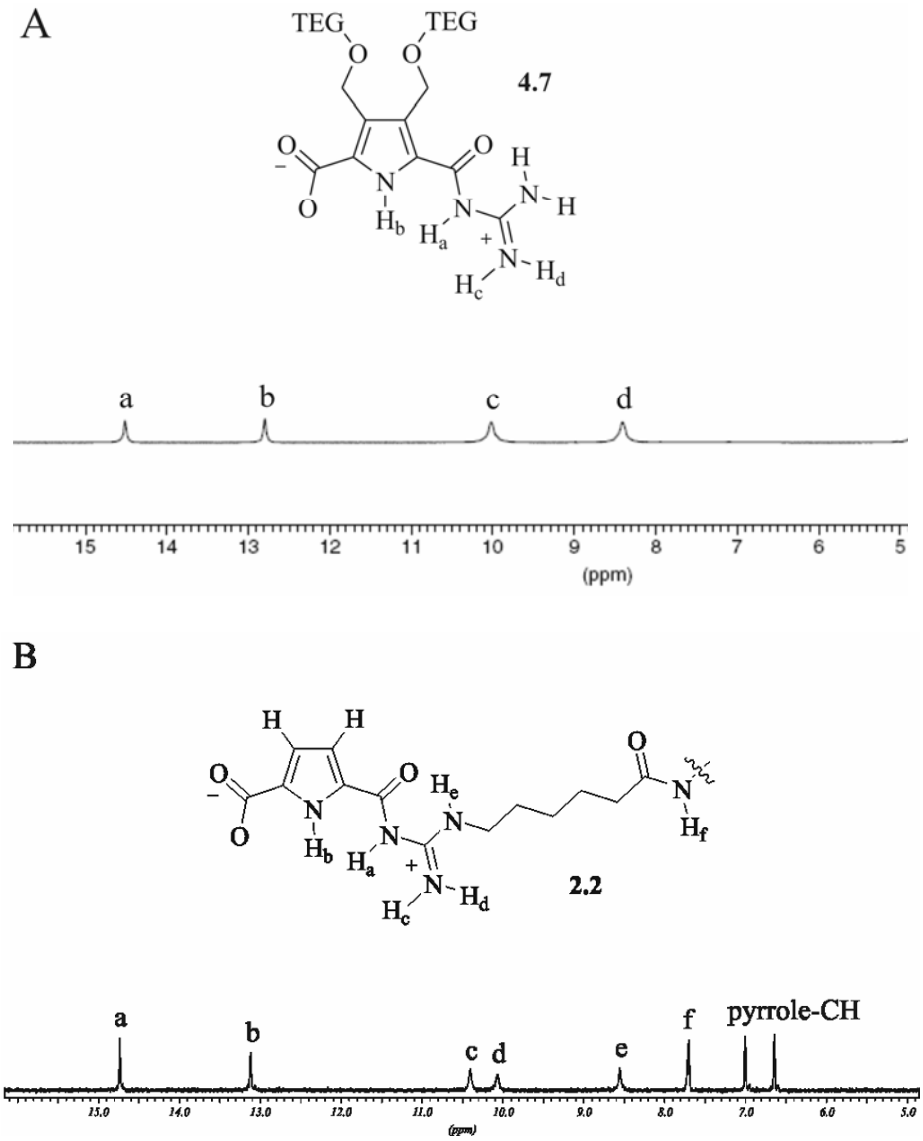

Fig. 4.3 *A) Part of the ^{1}H-NMR spectrum of dimeric **4.7** in DMSO-d_6 (picture taken and modified from reference 5); B) part of the ^{1}H-NMR spectrum of **2.2** (1 mM in DMSO-d_6).*

After verification of full dimerization NMR dilution studies were performed in a concentration range from 0.5 to 50 mM in DMSO-d_6.[6] The NMR data revealed a concentration-dependent equilibrium of two different species in solution as seen by two signal sets (Figure 4.4). Starting with a concentration 0.5 mM only one signal set is present. A closer look at the signals of the pyrrole-CH protons (δ = 6.64 and 7.00) and the amide-NH proton of the linker (δ = 7.70) shows clearly the fine structure of the signals (muliplets for the pyrrole-CH protons and a triplet for the amide-NH proton). With increasing concentration a second signal set appears which can be perfectly followed by the increasing signals of both pyrrole-CH protons (δ = 6.60 and 6.67), the pyrrole-NH proton (δ = 13.06) and the guanidinio amide NH proton (δ = 14.70). Furthermore the

second signal set is much broader compared to the first set (Figure 4.5A). This indicates an equilibrium between a monomer and a dimer or any higher oligomer.

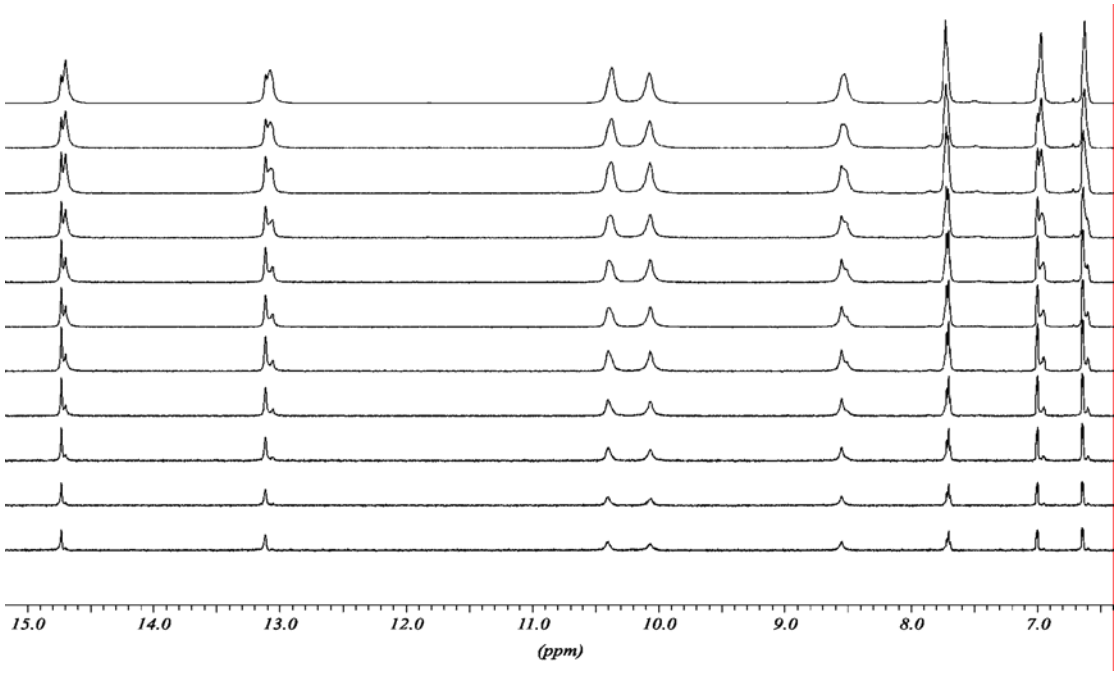

Fig. 4.4 *Part of the ^{1}H-NMR spectra of **2.2** (from bottom to top: c = 0.5, 1, 2.5, 5, 7.5, 10, 15, 20, 30, 40, 50 mM in DMSO-d_6).*

By integration of the signal intensity of the guanidinio amide-NH proton for both signal sets the transition of one species into the other can be displayed. At high dilution (c < 1 mM) **2.2** exists most likely as monomer (> 90 %), whereas with increasing concentration a transition takes place and the dimer population increases. Figure 4.5B displays this correlation. At a concentration of about 15 mM both species, monomer and dimer, exist in equal amounts. In order to get more information about the dimension of both species in solution DOSY NMR experiments were performed in DMSO-d_6. Beside the measurement of **2.2** in low (c = 1 mM) and high (c = 30 mM) concentration the fully protected precursor of **2.2** has also been analysed (c = 4 mM). This gave information about the dimension of an equally sized monomer of **2.2**, which is not able to self-assemble. The hydrodynamic radius of **2.2** in the diluted sample was r_H = 0.73 nm, which is in good agreement with the radius of the precursor molecule of r_H = 1.03 nm. In contrast to this the hydrodynamic radius of dimeric **2.2** in the high concentrated sample was twice as large having a value of r_H = 2.0 nm.

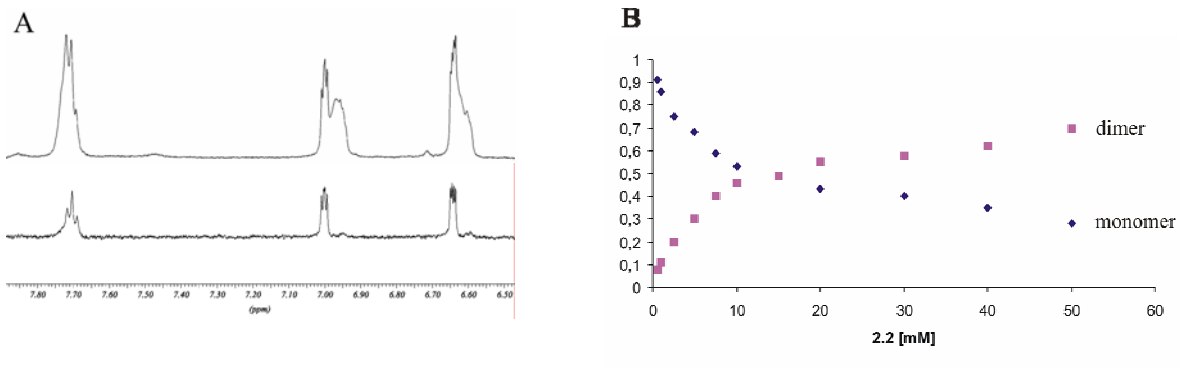

Fig. 4.5 *A) Comparing the ^{1}H-NMR spectra of **2.2** at two different concentrations: 0.5 mM (bottom) and 20 mM (top) in DMSO-d_6; B) concentration dependent transition of self-assembling species of **2.2** in solution.*

Beside the measurement in solution also mass spectrometry studies agreed with the coexistence of both monomer and dimer as verified by FAB MS experiments (Figure 4.6). Although the monomeric species was the predominant one in this case, dimeric **2.2** was also detected, but no larger aggregates.

Up to now all experiments point to a concentration dependent equilibrium of a monomeric and a dimeric species of **2.2** in solution. Due to the length and flexibility of the triethylene glycol chain bis-zwitterion **2.2** is able to fold into a loop which allows full dimerization of the zwitterionic binding motives. This mode of self-assembly, intramolecular folding, is limited to diluted solutions. With increasing concentration the population of dimeric **2.2** increases, leading to small spherical particles again with full association of the binding motives. Although DOSY NMR and FAB MS studies are useful for the study of monomers, dimers and small oligomers, they are not suitable for the analysis of large aggregates which self-assemble from an unknown number of monomers. For DOSY NMR line broadening prevents the formation of clear signals and their assignment. In case of FAB MS it could be already shown that dimeric **2.2** exists only in a small fraction compared to the dominant monomer. Higher aggregates would be most certainly outside the detection limit. Because of this lack of information further experiments had to be accomplished.

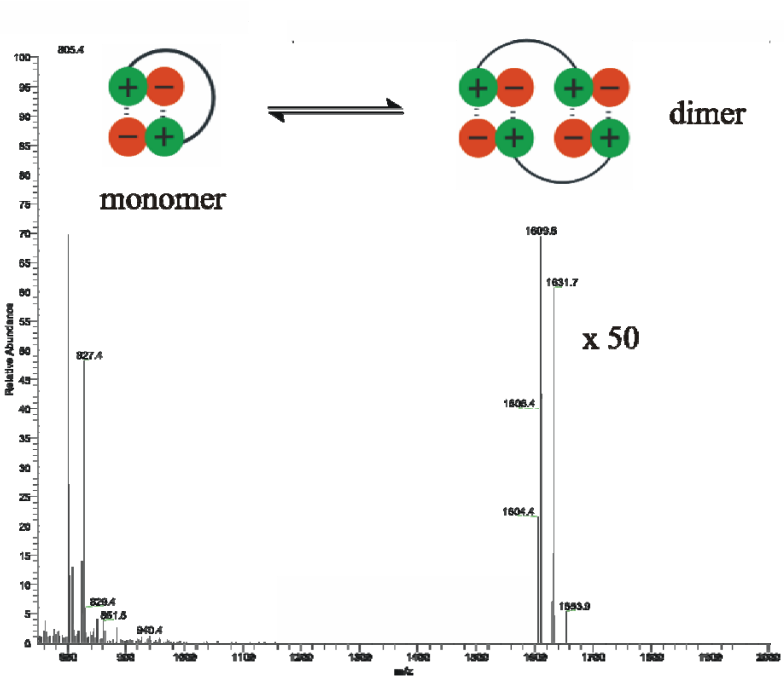

Fig. 4.6 *In FAB MS experiments both monomer and dimer could be detected in the protonated state or as sodium adduct (concentration of **2.2**: ~ 10 mM; matrix: 3-nitro-benzylalcohol); reprinted in part with permission from J. Am. Chem. Soc. **2006**, 128, 1430-1431. Copyright (2006) American Chemical Society; reprinted in part with permission from J. Am. Chem. Soc. **2006**, 128, 1430-1431. Copyright (2006) American Chemical Society.*

Since the detection of higher aggregates could not be ruled out so far, dynamic light scattering studies were performed in cooperation with Dr. F. Gröhn (Max Planck Institute for Polymer Research, Mainz). As the formation of higher aggregates might be as well concentration dependent the highest possible concentration of 50 mM of **2.2** in DMSO was used in order to investigate the formation of oligomers or polymers. But against all expectations DLS only shows a single diffusion mode corresponding to particles with a hydrodynamic radius of $r_H \approx 3.00$ nm.[7] This is in reasonably good agreement with the results of the DOSY NMR experiments. Unfortunately, DLS is not able to discriminate between monomer and dimer due to low resolution and too small size difference between the species. Here the size distribution method averages all hydrodynamic radii to one value. But nevertheless DLS can definitely exclude the formation of larger aggregates (Figure 4.7A). Additionally small angle neutron scattering experiments were performed.[8] Again, a highly concentrated solution of **2.2** with c = 45 mM in DMSO was used to determine the dimension of the particles as well as their shape. Figure 4.7B shows the *Guinier* plot resulting from the scattering curve of the SANS experiment. Its linearity is consistent with a spherical particle shape. Extracting the radius of gyration from the *Guinier* plot shows that **2.2** forms particles with a radius of r_G = 2.9 (± 0.2) nm in solution. This is again in good agreement with the

experimental data from DOSY NMR and DLS studies, although a closer analysis of the SANS data also showed a very small amount of particles with a maximum diameter of 11 nm. Beside the dimension also the interior structure of the spherical particles was determined. The ratio of the average radius of gyration (from SANS) and the hydrodynamic radius (from DLS) is $r_G/r_H \approx$ 1.0. This value points most likely to a "hollow sphere" type structure.

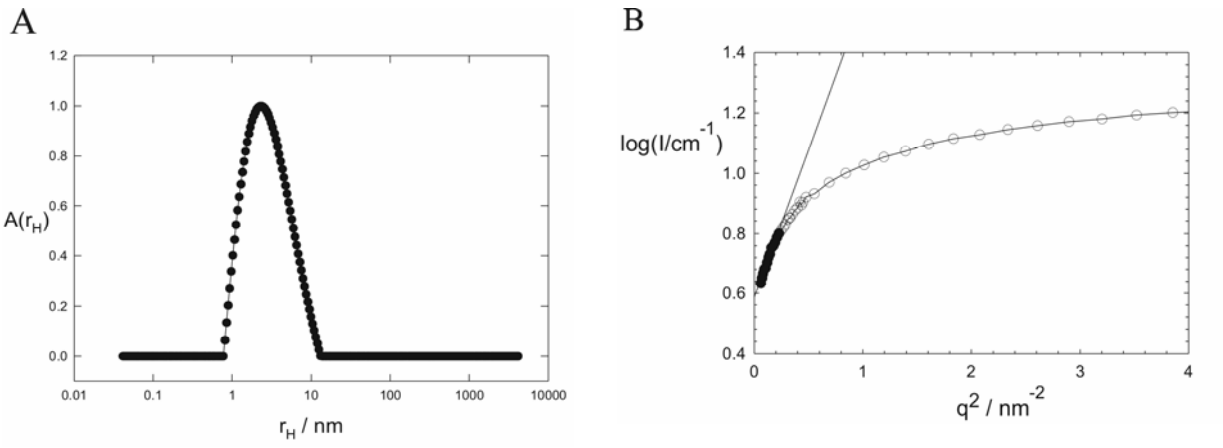

Fig. 4.7 *A) Intensity weighted distribution of hydrodynamic radii resulting from CONTIN analysis of the DLS data measured at a scattering angle of 90 ° (c = 50 mM in DMSO); B) Guinier plot resulting from the SANS experiments (c = 45 mM in DMSO); reprinted with permission from J. Am. Chem. Soc.* ***2006****, 128, 1430-1431. Copyright (2006) American Chemical Society.*

Molecular dynamic calculations are in good accordance with this suggestion (MacroModel 8.0, Amber* force field, GB/SA water solvation model, 100,000 steps). The interior of dimeric **2.2** consists of the flexible polyether chains and a significant number of solvent molecules (Figure 4.8). The hydrophilicity of the spacer is most likely the reason why **2.2** does not form any larger aggregates. The molecular design of the bis-zwitterion in total is rather polar which leads to a good interaction with the solvent. Therefore, no driving force is present which aspires bypassing any energetically disfavouring interactions between hydrophobic or unpolar moieties of the monomer with polar solvent molecules.

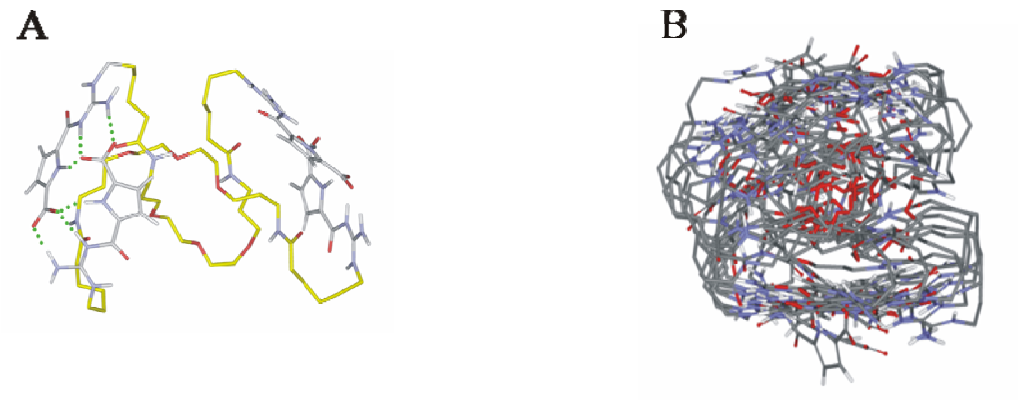

Fig. 4.8 *A) Calculated structure of dimeric **2.2**. The linker is shown in yellow, the interacting zwitterions in grey. At the left side the H-bonding pattern is highlighted in green (non-polar hydrogens omitted for clarity); B) structural stability of dimeric **2.2** as obtained from a MD simulation (500 ps at 300 K; snapshot taken every 50 ps); reprinted with permission from J. Am. Chem. Soc. **2006**, 128, 1430-1431. Copyright (2006) American Chemical Society.*

In conclusion bis-zwitterion **2.2** forms two species in solution, with the mode of self-assembly depending on the concentration. In both states full association of the binding motive is given. NMR dilution studies and FAB MS experiments showed the presence of a monomer-dimer equilibrium which was confirmed by DOSY NMR. In order to test if oligomer or polymer formation takes place, DLS and SANS experiments were performed. Interestingly both methods verified the already anticipated size of both species and ruled out the formation of any higher aggregates with comparable intensity. The SANS experiments also suggest a spherical and hollow structure of dimeric **2.2** which was fortified by molecular mechanics calculations. Hence, the fully flexible bis-zwitterion **2.2** is the first example for a homodimerization solely based on H-bond enforced ion pair formation which leads to stable nanometer-sized discrete particles in polar DMSO solutions even without any structural bias within the molecule.

4.1.2 Large vesicular structures via the self-assembly of a bis-zwitterion with a short and hydrophobic spacer[9]

Bis-zwitterion **2.2** has a long and hydrophilic spacer. In order to investigate the influence of the spacer on the self-assembly behaviour a second bis-zwitterion **2.3** (Figure 4.9) with a short and hydrophobic linker, 1,2-diaminoethane (**4.8**), was made. The synthesis of **2.3** is in analogy to the first one except for the last coupling step with the new spacer **4.8** which yielded 43 % of the fully protected monomer **4.9**. After deprotection and washing of the crude product bis-zwitterion **2.3** was subjected at first to NMR dilution studies.

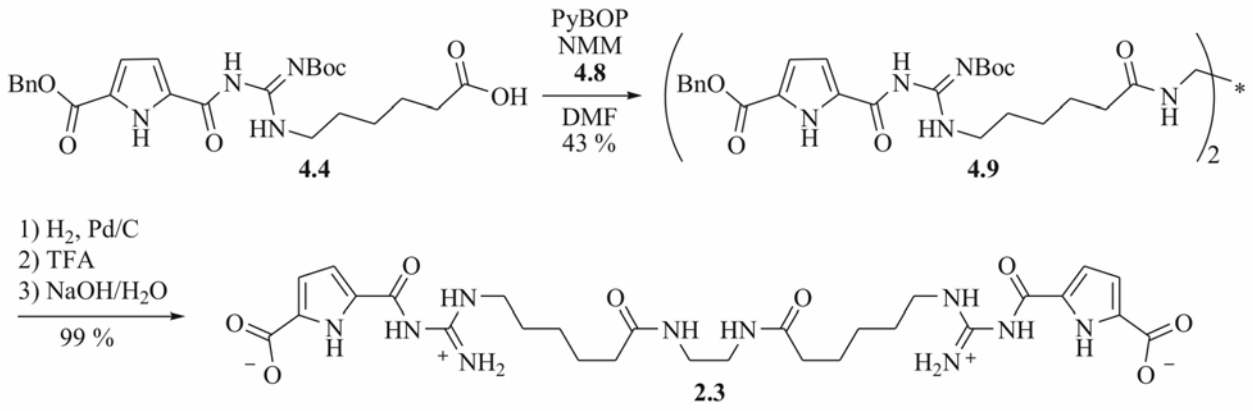

Fig. 4.9 *Synthesis of the second bis-zwitterion **2.3** starting with the free acid **4.4**.*

Figure 4.10 shows the stacked plot of ^{1}H-NMR spectra of **2.3** in DMSO-d_6 in a concentration range from 0.5 mM to 50 mM. In analogy to **2.2** bis-zwitterion **2.3** also forms two discrete species in solution, most likely monomers and dimers always with full association of the binding motives. Comparing the fractions of both species in relation to the concentration of the sample solution shows that in contrast to bis-zwitterion **2.2** both species of **2.3** exist equally at a concentration as low as 7.5 mM. This behaviour is certainly the consequence of the shorter linker. In the monomeric loop the binding motives are not able to dimerize intramolecularly in the perfect manner. The linker is not long enough to lead to a fully planar structure of the self-associated binding motives. This weakens the intramolecular association and serves also as driving force for the formation of dimeric **2.3** which allows intermolecular dimerization of the binding motives.

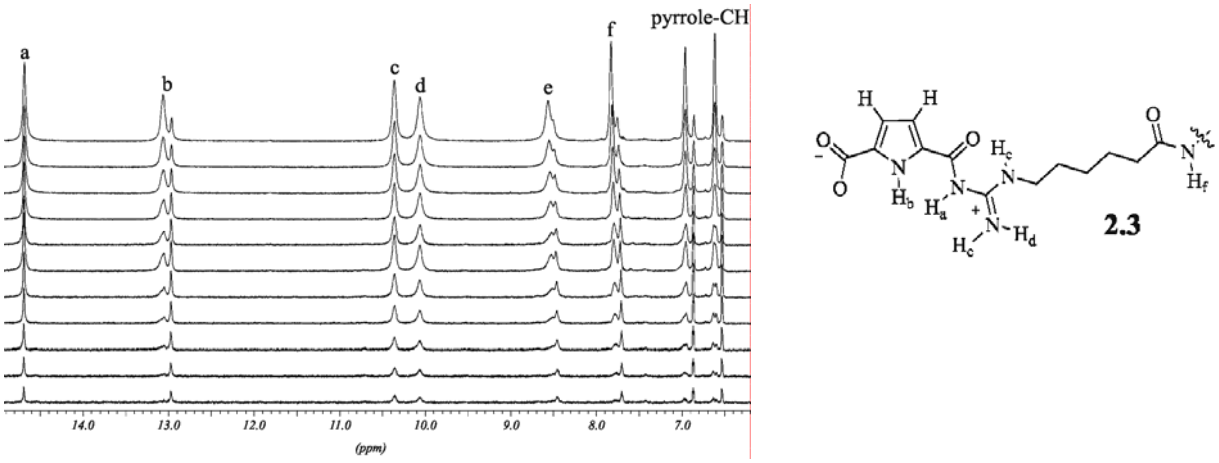

Fig. 4.10 *Part of the ^{1}H-NMR spectra of **2.3** (from bottom to top: 0.5, 1, 2.5, 5, 7.5, 10, 15, 20, 30, 40, 50 mM in DMSO-d_6); C. Schmuck, Th. Rehm. K. Klein, F. Gröhn: "Formation of Vesicular Structures through the Self-Assembly of a Flexible Bis-Zwitterion in Dimethyl Sulfoxide", Angew. Chem. Int. Ed. **2007**, 46, 1693-1697. Copyright Wiley-VCH Verlag GmbH & Co. KGaA. Reproduced with permission.*

To further confirm a concentration dependent monomer-dimer equilibrium in solution DOSY NMR studies were performed in DMSO-d_6. At low concentrations **2.3** has a hydrodynamic radius of r_H = 0.98 nm (c = 1 mM) which is in good agreement with the corresponding fully protected monomer **4.9** (0.78 nm, c = 1 mM). For the species present at higher concentrations (c = 30 mM) the hydrodynamic radius increased to a value of r_H = 1.42 nm. This increase is again in accordance with the formation of a dimeric particle of **2.3**. Unfortunately, all attempts to prove the dimer formation in the gas phase failed. But interestingly all higher concentrated samples showed a strong *Tyndall* effect at room temperature. This behaviour is in contrast to bis-zwitterion **2.2** and points also to the formation of larger aggregates rather than just monomers and dimers (Figure 4.11).

Fig. 4.11 *Solutions of bis-zwitterion **2.3** in DMSO show a strong Tyndall effect indicating the formation of large aggregates.*

First attempts to determine the dimension of the large aggregates were done by DLS measurements in cooperation with Dr. F. Gröhn (Max Planck Institute for Polymer Research, Mainz). In a concentration range from 0.2 to 2 mM solutions of **2.3** in DMSO were analysed. The resulting DLS data confirmed indeed the formation of separate particles with a mean diameter of 150 nm. Additionally, much larger structures with a size of about 5 µm were detected. In all likelihood these large aggregates are formed from the 150 nm sized particles in a dynamic equilibrium. Even after filtration of the large aggregates from the solution they reform upon standing within some hours. This is most likely also the reason for the colourless fluffy precipitate which appears after prolonged standing of the sample solution. Figure 4.12 shows the intensity-weighted distribution of all hydrodynamic radii extracted from the experimental DLS data of bis-zwitterion **2.3**. Since in light scattering experiments even very few large aggregates contribute strongly to the whole scattering intensity a more realistic view on the effective distribution can be given by the number distribution of the particles depending on their size ($I_{scattered\ light} \sim d^6$).[10] For this trans-

formation one has to assume that both aggregates consist of the same material and are homogeneous. This leads to a completely different result: in solution, only a small fraction of aggregates are 5 μm-sized (*ca*. 10^{-8}) and the majority of particles have a diameter of 150 nm.

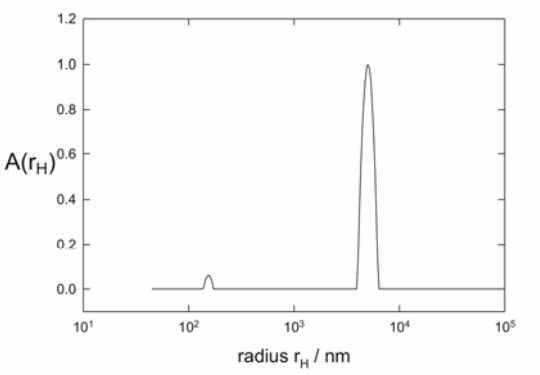

Fig. 4.12 *Intensity-weighted distribution of the hydrodynamic radii of **2.3** as obtained by dynamic light scattering in DMSO (c = 2 mM); C. Schmuck, Th. Rehm. K. Klein, F. Gröhn: "Formation of Vesicular Structures through the Self-Assembly of a Flexible Bis-Zwitterion in Dimethyl Sulfoxide", Angew. Chem. Int. Ed. **2007**, 46, 1693-1697. Copyright Wiley-VCH Verlag GmbH & Co. KGaA. Reproduced with permission.*

In order to take a snapshot of both aggregates from solution AFM experiments were performed in cooperation with V. Stepanenko and Prof. Dr. F. Würthner (Institute of Organic Chemistry, University of Würzburg). A 4 mM solution of **2.3** in DMSO was spin-coated (10,000 rpm) onto a freshly cleaved mica surface. The AFM phase image in Figure 4.13A shows discrete spherical particles with a mean diameter of 140 nm and a height of 6-7 nm. Due to the loss of solvent molecules AFM images show in general slightly smaller diameters than DLS.[11] As proposed these particles self-assemble into much larger aggregates with a size greater than 1 μm as depicted in the upper right region of Figure 4.13A. The dimension of the smaller aggregates in terms of diameter and height gives rise to the assumption that bis-zwitterion **2.3** forms vesicular structures in solution. During sample preparation (spin-coating) these hollow spheres interact with the surface and get distorted. The flattening process of the vesicle membrane leads to shoulders as seen in the section analysis (Figure 4.13B top). The inner part of the vesicle is still filled with some solvent and results in two different heights of the particle (schematically in Figure 4.13B bottom).

The possible formation of micellar structures can be certainly ruled out. Although micelles lead also to spherical structures in the AFM image, however, their diameter should be quite similar to their height. In case of bis-zwitterion **2.3** the diameter is nearly 20 times larger than the height. This clearly excludes the formation of micelles and is in excellent agreement with the DLS re-

sults. Up to now all experiments indicate that the self-assembly of bis-zwitterion **2.3** is based on two processes. On the smaller "molecular" level a concentration dependent equilibrium between monomers and dimers exists. On the higher supramolecular level bis-zwitterion **2.3** forms vesicles with a mean diameter of 150 nm in solution, which agglomerate further to larger structures with a size greater than 5 µm.

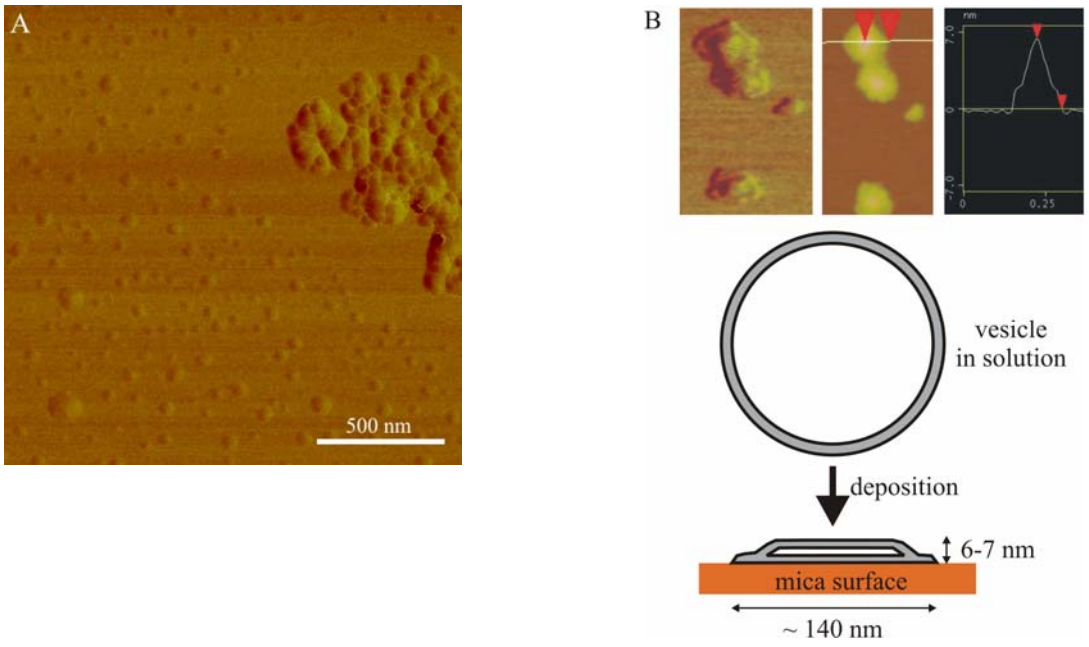

Fig. 4.13 *A) AFM phase image as overview of self-assembled **2.3** (spin-coated on mica; tapping mode); B) phase and height image of a representative vesicle and its schematic illustration based on the section plot (horizontal scale in µm; vertical scale in nm). The red markers indicate corresponding areas in the plot; C. Schmuck, Th. Rehm. K. Klein, F. Gröhn: "Formation of Vesicular Structures through the Self-Assembly of a Flexible Bis-Zwitterion in Dimethyl Sulfoxide", Angew. Chem. Int. Ed. **2007**, 46, 1693-1697. Copyright Wiley-VCH Verlag GmbH & Co. KGaA. Reproduced with permission.*

In order to investigate the interplay of both modes of self-assembly small angle neutron scattering studies were performed in cooperation with Dr. F. Gröhn (Max Planck Institute for Polymer Research, Mainz). Although several scattering experiments in a concentration range from 2 to 15 mM in DMSO were done (wavelength: 6 Å; wavelength spread 11 %) all detected aggregates were too large for a complete analysis. But this was expected from the data of DLS and AFM. Fortunately, the SANS experiments provided valuable information about the internal structure of the vesicles and their membranes, respectively. A thickness-*Guinier* plot was extracted from the SANS data showing a linear behaviour between log $I(q)q^2$ versus q^2 (I = scattering curve; q = scattering wave vector magnitude). This result confirms the presence of vesicle walls with a thickness radius of gyration of $r_{G,t}$ = 0.9 nm (Figure 4.14A). Assuming that the lamella has a

homogeneous scattering contrast in SANS, which is reasonable due to the chemical structure of the zwitterion, the $r_{G,t}$ translates into an average lamellae thickness of d = 3.1 nm. Further analysis of the nature of the vesicle wall was obtained by the calculation of the thickness density profile $p(x)$ of the lamellae through the thickness pair distance distribution function $P_t(r)$. This analysis confirms an average thickness of the lamellae of about 3.4 nm (Figure 4.14B).[12]

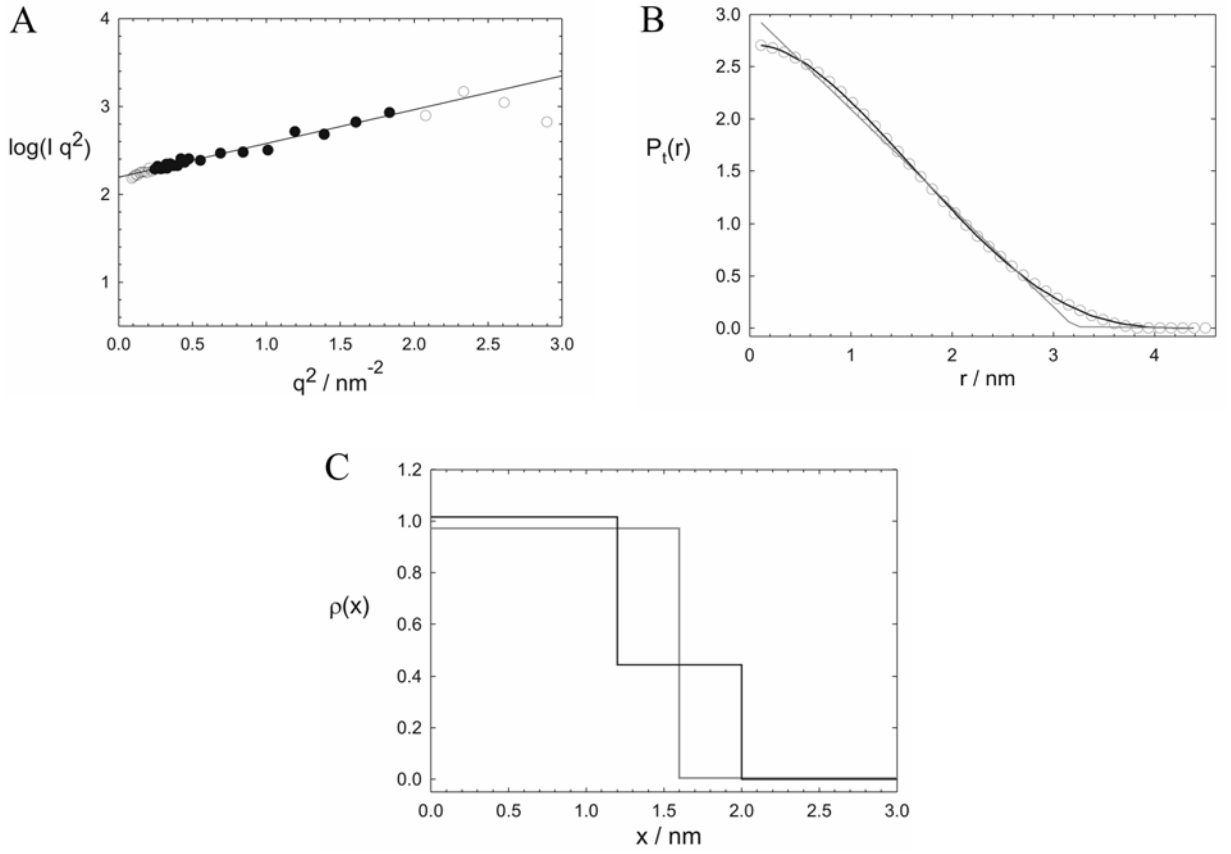

Fig. 4.14 *A) Thickness-Guinier plot for the data of a 4 mM solution in DMSO-d_6 as obtained from SANS measurements. Data points of the linear regime used for the Guinier fit are plotted as filled symbols; B) transversal pair distance distribution function resulting from the Fourier-Transformation of the experimental SANS data (circles). The grey line represents the fit of the data corresponding to a 1-step transversal density profile whereas the black line corresponds to a 2-step-transversal density profile; C) transversal density profile corresponding to the grey and the black curve in the top plot; C. Schmuck, Th. Rehm. K. Klein, F. Gröhn: "Formation of Vesicular Structures through the Self-Assembly of a Flexible Bis-Zwitterion in Dimethyl Sulfoxide", Angew. Chem. Int. Ed.* ***2007****, 46, 1693-1697. Copyright Wiley-VCH Verlag GmbH & Co. KGaA. Reproduced with permission.*

The $P_t(r)$ shown in Figure 4.14B has a $r_{G,t}$ = 0.9 nm, which is in very good agreement with the Thickness-*Guinier* plot from Figure 4.14A. Both analytical values are in accordance with the data from the DOSY NMR measurements as the dimer of **2.3** has a hydrodynamic radius of r_H = 1.42 nm and a diameter of about 2.8 nm, respectively. Assuming that the self-assembling process (from the dimers to the vesicles) leads to a small dilation of the molecules it is quite possible that

the vesicle membrane is formed by an unknown, but definitely high number of preorganized dimeric bis-zwitterions of **2.3** which string together as schematically depicted in Figure 4.15. The resulting membrane has never been detected by any analytical method, but it seems to be the most reasonable way to combine both modes of self-assembly. Interestingly the experimental data, displayed by the transversal pair distance distribution function in Figure 4.14B, can be best described by a two-step density profile. This leads to the assumption that the vesicle wall is not completely homogeneous, but is formed by two different membrane parts with two different thicknesses. The thinner part has a thickness of d = 2.4 nm, and the thicker part a value of d = 4 nm (Figure 4.14C: transversal radius of gyration of $r_{G,t}$ = 1.2 and 2 nm, respectively). The vesicle formation can be explained best by the postulation of an intermediate membrane with a thickness of 2.4 nm. However, a homogeneous wall would lead rather to a planar membrane (as considered in Figure 4.15) and not to a spherical structure. Therefore it is important to postulate a second structural element which deforms the initially planar membrane to a spherical vesicle. Most likely additional monomer form loops on the exterior and incorporate a certain degree of curvature. The formation of these trimers results in the thicker part of the membrane with a value of d = 4 nm (Figure 4.16).

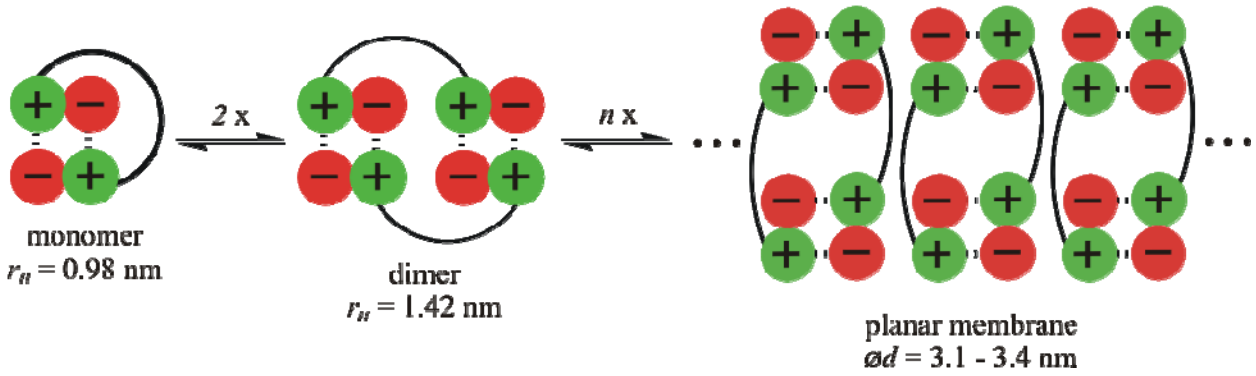

Fig. 4.15 *Initial mode of self-assembly of bis-zwitterion **2.3** with a possible intermediate planar membrane.*

Altogether this leads to the experimentally verified formation of the vesicles. Furthermore the outward pointing loops of the third monomer are most likely the reason why the vesicles agglomerate further on and precipitate in the end from the solution. The additional loops have hydrogen bond donors and acceptors at the amide groups of the linker. So it is possible that the vesicles interact through strong hydrogen bonding between whole vesicles.

The last point in this context is the question why bis-zwitterion **2.3** forms vesicles in contrast to the first bis-zwitterion **2.2** which "just" dimerizes. This can be most likely explained by compar-

ing the characteristics of the linkers. As already mentioned in Section 4.1.1 the ethylene glycol chain in **2.2** is hydrophilic and therefore nicely soluble in the polar solvent DMSO. In contrast the linker in **2.3** is short and hydrophobic which possibly is the driving force for the vesicle formation. In order to circumvent the energetically disfavouring interaction between the hydrophobic linker and the polar solvent the segregation of the polar and the unpolar parts of the bola-amphiphilic[13] bis-zwitterion **2.3** leads to the formation of the observed vesicles. This segregation opens the door for the formation of an unpolar region between the zwitterionic binding motives, which point to the interior and exterior vesicle membrane surfaces. Therefore the inner part of the membrane accommodates the alkyl chains of the linkers including their amide groups. Beside the *van der Waals* interactions between neighbouring alkyl chains the interactions between the amide groups might also be important due to the fact that they are able to form intermolecular hydrogen bonds. Since these hydrogen bonds are formed in an unpolar region without great exposure to the polar solvent they could be quite strong and enforce the vesicle membrane. The interplay of all interactions just mentioned is schematically depicted in Figure 4.17A.

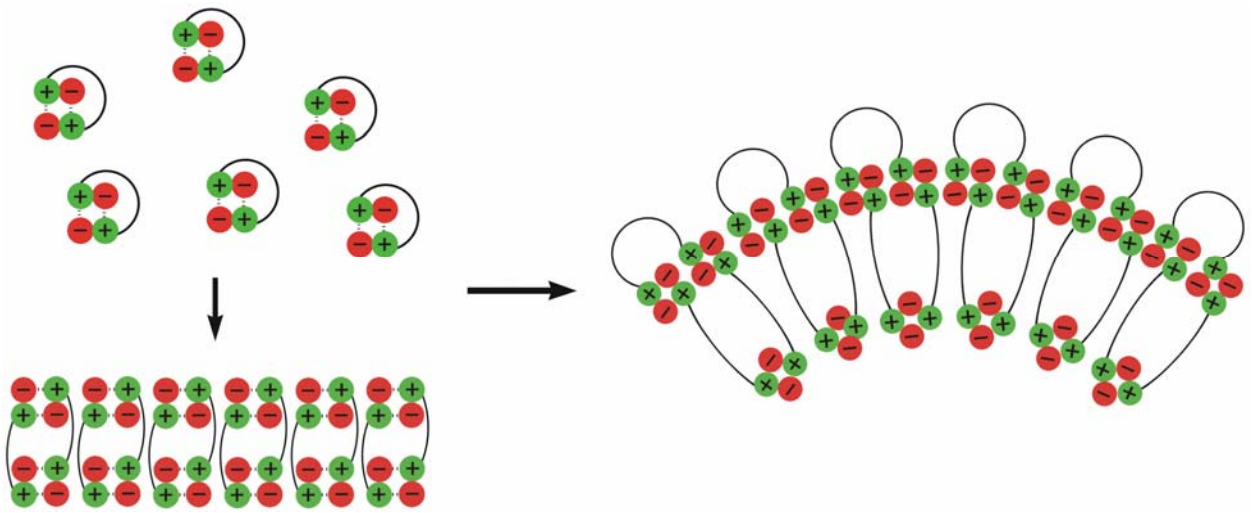

Fig. 4.16 *Second mode of self-assembly of bis-zwitterion **2.3** forces the proposed planar membrane into a spherical structure.*

This model of self-assembly was further confirmed by force-field calculations (Figure 4.17B; MacroModel 8.0, Amber* force field, GB/SA water solvation model, 50,000 steps). The arrangement proposed in Figure 4.16 exactly has the dimensions determined from the SANS measurements. Within the thinner monolayer of the vesicle membrane the bis-zwitterions **2.3** have a calculated length of approximately 2.5 nm, whereas the additional loop extends the thickness of the wall to about 3.9 nm according to the calculations. Beside this fact also the formation of the unpolar inner region with its hydrogen bond network was confirmed.

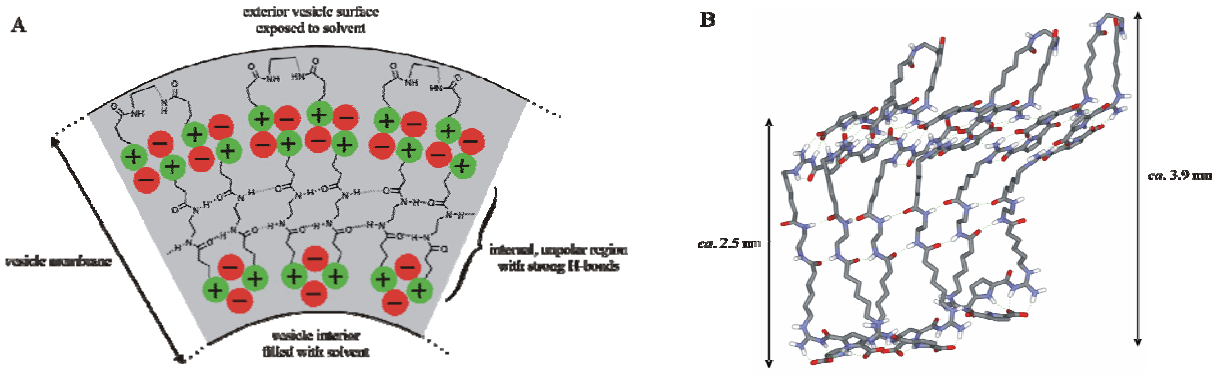

Fig. 4.17 *A) Schematic illustration of the vesicle membrane displaying the interplay of all non-covalent interactions for the vesicle formation; B) calculated structure of an assembly of nine bis-zwitterion monomers* ***2.3*** *confirming the postulated mode of self-assembly; C. Schmuck, Th. Rehm. K. Klein, F. Gröhn: "Formation of Vesicular Structures through the Self-Assembly of a Flexible Bis-Zwitterion in Dimethyl Sulfoxide", Angew. Chem. Int. Ed.* ***2007****, 46, 1693-1697. Copyright Wiley-VCH Verlag GmbH & Co. KGaA. Reproduced with permission.*

In conclusion flexible bis-zwitterion **2.3** can self-assemble in polar solutions to form large vesicular structures. The mode of self-assembly takes place in two steps. First on the "molecular" level a concentration dependent monomer-dimer equilibrium exists as seen in NMR dilution and DOSY NMR studies. Reaching the supramolecular level the preorganized cyclic dimers self-assemble into large vesicular structures. The main driving force in the polar solvent DMSO is of course the interaction of the zwitterionic binding motives. The specific mode for vesicle formation is determined by the interaction between the alkyl chains of the linker forming an unpolar region inside the vesicle membrane which is reinforced by a strong hydrogen bond network between the amide groups of the linker. Outward pointing loops of incorporated monomers, which provide the curvature of the spherical membrane, lead to the agglomeration of the vesicles due to "intersupramolecular" hydrogen bonding. Hence, bis-zwitterion **2.3** is an impressive example for the stepwise formation of large supramolecular architectures based on small molecular building blocks.

4.1.3 Concentration dependent transition from self-assembled vesicles to layer-like structures

The third example of self-assembling zwitterions introduces a new mode of aggregation, which is based on a modified linker. Bis-zwitterion **2.4**, in analogy to the former example, has a hydrophobic linker (Figure 4.18). The only difference is that this spacer extends over a length of ten CH_2 units, not only two as in bis-zwitterion **2.3**. The synthesis starts again with the free acid **4.4** and yields, after coupling with 1,10-diaminodecane (**4.10**), 32 % of the fully protected monomer

4.11. After deprotection the crude bis-zwitterion **2.4** was obtained in 90 % yield. Subsequent purification in terms of recrystallisation from water/dioxan resulted in the pure product, which was first subjected to NMR dilution studies.

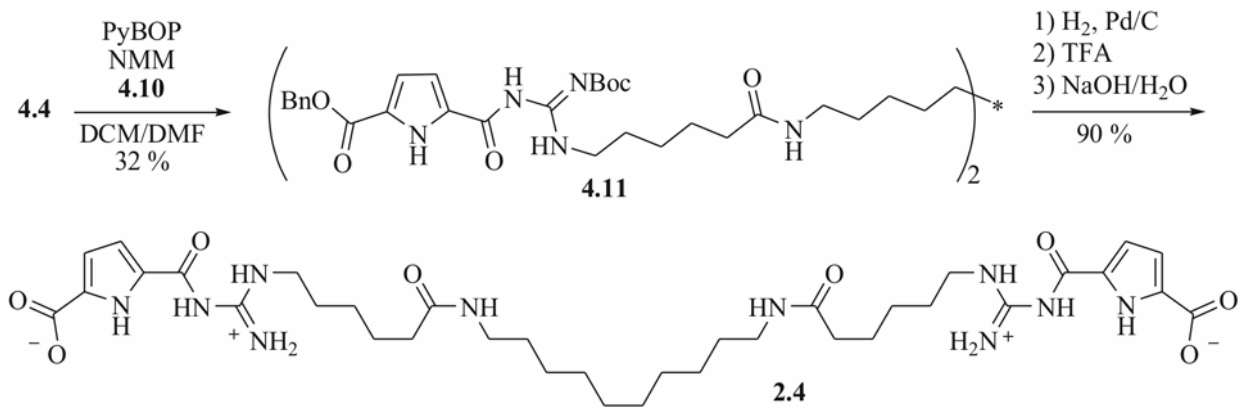

Fig. 4.18 *Synthesis of the third bis-zwitterion **2.4** starting with the free acid **4.4**.*

The self-assembly of bis-zwitterion **2.4** takes place in the same manner as already described for the vesicle forming bis-zwitterion **2.3** although there are some differences. However, these variations confirm the self-assembly mode of bis-zwitterions **2.3**. On the "molecular" level a concentration dependent equilibrium leads to the formation of monomer and dimer. In respect to the longer spacer in **2.4** the concentration, where equal shares of both monomer and dimer exist in solution, is c = 20 mM in DMSO-d_6 (Figure 4.19). This behaviour confirms the suggestion that the length of the spacer has a direct influence on the transition from monomer to dimer. The lower the strain is on the binding motives, the more stable the loop-like monomer is. DOSY NMR studies give the following dimensions: r_H = 0.81 nm for the monomer (c = 2.5 mM), r_H = 1.04 nm for the fully protected precursor **4.11** (c = 5 mM) and r_H = 1.33 nm for the dimer (c = 25 mM). This is again in good agreement with a monomer-dimer equilibrium. In cooperation with Dr. F. Gröhn (Max Planck Institute for Polymer Research, Mainz) DLS and SANS experiments were also performed which confirm the formation of spherical structures, although they are still under evaluation. But first results point to the formation of vesicles with a diameter of *ca*. 140 nm and a membrane thickness of up to d = 9 nm, but the membrane is not homogeneous at any part of the vesicle.

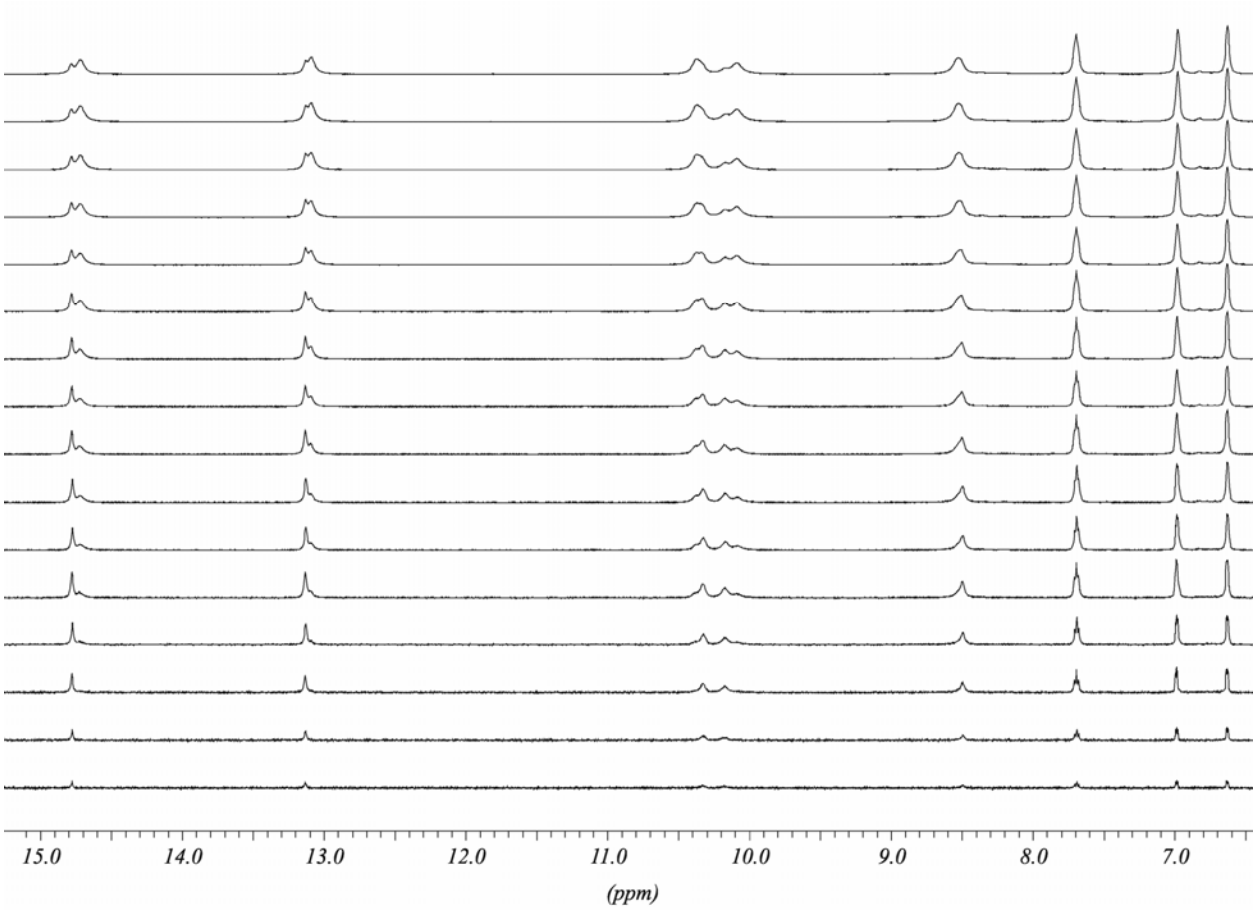

Fig. 4.19 *Part of the ^{1}H-NMR spectra of **2.4** (from bottom to top: 0.5, 1, 2.5, 5, 7.5, 10, 12.5, 15, 17.5, 20, 25, 30, 35, 40, 45, 50 mM in DMSO-d_6).*

Nevertheless without having the results from DLS and SANS the formation of vesicles by **2.4** was further investigated by AFM in cooperation with V. Stepanenko and Prof. Dr. F. Würthner (Institute of Organic Chemistry, University of Würzburg). A 2.5 mM solution of **2.4** in DMSO was spin-coated onto freshly cleaved mica (7000 rpm). In analogy to bis-zwitterion **2.3** spherical particles were found with a mean diameter of 55 nm and an average height of 2.7 nm (Figure 4.20). Interestingly **2.4** forms vesicles in solution which do not agglomerate into larger structures. This is in clear contrast to bis-zwitterion **2.3** but agrees with the stability of the sample solution of **2.4**. Even after days there is no evidence for precipitation of agglomerated **2.4**. As discussed above the agglomeration of the first vesicle forming bis-zwitterion **2.3** is most likely due to hydrogen bond networks between the vesicles. This was possible by the direct exposure of the amide groups of the linker. Now, in case of the extended linker length in **2.4** these hydrogen bond donors and acceptors might not point directly to the outside anymore. One possibility might be the formation of a second hydrogen bond network on the exterior of the vesicle membrane. However, in this model these hydrogen bonds might not be as stable as the hydrogen bonds in

the unpolar region of the membrane due to the closer contact to the solvent. But one thing is for sure: the pure interaction of the exposed alkyl chains is not strong enough to initiate the agglomeration of vesicles in solution (Figure 4.21).

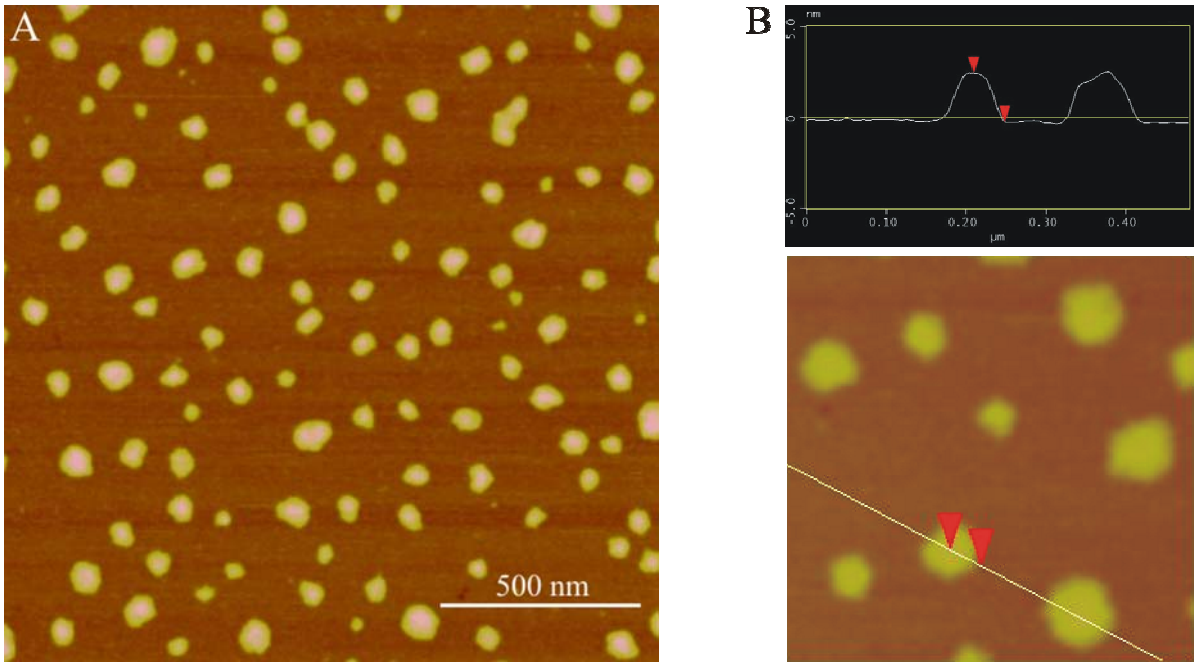

Fig. 4.20 *A) AFM height image of self-assembled **2.4** spin-coated on mica (c = 2.5 mM in DMSO); B) section analysis of a typical particle (horizontal scale in µm; vertical scale in nm). The red markers indicate corresponding areas in the plot.*

A closer look at the AFM images caused some confusion: the average height of all measured particles is about 2.7 nm. In comparison to the height of the vesicles based on bis-zwitterion **2.3** (6-7 nm) these new particles are thinner to a considerable degree. Additionally the shape extracted from the section analysis of **2.4** did not show any formation of shoulders (Figure 4.20 *vs.* Figure 4.13) which were a characteristic of the distorted vesicles of **2.3**. These two results give rise to the assumption that bis-zwitterion **2.4** indeed forms vesicles in solution but during the spin-coating process a different mode of self-assembly takes over and leads to significant changes in the shape and the dimension of bis-zwitterion **2.4**.

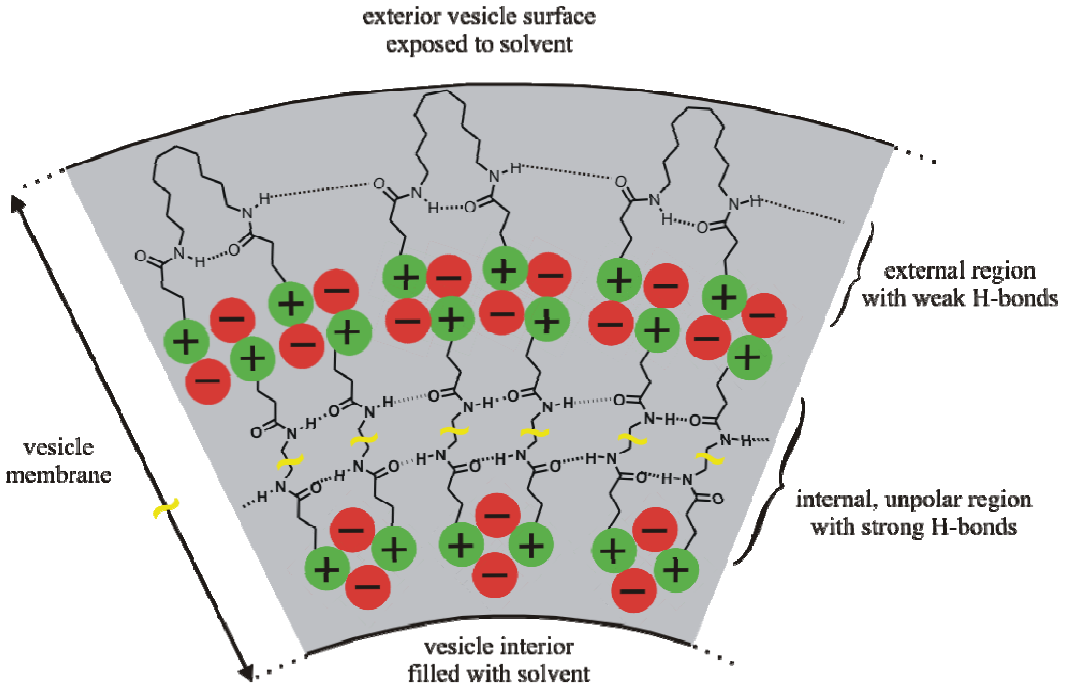

Fig. 4.21 *Proposed structure of vesicle membrane based on self-assembled **2.4** in solution (for clarity, the linker in the internal, unpolar region is presented shortened).*

In order to further investigate the self-assembly of bis-zwitterion **2.4** a higher concentrated solution (c = 10 mM in DMSO) was spin-coated onto freshly cleaved mica (9,000 rpm). Surprisingly no discrete particles were detected but widespread layers. Figure 4.22A displays an overview of a 25 μm^2 sized area with different parts of layer formation. Their expansion ranges up to some square micrometers but the layers do not seem to have a directed arrangement. Interestingly two different types of layers can be detected. One layer has an average thickness of d = 2.7 nm. This value is in perfect agreement with the height of the particles from the dilute sample in Figure 4.20. The other layer is by far thicker. But its height differs and has in one place a thickness of d = 13-14 nm and in other parts d = 11 or 8.5 nm. However, one thing is in common for all heights measured: they are multiples of 2.7 nm. This result points to the conclusion that the thinnest layer seems to be the original one. All other layers result from a repeated layer-by-layer deposition. Now with this information the AFM images of the dilute sample can be reinterpreted. The particles in Figure 4.20 seem to be parts of the thinnest layer but due to the low concentration they can not connect themselves in order to form the widespread layers. In addition the discrete particles in the AFM image also represent the former vesicles of the solution. In reverse this means that the deposition of the vesicles on the mica surface can be controlled by the concentration of the sample solution. At low concentrations the vesicles do not interact with each other during the deposition process and form island-like structures which always have the same height

of d = 2.7 nm. With increasing concentration the number of vesicles exceeds a certain limit which leads to the interconnection of the vesicles and therefore to their transformation into layers.

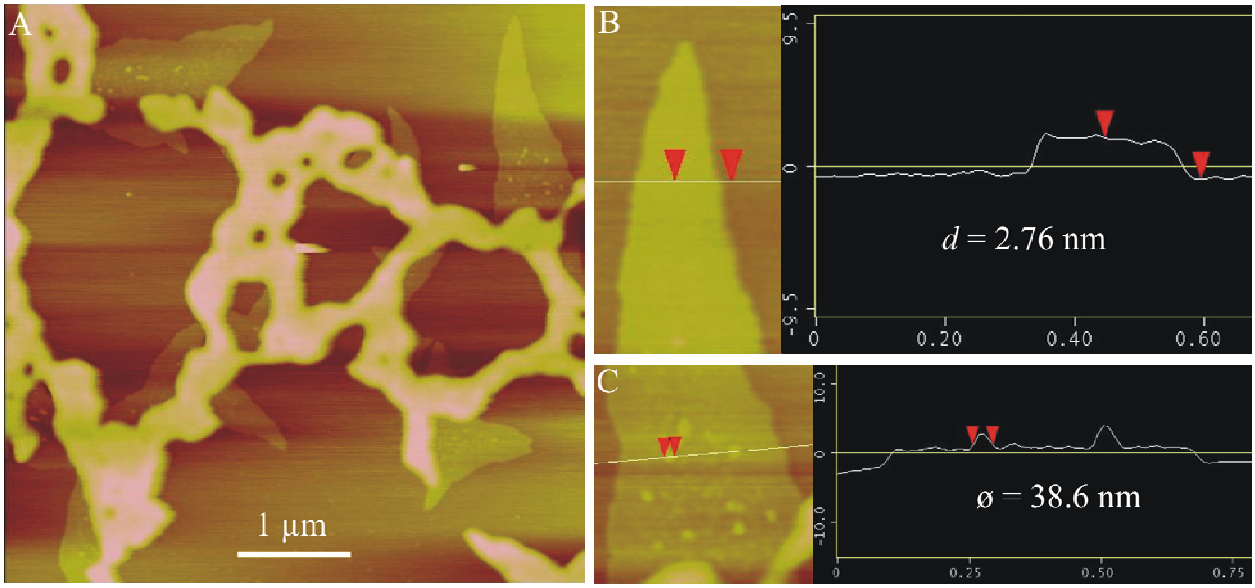

Fig. 4.22 *A) AFM height image of self-assembled layers of* ***2.4*** *on mica (c = 10 mM in DMSO). The thin layers have weaker contrast, whereas the thick ones are in bright-yellow; B) section plot of a typical monolayer; C) fusion of vesicles as basic principle for monolayer formation. (for B and C: horizontal scale in µm; vertical scale in nm) The red markers indicate corresponding areas in the plot.*

This transition can be compared with the reverse reaction of vesicle formation. In section 4.1.2 vesicle formation was explained by incorporation of curvature (in terms of a certain number of monomers) into a monolayer membrane. Now in case of bis-zwitterion **2.4** the vesicle membrane rearranges by contact with the surface and self-assembles at first as a monolayer. Afterwards free vesicles from solution stick on the layers and initiate the formation of a second layer on top of the primal one. This can be seen in Figure 4.22C. Several particles attached on a first layer are in the same size range as the discrete particles from the diluted solution. Furthermore the value of 2.7 nm for the thickness of the membranes fits perfect to the results from the DOSY NMR experiments. The hydrodynamic radius of the dimer has a value of r_H = 1.33 nm, *ergo* a diameter of 2.66 nm. This gives rise to the assumption that the observed layers are formed from stretched dimers, which stack together as depicted in Figure 4.23. Again, with formation of an unpolar region between the zwitterionic binding motives, strong hydrogen bonds and *van der Waals* interactions reinforce the monolayer structure. Most likely the loss of solvent molecules during the spin-coating process initiated the transformation from the curved vesicle membrane to the planar monolayer. Without any solvent surrounding the vesicles, the loop-like alkyl chains could move

from the exterior of the vesicles closer to the ionic binding motives. The repulsive interaction between the unpolar alkyl chains of the linker with the polar and ionic binding motives could lead to a transition of the alkyl chains from the outside to the interior, unpolar region. This rearrangement could lead to a strong stabilization of the alkyl chains and the hydrogen bonds, respectively. Therefore in case of bis-zwitterion **2.4** *van der Waals* interactions between the long alkyl chains might be the dominant forces which direct the mode of self-assembly at least on the surface.

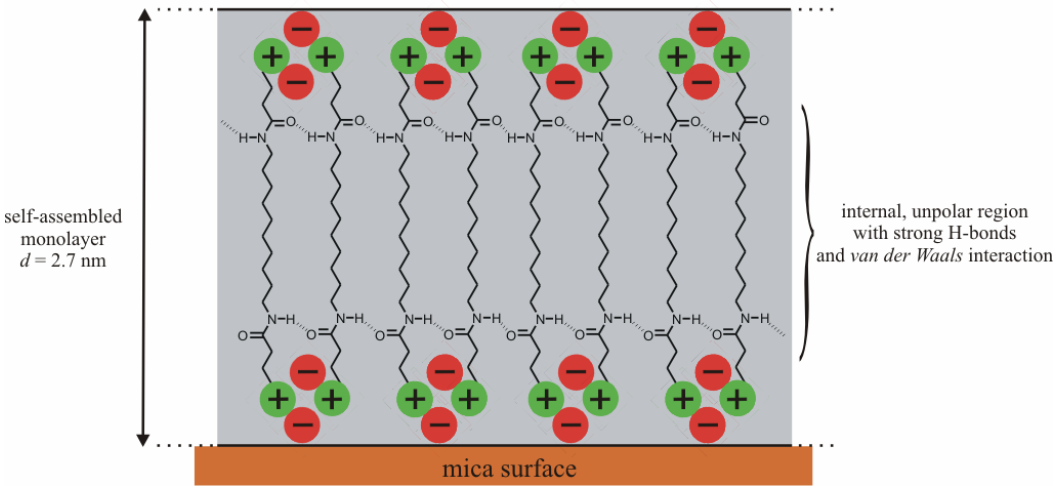

Fig. 4.23 *Proposed structure of the self-assembled monolayer of* ***2.4*** *on the mica surface.*

In conclusion, the use of a long and hydrophobic linker in the flexible bis-zwitterion **2.4** leads to new and different characteristics with respect to the self-assembly. In solution a distinct equilibrium exists between monomers and dimers on the "molecular" level. In the supramolecular state vesicle formation takes place and can be described in analogy to bis-zwitterion **2.3** whereas now the long linkers prevent the agglomeration of the vesicles to larger structures as they lack any specific binding site. Through contact with the surface during sample preparation for the AFM experiments the mode of self-assembly changes completely and leads to the formation of layer-like structures. Hence bis-zwitterion **2.4** is a first example for a change in self-assembly initiated by the modification of one monomer moiety, in this case the linker.

4.1.4 Hierarchical self-assembly of a triple-zwitterion: formation of three-dimensional supramolecular nanostructures from polymeric ribbons[14]

Beside the above mentioned building blocks **2.2**, **2.3** and **2.4**, in which two zwitterionic binding motives are connected with different types of linkers, also one building block was studied, which incorporates three binding motives in one monomer. Both the increased number of binding sites and the type of linker was different. In case of triple-zwitterion **2.5** (Figure 4.24) the binding motives are connected via the periphery of the pyrrole core with a linker, which connects three zwitterionic binding motives over a rather short distance.

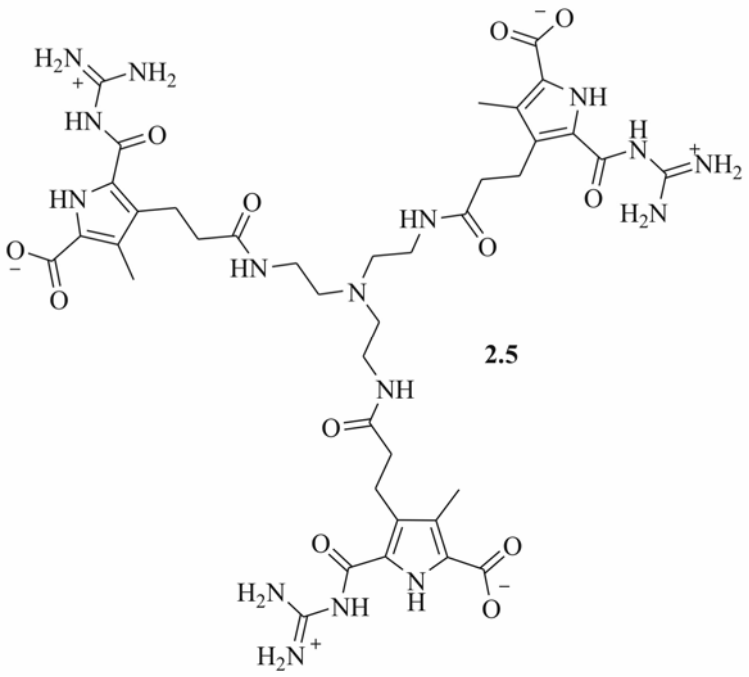

Fig. 4.24 *Triple-zwitterion **2.5** with three binding motives linked over the periphery of the pyrrole core.*

The synthesis of the triple-zwitterion is based on the *Triester route* and has been developed in earlier work. Therefore only a short summary will be given here (Figure 4.25). Coupling of *N*-boc-guanidine **4.12** to the free acid **4.13**[15] with PyBOP as coupling reagent resulted in the fully protected zwitterion **4.14** in 66 % yield. Deprotection of the benzyl ester with hydrogen and palladium on charcoal gave the free acid **4.15** in quantitative yield. Subsequent conversion with tris-(2-aminoethyl)-amine (**4.16**) and PyBOP as coupling reagent gave the fully protected precursor **4.17** in 44 % yield. After deprotection of **4.17** first with TFA and then with sodium hydroxide in methanol resulted in the crude product of **2.5,** which was extracted from water/dioxan.

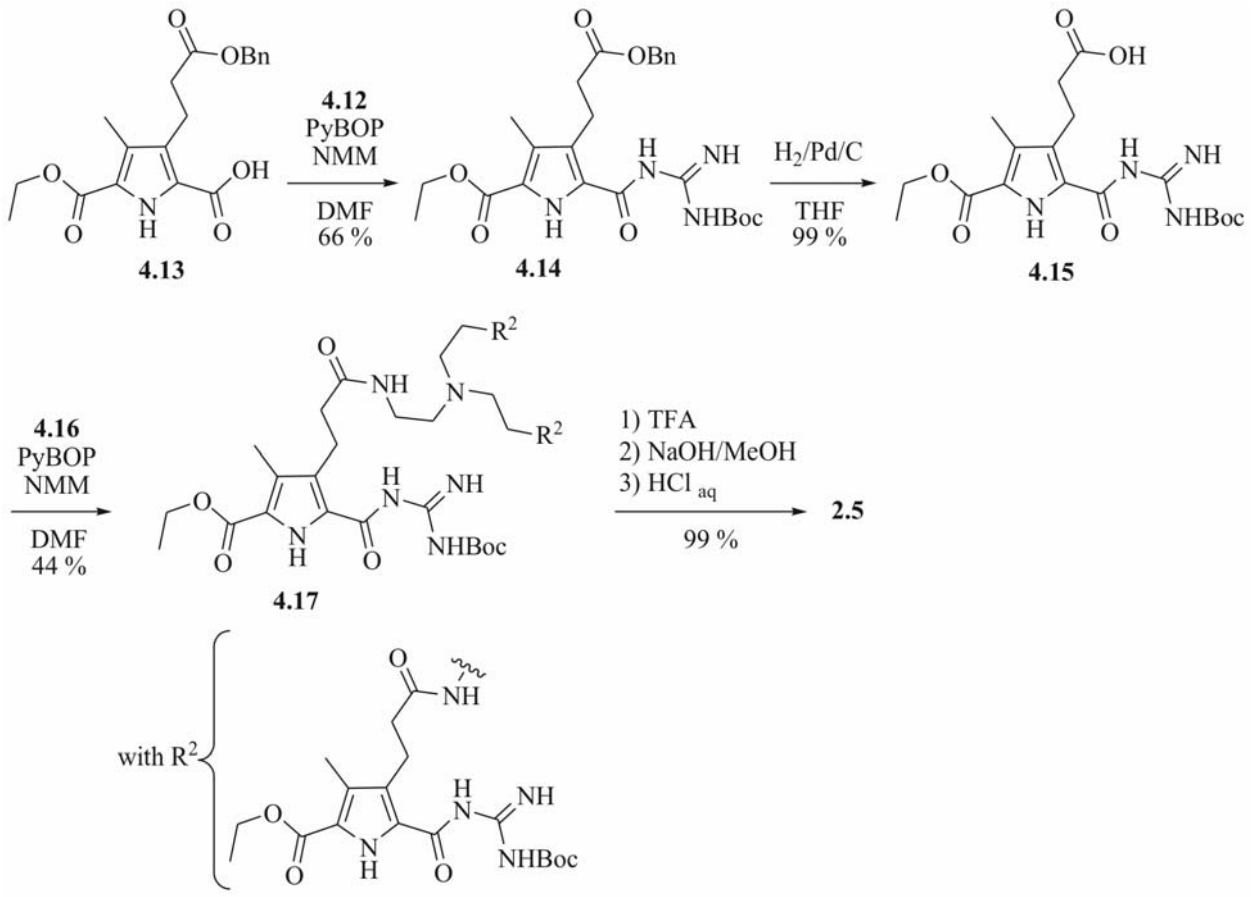

Fig. 4.25 *Synthesis of the triple-zwitterion **2.5** based on the Triester route.*

First results were obtained from NMR dilution studies of **2.5** in DMSO-d_6. All sample solutions showed a strong *Tyndall* effect which points to the formation of larger aggregates, also in highly diluted solutions. The ^{1}H-NMR spectra evidence that the triple-zwitterion **2.5** is fully ion paired over the whole concentration range (Figure 4.26). Due to the fact that in a triple-zwitterion principally only two binding motives can interact at the same time *intra*molecularly, at least one free zwitterion must interact *inter*molecularly with a second "monomer". Therefore the smallest building block in the self-assembly of **2.5** must be a dimer. The characteristic signal set of the guanidinio amide NH proton at $\delta \approx 14.7$ and the pyrrole NH proton at $\delta \approx 12.5$ is detected twice due to the different binding environment of either *intra*molecular or *inter*molecular ion pairing. With increasing concentration one signal of each pair also increases. This change suggests, that with increasing concentration the *intra*molecular ion pair is converted into the *inter*molecular ion pair, most likely under formation of oligomers or network-like structures. Simple force-field calculations were used to demonstrate the dimerization of **2.5** (MacroModel 8.0, Amber* force field, GB/SA water solvation model, 50,000 steps). In Figure 4.27 both intra- and intermolecular ion pairs are shown. Although there is full association of the zwitterions they differ in the angles

between two binding motives (intramolecular: ~ 60 °; intermolecular: ~ 175 °). The two signal sets in the ^{1}H-NMR spectra might be the result of these different angles between the dimerizing zwitterions. This behaviour has already been discussed in the previous sections in the discussion of the monomer-dimer equilibrium of the bis-zwitterions.

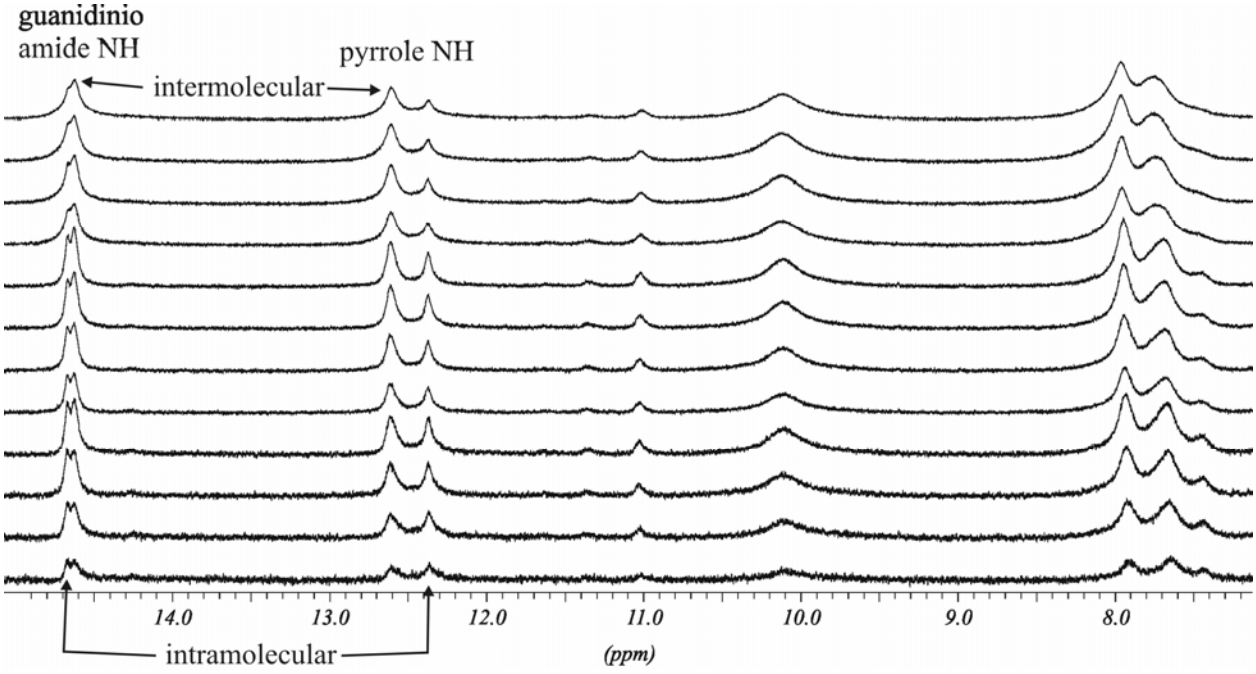

Fig. 4.26 *Part of the ^{1}H-NMR spectra obtained from the NMR dilution studies of **2.5** (from bottom to top: c = 2.5, 5, 7.5, 10, 12.5, 15, 17.5, 20, 25, 30, 35, 40 mM in DMSO-d_6).*

In addition DOSY NMR studies confirm the presence of dimeric **2.5** as the smallest building block even at low concentrations. At a concentration of c = 2.5 mM triple-zwitterion **2.5** has a hydrodynamic radius of r_H = 1.37 nm which is twice as large as the value for the hydrodynamic radius of the fully protected precursor **4.17** with r_H = 0.70 nm. With increasing concentration (c = 25 mM) r_H of **2.5** rises to a value of 1.60 nm. This is in agreement with the dilution studies and the increasing signal of the intermolecularly bound ion pair. The increasing value of r_H represents the shift in the equilibrium from dimeric **2.5** to the resulting oligomers. Higher aggregates like polymeric networks are not detectable by DOSY NMR due to signal broadening, but they have also an influence on the diffusion of the smaller structures.

The presence of larger particles than just dimers was already assumed in the beginning due to the strong *Tyndall* effect present in the solutions of **2.5**. Hence, in cooperation with Dr. F. Gröhn (Max Planck Institute for Polymer Research, Mainz) a set of dynamic light scattering experiments were performed and confirmed the existence of large aggregates with a diameter up to 100

nm. Unfortunately, small amounts of even larger structures (> 1 µm) prohibited the quantitative analysis of the DLS data.

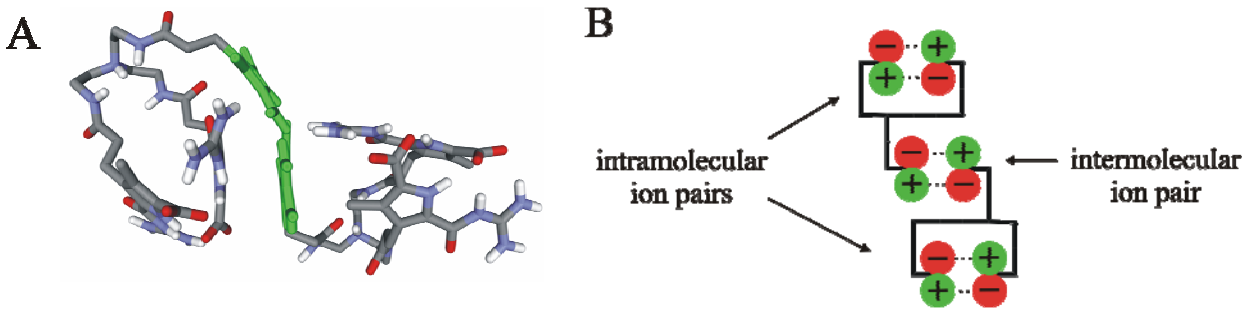

Fig. 4.27 *A) Force-field calculations of dimeric* ***2.5*** *show the different angles between the intra- and intermolecular ion pair, respectively (intermolecular ion pair is depicted in green; non-polar hydrogens are omitted for clarity); B) schematical illustration of dimeric* ***2.5*** *with its distinct ion pairs.*

Therefore, in cooperation with Dr. F. Gröhn (Max Planck Institute for Polymer Research, Mainz) small angle neutron scattering experiments were used for further investigations of the self-assembly of **2.5** in solution. All studies were performed with a wavelength of 6 Å for the neutron radiation, a wavelength spread of 11 % and a sample concentration of c = 2.5 mM in pure DMSO. Figure 4.28A shows the scattering curve *I(q)* which was *Fourier* transformed into the pair distance distribution function *P(r)* which is displayed in Figure 4.28B. Without assuming any certain particle shape the analysis of the SANS data clearly proved the presence of spherical particles with an average diameter of 90 nm in solution (r = 45 nm). However, no larger particles could be detected. Further *Guinier* analysis of the SANS data yields a radius of gyration of r_G = 32.5 nm. Both values, r and r_G, indicate the formation of solid spheres and not vesicles as in the case of bis-zwitterions **2.3** and **2.4**. Now the characteristic ratio of r/r_G has a value of 0.72 and is therefore in good agreement with the theoretical value for solid spheres of 0.75. Furthermore, the SANS data also give reliable information for the presence of a second structural level. On a smaller size scale (higher q-values) the solid spheres do not seem to be homogenously in the interior, but consist of organic material and solvent. A cross-section *Guinier* plot representing $\log(I \cdot q)$ versus q^2 shows a linear behaviour in the distinct q-region (Figure 4.28C). This information points to the formation of cylindrical, worm-like structures. A quantitative analysis yields a cross-sectional radius of gyration of $r_{G,c}$ = 1.1 nm. Under the assumption that the cylinders have a spherical cross-section and a homogenous contrast inside this radius of gyration can be transformed into a diameter of 3.2 nm for the cylindrical substructure. The SANS data can also be transformed into a cross-sectional pair distance distribution function $P_c(r)$ which reflects the

characteristics of the cross-sectional dimension and shape for a cylinder-like structure. This transformation yields a diameter of 3.3 nm, which confirms the first value of the cross-sectional radius of gyration (Figure 4.28D). In addition the data also show that the interior of the cylindrical substructure is not homogenous and not centro-symmetric.[16] Unfortunately the size resolution of the SANS data is not sufficient for a more detailed model.

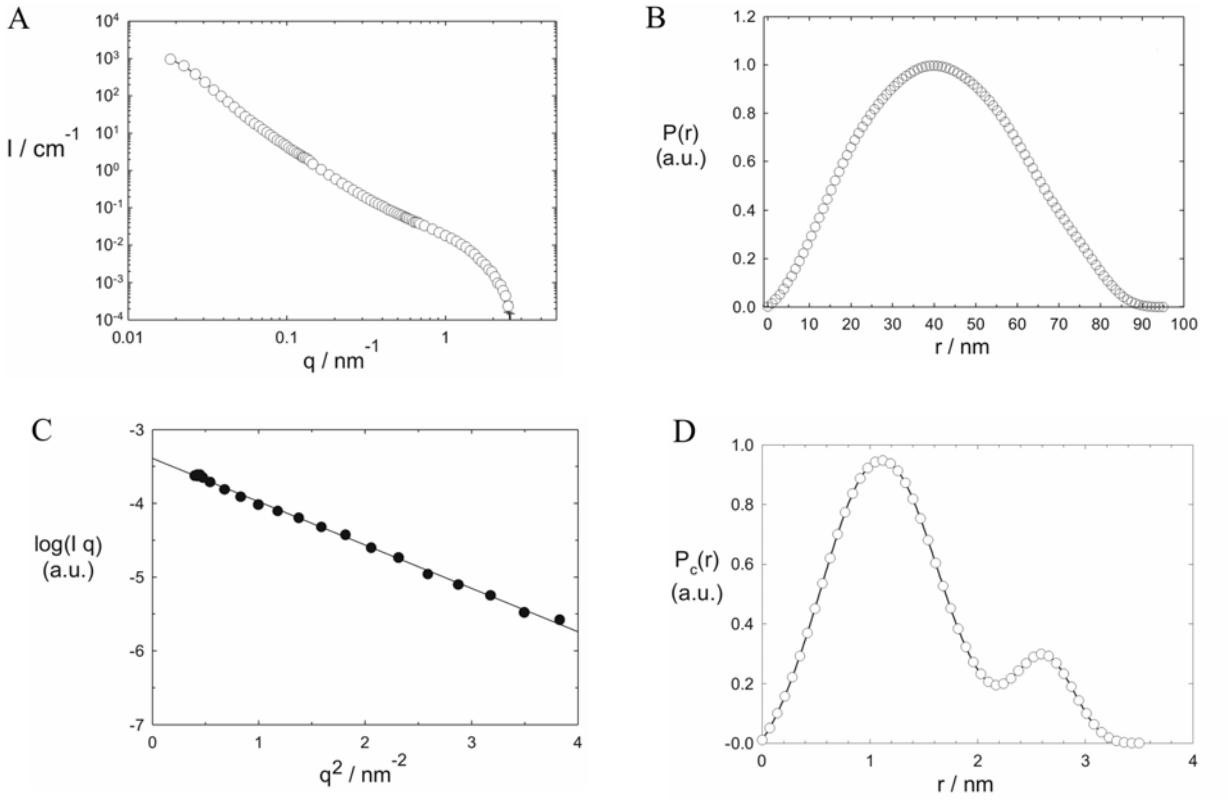

Fig. 4.28 *Results from the SANS experiments of **2.5** (c = 2.5 mM in DMSO): A) scattering curve I(q); B) pair distance distribution function P(r) resulting from the Fourier transformation of the experimental SANS data; C) cross section Guinier plot for the SANS data at higher q-values; D) pair distance distribution function $P_c(r)$ for the cylindrical substructure.*

In conclusion, the results from the SANS experiments show clearly that triple-zwitterion **2.5** forms spherical structures with a mean diameter of 90 nm. In contrast to the bis-zwitterionis **2.3** and **2.4** the triple-zwitterion **2.5** forms solid spheres as the characteristic ratio of r/r_G has a value of 0.72, which is close to the theoretical value of 0.75 for solid spheres. It could also be shown that the internal structure of the solid spheres is not homogenous, but consists of a combination of organic material and solvent molecules. Additionally, a second structural level could be detected which also seems to be part of the self-assembly process of **2.5**. On this smaller level a worm-like structure exists with a cylindrical shape, which has a diameter of 3.3 nm.

Subsequently, in cooperation with V. Stepanenko and Prof. Dr. F. Würthner (Institute of Organic Chemistry, University of Würzburg) AFM experiments were performed in order to examine the self-assembly of triple-zwitterion **2.5** on a solid substrate. All samples were prepared by spin-coating solutions of different concentrations on freshly cleaved mica (c = 2.5, 5, 10 mM in pure DMSO). The experiments were analysed in tapping mode under ambient conditions. First results showed that the deposition on the surface is strongly depending on the concentration of the sample solution. Images taken from samples with concentrations of *c* = 10 and 5 mM show the same rather unspecific pattern throughout all parts of the examined surface: layers of undefined height based on spherical particles. Unfortunately, a quantitative analysis of the diameter of these particles is not possible due to their strong agglomeration. But with decreasing concentration more defined structures can be detected. At a concentration of *c* = 2.5 mM large cylindrical plates with a diameter of *ca*. 450 nm and a height of about 2-3 nm can be observed in some parts of the surface (Figure 4.29). Interestingly, these plates have the same volume like the solid spheres detected by SANS in solution. The volume of a representative plate (AFM) has a value of

$$V_{plate} = \pi \cdot r_{plate}^2 \cdot h = 3.9 \cdot 10^5 \, nm^3 \qquad \text{(Eq. 4.1)},$$

whereas the solid spheres (SANS) have a mean volume of

$$V_{sphere} = \frac{4}{3} \cdot \pi \cdot r_{sphere}^3 = 3.8 \cdot 10^5 \, nm^3 \qquad \text{(Eq. 4.2)}.$$

This accordance points to the possibility that the large plates represent snapshots of the solid spheres deposited on the mica surface. More importantly, the AFM image also confirms that the spheres are not homogenous. Figure 4.29C clearly shows a network-like interior of the plate with several gaps between the network ribbons. These empty spaces most likely were filled with solvent as predicted by the SANS experiments. Larger areas of this kind of network can be observed in most of the other regions of the surface as depicted in Figure 4.29B. Now it is possible to further investigate the dimension of the particles, which form the networks. The best explanation of their network structure might be given by the comparison with pearls on a chain. A closer analysis of the ribbons shows that they consist of spherical particles with a mean diameter of *ca*. 22 nm and a height of about 3 nm (Figure 4.29A). The small plates interact with each other upon formation of ribbons. Since the large network-like structure covers most of the surface and only very few single cylindrical plates can be observed one can assume that with increasing concentration (because of the loss of solvent) the larger solid spheres interact with each other, lose their cylindrical shape and merge during the AFM sample preparation into the large network. A first step of this intersupramolecular interaction can be seen in Figure 4.29C. A kind of bridge connects two plates and former spheres, respectively. This behaviour is also in agreement with the

results from the higher concentrated sample solutions. There, the interaction of the spheres was so large that no single plate can be detected, but only small particles forming a close network without any space between the ribbons. This transition from single solid spheres or plates to large area networks can be also observed using a slightly different sample preparation. By reducing the rotation speed during the spin-coating process (7000 rpm → 5000 rpm) some spheres were able to keep their shape while they were deposited in the state of interaction (Figure 4.30A).

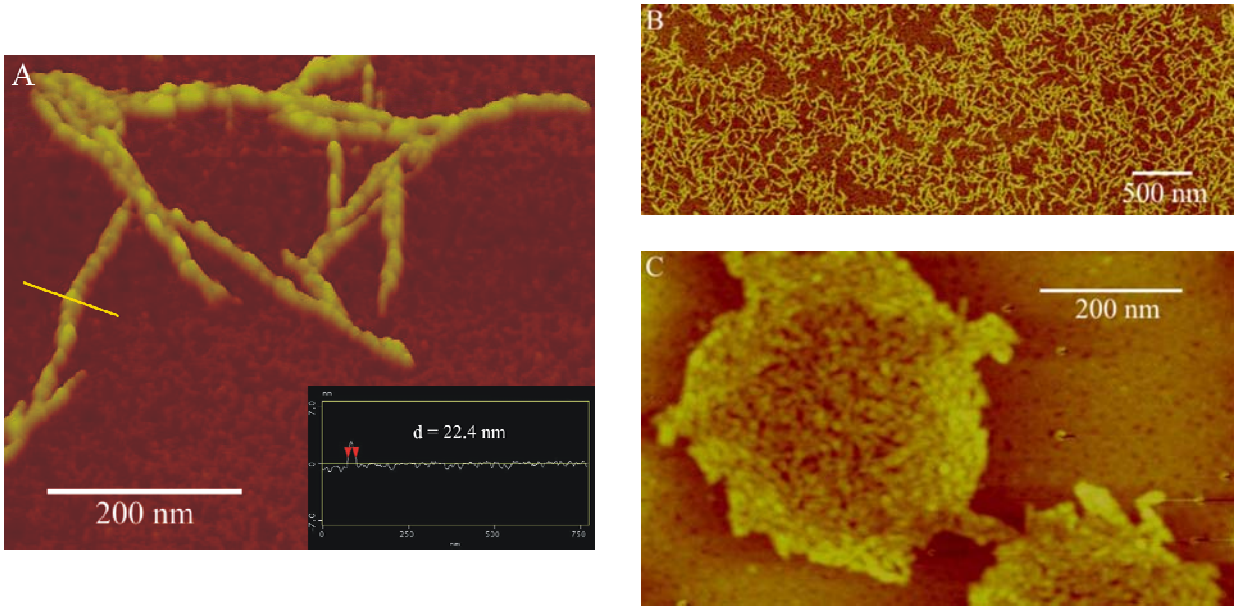

Fig. 4.29 *AFM images of self-assembled* ***2.5*** *(c = 2.5 mM in DMSO): A) small plates self-assemble like pearls on a chain (inset: section plot of a representative sphere); B) formation of an extensive network based on small, interacting plates; C) large, flat plates with internal network-like structure resulting from the interaction solid spheres with the mica surface.*

In conclusion, the AFM experiments confirm in an indirect way the formation of large particles with an inhomogeneous interior. The large cylindrical plates represent the former solid spheres from solution, which were deposited on the mica surface during the sample preparation. Their interior shows a network-like structure which is in agreement with the SANS data predicting an inhomogeneous interior. The ribbons of the network are based on the interaction of a smaller spherical particle species. They arrange themselves like pearls on a chain and form an expanded network. Its density is strongly depending on the concentration of the sample solution. All images taken from higher concentrated solutions than 2.5 mM only show the small spheres covering the whole surface (Figure 4.30B).

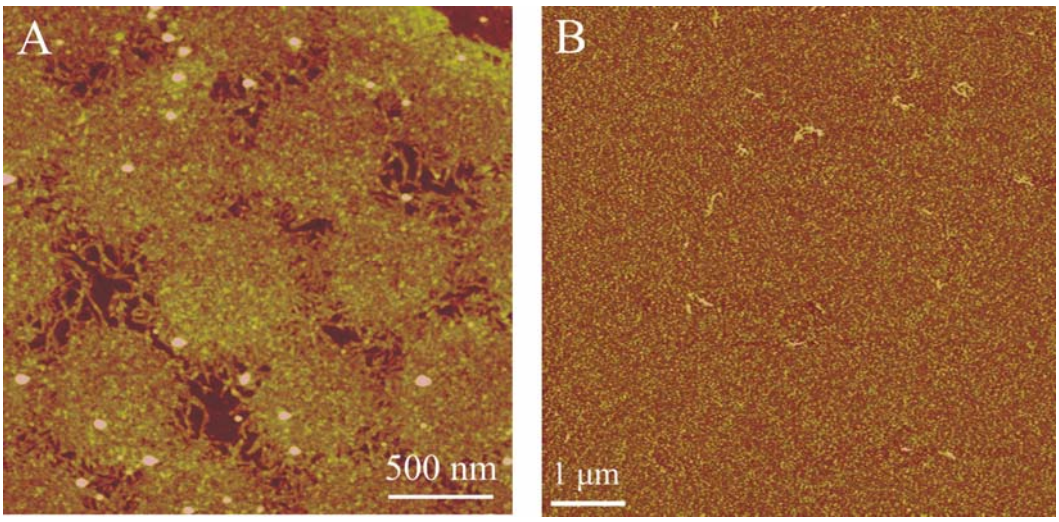

Fig. 4.30 *A) The last step in the self-assembly of triple-zwitterion **2.5**: intersupramolecular interaction of solid spheres deposited on the mica surface (c = 2.5 mM in DMSO); B) AFM image of **2.5** with a sample concentration of c = 10 mM in DMSO.*

Now, with the complete information derived from all analytical methods the hierarchical mode of self-assembly of triple-zwitterion **2.5** can be explained stepwise. For a better overview all experimental data are summarized in Table 4.1.

Tab. 4.1 *Overview of the experimental data obtained from all analytical methods for triple-zwitterion **2.5**.*

METHOD	RESULTS
NMR dilution	two signal sets representing *intra*- and *inter*molecular ion pairing; concentration dependent transition from dimeric **2.5** to higher oligomers
DOSY	concentration *independent* dimerization of **2.5**: r_H = 1.37 nm (2 mM) and r_H = 1.60 nm (25 mM); r_H (**4.17**) = 0.70 nm (2 mM)
DLS	large aggregates with a size up to 100 nm
SANS	solid and spherical particles with a diameter of 90 nm; inhomogeneous interior; worm-like structures with cylindrical shape and a diameter of 3.3 nm
AFM	large, cylindrical plates with a mean diameter of 450 nm and a height of 2-3 nm; inhomogeneous and network-like interior; small spherical particles with a mean diameter of 22 nm and a height of 2-3 nm

Starting on the molecular level the smallest building block consists of the dimerized triple-zwitterion **2.5**. DOSY experiments evidence the dimension of the dimer throughout a concentration range from 2 mM (r_H = 1.37 nm) to 25 mM (r_H = 1.60 nm). The fully protected precursor **4.17** has a hydrodynamic radius of r_H = 0.70 nm. Both the increasing hydrodynamic radius of **2.5** and the intensity change in the ^{1}H-NMR spectra of the NMR dilution row points to an equilibrium between the dimer and higher oligomers. The formation of larger aggregates than dimers is also in accordance with the strong *Tyndall* effect of the solution samples of **2.5**. The next step is most likely the formation of worm-like structures as revealed by SANS experiments. Assuming a spherical diameter these worm-like aggregates are formed from oligomers of dimeric **2.5**. The hydrodynamic radius r_H = 1.60 nm of dimeric **2.5** is in good agreement with the diameter of the oligomers (3.3 nm). This striking resemblance points to a stack-like assembly of dimers along the long axis of the dimer as schematically depicted in Figure 4.31. This mode of ribbon-formation is also in agreement with the data from the SANS experiments concerning the inhomogeneous interior of the worm-like structure. The stacked dimers are more or less flat building blocks which are twisted along the ribbon axis but do not fill the whole cylinder volume of the worm-like substructure. Therefore solvent molecules are also incorporated and fill up the empty spaces between the organic materials. Under equilibrium conditions open valencies in terms of free binding motives interact at the surface of the oligomers with each other and lead to the formation of long ribbons based on oligomeric **2.5**.

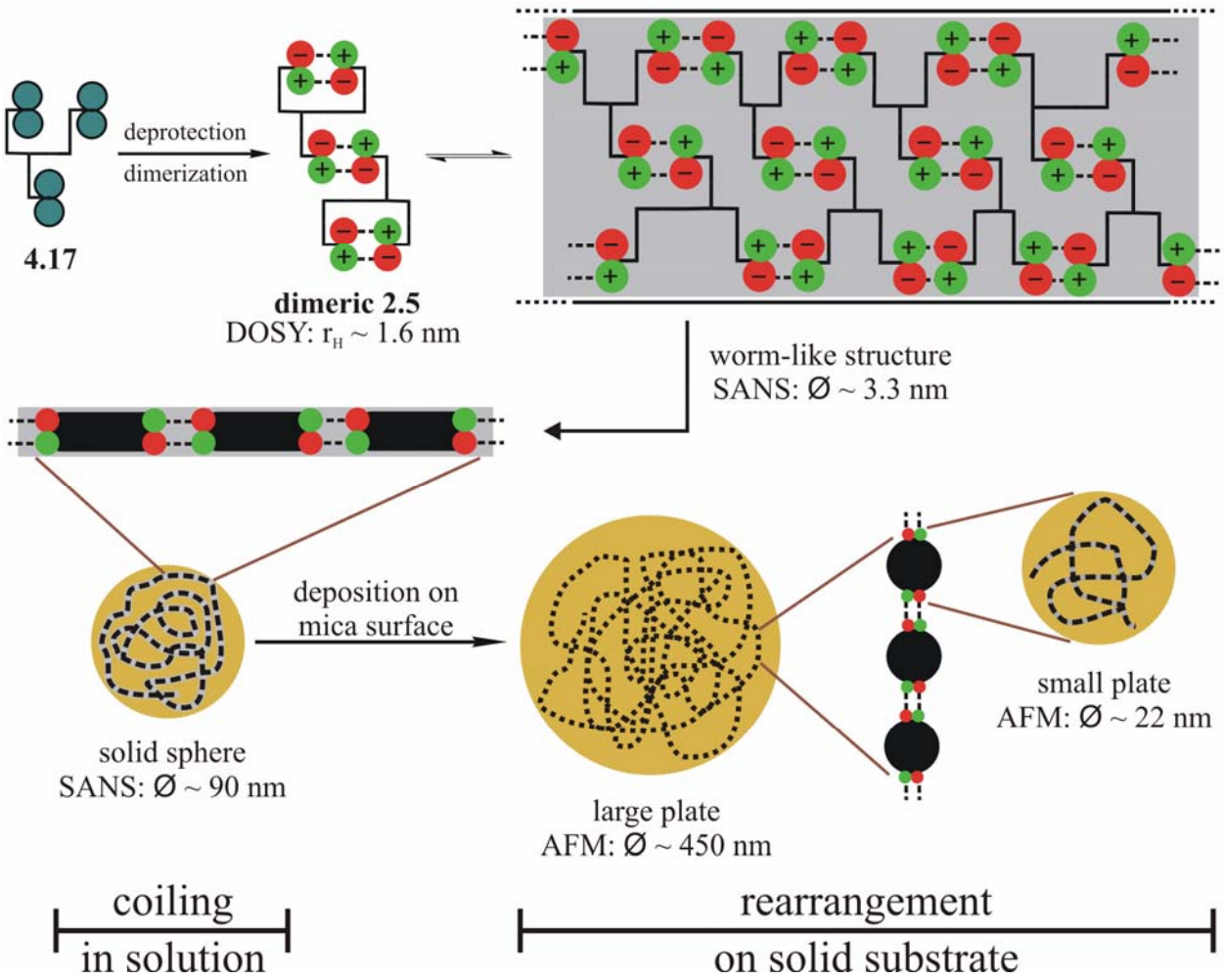

Fig. 4.31 *Schematical illustration of the hierarchical self-assembly process of **2.5** separated into the coiling process in solution and the rearrangement on the solid substrate.*

In solution the next level in the hierarchical self-assembly of **2.5** is the formation of the spherical particles as observed by SANS experiments. They have a mean diameter of about 90 nm and an inhomogeneous internal structure. The solid spheres are most likely formed from the worm-like ribbons which coil forming the ball-like structure. Upon deposition of the spheres on the mica surface a rearrangement takes place. As already discussed these spheres from solution are the counterparts of the large plates on solid substrate which were observed by AFM (mean diameter: 450 nm; height: 2-3 nm). Beside this flattening process also a change of the internal structure of the former spheres takes place. As observed in the AFM experiments, the interior of the large plates consists of small plates which have a diameter of about 22 nm and a height of 2-3 nm. One possibility is that upon interaction with the mica surface the worm-like structures coil themselves to small solid spheres which lose their spherical shape and spread on the mica surface as already seen for the large solid spheres. As these spheres were not detected by either SANS or DLS experiments their existence seems to be limited to the surface contact.

In conclusion, triple zwitterion **2.5** passes through a complex hierarchical self-assembly process. It starts with a rather simple dimeric triple-zwitterion which stacks together to worm-like structures with cylindrical shape. These ribbons coil together forming solid spheres in solution. By interaction with the mica surface these spheres spread out to large plates under rearrangement of their internal structure. Therefore triple-zwitterion **2.5** shows, in contrast to all other zwitterions discussed so far, new and very different properties concerning its mode of self-assembly.

4.1.5 Conclusion and outlook

The first part of this thesis reviews the application of guanidiniocarbonylpyrrole carboxylate zwitterions as building blocks for a variety of supramolecular structures. Four different monomers were introduced and their mode of self-assembly was discussed. The first three building blocks are so-called bis-zwitterions. They feature the combination of two binding motives in one molecule linked by different linkers via the guanidinio group. Although this project had its focus on the synthesis of water-soluble, supramolecular polymers in the beginning it emerged that the introduced linkers and their properties had an enormous influence on the self-assembly of the building blocks. The first bis-zwitterion **2.2** possesses a long and hydrophilic linker, which leads to the formation of discrete nanometer-sized cyclic dimers as confirmed by DOSY NMR, DLS and SANS experiments. By use of a short and hydrophobic linker in bis-zwitterion **2.3** the self-assembly did not stop on the state of dimerization, which is in clear contrast to building block **2.2**. Via DLS, SANS and AFM experiments the formation of vesicular structures with a size of *ca*. 140 nm could be observed. Just by the change of some properties of the linker a massive change in the mode of self-assembly occurred. This could also be examined by the third example. In bis-zwitterion **2.4** a long and hydrophobic linker was introduced. This combination led to a related mode of self-assembly compared to the short linker in **2.3**. But beside the formation of well-defined vesicles in solution also the deposition of wide-spread layers of self-assembled **2.4** on the mica surface could be observed. Extensive *van der Waals* interactions forced the vesicular structure back to a planar membrane architecture, whereas in case of **2.3** hydrogen bonds played the dominant role and lead to a undefined agglomeration of the vesicles already in solution. With these three examples a first step in the synthesis and analysis of programmable, supramolecular architectures based on zwitterionic building blocks was done. Thereby the mode of self-assembly was changed by the specific variation of the attributes of the linker which were used to connect the binding motives.

In the last example the number of binding sites was raised to three. They were linked by a short triamine over the periphery of the pyrrole core. Interestingly this monomer passed through a very

complex mode of self-assembly. Beside the concentration independent formation of dimers triple-zwitterion **2.5** also arranges into worm-like oligomers, which further self-assemble into solid spheres in solution. They were observed by SANS as solid structures with an inhomogenous interior, which is in agreement with the results from the AFM experiments. On the mica surface the solid spheres spread out and form large plates. The AFM images clearly show the network-like interior of the former spheres, which is most likely based on the coiling of the worm-like structure to small particles. The last step in the self-assembly of **2.5** is the intersupramolecular agglomeration of some large spheres under the formation of expanded networks of the small plates, which seems to be reserved to higher concentrated solutions. In contrast to all bis-zwitterions discussed triple-zwitterion **2.5** carries out a complex hierarchical mode of self-assembly. This mode is exceptionally affected by the introduction of a third binding motive into the monomeric building block.

For future work one important result has to be pointed out again. The self-assembly of all monomers is based on the outstanding properties of the binding motive. However, the specialties of the examples discussed are strongly influenced by the properties of the linker molecule (e.g. vesicle or layer formation). Now, in order to mould the structural attributes of the resulting supramolecules, the influence of the linker has to be examined in more detail. First attempts were already achieved by changing the linker length from two to ten CH_2 units, which caused a significant change in self-assembly. But where is the critical length which initiates the formation of layers? How stable are the vesicles based on a linker with 18 CH_2 units? What happens if the linker is not only composed of alkyl chains but also has some aromatic parts incorporated? What happens if the ethylene glycol chain in **2.2** is substituted by a spermine linker which imports further positive charges? What happens if the whole flexibility of the linker is removed? These questions show the high potential of this concept for supramolecular architectures. The main binding motive in terms of the zwitterionic guanidiniocarbonylpyrrole carboxylate is the inherent part with its well-defined properties for the formation of supramolecular structures in polar solvents. With the possibility of selective derivatisation of the binding motive tailor-made monomers with new and particular qualities can be designed.

4.2 Changing the binding mode: supramolecular structures via the self-assembly of α-amino acid derived zwitterions[17]

In the following section the first results of the self-assembly of four new derivatives of the primal zwitterion **2.1** will be presented and discussed. The idea of this project is based on a concept which changes the structure of the primal zwitterion by separation of the cation binding side and

the carboxylate. First attempts were already done by the incorporation of flexible linkers ranging from one to five CH_2 units (Figure 4.32). With this experimental series it was possible to test the influence of the linker length on the mode of self-assembly.[18] The zwitterion with the shortest linker showed extensive oligomerization whereas with increasing linker length the intramolecular stabilization of the monomer exceeds the intermolecular interaction. Therefore, from three CH_2 units onwards only weak intermolecular self-association takes place. As already discussed in section 3.2 not only the strength of the interaction between the self-complementary end groups is important but also any stabilization within the monomer itself resulting from the rigidity or flexibility of the building block.

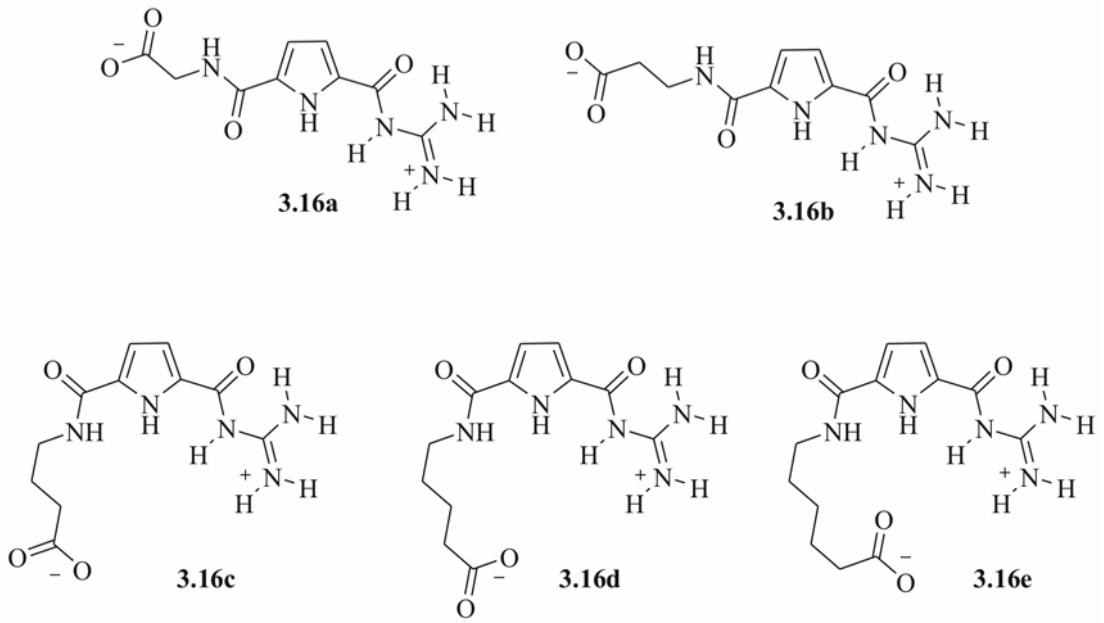

Fig. 4.32 *Increasing separation of charged end groups by alkyl chains as probe for the influence of the linker flexibility on the self-association behaviour.*

With the results of this test series and the knowledge that zwitterion **3.16a** tends to oligomerize, the idea was born to introduce a centre of chirality in order to shape the resulting self-assembled structures. In the next section four new zwitterions will be presented in detail, which are derived from the substitution of glycine in **3.16a** by the natural amino acids *L*-alanine, *L*-serine, *L*-phenylalanine and *L*-tyrosine.

4.2.1 Synthesis of the chiral zwitterions

As the synthesis of the main building block in terms of 5-(*N*-Boc-guanidinocarbonyl)-1H-pyrrole-2-carboxylic acid **4.18** is well established in our work group[19] the whole preparation of the chiral zwitterions is rather simple. It starts with the protection of the free amino acids as

methyl esters according to literature.[20] Hence, all amino acids **4.19a-d** were suspended in 2,2-dimethoxypropane and after addition of concentrated hydrochloric acid the solution was stirred over night at room temperature. From this point onwards the workup was different for every amino acid. Table 4.2 summarises the course including the yields for the pure products.

Tab. 4.2 *Workup for the methoxylation depending on the used amino acids.*

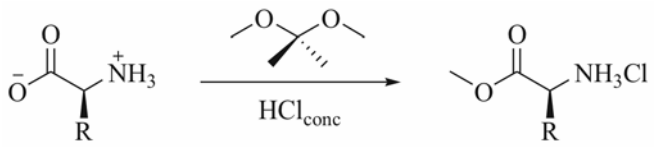

4.19a-d **4.20a-d**

product	workup	yield
4.20a R = CH_3	The solution was concentrated *in vacuo*. The resulting brown solid was dissolved in water and washed with ethyl acetate. The aqueous phase was lyophilized resulting in a colourless oil which crystallised in diethyl ether.	70 %
4.20b R = CH_2OH	The solution was concentrated *in vacuo*. The resulting brown solid was elutriated with diethyl ether, filtrated and recrystallised from isopropanol. The pure product was filtrated and washed with diethyl ether.	72 %
4.20c R = CH_2Ph	The solution was concentrated *in vacuo*. The resulting brown solid was elutriated with diethyl ether, filtrated and recrystallised from ethanol and ethyl acetate. The pure product was filtrated and washed with diethyl ether.	70 %
4.20d R = $CH_2(C_6H_4)OH$	The solution was concentrated *in vacuo*. The resulting brown solid was dissolved in water and washed with diethyl ether. The aqueous phase was lyophilized resulting in a colourless solid.	93 %

In the following step the protected amino acids were coupled with the *N*-boc-protected guanidinocarbonylpyrrole carboxylic acid **4.18**. For an efficient coupling carboxylic acid **4.18** was dissolved in DMF and NMM in order to assure a high availability of the active ester. Therefore after addition of the respective coupling reagent the reaction solution was stirred for 60 minutes at room temperature. Subsequently, the protected amino acids **4.20a-d** were added to the solution, which was further stirred for 24 hours at room temperature. The workup was the same for all

systems. The reaction solutions were hydrolysed with water and extracted several times with diethyl ether. The organic phases were then dried with magnesium sulphate and concentrated *in vacuo*. All crude products were purified by column chromatography yielding colourless or slightly yellow powders. Figure 4.33 shows the ^{1}H-NMR spectrum of **4.21a** as an example. The results of this second step are summarised in Table 4.3. The first coupling of **4.20a** with **4.18** using PyBOP as coupling reagent resulted in 63 % product. Usually these peptide couplings have yields of 95 %. Therefore HCTU was used as a second coupling reagent in order to achieve higher yields. Unfortunately it was not possible to reach better yields than 76 % with PyBOP.

Tab. 4.3 *Respective conditions for the coupling of **4.18** with **4.20a-d** including the yields for the pure products.*

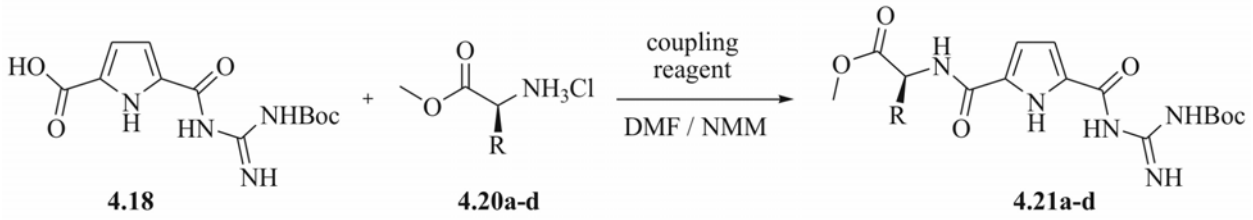

product	coupling reagent	yield
4.21a R = CH_3	PyBOP	63 %
4.21b R = CH_2OH	HCTU	70 %
4.21c R = CH_2Ph	PyBOP	76 %
4.21d R = $CH_2(C_6H_4)OH$	HCTU	74 %

The last step in the synthesis of the chiral zwitterions is the removal of both the boc group and the methyl ester. By dissolving the fully protected zwitterions in trifluoracetic acid first the boc group was removed. After stirring the solution for 30 minutes at room temperature the remaining TFA was evaporated *in vacuo* yielding a brownish oil in all cases. This oil was dissolved in a mixture of tetrahydrofuran and water (v/v, 4/1). Under vigorous stirring lithium hydroxide monohydrate was added. The reaction solution was stirred at room temperature until TLC control did not show starting material any more and therefore the complete cleavage of the methyl ester. At this point all organic solvents were removed *in vacuo* from the reaction mixture. The resulting viscous solution was diluted with water. In order to establish the zwitterionic state of the compounds 1N hydrochloric acid was added under vigorous stirring. The pH value was verified with litmus paper. Reaching the desired pH value of about 5 to 6 caused the precipitation of

a colourless and fine solid, which was filtrated and washed several times with pure water and diethyl ether.

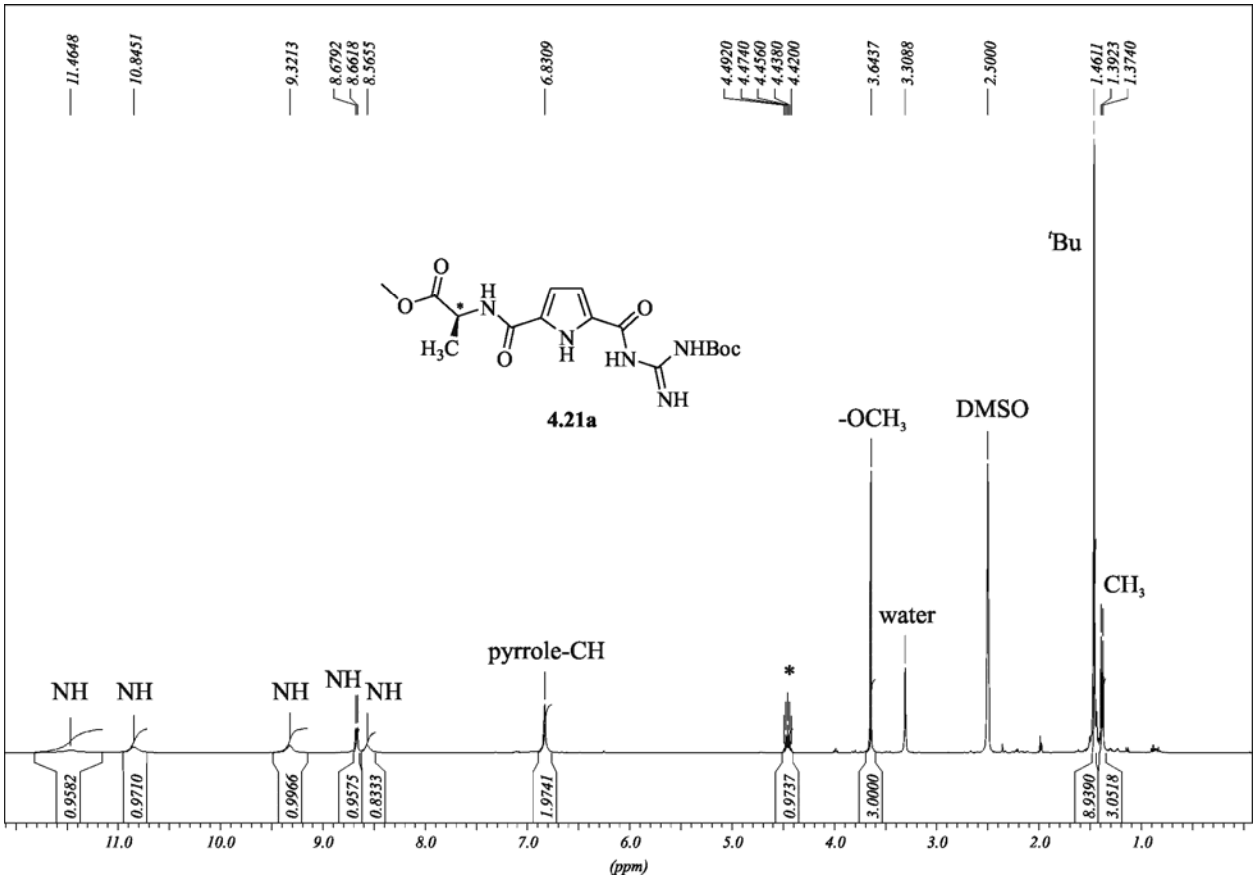

Fig. 4.33 *^{1}H-NMR spectrum of **4.21a** in DMSO-d_6.*

The last step in the purification of the chiral zwitterions was performed in order to remove all inorganic salts which resulted from the deprotection and pH adjustment. Therefore all zwitterionic compounds were recrystallised from water and dioxane. After filtration and subsequent washing with water the pure products were dried over phosphorous pentoxid. The yields over both steps of deprotection and purification are listed in Table 4.4. Due to analytical reasons and detailed integration of the NMR signals all zwitterions were also transformed into the picrate salts. Figure 4.34 shows the ^{1}H-NMR spectrum of the picrate salt of **2.6** in DMSO-d_6.

Tab. 4.4 *Product yields after the deprotection of the fully protected chiral zwitterions* ***4.21a-d*** *including the purification.*

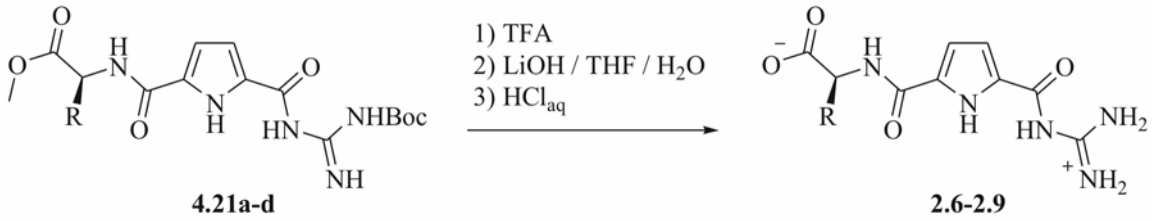

4.21a-d **2.6-2.9**

product	yield
2.6 R = CH_3	80 %
2.7 R = CH_2OH	80 %
2.8 R = CH_2Ph	71 %
2.9 R = $CH_2(C_6H_4)OH$	92 %

In conclusion the synthesis of all four zwitterionic building blocks **2.6** to **2.9** could be performed without any problems as all synthetical procedures are well-established. The recrystallisation from water and dioxane as the last step of purification rules out any contamination by inorganic salts, which could interfere with the self-assembly process. Now, these new chiral zwitterions can be subjected to NMR experiments.

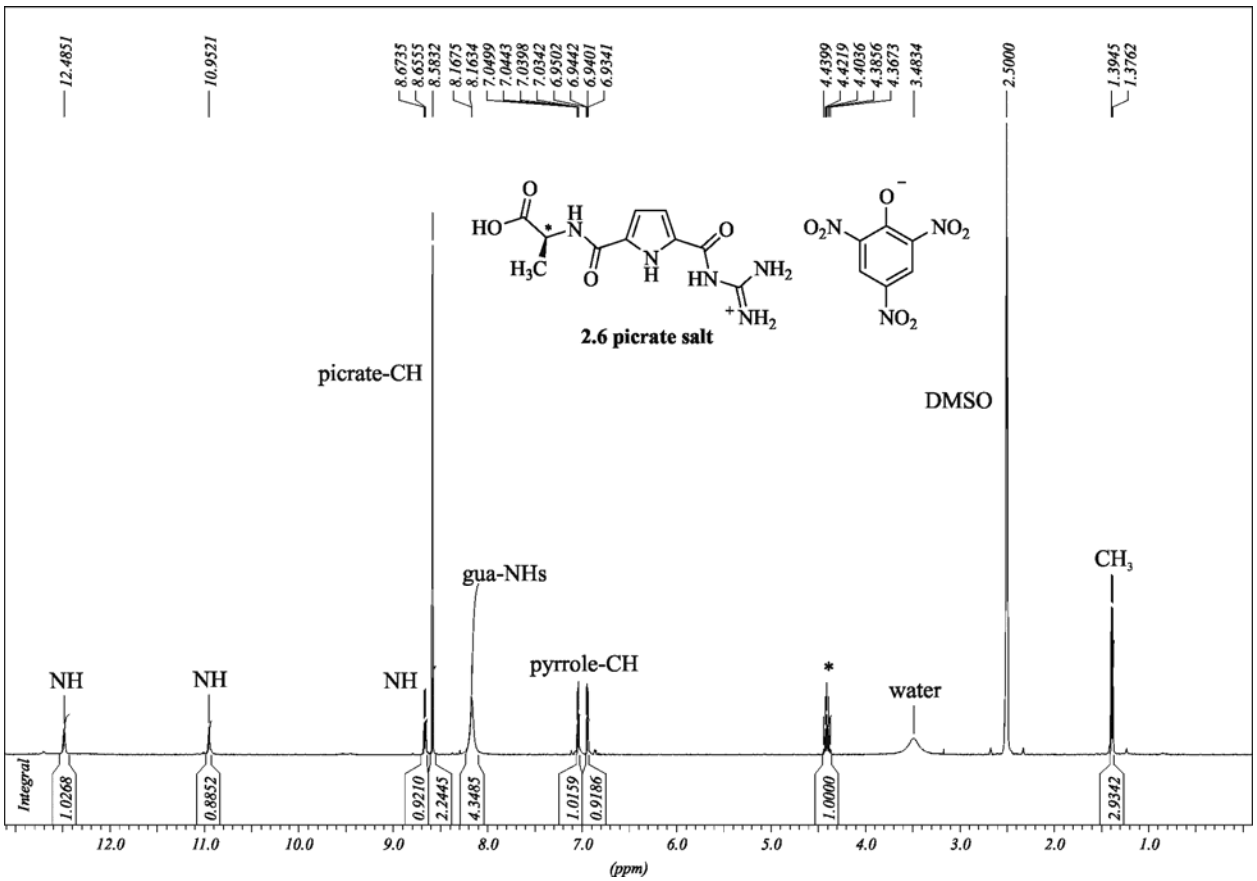

Fig. 4.34 *^{1}H-NMR spectrum of the picrate salt of **2.6** in DMSO-d_6; the signal of the free acid is not visible due to fast exchange with the solvent.*

4.2.2 Results from the NMR experiments

The analysis of the chiral zwitterions starts with the investigation of their behaviour in solution. Therefore ^{1}H-NMR dilution experiments in DMSO-d_6 were performed. A first and surprising result was the very different solubility of all zwitterions. Whereas the glycine derivative **3.16a** precipitates already at 25 mM almost completely the chiral zwitterions **2.6** and **2.7** are far better soluble up to a concentration of 100 mM. Solutions of both zwitterions with a concentration $c >$ 10 mM show a *Tyndall* effect which vanishes after some hours in case of **2.6**. Solutions of **2.7** with the same concentration keep the *Tyndall* effect for some days. This effect hints to the formation of larger aggregates in a range of up to 1 µm. The zwitterions based on *L*-phenylalanine (**2.8**) and *L*-tyrosine (**2.9**) are very good soluble and yield absolute clear solutions of high concentrations in DMSO (100 mM). But after a very short time (< 2 minutes) these solutions abruptly precipitate yielding suspensions which can not be dissolved again neither with heat nor ultrasonic treatment. Unfortunately this behaviour anticipates the performance of reproducible NMR dilution, COSY and NOESY experiments since the solutions also precipitate at concentra-

tions as low as 10 mM. But further analysis of these suspensions revealed another very surprising result. Up to now several attempts were done to crystallise any available zwitterions which are under investigation in our work group in order to get a deeper insight into their self-assembled structure. But unfortunately only the crystal structure of the primal zwitterion **2.1** could be obtained. In case of **2.8** and **2.9** images could be taken with a common light microscope. They show needle-like crystals which further develop urchin-like crystals (Figure 4.35). Even though these structures are most likely unsuitable for x-ray diffraction they nevertheless evidence the possibility to crystallise new zwitterions. But further experiments have to be done in order to obtain suitable results.

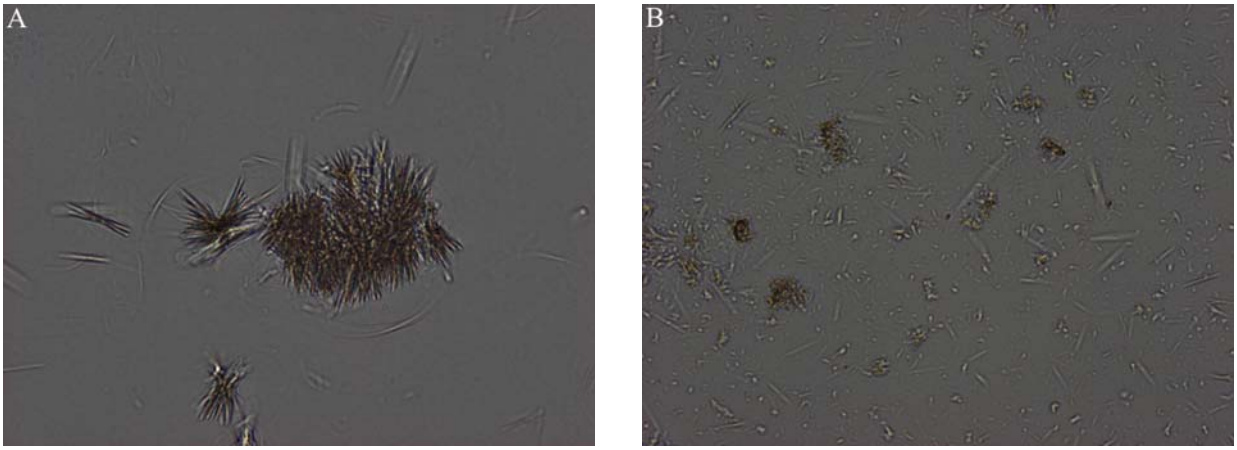

Fig. 4.35 *Light microscope images from the crystalline precipitate of solutions of A)* ***2.8*** *and B)* ***2.9*** *(c = 10 mM in DMSO).*

In contrast to this the solutions of **2.6** and **2.7** are far more stable which allows the performance of NMR dilution experiments. Starting with the *L*-alanine derived zwitterion **2.6** the results show again a completely different behaviour in comparison to the glycine derivative. The concentration dependent shift of the guanidinium amide NH *a* starts at δ = 11.09 (c = 1 mM) and ends at δ = 11.53 (c = 100 mM). Beside proton *a* only pyrrole CH proton *d* shifts slightly to a higher δ until it merges with the second pyrrole CH proton *c* (Figure 4.36). The assignment of the signals based on COSY and NOESY experiments (*vide infra*). Two things are in clear contrast to the glycine derivative **3.16a**: first, at a comparable low concentration of c = 0.5 mM the signal of proton *a* is shifted about 0.23 ppm to lower field compared to the guanidinium NH proton in **3.16a** which starts at δ = 10.83. This difference points to the possibility of weak *inter*molecular interactions of **2.6** already at low concentrations as the linker is too short for *intra*molecular interactions. Secondly, the proton signal *a* does not reach to a plateau but increases steadily. This

result implicates that with increasing concentration the intermolecular interaction gains in strength but does not reach a endpoint like **3.16a** (Figure 4.37A).

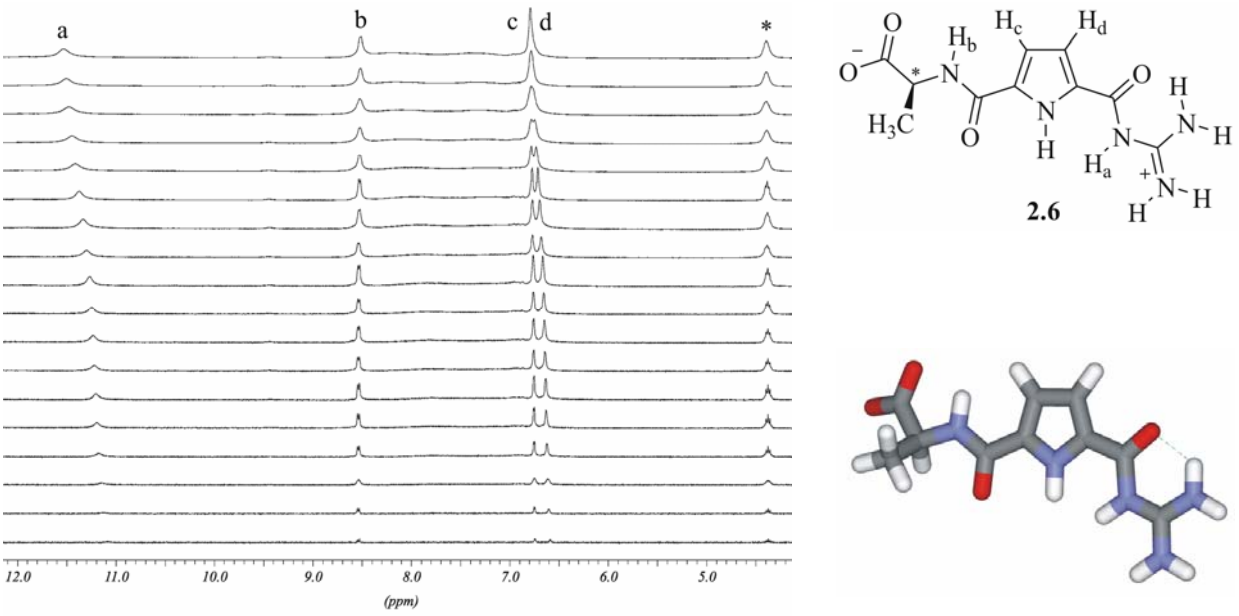

Fig. 4.36 *Part of the ^{1}H-NMR spectra of **2.6** in a concentration range from 1 to 100 mM in DMSO-d_6 (from bottom to top); minimized structure of monomeric **2.6** obtained from molecular mechanics calculations (MacroModel 8.0, Amber* force field, GB/SA water solvation model, 20,000 steps; hydrogen bonds are illustrated in green); reprinted in part with permission from Org. Lett. **2008**, 10, 1469-1472. Copyright (2008) American Chemical Society.*

One further point supports the assumption of weak intermolecular interactions at low concentrations. In case of ion pairing between the carboxylate and the guanidinium group the signal of the guanidinium NHs splits into two signals. This is depicted in Figure 4.37B for zwitterion **2.6**. Here the signal splitting can be observed at low and high concentrations although the signal intensity is rather weak due to exchange with the solvent. Two other results have to be mentioned as well. First, due to the fact that amide NH proton *b* does not shift at all over the whole concentration range, it seems that this proton does not participate in the self-association. This is quite interesting, because in other cases of ion pairing between a receptor and its substrate in terms of amino acids or small peptides this interaction is observed rather often.[21] Secondly, nearly all signals get broader with increasing concentration. This loss in signal sharpness is most likely based on the formation of larger aggregates with rather undefined structure.

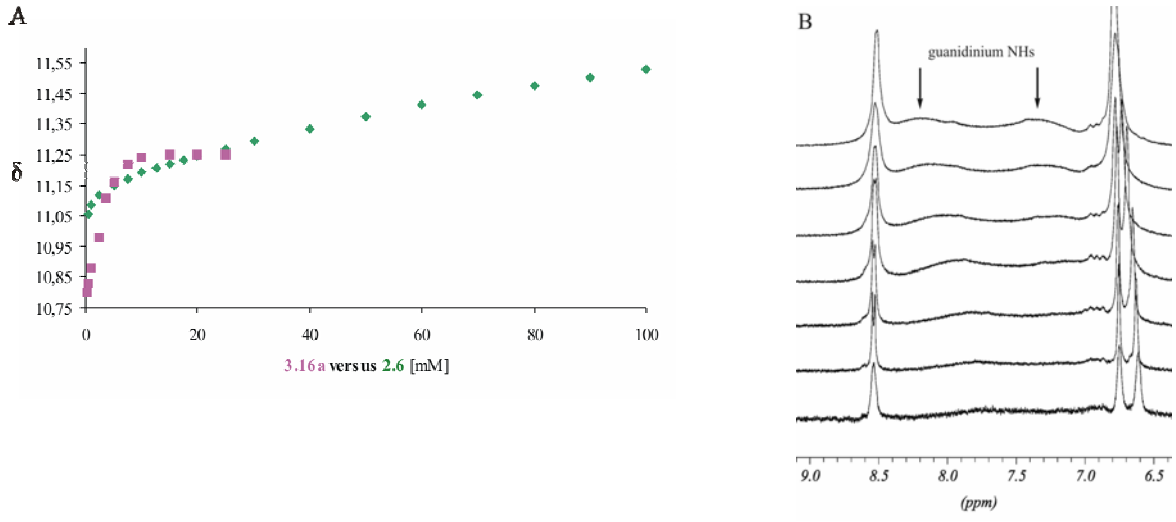

Fig. 4.37 *A) Shift of the guanidinium amide NH proton illustrating the difference between the glycine (pink) and the L-alanine (green) zwitterion; B) signal splitting of the guanidinium NHs in* ***2.6*** *(from bottom to top: c = 5, 10, 20, 40, 60, 80, 100 mM in DMSO-d_6).*

The ^{1}H,^{1}H-NOESY NMR spectrum of **2.6** (*c* = 15 mM in DMSO-d_6) proves the assumption that proton *b* does not participate in the complexation of the carboxylate. A clear NOE-contact between proton *b* and the pyrrole-CH proton *c* shows that proton *b* points away from the binding site and has therefore no contact to the carboxylate. A second NOE-contact between proton *b* and the methyl group of the amino acid side chain proves the rather planar structure of the whole monomer. The methyl group is definitely not in the molecular plane. This would lead to a repulsive contact either between the methyl group and the carbonyl oxygen or between the carboxylate group and the carbonyl oxygen. At last, since there is no NOE-contact between the amide NH proton *a* and the pyrrole-CH proton *d* one can assume a monomeric structure of **2.6** as depicted in Figure 4.38.

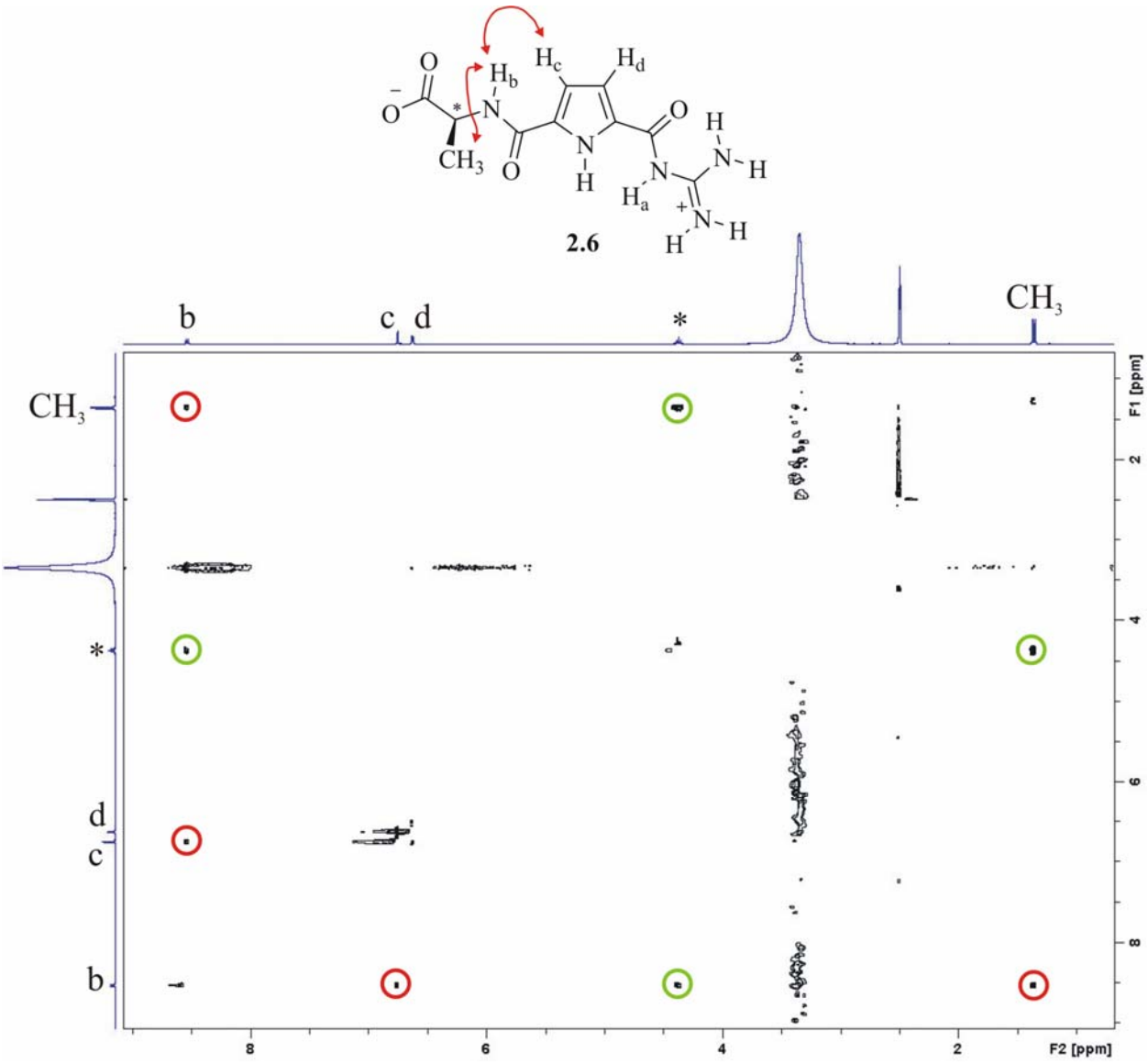

Fig. 4.38 *$^{1}H,^{1}H$-NOESY NMR spectrum of* ***2.6*** *(c = 15 mM in DMSO-d_6): the green circles represent the COSY-contacts; the red circles represent the NOE-contacts.*

In case of the chiral zwitterion **2.7** nearly the same results were observed. The ^{1}H-NMR dilution experiments show, in analogy to zwitterion **2.6**, only two shifting protons: the guanidinium amide NH *a* shifts from δ = 11.21 (*c* = 1 mM) to δ = 11.68 (*c* = 100 mM); the pyrrole CH proton *d* starts at δ = 6.6 and shifts to higher δ values until it merges with the second pyrrole CH proton *c*. The higher starting value of proton *a* might be based on a certain preorganisation within the monomer of the *L*-serine zwitterion. A hydrogen bond between the carbonyl oxygen and the hydroxyl group of the amino acid side chain leads to an enforced 7-membered ring, which reduces also the flexibility of the carboxylate group (Figure 4.39). A hydrogen bond to the carboxylate group was energetically less favoured (ΔE = 34 kJ/mol) as demonstrated by molecular mechanics calculations (MacroModel 8.0, Amber* force field, GB/SA water solvation model, 10,000 steps).

Due to this fact a more effective ion pairing is possible between two preorganized monomers of **2.7**.

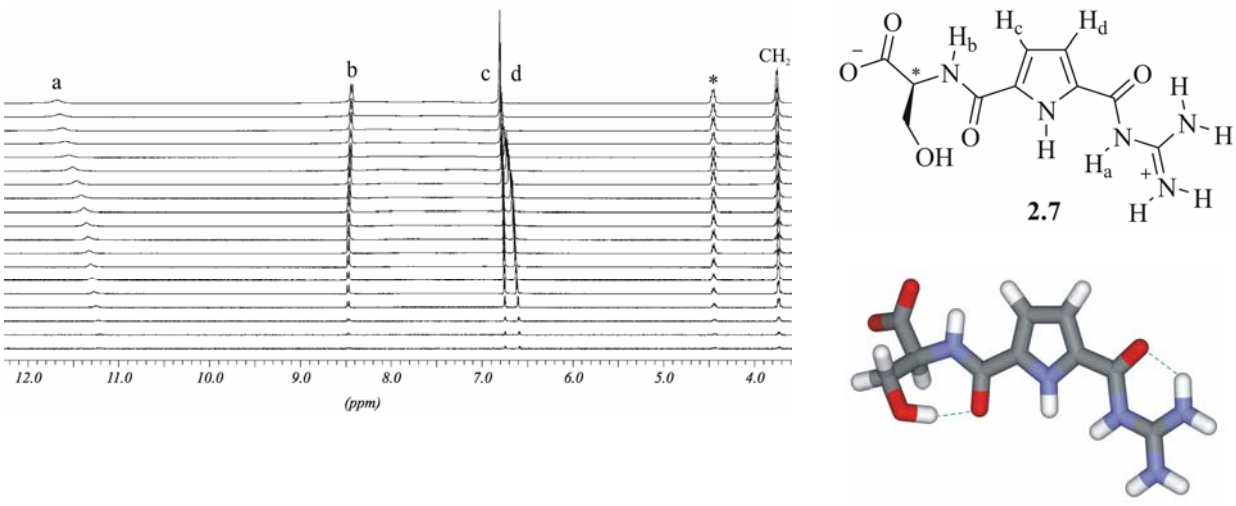

Fig. 4.39 *Part of the ^{1}H-NMR spectra of **2.7** in a concentration range from 1 to 100 mM in DMSO-d_6 (from bottom to top); minimized structure of monomeric **2.7** obtained from molecular mechanics calculations (hydrogen bonds are illustrated in green; MacroModel 8.0, Amber* force field, GB/SA water solvation model, 10,000 steps).*

A further evidence for this intramolecular stabilisation of the *L*-serine derived zwitterion is the regularity between the increasing δ values of proton *a* in comparison to **2.6**. Figure 4.40A shows that the mean difference between both curves is about $\Delta\delta = 0.12$. Since any intramolecular hydrogen bond is concentration independent the stabilisation of the carboxylate group is not affected by concentration changes, too.

In analogy to **2.6** amide NH proton *b* does not shift with increasing concentration. A splitting of the guanidinium NH signal was observed for the *L*-serine zwitterion as well, indicating weak intermolecular interactions already at low concentrations but again proton *b* does not take part in this process (Figure 4.40B. However, one thing is in contrast to the *L*-alanine zwitterion: the loss in signal sharpness is by far not as distinctive as for **2.6**. This difference points to the assumption that the self-assembled structures of **2.7** are more defined due to their stronger interaction based on the preorganized monomer.

Finally the interpretation of the ^{1}H,^{1}H-NOESY-NMR spectrum of **2.7** leads to the same conclusion as already discussed for the *L*-alanine zwitterion (Figure 4.41). The NOE-contact between the protons *b* and *c* clearly supports the assumption that proton *b* does not take part in the complexation process between the carboxylate and the binding site. Also the fact that there is no NOE-contact between the protons *a* and *d* results in the same structural characteristics found for **2.6**. The NOE-contact between the CH_2 protons of the amino acid side chain and the proton *b*

shows that at least one of the CH_2 protons points at proton *b*. This structural characteristic is best explained by the proposed intramolecular hydrogen bond between the OH group and the carbonyl oxygen. Molecular mechanics calculations proved that in case of a hydrogen bond between the OH group and the carboxylate group the CH_2 protons point completely away from proton *b* (Figure 4.40C).

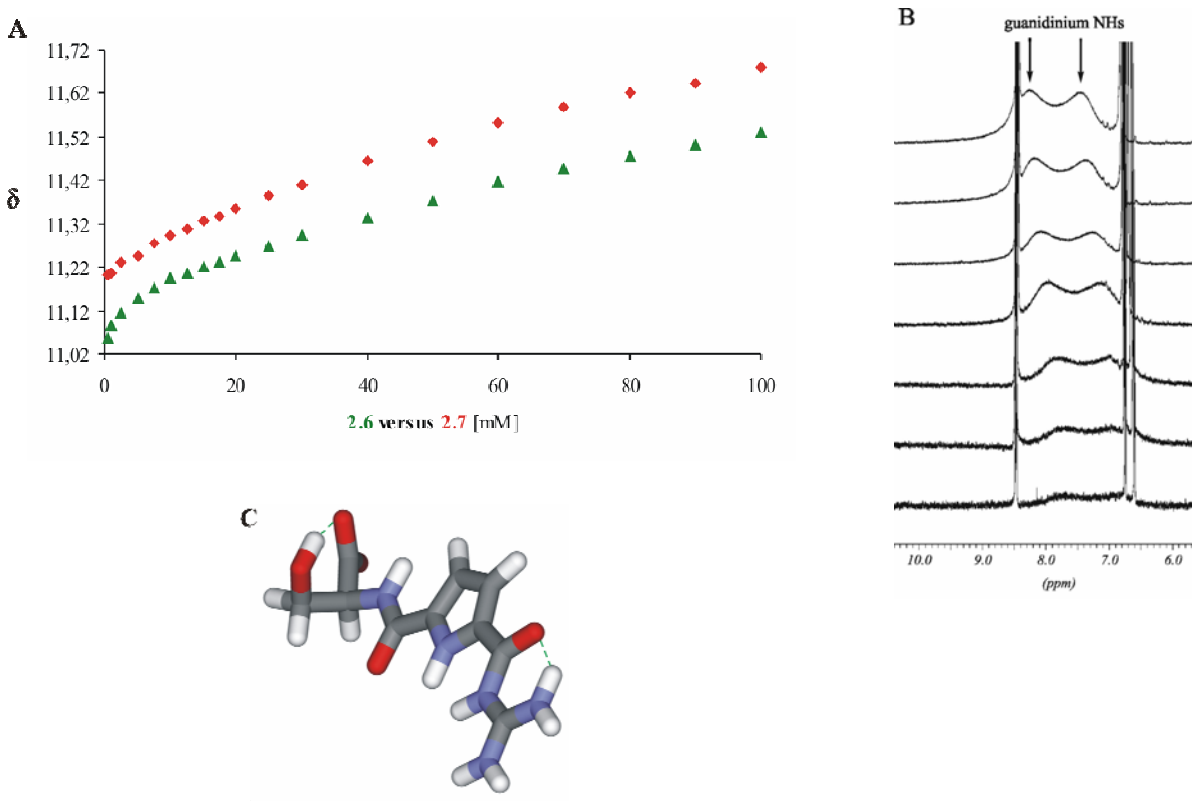

Fig. 4.40 *A) Shift of the guanidinium amide NH proton illustrating the difference between the L-alanine (green) and the L-serine (red) zwitterion; B) Signal splitting of the guanidinium NHs in* ***2.7*** *(from bottom to top: c = 5, 10, 20, 40, 60, 80, 100 mM in DMSO-d_6); C) minimized structure of 2.7 with energetically disfavouring hydrogen bond to the carboxylate group (hydrogen bonds are illustrated in green; MacroModel 8.0, Amber* force field, GB/SA water solvation model, 10,000 steps).*

In conclusion both zwitterions **2.6** and **2.7** are quite similar according to their behaviour in solution. The NMR data obtained from NMR dilution, COSY and NOESY experiments show three important things: 1) weak intermolecular interactions occur already at low concentrations; 2) amide NH proton *b* does not take part in the association process; 3) the solubility of both compounds exceeds the solubility of the glycine derivative. But one speciality distinguishes the *L*-serine zwitterion: due to one intramolecular hydrogen bond between the OH group of the amino acid side chain and the carbonyl oxygen the whole monomer is more rigid. This preorganized

structure is reflected in a better self-association leading to NMR shifts to lower field for the guanidinium amide NH *b* in comparison to the *L*-alanine derived zwitterion.

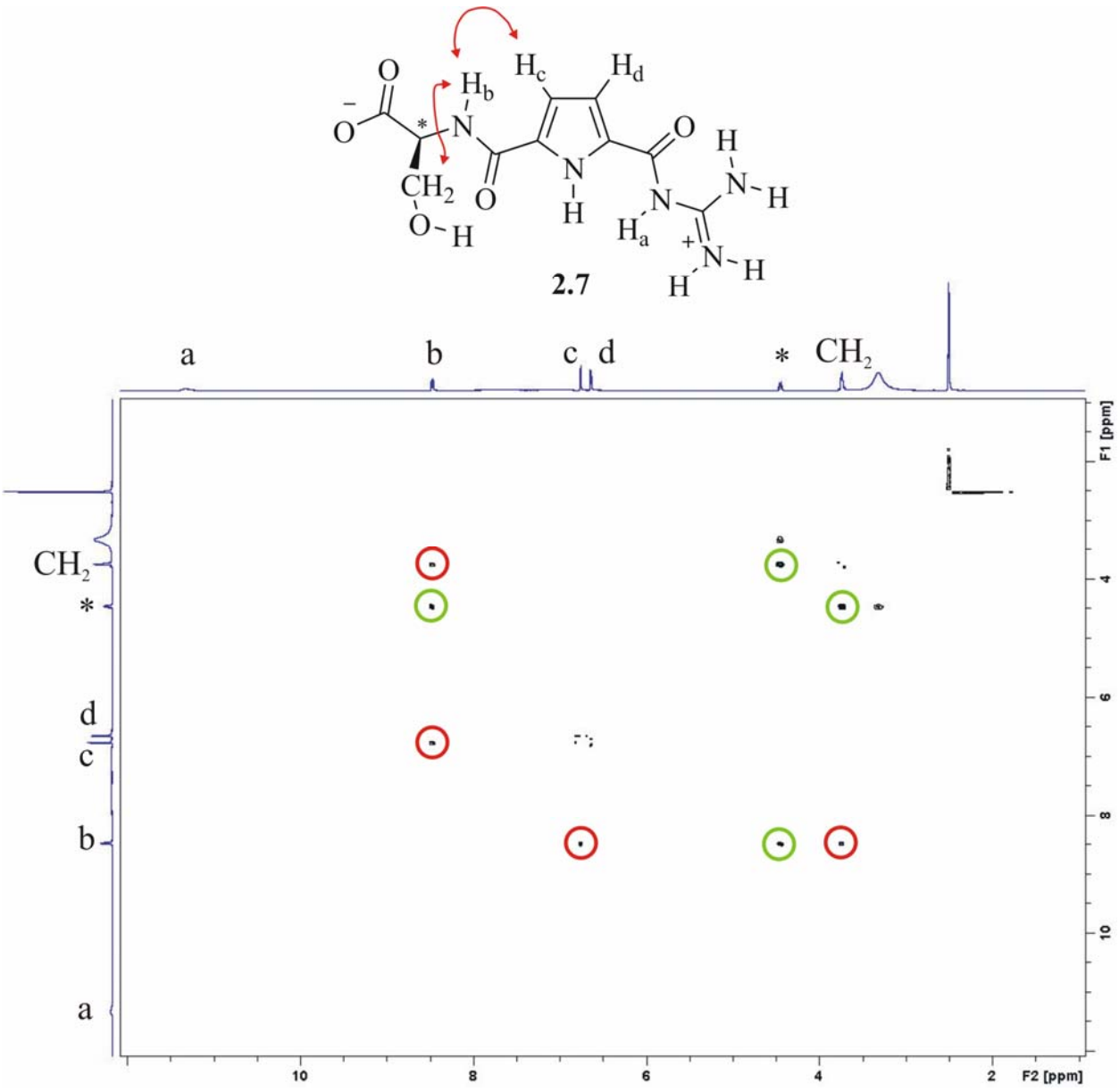

Fig. 4.41 *^{1}H,^{1}H-NOESY NMR spectrum of **2.7** (c = 15 mM in DMSO-d_6): the green circles represent the COSY-contacts; the red circles represent the NOE-contacts.*

With this information a first model for the structure of both chiral zwitterions **2.6** and **2.7** can be developed. The zwitterions **2.8** and **2.9** will not be included here due to the insufficient data concerning their behaviour in solution. Beside this lack of information also the influence of the aromatic amino acid side chain on the self-assembly of **2.8** and **2.9** might lead to different results.

The main driving force for the self-assembly is still the interaction between the ionic parts of the molecule. Normally the ion pairing process is due to a four-dentate interaction of the cationic

binding site with the carboxylate group as depicted in Figure 4.42A. But the amide NH group (proton *b*), which connects the amino acid to the pyrrole core, does not participate in the complexation. This fact suggests a three-dentate binding mode (Figure 4.42B). Concerning this fact, also the small shift of the guanidinium amide NH *a* has to be remembered. Normally this proton undergoes the strongest shift during the interaction with the carboxylate group. In case of the primal zwitterion **2.1** a shift change of more than $\Delta\delta \approx 4.5$ occurs upon dimerization. In case of a receptor-substrate interaction (i.e. peptide) smaller shifts are observed. But they still have a value of $\Delta\delta \approx 1$ (comparing the picrate salt of the receptor with the receptor-peptide complex). Since in the observed concentration range the shift changes of proton *a* are quite small ($\Delta\delta = 0.43$ for **2.6**; $\Delta\delta = 0.47$ for **2.7**) a participation of this proton in the complexation of a carboxylate group is rather improbable. Therefore the signal shift is most likely indirectly induced. This assumption leads then to a bi-dentate binding mode between the carboxylate and the guanidinium group as illustrated in Figure 4.42C.

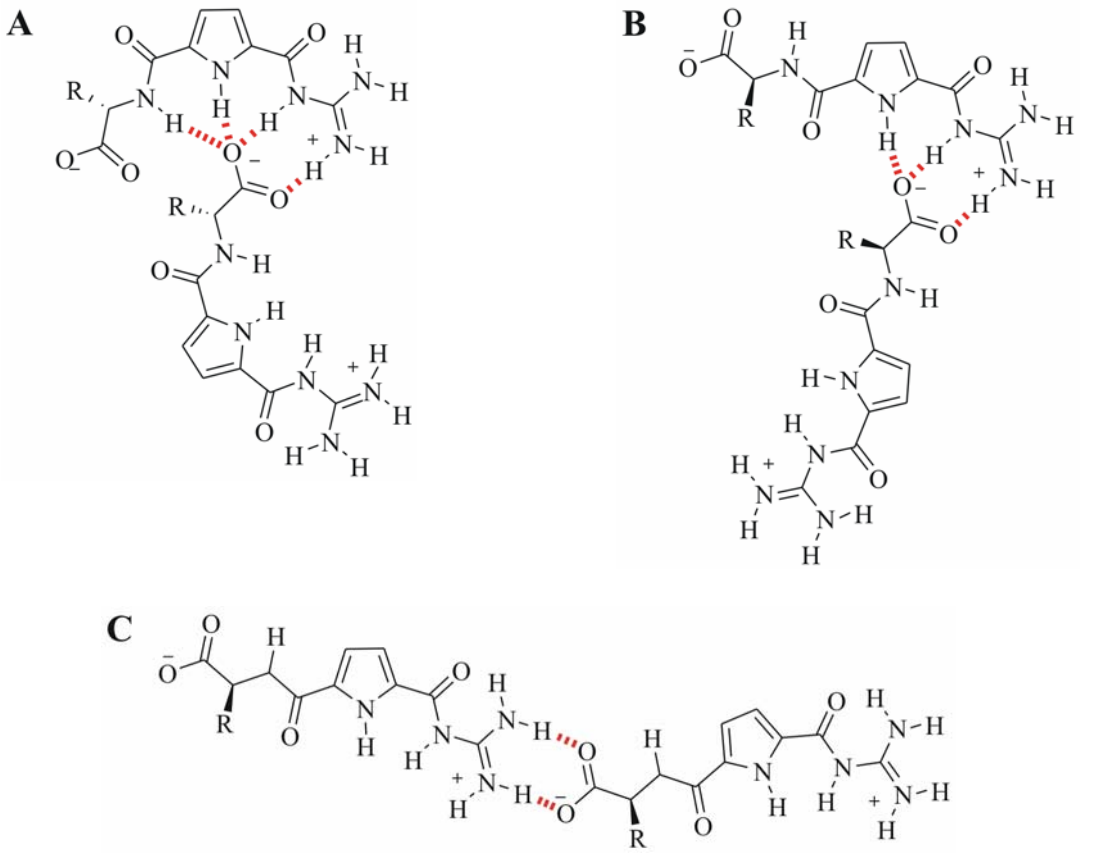

Fig. 4.42 *Possible modes of complexation of the carboxylate group: A) four-dentate with U-shaped binding site; B) three-dentate with one additional hydrogen bond from the pyrrole NH; C) bi-dentate in analogy to simple guanidinium cations.*

A second fact points to the formation of a bi-dentate ion pair. Comparing the complexation induced shift of the guanidinium NH protons of a three- or four-dentate binding mode with the bi-dentate mode shows that the latter one results in a far smaller shift. In case of the primal zwitterion **2.1** the signal of the guanidinium NH protons splits and leads to a maximum of $\Delta\delta = 1.5$ at lowest concentrations. Receptor-substrate complexes, representing the three-dentate binding mode, also lead to comparable values. But the signal split just reaches values of $\Delta\delta = 0.7$ and 0.8 in case of **2.6** and **2.7**, respectively, at a concentration of 100 mM. This small change points to a weak ion pair formation. Interestingly the signal splits although a weak bi-dentate binding mode allows free rotation of the guanidinium group, resulting in one ^{1}H-NMR signal.[22] In case of the zwitterions **2.6** and **2.7** another interaction seems to exert influence on the self-assembly, already at low concentrations. Most likely intermolecular π-stacking between the aromatic parts of the monomers hinders the rotation in a certain manner. But this point will be discussed later in more detail. Due to the uncomplexed end groups resulting from the bi-dentate binding mode the formation of longer oligomers should be possible. Hence, these oligomers will be in a quick equilibrium with the smallest structures due to the weak binding mode.

In conclusion the NMR data point to the formation of dimers and oligomers, respectively, based on the intermolecular, bi-dentate interaction of the charged end groups of **2.6** and **2.7**. This result is quite different to the common binding mode of guanidiniocarbonyl pyrroles which complex a carboxylate group with at least three hydrogen bonds. This bi-dentate binding mode is only possible if the zwitterion is rather rigid, which prevents intramolecular ion pairing, or some external influence hinders the formation of discrete dimers.

4.2.3 Results from the AFM experiments

Since the NMR samples of **2.6** and **2.7** show a strong *Tyndall* effect the aggregation of larger structures has to be assumed. Although the solutions of **2.8** and **2.9** did not show any *Tyndall* effect at first the formation of larger particles needs also to be assumed due to the sudden precipitation of a crystalline solid. Therefore, in cooperation with V. Stepanenko and Prof. Dr. F. Würthner (Institute of Organic Chemistry, University of Würzburg), AFM experiments were performed with freshly prepared solutions of all four zwitterions in DMSO. Table 4.5 summarises the data concerning the dimension of the observed particles, also including the data for the sample preparation.

Tab. 4.5 *AFM data concerning the dimension of the observed particles including sample preparation (diameter measured at half-height).*

	2.6 (*L*-Ala)	**2.7 (*L*-Ser)**	**2.8 (*L*-Phe)**	**2.9 (*L*-Tyr)**
number of particles analysed	105	57	68	51
mean diameter [nm]	25	17	16	31
mean height [nm]	3.9	3	4.2	3
sample surface	Si wafer	Si wafer	mica	mica
spin coating [rpm]	8000	4000	5000	4000
sample concentration [mM]	5	5	5	5

In all cases spherical particles were observed. The mean diameter of the particles was not in the same size range as the height of the objects. This result points to the formation of hollow spheres. In other words, the amino acid derived zwitterions **2.6** to **2.9** seem to self-assemble into vesicles. During the sample preparation and therefore within contact to the surface the vesicles get distorted with formation of the observed pancake-like structures. Micelle formation can be ruled out due to the fact that a micellar structure would lead to height and diameter values within the same range. Figure 4.43 shows an assortment of representative images with a general overview of the observed structures and an appropriate section plot.

First experiments with the *L*-alanine and *L*-serine derived zwitterions on mica surface lead to poor results. No clear data about the height and the diameter could be achieved. Changing to a surface with lower polarity, like Si wafer, resulted in reproducible data. In contrast to this the vesicles based on monomers with aromatic side chains are more stable and keep their structure also on mica. This different behaviour is most likely based on the stronger interaction of the aromatic moieties inside the membrane. Yet another difference can be observed which is most likely based on the polarity of the amino acid side chain. Zwitterions **2.7** and **2.9** have both free hydroxyl groups in the side chain. In comparison to their derivatives without free hydroxyl groups their height is smaller (**2.7**, **2.9**: *ca*. 3 nm; **2.6**, **2.8**: *ca*. 4 nm). This might be due to a stronger interaction between the hydroxyl function and the surface. So two facts have to be considered for the interpretation of the results: 1) aromatic side chains yield more stable structures most likely due to efficient π-stacking interactions between the monomers and 2) the more polar the side chain is, the stronger the interaction is with polar surfaces resulting in lower heights. Additionally, since the self-assembled vesicles are based on rather soft materials the interaction with the

AFM tip also leads to a reduction of the height.[23] Therefore one can estimate that the real height of the vesicles is about 2-3 nm bigger.

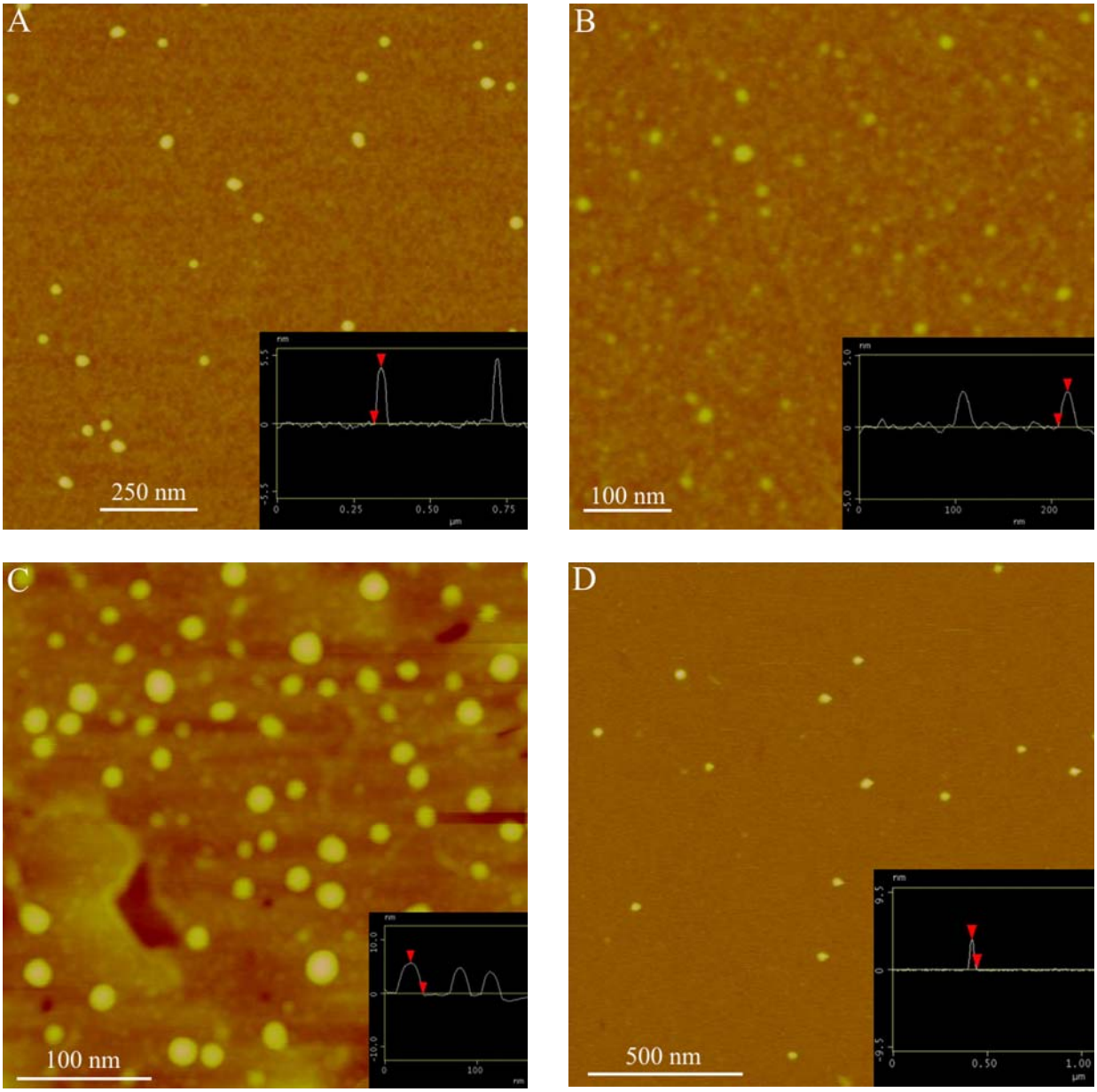

Fig. 4.43 *AFM height images of A) L-alanine zwitterion; B) L-serine zwitterion; C) L-phenylalanine zwitterion; D) L-tyrosine zwitterion; reprinted in part with permission from Org. Lett.* ***2008****, 10, 1469-1472. Copyright (2008) American Chemical Society.*

In conclusion all four zwitterions most likely self-assemble into vesicles. It could be shown that both the polarity of the amino acid side chain and the membrane rigidity have an influence on the deposited structures due to the interaction with the surface.

4.2.4 Results from DLS and TEM experiments

Up to now these two analytical methods were only used for the examination of the *L*-alanine derived zwitterion. In order to confirm the formation of vesicles based on **2.6** DLS experiments were performed in cooperation with Dr. F. Gröhn (Max Planck Institute for Polymer Research, Mainz). For a 5.55 mM solution of **2.6** particles with a hydrodynamic radius of r_H = 20-25 nm were observed. In addition some even larger aggregates with a size of some hundred nm could be detected although a species of this size was never observed by AFM. A second time dependent measurement demonstrated the stability of the particles over a time periode of at least 80 hours. The dimensions of the particles are larger compared to the AFM data. This is most likely based on the fact that the AFM data is collected in the dry state, which leads to a shrinking of the vesicles. Unfortunately all attempts to use SANS for a further investigation of the vesicle membrane failed due to an insufficient contrast in experiments.

As a last experiment TEM images were taken of the self-assembled structures of the *L*-alanine derived zwitterion in cooperation with Dr. X. Zhang, Prof. Dr. F. Würthner (Institute of Organic Chemistry, University of Würzburg) and Prof. Dr. G. Krohne (Theodor Boveri Institute for Life Science, University of Würzburg). A freshly prepared solution of **2.6** (5 mM in DMSO) was placed on 400-mesh formvar copper grid coated with carbon. After removal of remaining solvent the sample was negatively stained with aqueous uranyl acetate solution. Figure 4.44 shows an image of a representative vesicle of **2.6**. The vesicle has an estimated diameter of about 70 nm and a membrane thickness of 2-3 nm. Hence, the diameter of the vesicle is even larger compared to the data obtained from the DLS experiments. This result is very likely based on a swelling process during the sample preparation. Since the vesicles are formed in a DMSO solution the inner part of the vesicle is still filled with DMSO, after removal of the organic solvent. Subsequently use of water during the staining process leads to the permeation of water molecules into the vesicle resulting in an increasing solvent volume inside the vesicle. This process finally results in the destruction of the vesicles. First damages can be seen in the upper left part of the vesicle in Figure 4.44.

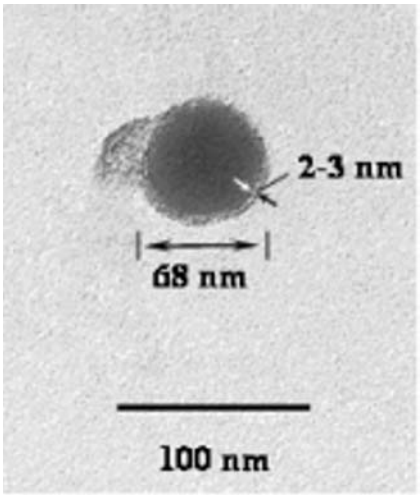

Fig. 4.44 *TEM image of a self-assembled vesicle based on **2.6**; on the left side a rupture can be seen due to prolonged exposure to water.*

According to literature[24] TEM images of soft vesicles show a weak contrast compared to hard vesicles. In case of collapsed vesicles the thickness of the resulting particles is almost constant from the periphery to the centre. This is in accordance to the AFM results from the height measurements which do not show any deviation in height within one particle. As discussed above due to the permeation of water into the vesicle interior also uranyl acetate is transported into the vesicle. Since the organic solvent DMSO has a strong affinity for the uranyl cation the concentration of the staining agent inside the vesicle is higher than in the membrane itself. This effect leads to an inverse contrast between the darker inside area and the membrane.

In conclusion both analytical methods prove the existence of vesicles on surfaces and, in case of DLS, also in solution. Due to different surrounding media and sample preparation (AFM: dry state; DLS: pure solvent; TEM: solvent mixture and finally dry state) a first examination concerning the stability of the membrane was possible. Although a more detailed examination of the membrane is not possible due to insufficient data from SANS a proposed model for the self-assembly of the *L*-alanine and *L*-serine derived zwitterion can be given.

4.2.5 Proposed model for the self-assembly of *α*-amino acid derived zwitterions 2.6 and 2.7

With the information obtained about the behaviour of **2.6** and **2.7** in solution and on a surface, the mode of self-assembly for these two *α*-amino acid derived zwitterions can be discussed. At first on the molecular level the zwitterion building blocks do not seem to form discrete dimers as suggested in Figure 4.45A. Several results from the NMR experiments point to the formation of linear aggregates based on a weak, intermolecular bi-dentate binding between the charged end

groups of the monomers. Figure 4.45B depicts the more realistic structure of dimeric **2.6**. In case of the *L*-serine derived zwitterion the intramolecular hydrogen bond between the amino acid side chain and the carbonyl oxygen increases the molecular rigidity. This is a special case which leads to a slightly better association due to the reduced flexibility of the carboxylate group. But in principle the depicted structure of **2.6** in Figure 4.45B can also be used for **2.7**.

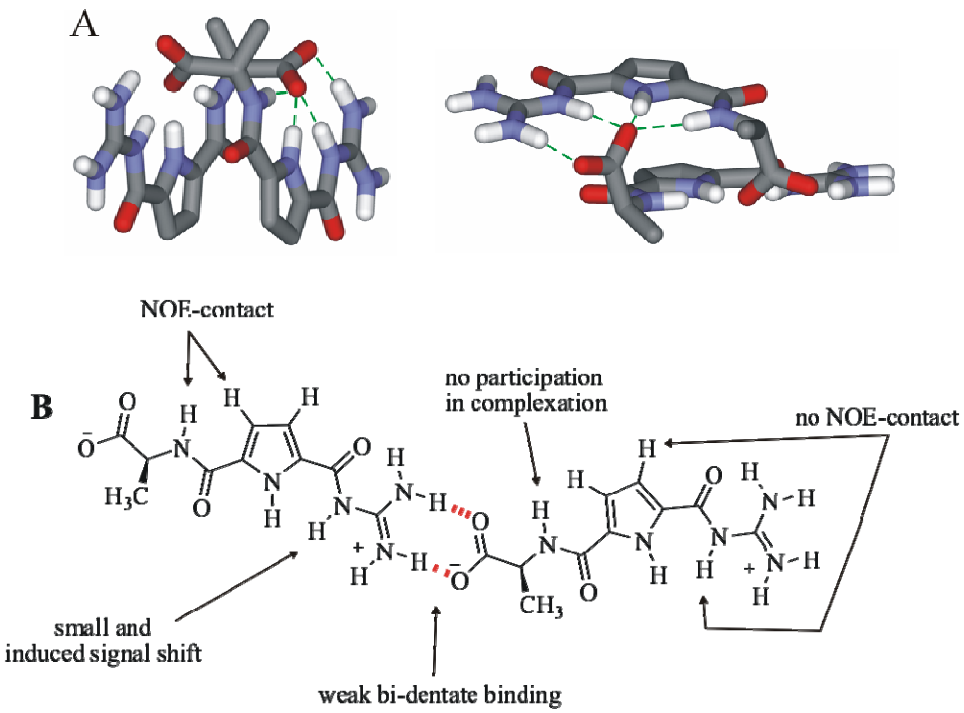

Fig. 4.45 *A) A discrete dimer of **2.6** would lead to different NMR data; the participation of all four hydrogen bond donors could be ruled out; B) a more realistic mode of self-assembly of **2.6** according to the experimental data; reprinted in part with permission from Org. Lett. **2008**, 10, 1469-1472. Copyright (2008) American Chemical Society.*

Now the last point of discussion concerns the signal splitting of the guanidinium NH protons. As already mentioned another influence in terms of a third non-covalent interaction leads to the hindered rotation of the guanidinium group. Most likely intermolecular aromatic or hydrophobic interactions lead to stack-like structures as depicted in Figure 4.46B. These obviously rather strong stacking interactions prevent the rotation of the guanidinium group to a certain degree resulting in the split of the NMR signal. Since the zwitterions are rather planar, except for the amino acid side chain, such an aromatic stacking interaction might also be supported by ionic interactions between the stacks. Now the results of both AFM and TEM experiments confirm this association model. The TEM image in Figure 4.44 shows a membrane thickness of about 3 nm. The AFM images give the height of the complete vesicle. In other words this height value has to be divided by two. Taking again into account that the realistic height of the vesicle is

about 2-3 nm bigger than observed by AFM, thisleads also to a value of about 3 nm for the vesicle membrane. This value for the membrane thickness points to the formation of linear dimers of **2.6** or **2.7** which stack together via aromatic interactions as already discussed. Additional molecular mechanics calculations of a membrane segment based on 64 monomers of **2.6** confirm the dimension of the dimeric stacks with a value of 2.7 nm in length and a kink of 38 ° (MacroModel 8.0, Amber* force field, GB/SA water solvation model, minimization) (Figure 4.46A, B and C). Additionally, all methyl groups are presented at the same side which results in a steric bulk, especially in the middle part of the membrane. This fact, together with the tilt of each dimer, induces a membrane curvature. In Figure 4.46D the whole mode of self-assembly is presented schematically.

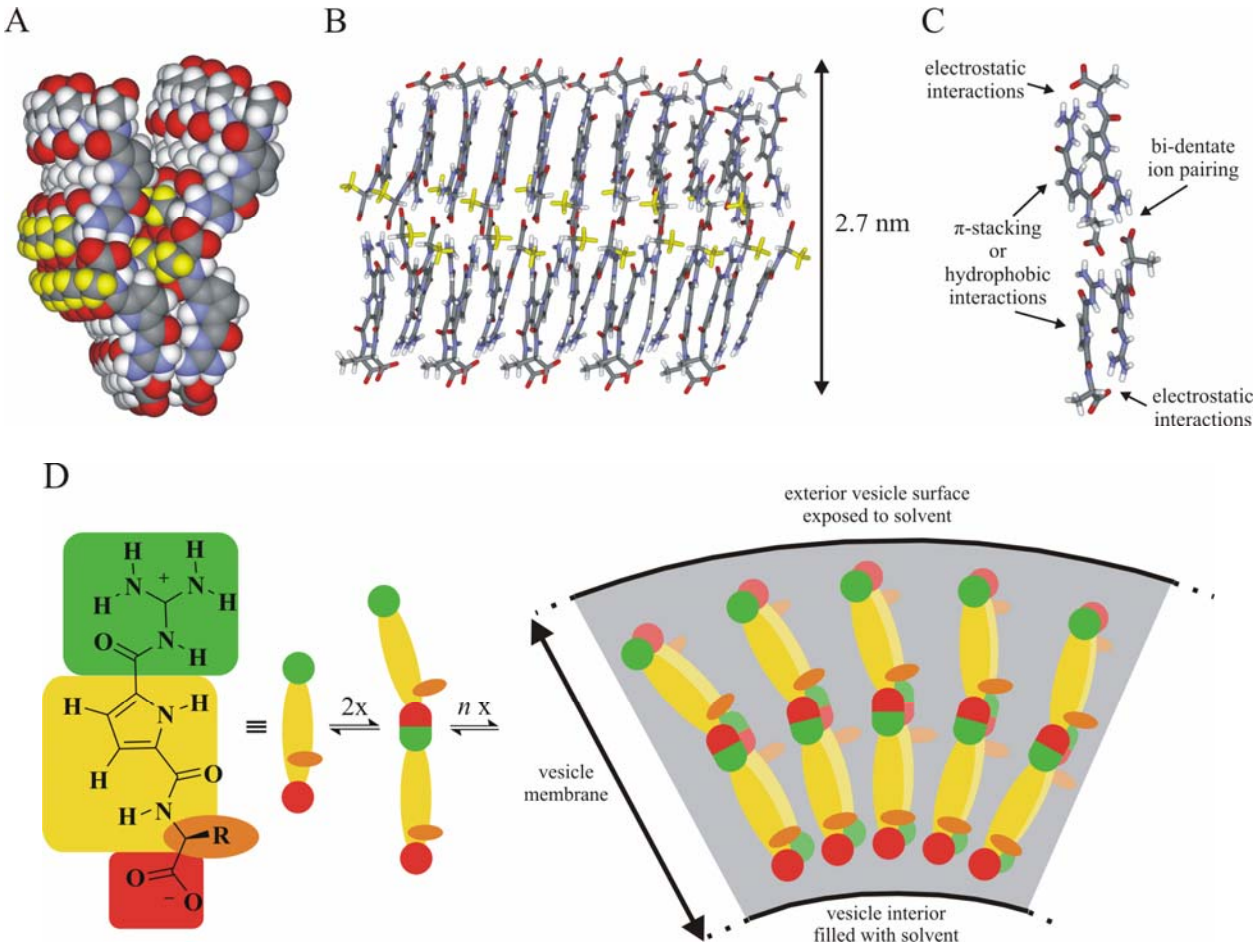

Fig. 4.46 *A) Vesicle membrane segment based on 40 monomers of **2.6** (the methyl groups are highlighted in yellow); B) side view of membrane segment showing the stacked dimers in their antiparallel orientation; C) tetrameric **2.6** showing the distinct intermolecular interactions; D) schematical representation of the self-assembly of chiral zwitterions **2.6** and **2.7** (amino acid side chain is illustrated in orange); reprinted in part with permission from Org. Lett. **2008**, 10, 1469-1472. Copyright (2008) American Chemical Society.*

With this mode of self-assembly the vesicle formation is in very good agreement with the experimental data. Due to the allover weak interactions between the monomers it is also reasonable that the formed vesicles are soft materials and are pretty sensitive to external stimuli. But in comparison to other vesicle forming monomers the chiral zwitterions are fairly small. So the instance that these small molecules are able to form such big structures is very astonishing.

4.2.6 Conclusion and outlook

In the second part of this thesis four new derivatives of the primal zwitterion were presented. With the introduction of chiral centres into the zwitterion structure by incorporation of α-amino acids, completely new features concerning the self-assembly were observed. Beside the enhanced solubility compared to known achiral zwitterions also the mode of interactions is quite different to the behaviour of the zwitterions presented earlier. In case of the zwitterions with aromatic amino acid side chains (*L*-phenylalanine, *L*-tyrosine) a full examination was not possible due the formation of fine crystalline structures. Since this behaviour is also quite exceptional the future work should be focused on the specific formation of crystals which are suitable for X-ray diffraction experiments. In case of the zwitterions based on *L*-alanine and *L*-serine a far better examination was possible. The experimental data support a rather unusual binding mode in terms of bi-dentate interactions leading to linear dimers as smallest supramolecular structures. But the most surprising fact is that small molecules like **2.6** and **2.7** lead to the formation of large architectures like the observed vesicles. As these vesicles are rather soft materials the fortification of the membrane should be an important part in the future work.

4.3 Concluding remarks

The latter two sections of this thesis introduced and discussed a new class of supramolecular building blocks. Beside their varying binding mode and association strength these building blocks have one thing in common: the powerful ability to form defined supramolecular structures in polar solutions. In contrast to metal-ligand interactions, which represent an alternative for self-assembly in polar solutions, no heteroassociation takes place, but homoassociation of pure organic compounds. The self-assembly process is based on the mutual interaction of hydrogen-bond enforced ion pairs and delivers therefore enough association strength for stable, supermolecular structures in polar solutions. The design of these architectures benefits from the combination of one main driving force and one texturing force. This principle is suitable for programmable building blocks where you keep the ion pair formation as the main driving force under variation of the texturing force in terms of other moieties in the monomer. Since the derivatisation of

the main binding motive is rather simple, this new compound class offers a great number of new supramolecular structures with tailor-made features. In consequence to this fact the last section of this chapter will present some promising ideas.

4.4 Concepts for the syntheses of boxes, cages and new zwitterions

The last part of this chapter is mostly an introduction to future projects. Some ideas and first tries concerning the synthesis and the probable structure of new and fascinating supramolecular architectures are presented. The first part in this section introduces a concept for the preparation of more defined supramolecular structures based on the self-assembly of primal zwitterion **2.1**. The main focus will be on the dimerization of preorganized monomeric building blocks with less flexible spacers between the binding sites. The second part will describe the synthesis of a new derivative of the primal zwitterion based on the introduction of water-solubility enhancing groups in the periphery of the pyrrole core. The third part will introduce structural elements into the primal zwitterion, which are capable of aromatic stacking interactions. Therefore the number of non-covalent interactions used for the dimerization process would be increased. All ideas were primarily developed by molecular mechanics calculations (MacroModel 8.0, Amber* force field or MMFF, Monte Carlo conformational search or minimization). Hence, the syntheses of all systems are based on the obtained results of foregoing theoretical work. In addition it should be noted that this section comprises all steps of syntheses except from the final deprotection of the binding motive. This will be part of future work.

4.4.1 Introduction of semi-flexible linkers for tailor-made boxes and cages

The formation of well-defined and hollow structures is a particular challenge in supramolecular chemistry,[25] since these nanometer-sized boxes and cages[26] can work as structural catalysts for reactions inside a supramolecular matrix.[27] In addition the strong tendency of zwitterion **2.1** to dimerize in aqueous solutions is another important point for the use of these nanostructures for biomimetic applications.[28]

All zwitterions discussed in the foregoing chapters are based on flexible linkers, which connect two or three binding motives. Depending on their length and chemical attributes the resulting monomers self-assemble into loops, cyclic dimers or larger structures like vesicles. Due to the flexibility of the linker the small aggregates lack of a defined structure in terms of interior volume and rigidity. The idea is now to decrease the degrees of freedom by the substitution of the flexible linker with semi-flexible linkers. The rigidity of the linker should result in a preorganiza-

tion of the monomer. In consequence to this the dimerization should lead to structures of defined volume at least in dilute solutions (Figure 4.47).

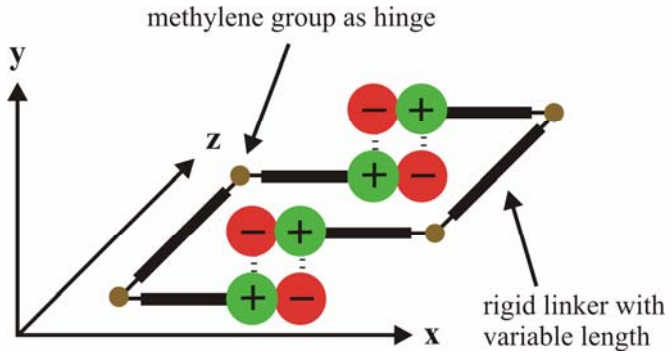

Fig. 4.47 *Dimerization of preorganized monomers illustrating the decrease of linker flexibility.*

In the beginning a fully protected zwitterion was needed, which has solubility enhancing groups in the periphery of the pyrrole core. These groups were necessary due to the rather poor solubility of the primal zwitterion in polar solvents. Hence, a pyrrole core which incorporates two ethyl groups in the positions 3 and 4 was used (Figure 4.48). The synthesis of the fully protected binding motive with solubility enhancing groups starts with the coupling of *N*-boc-guanidine **4.12** to the free acid **4.22**. Under standard reaction conditions (PyBOP as coupling reagent, NMM as base and DMF as solvent) fully protected zwitterion **4.23** could be obtained with a yield of 72 % after column chromatography.

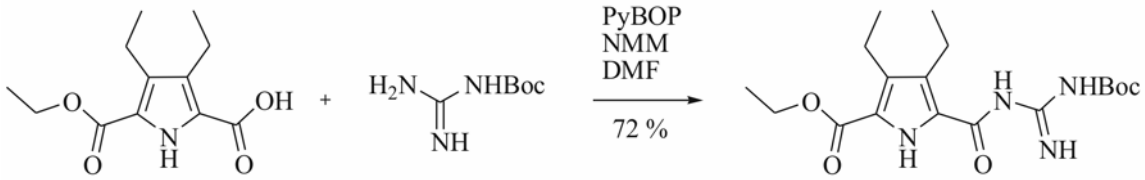

Fig. 4.48 *Synthesis of the fully protected zwitterion **4.23**.*

With the deprotected zwitterion derived from **4.23** first calculations were performed concerning the self-assembly of the smallest box. It consists of two zwitterionic binding motives, which are linked over the guanidino group by a short and semi-flexible spacer. The linker is composed of a simple benzene ring which incorporates two methylene groups as hinges in *para*-position. Figure 4.49 shows the theoretical result of the desired self-assembly.

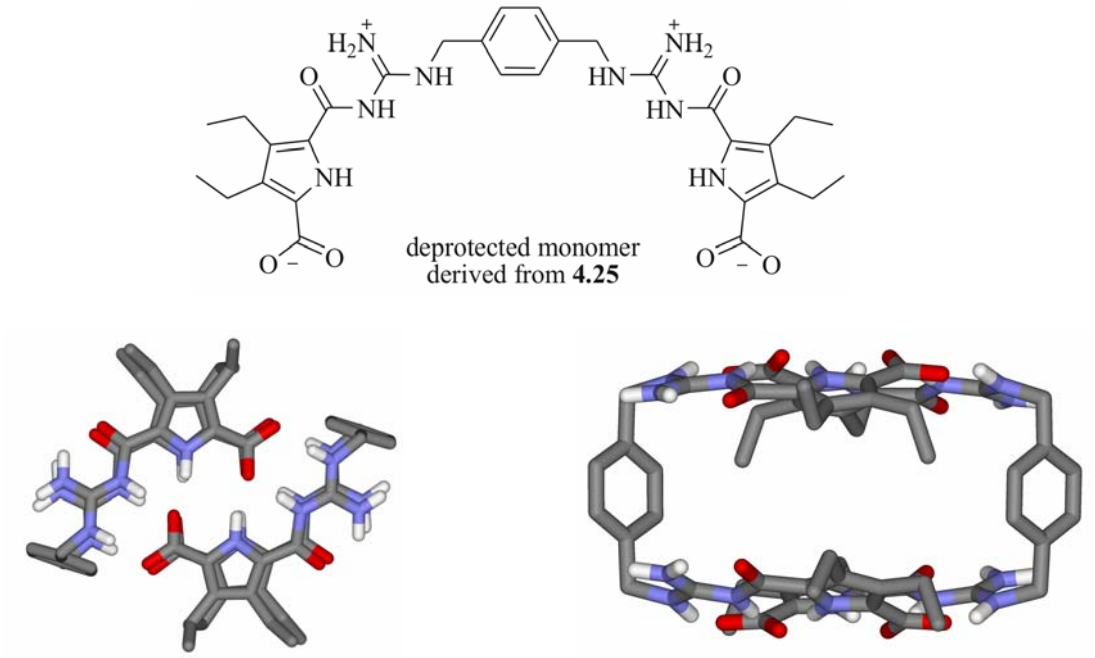

Fig. 4.49 *Top: deprotected monomer derived from* ***4.25****; small self-assembled box (left: side view; right: top view; non-polar hydrogens are omitted for clarity).*

Synthetically two routes are possible. The *Triflate route* is well established for the incorporation of alkyl linkers into the zwitterion by activation of the guanidino group with triflic anhydride. But, unfortunately, all attempts were in vain to attach the benzylic linker. In either case only the starting materials or the activated pyrrole compound could be reisolated. Therefore another route had to be developed. In contrast to the *Triflate route* now the guanidino group was used as nucleophile (Fig 4.50).

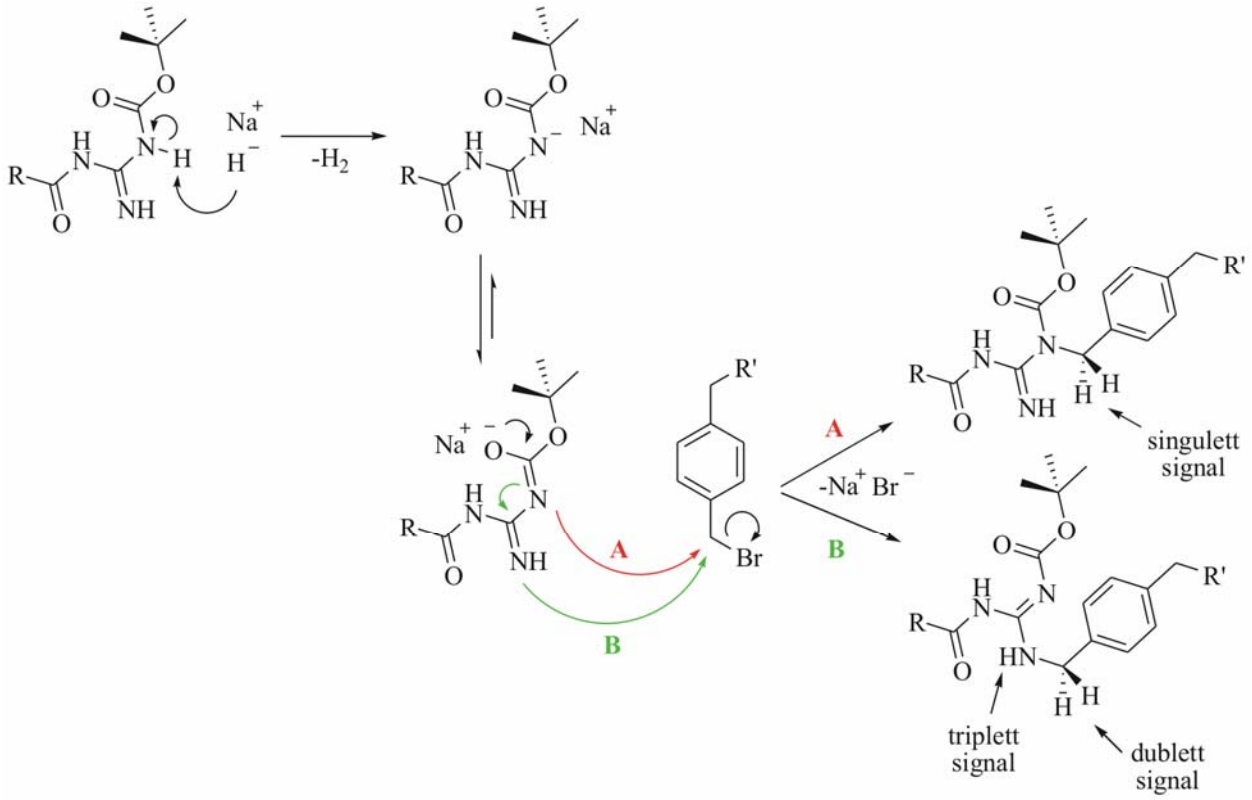

Fig. 4.50 *Possible reaction pathways of the nucleophilic substitution of the bromide substituent leading to the attachment of a benzylic linker to the protected guanidino group.*

Compound **4.23** was dissolved in DMF and deprotonated with sodium hydride.[29] Subsequent addition of the linker **4.24** in terms of *α*, *α´*-dibromo-*p*-xylene resulted in colour change of the solution from colourless to yellow. After stirring the reaction solution over night at room temperature TLC control detected no more dibromide linker. Then the solution was quenched with water and extracted with ethyl acetate. The crude product was purified by column chromatography yielding 71 % of pure product **4.25** as a colourless, fluffy powder (Figure 4.51).

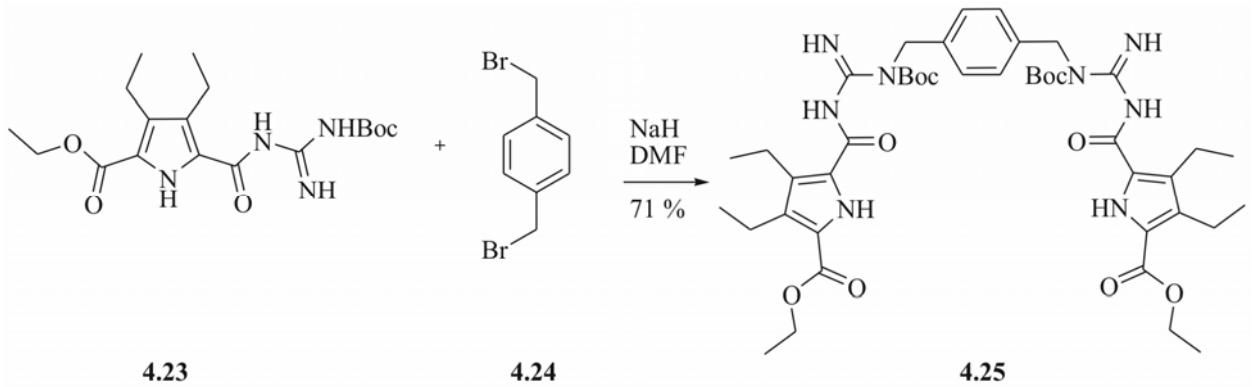

Fig. 4.51 *Synthesis of the fully protected monomer **4.25**.*

In conclusion the *Bromide route* is an efficient and, compared to the *Triflate route*, easy way to incorporate benzylic linkers into the fully protected zwitterion. Figure 4.52 shows the ^{1}H-NMR spectrum of compound **4.25**. Reaction pathway **A** could be confirmed since the proton signal of the benzyl CH_2 group is a singulett and does not couple with any other proton as it would be the case in route **B**.

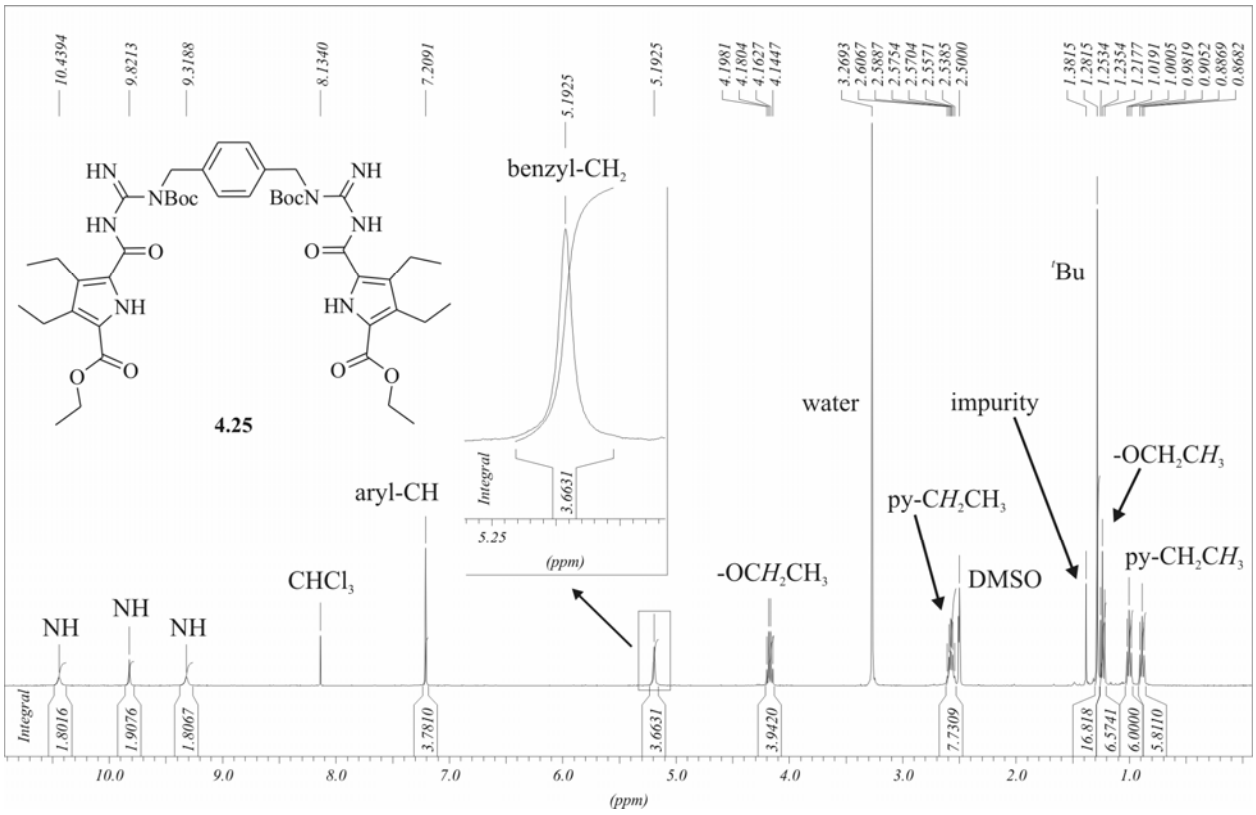

Fig. 4.52 *^{1}H-NMR spectrum of **4.25**; as solvent a mixture of DMSO-d_6 and $CDCl_3$ (v/v, 5/3) was used due to solubility problems in pure solvents and signal overlap.*

The synthesis of **4.25** proved that it is possible to connect two binding motives with a small and semi-flexible linker. Since the distance between the zwitterions should also be varied a new building block had to be developed. This multi-purpose zwitterion should incorporate both rigidity and semi-flexibility and additionally a reactive function, which can be further linked to other moieties. For the synthesis of this new building block the *Bromide route* was applied again to attach a bifunctional linker to the zwitterion. After deprotonation of **4.23** with sodium hydride in DMF, 4-nitro-benzylbromide was added to the solution resulting in a quick colour change from yellow to purple and finally deep red. The reaction solution was worked up in the same manner as for **4.25**. The main part of the pure product (75 %) was obtained by subsequent crystallisation of the crude product from methanol resulting in a colourless solid. The remaining crude product

was purified by column chromatography yielding further 10 % of pure product as colourless fluffy powder. The subsequent step was the reduction of the nitro group under a hydrogen atmosphere with palladium on charcoal as catalyst (Figure 4.53).

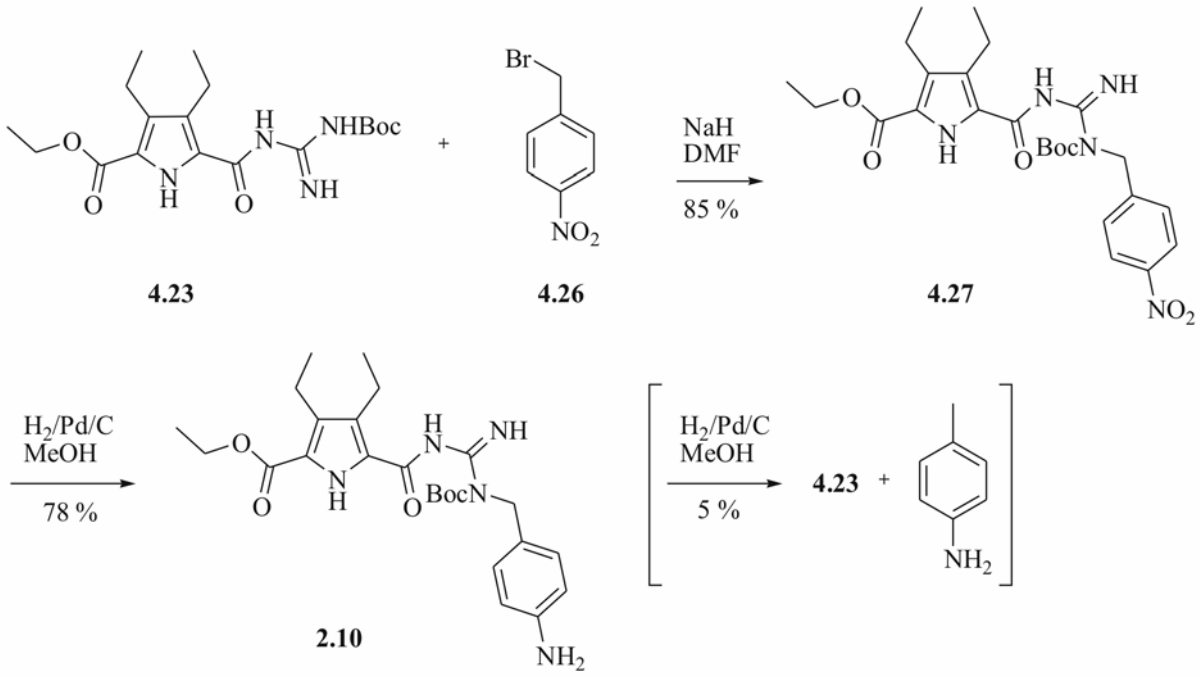

Fig. 4.53 *Synthesis of the fully protected multi-purpose zwitterion **2.10**.*

This reaction was performed in methanol resulting in three spots on the TLC plate with very different intensities. The largest spot could be identified as the desired product **2.10** with the free amino group in the *para*-position of the benzyl ring. The second spot was identified as the former starting material **4.23** which results from the hydrogenolysis of the benzyl substituent at the guanidino group. This side product had a yield of only 5 % (as confirmed by column chromatography) and can be recycled in the synthesis of compound **4.27**. The last spot remained on the starting line of the TLC plate. It is most likely *para*-toluidine as the byproduct of the hydrogenolysis of **2.10**. After work up of the reaction solution by filtration over a celite pad the crude product was purified by column chromatography yielding 78 % of the pure product **2.10** as slightly yellow powder. In conclusion, the synthesis of the fully protected multi-purpose zwitterion **2.10** could be achieved in two steps with an overall yield of 66 %. Figure 4.54 shows the ^{1}H-NMR spectrum of compound **2.10** in DMSO-d_6.

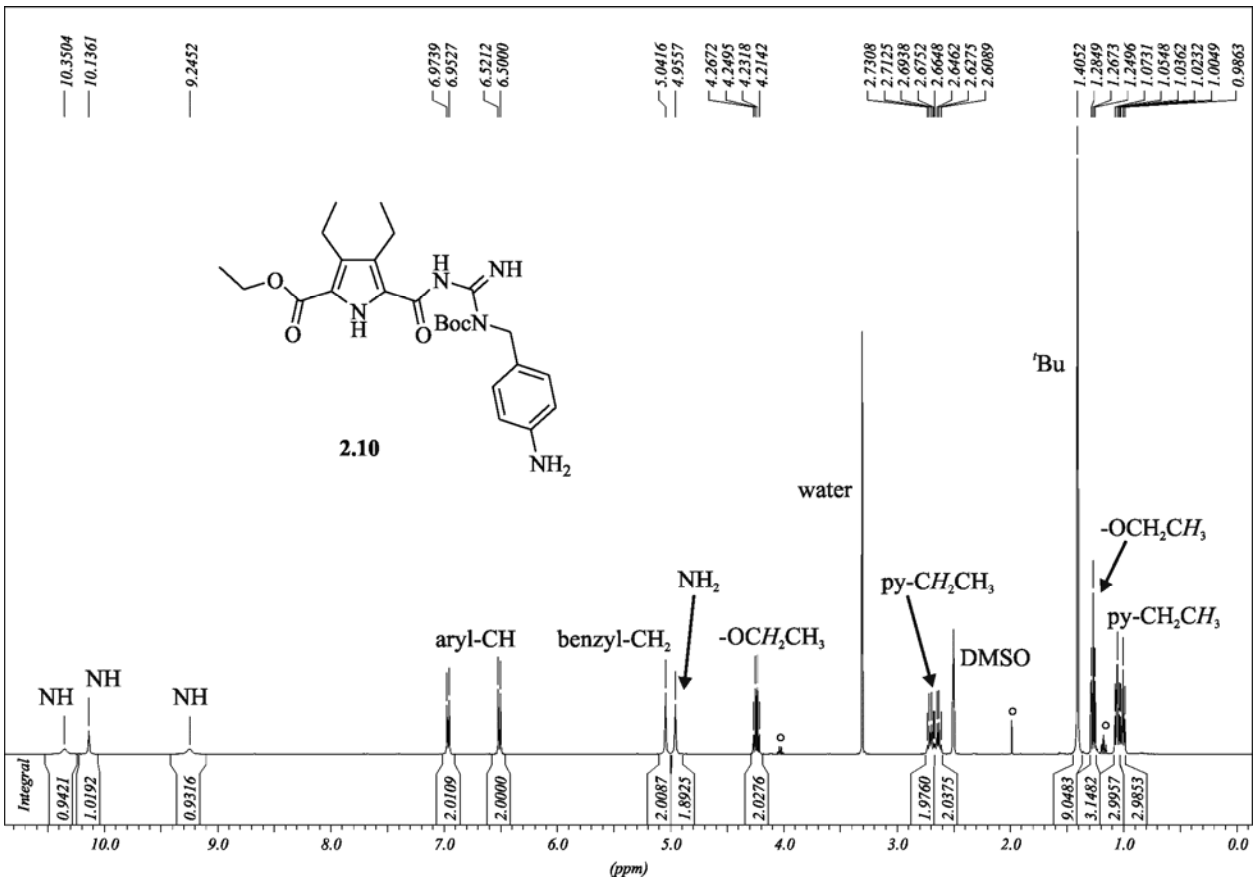

Fig. 4.54 *^{1}H-NMR spectrum of **2.10** in DMSO-d_6 (signals from ethyl acetate impurities are marked with °).*

The free amino group in compound **2.10** offers the possibility to link the binding motive to varying linkers. Here, the use of rigid dicarboxylic acids like terephthalic acid is feasible, whereas the resulting amide bonds might be too flexible for the desired purpose. Therefore the use of naphthalene tetracarboxylic acid dianhydride **4.28** was considered (Figure 4.55). This linker combines all necessary attributes in terms of rigidity and larger spacer length and provides interesting optical and electrochemical characteristics.[30]

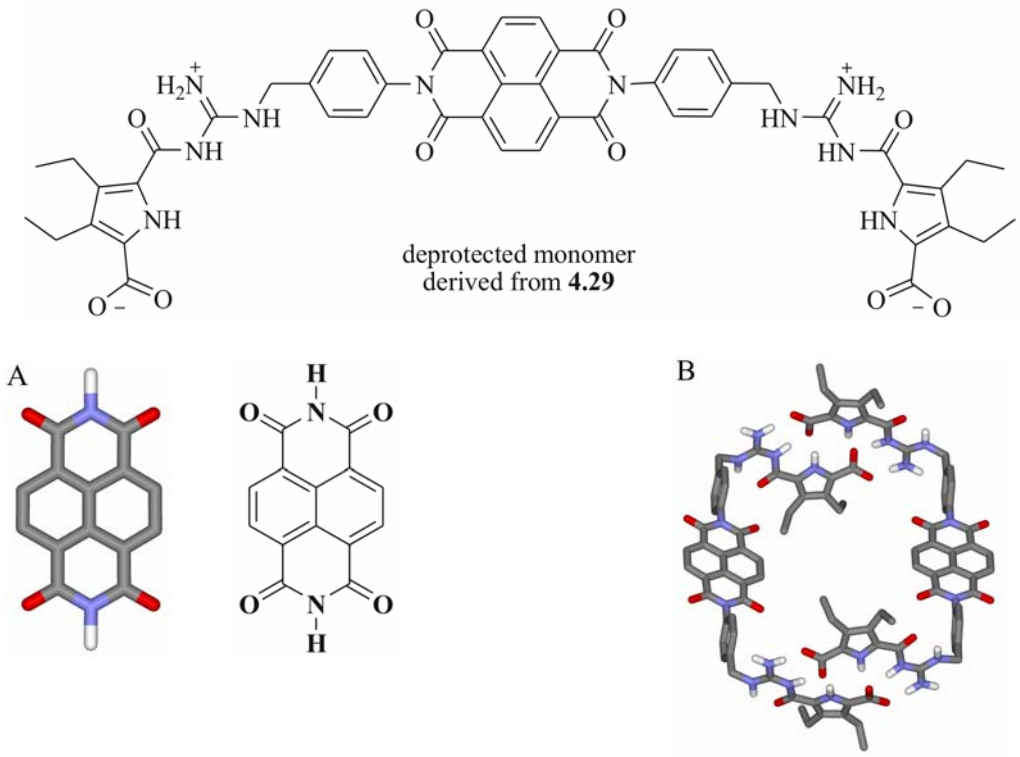

Fig. 4.55 *Top: deprotected monomer derived from **4.29**; bottom: A) Principle structure of a naphthalene diimide; B) molecular mechanics calculations of deprotected **4.29** show a well-defined dimer (non-polar hydrogens are omitted for clarity).*

The synthesis of **4.29** starting from compound **2.10** is quite simple. By stirring **2.10** and **4.28** in a ratio of 2:1 in DMF at 80 °C an imidization takes place.[31] Under the elimination of water the free amino group of compound **2.10** opens the anhydride of **4.28** and reacts to the thermodynamical stable imide. After a reaction time of 12 hours the solution was quenched with water and extracted with ethyl acetate. The resulting brown product **4.29** was dissolved in chloroform and precipitated with methanol resulting in a fine brown powder with 94 % yield. Figure 4.56 shows the ^{1}H-NMR spectrum of naphthalene bridged compound **4.29**. Beside the naphthalene derivative also larger and smaller spacers of this kind are conceivable. Through the application of perylene or pyromellitic anhydride the size of the expected box should be controlled. But one has to remember that with increasing size of the hydrophobic parts the solubility of the box in polar solvents decreases rapidly. Therefore linkers with functionalities which prevent stacking interactions or increase the hydrophilicity are necessary.[32]

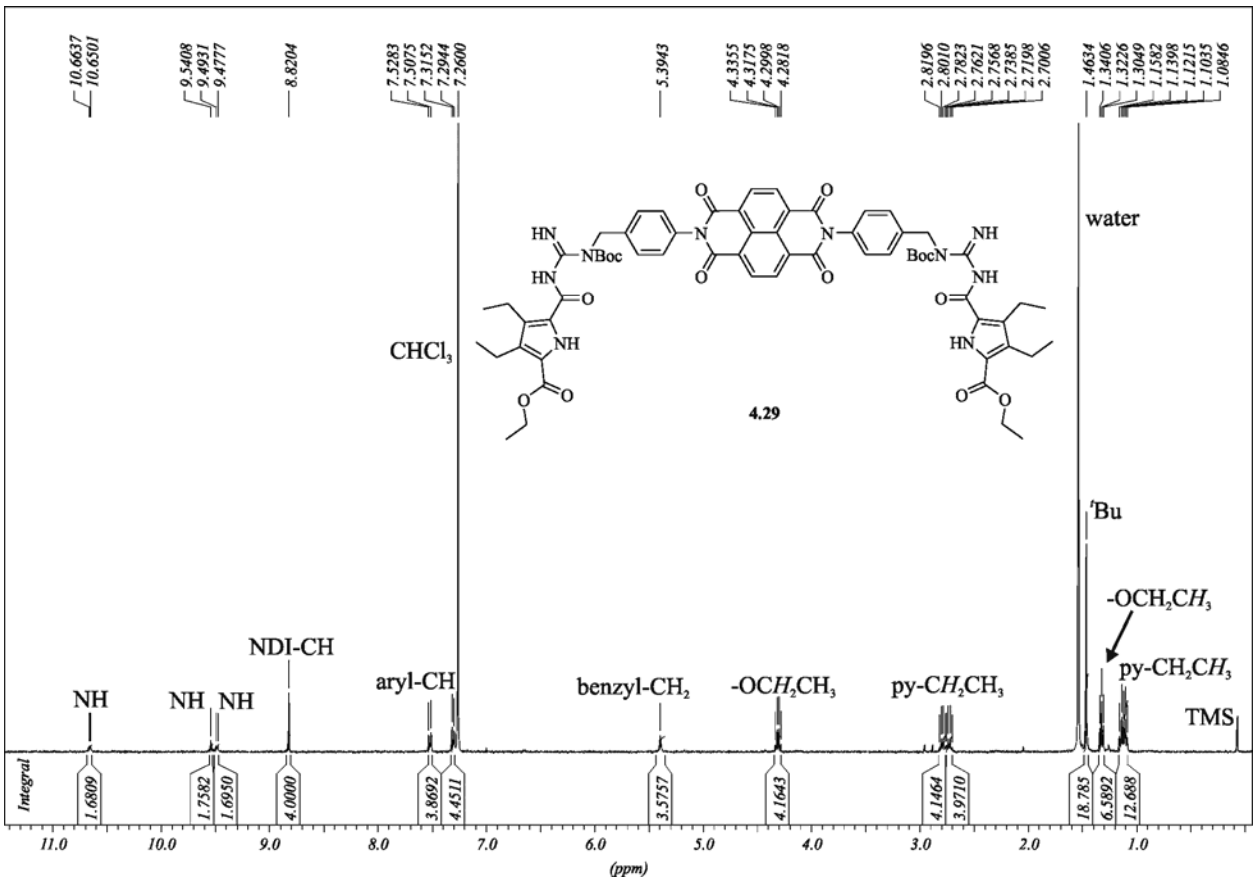

Fig. 4.56 *^{1}H-NMR spectrum of **4.29** (NDI = naphthalene diimide).*

Beside spacer types like **4.28**, which connect two binding motives, also the use of a C_3 symmetric spacer is possible. One example is cyanuric acid chloride **4.30**. Through the substitution of the chloride atoms a small and rigid linker connects three binding motives. Molecular mechanics calculations provided a well-defined cage for the self-assembly of such a building block (Figure 4.57).

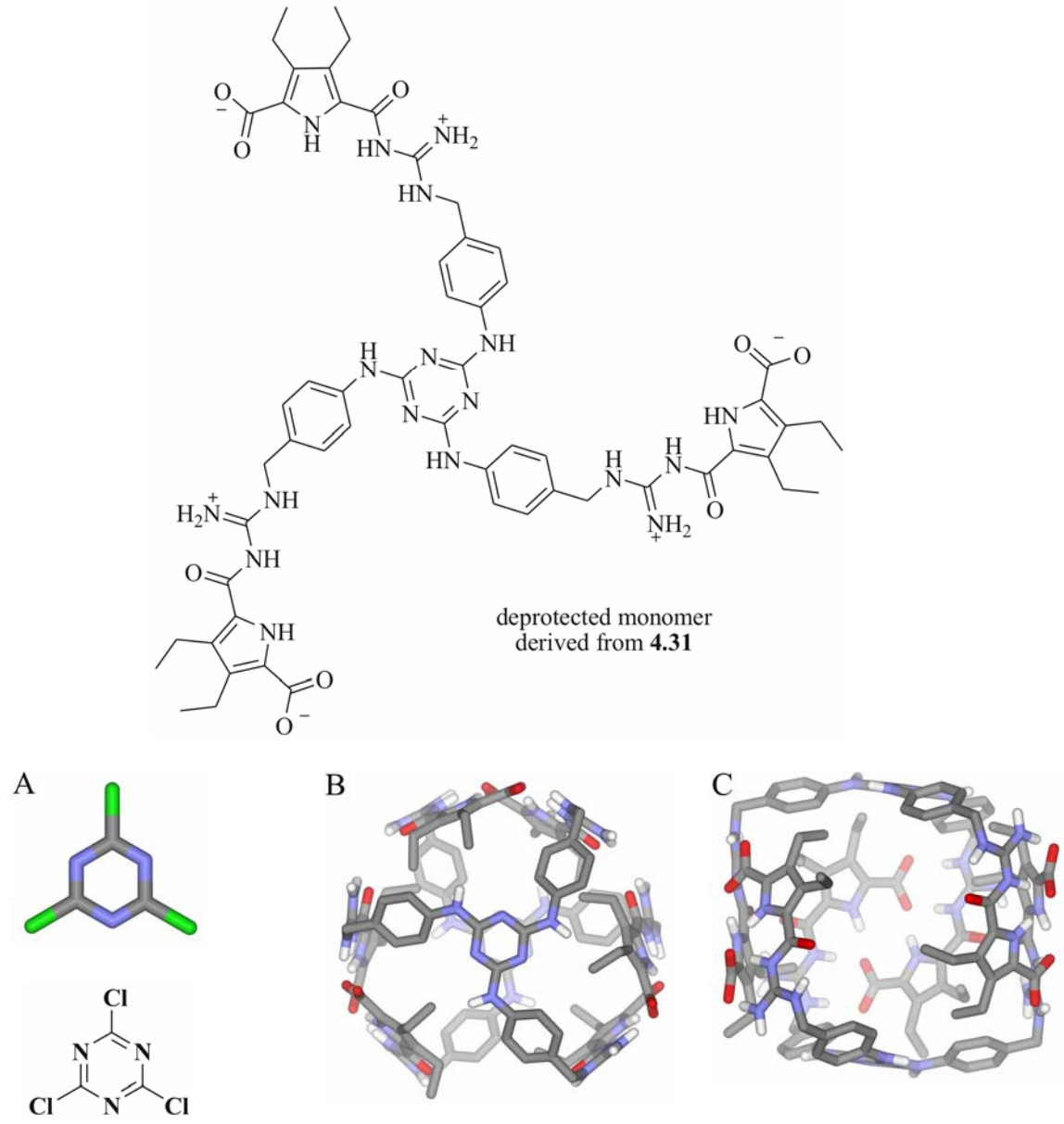

Fig. 4.57 *Top: deprotected monomer derived from **4.31**; bottom: A) Cyanuric acid chloride as C_3 symmetric linker; B) top view and C) side view of the self-assembled cage (non-polar hydrogens are omitted for clarity).*

Synthetically the preparation of this C_3 symmetric monomer was again rather simple. Multipurpose building block **2.10** was dissolved in THF. After addition of triturated potassium carbonate a solution of cyanuric acid chloride **4.30** in THF was added drop wise at room temperature. Subsequently the reaction suspension was stirred over night. The TLC plate of this solution showed three spots. The first spot is most likely the desired product. Although the ^{1}H-NMR spectrum shows the correct integrals and shifts for the product one can not be completely sure since no clear mass spectrum could be obtained trying ESI, MALDI, APCI and EI. Additionally, the ^{1}H-NMR spectra of the mono- and disubstituted product will look similar due to the symme-

try of each molecule. This could be proved by the second spot on the TLC which represents the product of the disubstitution. In this case both ^{1}H-NMR and MALDI-MS spectra were consistent. The only difference to **4.31** in the NMR spectrum was the downfield shifted signal of the NH protons directly bound to the linker core (δ_{NH} = 9.43). This is the result of the electron withdrawing effect of the last chloride substituent at the linker core. Compared to the same NH proton signal in the triple substituted product (δ_{NH} = 7.51) the signal shifts 1.92 ppm. Additionally, according to literature[33] mono-substituted triazines are always prepared at low temperatures (≤ 0 °C) and with equimolar ratios of cyanuric acid chloride and the corresponding amine in order to prevent higher substitutions. In case of **4.31** the ratio of the starting materials was 1:3 and the temperature was > 20 °C. But a definitive evidence for the triple substitution still has to be obtained. The last spot on the TLC plate was the starting material **2.10**. Figure 4.58 shows the ^{1}H-NMR spectrum of the presumed triple substituted product **4.31** according to the first spot on the TLC plate.

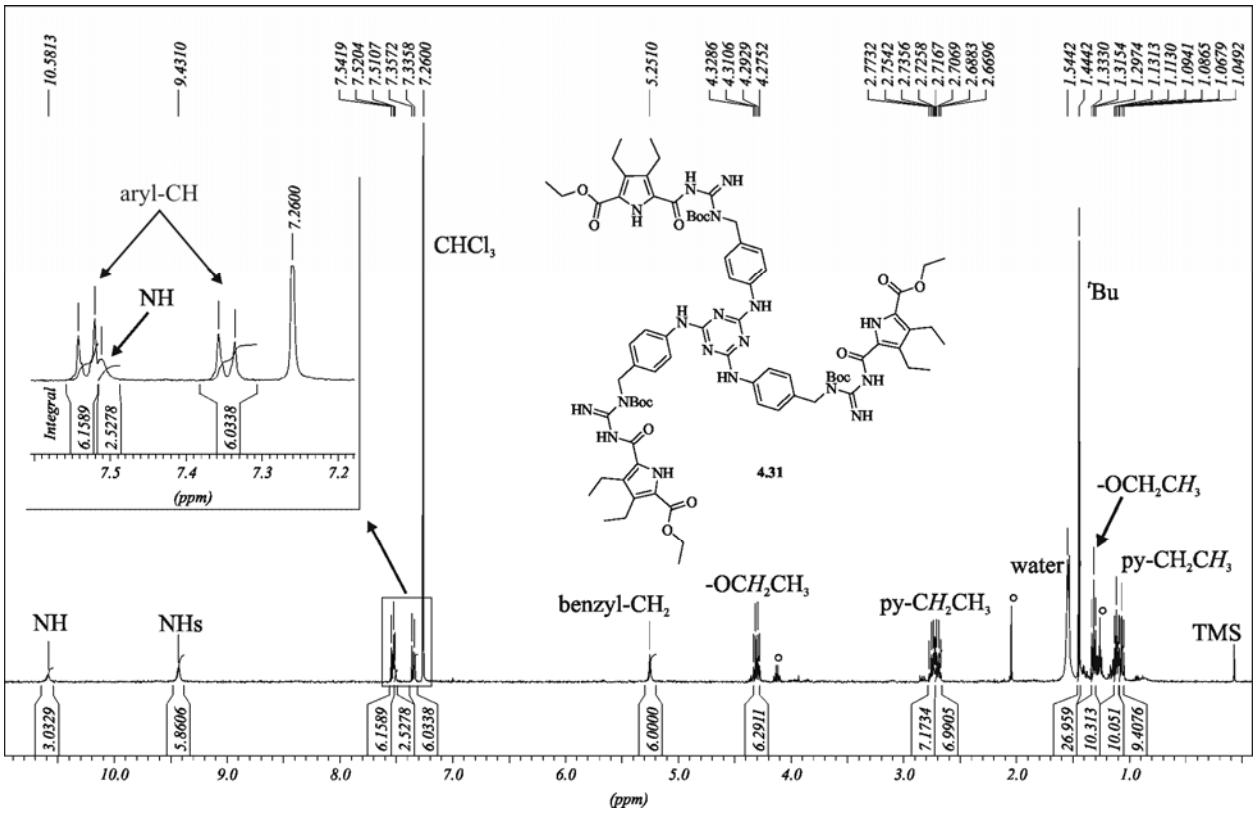

Fig. 4.58 *^{1}H-NMR spectrum of **4.31** in $CDCl_3$ (signals of ethyl acetate impurities are marked with °).*

In conclusion the key step in the synthesis of the supramolecular structures discussed is the *Bromide route*. Via a nucleophilic substitution of the bromide substituents in the corresponding ben-

zylic linkers the fully protected monomer **4.25** could be synthesized for example. In order to have the possibility to vary the size of the box the multi-purpose building block **2.10** was synthesized which was connected over a free amine group to a naphthalene dianhydride or cyanuric acid chloride. The latter synthesis should result in a cage-like structure due to the C_3 symmetric preorganisation of the linker. Subsequently, the deprotection of these fully protected systems has to be achieved. In case of the compounds with diimide functionalities the synthesis might be changed from the beginning since the deprotection of the ethyl ester under basic conditions might also cleave the diimides.

In the end one more idea shall be presented here. The introduction of a second supramolecular binding site offers the possibility to connect the boxes or cages intersupramolecularly. Since the primal zwitterion **2.1** was designed for aqueous solutions, the second non-covalent interaction needs to be very stable and must be able to interact with the zwitterion in a non-destructive way. Therefore metal-ligand interactions are the right choice. As consequence to these necessary conditions porphyrins seem to be one possible type of linker. According to literature the synthesis of a 5,10,15,20-tetrakis-(*α*-bromo-*p*-tolyl)-porphyrin[34] is rather easy and this linker should also be suitable for the *Bromide route*. The theoretical result of the self-assembled 'porphyrin box' is depicted in Figure 4.59 (top). Due to the defined size of this box the intersupramolecular linker should be larger than the mean distance between two associated porphyrins. A first example is the use of a rigid compound like *N*,*N*'-di-(4-pyridyl)-1,4,5,8-naphthalene tetracarboxydiimide.[35] The possible association between two 'porphyrin boxes' and one linker is presented in Figure 4.59 bottom.

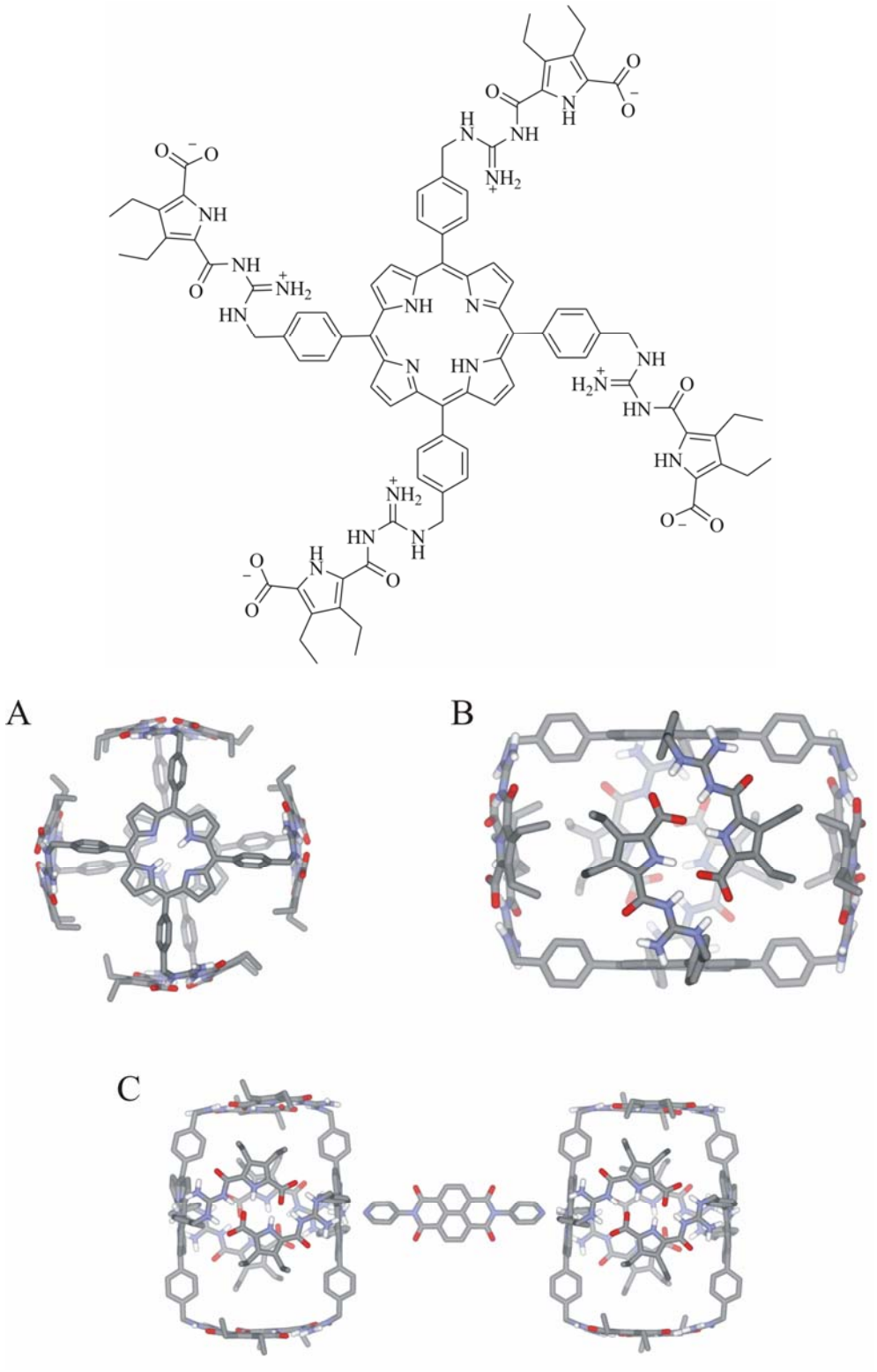

Fig. 4.59 *Top: deprotected monomer based on a porphyrine spacer; bottom: theoretical structure of the 'porphyrin box': A) top view; B) side view and C) its dimerized derivative (MacroModel 8.0, Amber* force field, GB/SA water solvation model, 10,000 steps for the box; MMFF, gas phase and minimization for its dimerized derivative; non-polar hydrogens are omitted for clarity).*

In conclusion the concept of semi-flexible monomers seems to have good potential for the construction of well-defined supramolecular structures with interesting characteristics in terms of encapsulation, photophysics and electrochemistry.

4.4.2 Enhancing the solubility of the primal zwitterion: the morpholine derivative

This idea was developed for two reasons. First, the application of the primal zwitterion **2.1** in pure water is an important point of interest. Since structures, which mimic biological systems, should work under physiological conditions a good solubility of the binding site in polar solvents has priority. A second and more technical reason is the incorporation of additional and permanent charges into the zwitterion. This modification should result in better mass spectra, since the signal intensity of overall uncharged zwitterions is rather bad. So, in consequence to these desired abilities, the incorporation of morpholine groups in the periphery of the pyrrole core was considered (Figure 4.60).

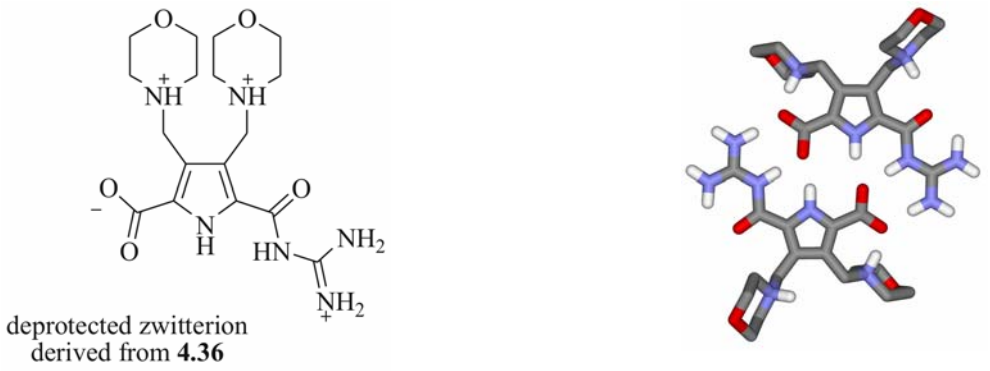

Fig. 4.60 *Theoretical structure of the dimeric zwitterion with fully protonated morpholine groups (non-polar hydrogens are omitted for clarity).*

The starting material for the synthesis is the well-established, fully protected bisbromo pyrrole dicarboxylic acid **4.32** (Figure 4.61). The first step is a nucleophilic substitution of the bromides by morpholine **4.33**. The starting material **4.32** was dissolved in DMF together with six equivalents of morpholine. After one hour of stirring at room temperature the reaction solution was quenched with water and extracted with diethyl ether. The resulting yellow oil was purified by column chromatography yielding 99 % of pure product **4.34** as a colourless oil which crystallised within two days. Interestingly the boc group at the pyrrole nitrogen was removed during this first step. This is rather surprising since the boc protecting group is not base sensitive. The second step is the deprotection of the *tert*-butyl ester. This was performed not with trifluoracetic acid in DCM, but with concentrated hydrochloric acid in methanol (v/v 1:20). The first method resulted

always in complete decomposition of the starting material. Although the latter method takes quite longer it is a mild and efficient way for deprotecting a *tert*-butyl ester. The chloride salt **4.35** was obtained in 99 % yield.

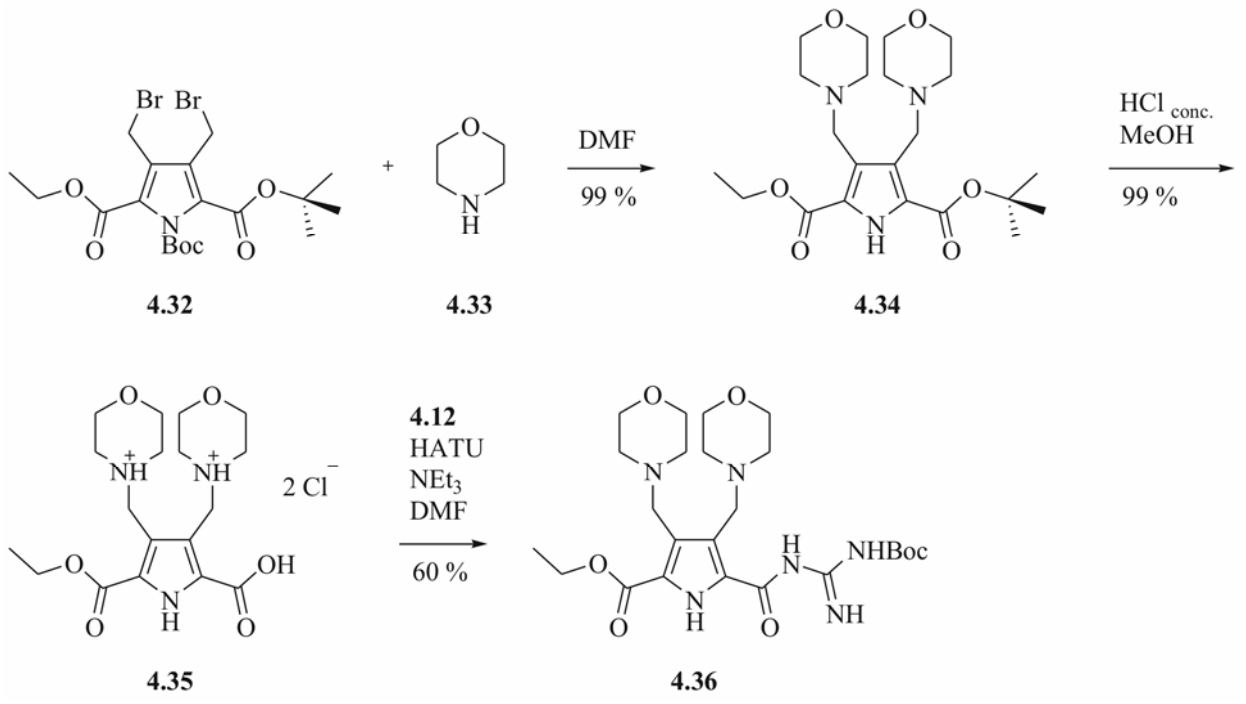

Fig. 4.61 *Synthesis of the fully protected zwitterion **4.36**.*

The last step is the attachment of *N*-boc-guanidine **4.12** to the free acid **4.35** which was performed under slightly changed standard conditions with HATU as coupling reagent and DMF as solvent. Triethyl amine was applied as base since the use of the standard base NMM resulted in low yields. Now the fully protected zwitterion **4.36** with morpholine groups in position 3 and 4 of the pyrrole core could be obtained in 60 % yield. Figure 4.62 shows the ^{1}H-NMR spectrum of **4.36** in $CDCl_3$. The strong downfield shift of one proton of the guanidino group is most likely the result of an intramolecular hydrogen bond to the adjacent morpholine substituent.

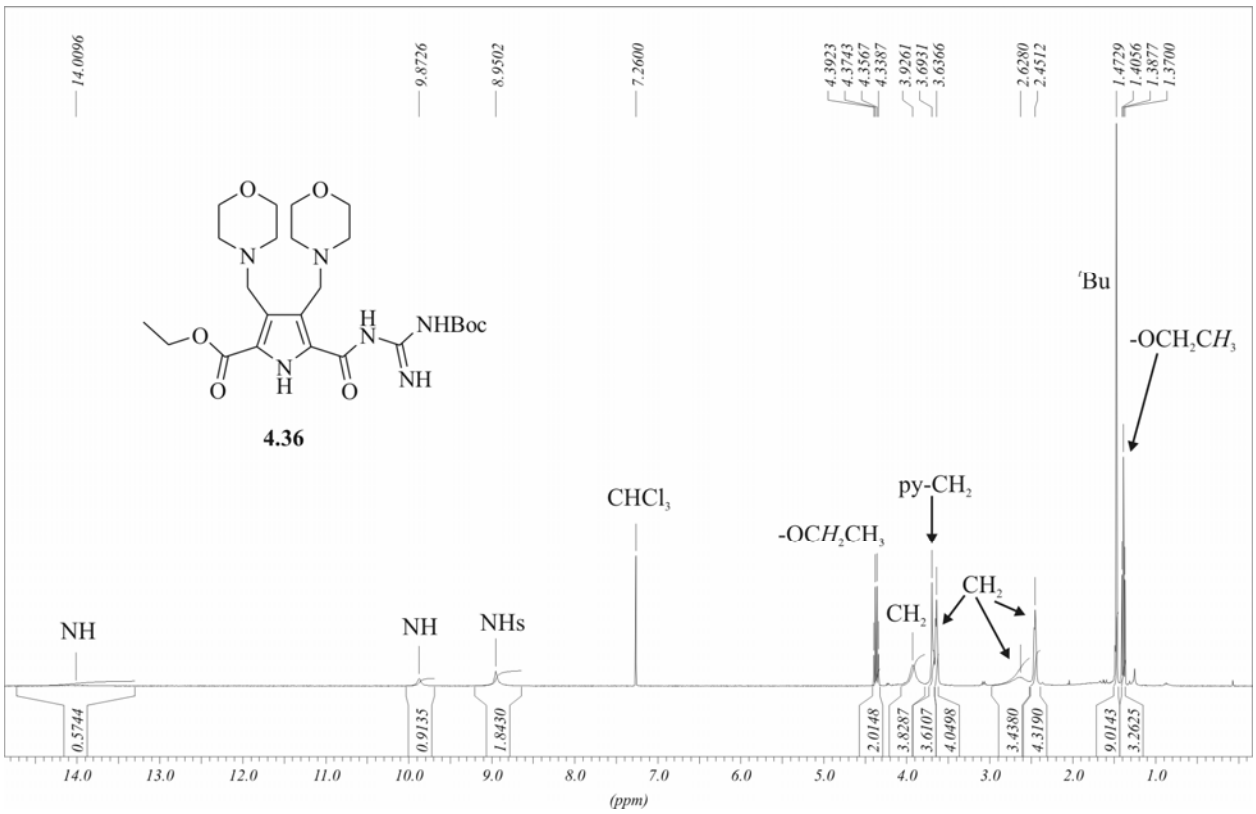

Fig. 4.62 *^{1}H-NMR spectrum of **4.36** in $CDCl_3$.*

In conclusion the fully protected zwitterion **4.36** could be obtained within a three-step synthesis and an overall yield of 59 %. Although the preparation and subsequent work up of each reaction caused no problems one should consider a small change in the synthesis in future work. The last step in terms of coupling **4.12** to the free acid **4.35** yielded just 60 % product. Usually these coupling reactions provide products with yields of 80 to 95 %. Most likely the interaction with the morpholine substituents decreased the efficiency of this reaction by a certain shielding effect of the reaction centre. Therefore the introduction of the morpholine substituents should be done after this step. But this requires also that the radical bromination of the pyrrole side chain has to done after the coupling of *N*-boc-guanidine. Figure 4.63 shows the retro-synthesis of this proposal.

After removal of both the boc group and the ethyl ester the examination of the dimerization of this zwitterion has to be done. One interesting point is the question if the additional charges have a negative influence on the binding ability of the zwitterion. A second point might be the question whether the charges in the periphery of the pyrrole core are stable enough for experiments in the gas phase, hopefully resulting in stronger signal intensity. Therefore one can also consider the quaternisation of the morpholine nitrogens or at least one of them.

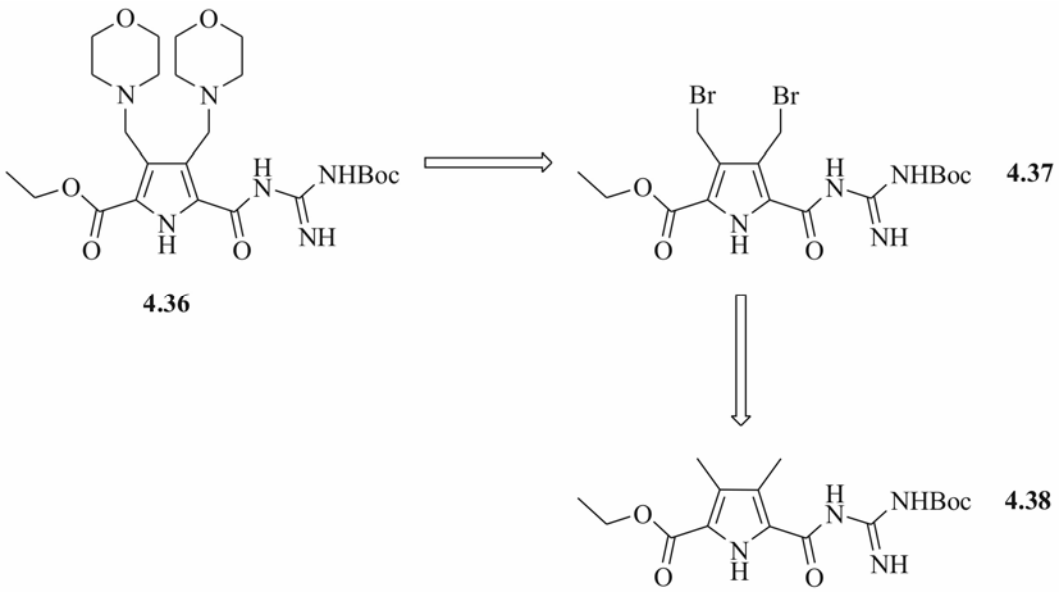

Fig. 4.63 *Retro synthesis of **4.36**: both radical bromination and subsequent substitution as last steps in the synthesis.*

4.4.3 Introduction of a third non-covalent interaction: zwitterions capable of π-stacking

The last concept presents the idea to strengthen the dimerization of the primal zwitterion **2.1** in aqueous solutions by a third non-covalent interaction. The intention here is to use hydrophobic contacts in terms of π-π interactions. It is known from literature[36] that this type of supramolecular interaction can be rather strong in polar solvents, but needs structural preorganization for efficient association. Now in case of zwitterion **2.1** these requirements are given by the ion pair. The idea is to separate the charges by an aromatic spacer, so that, due to defined ion pairing, the aromatic parts of the dimerizing monomers are stacked with each other. Further on, an extended dipole moment should also lead to an increased dimerization efficiency. The first idea was the introduction of a simple benzene ring in form of *p*-amino benzoic acid **4.39**. Molecular mechanics calculations of the resulting zwitterion indicate a mean distance of 3 Å between the aromatic benzene rings (Figure 4.64). Although the aromatic linker like the benzene ring is too displaced for real stacking interactions it was used as model for the synthetical part of the project.

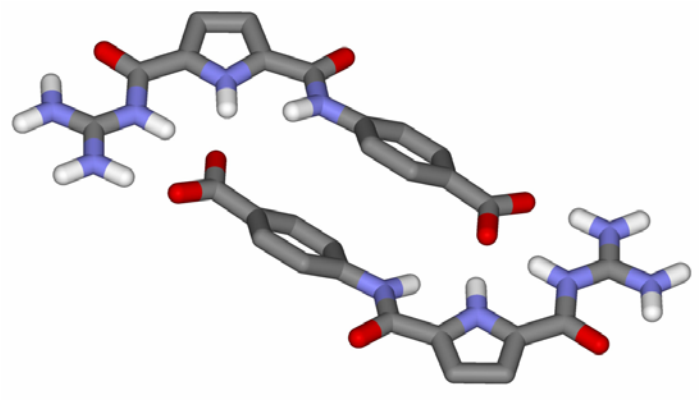

Fig. 4.64 *Theoretical structure of dimerized zwitterion capable of π-stacking (non-polar hydrogens are omitted for clarity).*

The synthesis starts with the protection of the carboxylic acid in the spacer as the methyl ester (Figure 4.65). This was performed according to literature[37] by stirring *p*-amino benzoic acid **4.39** with thionyl chloride in dry methanol. The resulting methyl ester **4.40** was obtained in 99 % yield. Due to the low nucleophilicity of the deactivated aromatic amine the corresponding acid had to be activated as acid chloride. Attempts to couple them with standard coupling reagents like PyBOP, HCTU or HATU were in vain. Therefore the free acid **4.41** was transformed to the acid chloride with oxalyl chloride in DCM with catalytic amounts of DMF. Subsequently, the remaining oxalyl chloride was removed. The intermediate product was immediately reacted at 0 °C with the free amine **4.40** and triethyl amine as base. After 30 minutes at 0 °C the reaction solution was stirred further for two hours at room temperature. The reaction solution was washed with 0.5 N hydrochloric acid. Finally, the crude resulting product was purified by column chromatography yielding 93 % pure product **4.42** as white powder.

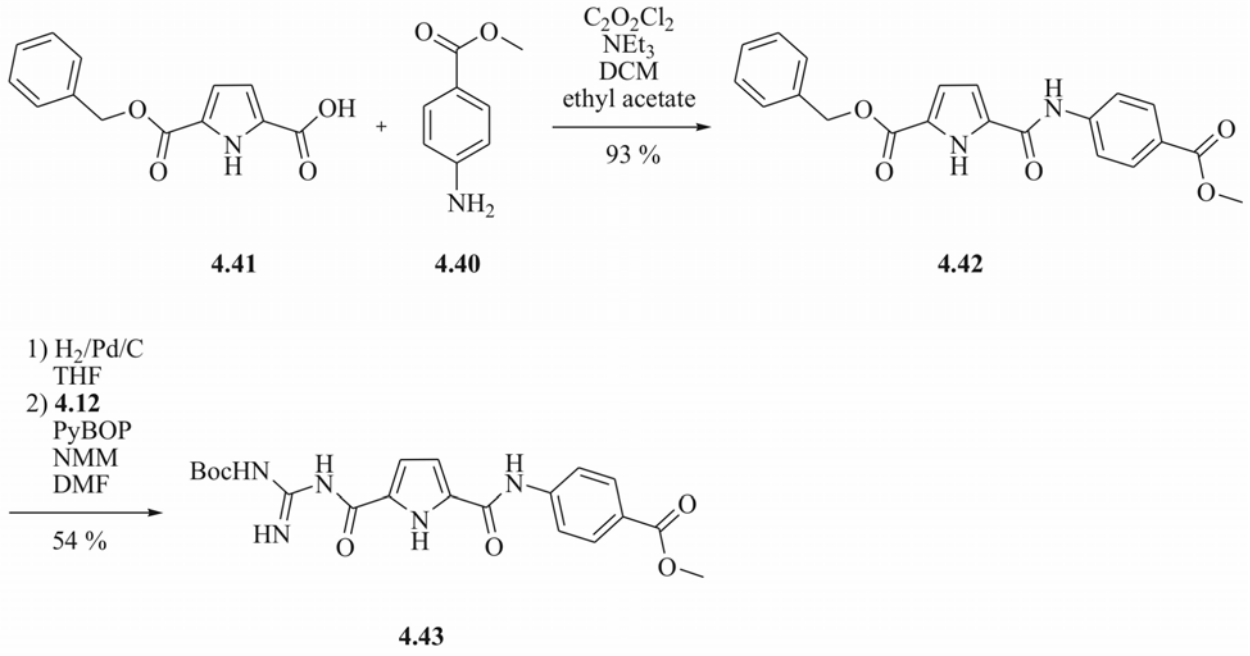

Fig. 4.65 *Synthesis of the fully protected zwitterion **4.43**.*

The next step in the preparation of the extended zwitterion was the removal of the benzyl group via hydrogenolysis with palladium on charcoal in THF. Subsequent coupling of *N*-boc-guanidine **4.12** to the free acid under standard conditions with PyBOP as coupling reagent, DMF as solvent and NMM as base resulted in the final, fully protected zwitterion **4.43** in 54 % yield after column chromatography. Figure 4.66 shows the ^{1}H-NMR spectrum of **4.43** in $CDCl_3$ with 5 % DMSO-d_6.

In conclusion the introduction of a rigid spacer which separates the charges of the zwitterion could be achieved in three steps with an overall yield of 50 %. After removal of the boc group and the methyl ester the first point of interest will be the examination of the dimerization abilities of this new zwitterion. Further theoretical investigations concerning the size of the aromatic unit will give hints for detailed modifications of this system. A first test was already performed by the calculation of a naphthalene derivative. Annealing one more aromatic ring to the central spacer structure results in larger hydrophobic surface, which should stabilize the dimer (Figure 4.67).

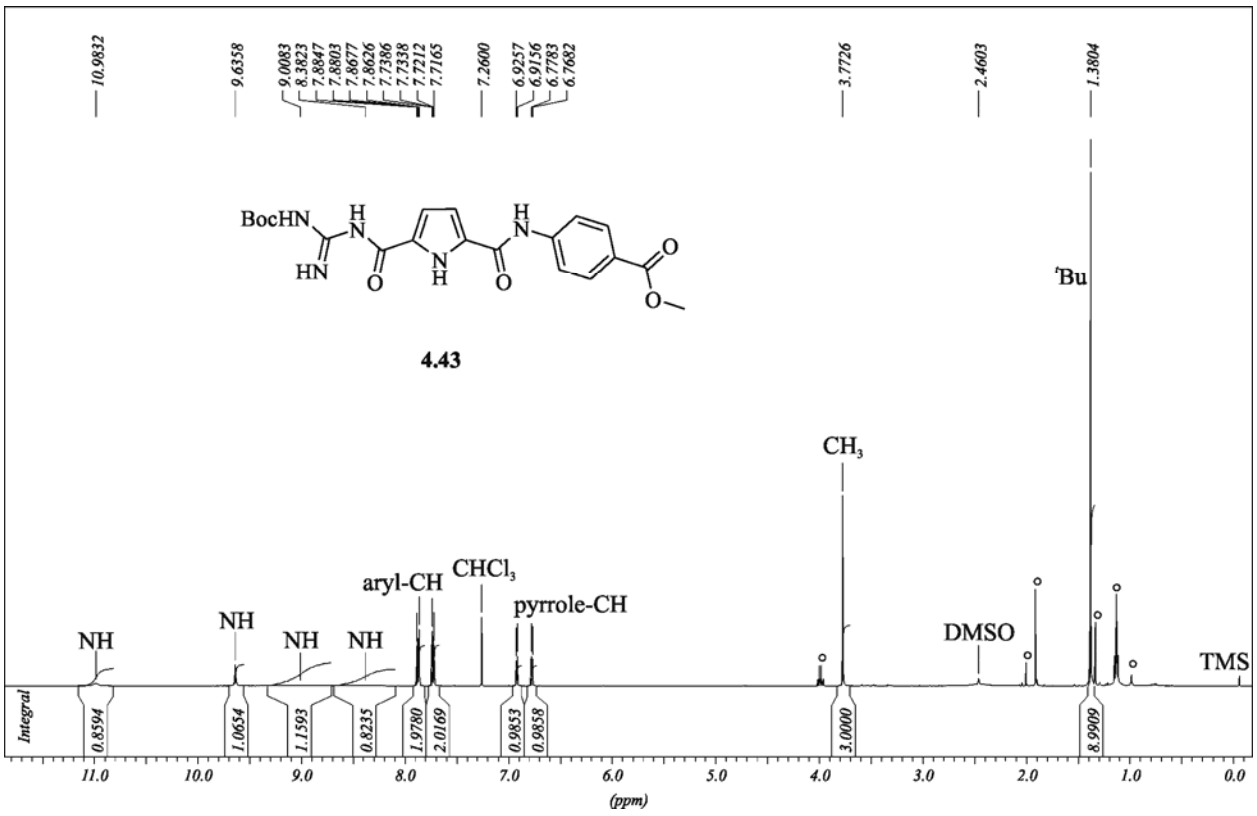

Fig. 4.66 *^{1}H-NMR spectrum of **4.41** in $CDCl_3$ with 5 % DMSO-d_6; due to fast exchange with the solvent one NH proton is not detected (signals of impurities, acetone and ethyl acetate are marked with °).*

Unfortunately, first theoretical calculations on DFT level[38], performed by Dr. S. Schlund (Institute of Organic Chemistry, University of Würzburg), show that both benzene and naphthalene zwitterions are slightly weaker than the primal one. Two opponent factors have to be considered here. Due to the larger distance between the charges a stronger dipole moment exists in the extended zwitterions. First estimations show a dipole moment with a value of 40 *Debye* which is twice the value of the primal zwitterion **2.1**. This points to a very high dimerization constant although in case of the benzene derivative no stacking interactions occur since both aromatic partners are too displaced for efficient stacking. In case of the naphthalene derivative the aromatic surfaces of the naphthalene linkers are stacked above each other promising efficient aromatic interaction as depicted in Figure 4.67.

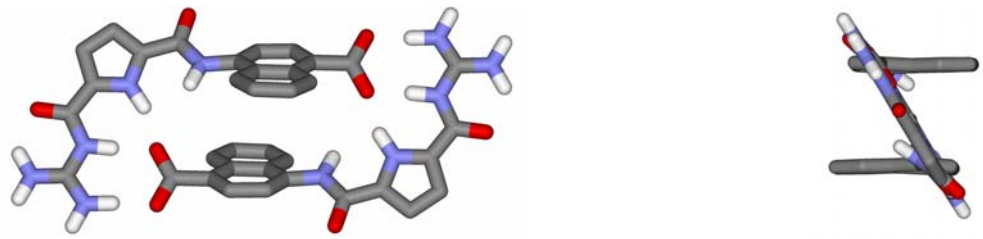

Fig. 4.67 *Enhanced aromatic surface for a stronger stacking interaction (left: top view; right: side view; non-polar hydrogens are omitted for clarity).*

Although the aromatic surfaces have enough contact for π-stacking this interaction does not lead to a stronger dimerization in combination with the larger dipole character because a third point has to be remembered. If both processes occur parallel, a distortion of the monomeric units within the dimer is the result. The twisting process leads to a conformational change from a planar monomer to a tilted one; a process which needs energy which has to be taken from the dimerization energy. Beside this fact a detailed look at the images shows that only three instead of four hydrogen bonds are complexing one carboxylate. This is most likely another reason for the predicted lower dimerization efficiency. Although this project is still in its infancy it offers interesting perspectives for the improvement of the primal zwitterion **2.1**. The next step will be the evaluation of an anthracene derivative with an axially symmetric and even larger aromatic unit. Maybe the size of the anthracene linker is big enough to lead to a crossbred structure of the monomer. Here no more twisting process would be necessary to perform both efficient ion pairing and π-stacking.

4.4.4 Conclusion and outlook

The third part of this thesis introduced building blocks for the formation of more defined supramolecular structures by dimerizing preorganized monomers. The concept is to reduce the structural flexibility of the monomer by introduction of semi-flexible linker and rigid spacers. For this reason the *Bromide route* was introduced in order to attach semi-flexible benzyl-linkers to the guanidino group of the binding site. Three different monomers were synthesized which all differ in their spacer length. Molecular mechanics calculations presented the resulting dimers of the preorganized monomers, starting with a small box based on a toluene linker and a larger box via the use of a naphthalene spacer. A molecular cage was obtained by the introduction of cyanuric acid as a C_3 symmetric linker. In future work the introduction of a second non-covalent binding site (metal-ligand interactions) should lead to the oligomerization of the dimerized structures. Another idea discussed the modification of the primal zwitterion. The first synthesis introduced morpholine groups in the periphery of the pyrrole core in order to increase the solubility of the

binding motive in water. The protonation of the morpholine nitrogen atoms should result in an additional charge which is also desired for stronger signal intensity in gas phase experiments. A second modification should strengthen the dimerization of the primal zwitterion. Via the introduction of a third non-covalent interaction (hydrophobic contacts, π-stacking) the association constant of the binding motives should be increased particularly in polar solvents like water. Unfortunately, theoretical calculations on DFT level predicted that both benzene and naphthalene spacers are not the ideal choice for this project. Future work should give better results by using anthracene as binding motive for aromatic interactions.

In conclusion, the third part of this thesis gives an overview of several new and promising ideas for the use and modification of the primal zwitterion **2.1**.

1 C. Schmuck, T. Rehm, F. Gröhn, K. Klein, F. Reinhold, *J. Am. Chem. Soc.* **2006**, *128*, 1430-1431.
2 Th. Rehm, Diploma thesis, University of Würzburg, **2004**.
3 a) K. Feichtinger, H. Sings, T. Baker, K. Matthews, M. Goodman, *J. Org. Chem.* **1998**, *63*, 8432-8439; b) C. Schmuck, V. Bickert, *Org. Lett.* **2003**, *5,* 4579 - 4581.
4 K. Connors, *Binding Constants* **1987**, Wiley & Sons, Chichester.
5 C. Schmuck, W. Wienand, *J. Am. Chem. Soc.* **2003**, *125*, 452-459.
6 a) Y. Cohen, L. Avram, L. Frish, *Angew. Chem. Int. Ed.* **2005**, *44*, 520-554; b) C. Johnson, *Prog. Nucl. Magn. Reson.* **1999**, *34*, 203-256.
7 S. Provencher, *Comput. Phys. Commun.* **1982**, *27*, 229-242.
8 P. Lindner, T. Zemb (Eds.), *Neutron, X-rays and Light: Scattering Methods Applied to Soft Condensed Matter* **2002**, Elsevier, Amsterdam.
9 C. Schmuck, T. Rehm, K. Klein, F. Gröhn, *Angew. Chem. Int. Ed.* **2007**, *46*, 1693-1697.
10 M. Kerker, *The Scattering of Light* **1969**, Academic Press, New York.
11 a) E. Minatti, P. Viville, R. Borsali, M. Schappacher, A. Deffieux, R. Lazzaroni, *Macromolecules* **2003**, *36*, 4125-4133; b) N. Ouarti, P. Viville, R. Lazzaroni, E. Minatti, M. Schappacher, A. Deffieux, R. Borsali, *Langmuir* **2005**, *21*, 1180-1186.
12 a) O. Glatter, *Acta Phys. Austriaca* **1977**,*47*, 83-102; O. Glatter, *J. Appl. Cryst*. **1977**, *10*, 415-421; b) O. Glatter *J. Appl. Cryst.* **1980**, *13*, 7-11; O. Glatter *J. Appl. Cryst.* **1980**, *13*, 577-584; c) O. Glatter *J. Appl. Cryst.* **1981**, *14*, 101-108; d) O. Glatter, B. Hainisch, *J. Appl. Cryst.* **1984**, *17*, 435-441; e) O. Glatter, *J. Appl. Cryst.* **1988**, *21*, 886-890; f) D. J. Iampietro, L. L. Brasher, E.W. Kaler, A. Stradner, O. Glatter, *J. Phys. Chem. B* **1998**, *102*, 3205-3113; f) F. Gröhn, B. Bauer, E. Amis, *Macromolecules* **2001**, *34*, 6701-6707.
13 J.-H. Fuhrhop, T. Wang, *Chem. Rev.* **2004**, *104*, 2901-2937.
14 C. Schmuck, T. Rehm, V. Stepanenko, F. Würthner, F. Gröhn, K. Klein, *under preparation.*
15 C. Schmuck, D. Rupprecht, C. Urban, N. Walden, *Synthesis* **2006**, 89-96.
16 F. Gröhn, B. Bauer, Y. Akpalu, C. Jackson, E. Amis, C. Jackson, *Macromolecules* **2000**, *33*, 6042-6050.
17 Th. Rehm, V. Stepanenko, X. Zhang, F. Würthner, F. Gröhn, K. Klein, C. Schmuck, *Org. Lett.* **2008**, *10*, 1469-1472.
18 C. Schmuck, Th. Rehm, L. Geiger, M. Schäfer, *J. Org. Chem.* **2007**, *72*, 6162-6170.
19 C. Schmuck, V. Bickert, M. Merschky, L. Geiger, D. Rupprecht, J. Dudaczek, P. Wich, Th. Rehm, U. Machon, *Eur. J. Org. Chem.* **2008**, *21*, 324-329.
20 W. Oelofson and C. H. Li, *J. Org. Chem.* **1968**, *33*, 1581-1583.
21 a) C. Schmuck, *Chem. Commun.* **1999**, 843-844; b) C. Schmuck, *Chem. Eur. J.* **2000**, *6*, 709-718; c) C. Schmuck, U. Machon, *Chem. Eur. J.* **2005**, *11*, 1109-1118; d) C. Schmuck, L. Geiger, *J. Am. Chem. Soc.* **2005**, *127*, 10486-10487; e) C. Schmuck, S. Graupner, *Tett. Lett.* **2005**, *46*, 1295-1298; f) C. Schmuck, V. Bickert, *J. Org. Chem.* **2007**, *72*, 6832-6839.
22 A rigid zwitterion with the same association mode shows this behaviour in a comparable concentration range: C. Schmuck, *Tetrahedron* **2001**, *57*, 3063-3067.
23 a) H. Hansma, *J. Vac. Sci. Technol. B* **1996**, *14*, 1390-1394; b) J. Tamayo, R. Garcia, *Langmuir* **1996**, *12*, 4430-4435.
24 a) M. Yang, W. Wang, F. Yuan, X. Zhang, J. Li, F. Liang, B. He, B. Minch and G. Wegner, *J. Am. Chem. Soc.* **2005**, *127*, 15107-15111; b) D. Xie, M. Jiang, G. Zhang, D. Chen, *Chem. Eur. J.* **2007**, *13*, 3346-3353.
25 a) C. Schmuck, *Angew. Chem. Int. Ed* **2007**, *46*, 5830-5833; b) L. Palmer, J. Rebek, Jr. *Org. Biomol. Chem.* **2004**, *2*, 3051-3059.
26 a) S. Biros, J. Rebek, Jr. *Chem. Soc. Rev.* **2007**, *36*, 93-104; b) K. Fujita, M. Tominaga, A. Hori, B. Therrien, *Acc. Chem. Res.* **2005**, *38*, 371-380.
27 a) M. Yoshizawa, M. Tamura, M. Fujita, *Science* **2006**, *312*, 251-254; b) R. Hooley, T. Iwasawa, J. Rebek, Jr., *J. Am. Chem. Soc.* **2007**, *129*, 15330-15339.
28 a) J. Sessler, C. Lawrence, J. Jayawickramarajah, *Chem. Soc. Rev.* **2007**, *36*, 314-325; b) S. Zhang, *Nature Biotechnology* **2003**, *21*, 1171-1178.
29 G. Vaidyanathan, S. Shankar, D. Affleck, K. Alston, J. Norman, P. Welsh, H. LeGrand, M. Zalutsky, *Bioorg. Med. Chem.* **2004**, *12*, 1649-1656.
30 S. Bhosale, C. Jani, S. Langford, *Chem. Soc. Rev.* **2008**, *37*, 331-342.
31 C. Hunter, R. Tregonning, *Tetrahedron* **2002**, *58*, 691-697.
32 a) C. Röger, F. Würthner, *J. Org. Chem*. **2007**, *72*, 8070-8075; b) R. Kishore, V. Ravikumar, G. Bernardinelli, N. Sakai, S. Matile, *J. Org. Chem.* **2008**, *73*, 738-740.
33 a) S. Mandal, G. Berube, E. Asselin, I. Mohammad, V. Richardson, A. Gupta, S. Pramanik, A. Williams, S. Mandal, *Bioorg. Med. Chem. Lett.* **2007**, *17*, 4955-4960; b) M.-X. Wang, H.-B. Yang, *J. Am. Chem. Soc.* **2004**, *126*, 15412-15422; c) P. Anelli, F. Montanari, S. Quici, *Chem. Commun.* **1983**, *4*, 194-195.

34 a) B. Bookser, T. Bruice, *J. Am. Chem. Soc.* **1991** *113*, 4208-4218; b) L. Wen, M. Li, J. Schlenoff, *J. Am. Chem. Soc.* **1997**, *119*, 7726-7733; c) J. Buchler, J. Simon, *Eur. J. Inorg. Chem.* **2000**, 2615-2621.

35 P. Dinolfo, M. Williams, C. Stern, J. Hupp, *J. Am. Chem. Soc.* **2004**, *126*, 12989-13001.

36 a) A. Zych, B. Iverson, *J. Am. Chem. Soc.* **2000**, *122*, 8898-8909; b) G. Gabriel, B. Iverson, *J. Am. Chem. Soc.* **2002**, *124*, 15174-15175; c) V. Bradford, B. Iverson, *J. Am. Chem. Soc.* **2008**, *130*, 1570-1524.

37 B. Hosangadi, R. Dave, *Tett. Lett.* **1996**, *37*, 6375-6378.

38 All geometry optimizations were performed on DFT level with density fitting using the TURBOMOL program package, version 5.8. The applied functional was BLYP with the TZVPP+ basis set. Since only the relative energies of all compounds were correlated no BSSE correction was done. For optimizations in solvent the COSMO approach was used as implemented in TURBOMOL with a dielectric constant of $\varepsilon = 78$ to simulate a water-like solvent.

5 Summary

The main focus of this thesis is the synthesis and analysis of supramolecular architectures based on guanidiniocarbonylpyrrole carboxylate zwitterions as main building block (Figure 5.1). Due to its self-complementarity and outstanding self-association properties in polar solvents this building block was used to synthesize monomers for supramolecular structures which self-assemble in DMSO solutions. The subsequent analysis allowed a fascinating insight into the self-assembly of this new compound class.

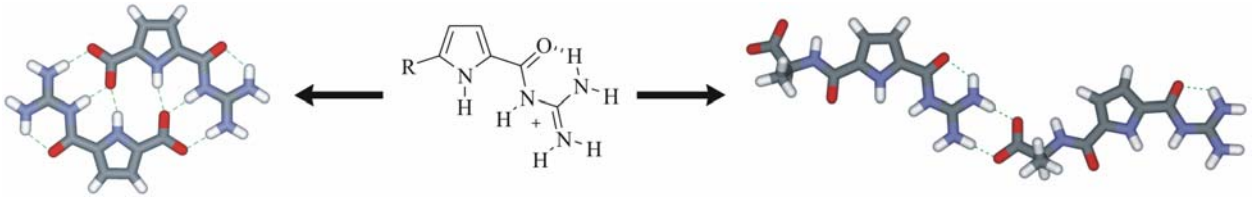

Fig. 5.1 *Guanidiniocarbonylpyrroles as receptors for carboxylates representing new self-complementary building blocks for supramolecular architectures (hydrogen bonds are shown as green, dotted lines).*

5.1 Architectures based on the self-assembly of bis- or triple-zwitterions

Three bis-zwitterions and one triple-zwitterion were synthesized, which self-assemble in polar DMSO solutions. The zwitterions were connected covalently by flexible alkyl chains of different length and chemical constitution. The analysis of the resulting supramolecular architectures proved the strong influence of the linker on the mode of self-assembly. Although the ion pairing process between the binding motives is the main driving force, the additional interaction of the linker with either the solvent or itself is necessary for the exact structure of the aggregates. The first example is bis-zwitterion **2.2** which links two binding motives via a hydrophilic triethylene glycol chain (Figure 5.2). The self-assembly of **2.2** leads to nanometre-sized cyclic dimers with a well defined dimension. In DMSO solutions **2.2** exists in a concentration dependent monomer-dimer equilibrium with the dimer as the dominant species in higher concentrated solutions. DOSY NMR, dynamic light scattering and small angle neutron scattering evidence the size of dimeric **2.2** (r_H = 2.00 nm) and rule out the presence of larger aggregates under these conditions at least in detectable quantities.

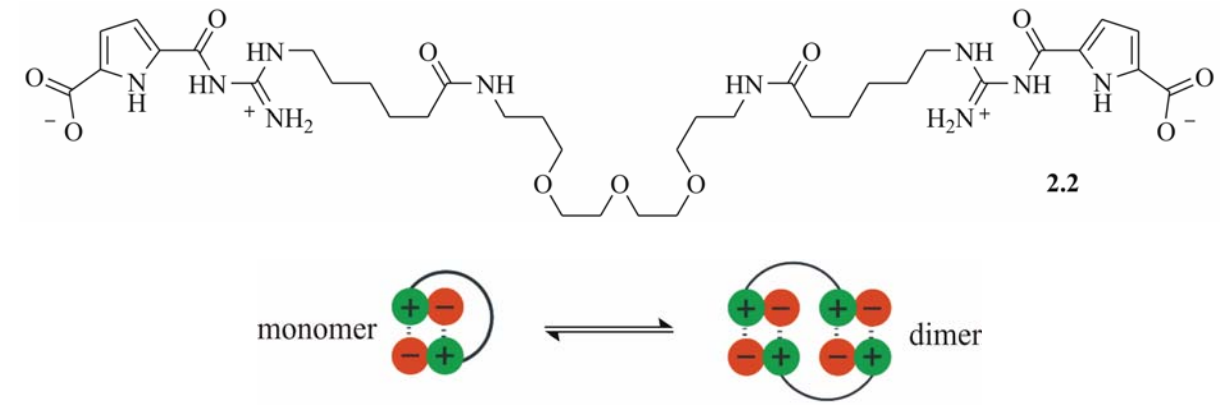

Fig. 5.2 *Bis-zwitterion **2.2** forms nanometre-sized cyclic dimers.*

The second example, bis-zwitterion **2.3**, contains a short and hydrophobic linker (Figure 5.3). In solution bis-zwitterion **2.3** again exists in a concentration dependent monomer-dimer equilibrium, however, followed by the formation of larger aggregates of vesicular structure. This new level of self-assembly was evidenced by DLS and gave a mean diameter of 140 nm for the vesicles. With AFM and SANS experiments a structure model of the membrane was evaluated. Compared to **2.2** bis-zwitterion **2.3** is a bolaamphiphil. The unpolar middle-section of the monomer most likely initiates the formation of the vesicles. In this unpolar region both strong hydrogen bonding and *van der Waals* interactions lead to a stable vesicle membrane.

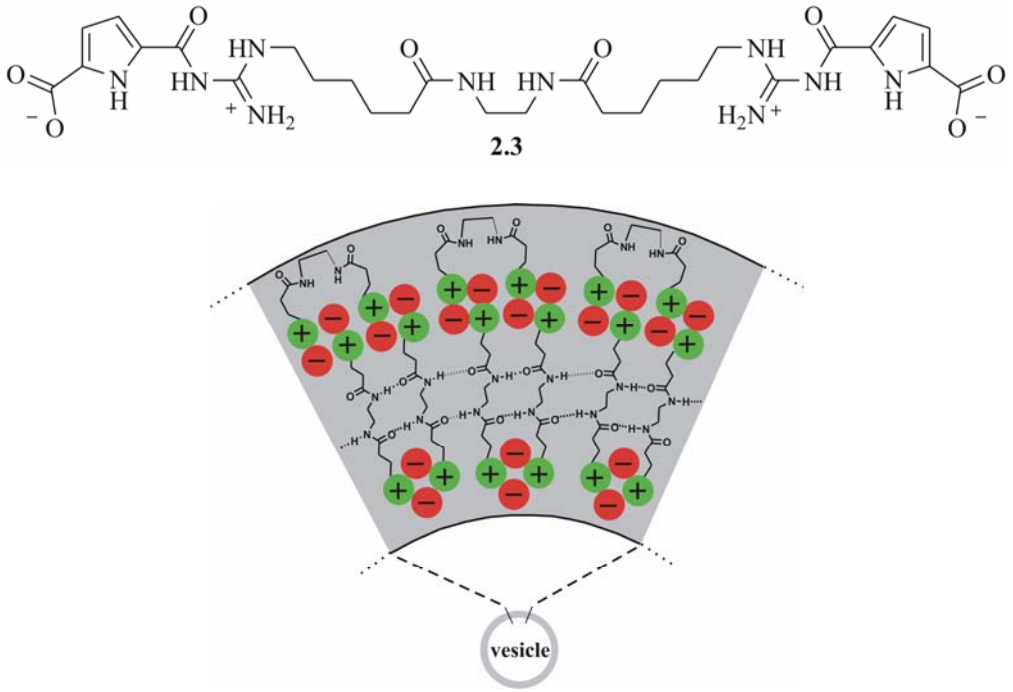

Fig. 5.3 *Bis-zwitterion **2.3** self-assembles to large vesicular structures based on the bola-amphiphilic structure of the monomer.*

The third example, bis-zwitterion **2.4,** only differs in the length of the unpolar linker which has ten CH_2 units instead of just two as in **2.3** (Figure 5.4). In analogy to **2.3** bis-zwitterion **2.4** exists in solution in a concentration dependent monomer-dimer equilibrium and forms vesicles with a diameter of about 140 nm. However, upon deposition on a solid surface **2.4** forms layer-like structures. AFM experiments proved the formation of monolayers from dilute samples and multi-layered structures from higher concentrated solutions. All available experimental data point to the strong influence of the longer alkyl linker as the main driving force for the layer formation on solid substrate.

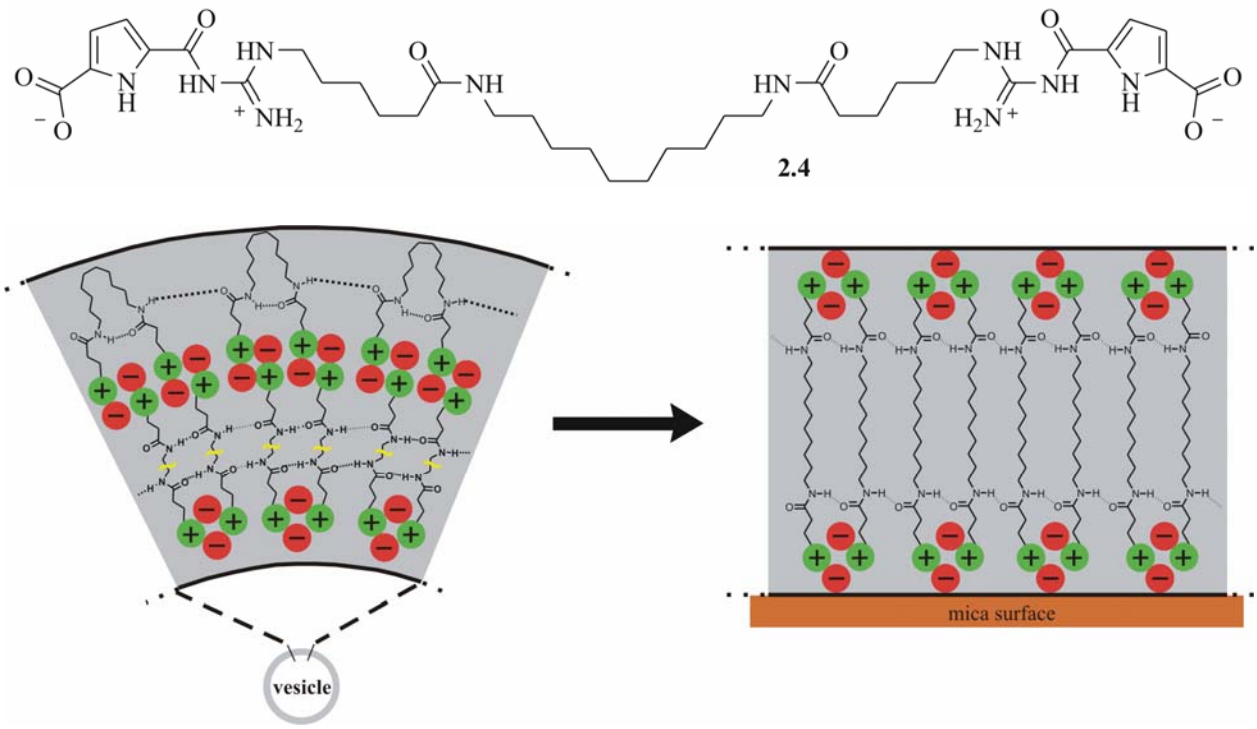

Fig. 5.4 *Bis-zwitterion **2.4** self-assembles into vesicles in solution and rearranges to wide-spread layers on a solid surface (the alkyl linker in the vesicle membrane is illustrated shortened as a yellow line).*

The last example in this project is the triple-zwitterion **2.5**. This building block is so far the first one, which incorporates three binding motives within one molecule (Figure 5.5). This significant change in the molecular structure also leads to a different mode of self-assembly. In solution the smallest supramolecular structure of **2.5** is the dimer, which is in equilibrium with larger oligomers of cylindrical shape. These worm-like structures coil together in solution forming solid

and spherical particles with a mean diameter of 90 nm and an inhomogeneous interior which is in contrast to the vesicle formation of the bis-zwitterions **2.3** and **2.4**.

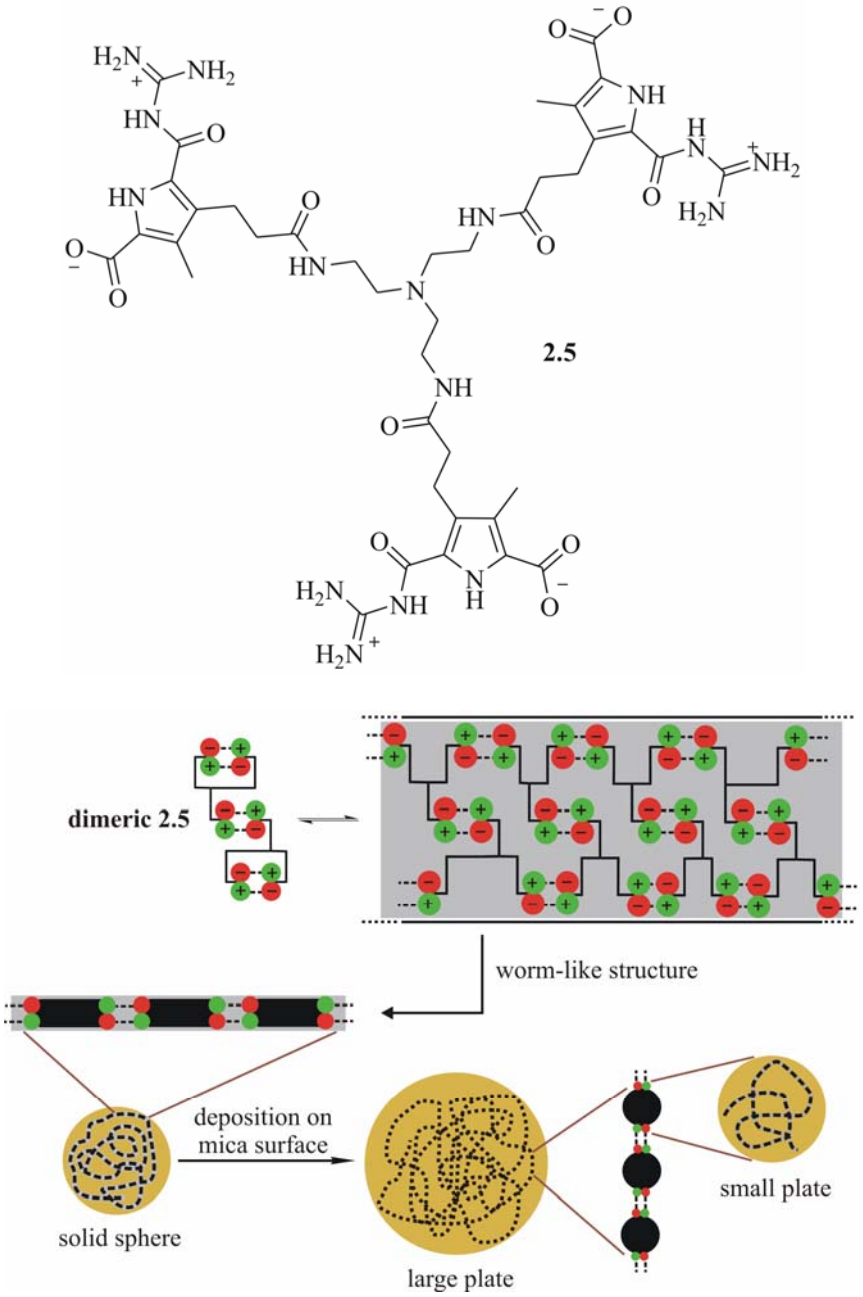

Fig. 5.5 *Triple-zwitterion **2.5** forms solid spheres with a network-like internal structure in a complex self-assembly process.*

Upon deposition on mica the spherical structures from solution rearrange into large plates. Their internal network-like structure is based on small plates which are most likely formed from the coiled worm-like structures as seen in solution. Concentration dependent AFM studies showed the formation of separate plates from dilute solutions which rearranged to a large network-like structure with increasing concentration. This is most likely based on the fusion of a large number

of solid spheres during sample preparation. The self-assembly process of triple-zwitterion **2.5** is in clear contrast to all bis-zwitterions.

In conclusion these four examples show that the features of the linker moieties have a great influence on the self-assembly of the monomers. The combination of one strong driving force in terms of the ion pairing binding motive with a second texturing force, introduced by the linker functionalities, opens the door for the formation of diverse nanostructures.

5.2 Changing the binding mode: vesicular structures from *α*-amino acid derived zwitterions

The second part of this thesis discusses the synthesis and analysis of four new zwitterionic building blocks. The idea of this part is the separation of the charges within the zwitterion by incorporation of *α*-amino acids. Figure 5.6 shows the synthesized compounds derived from *L*-alanine, *L*-serine, *L*-phenylalanine and *L*-tyrosine.

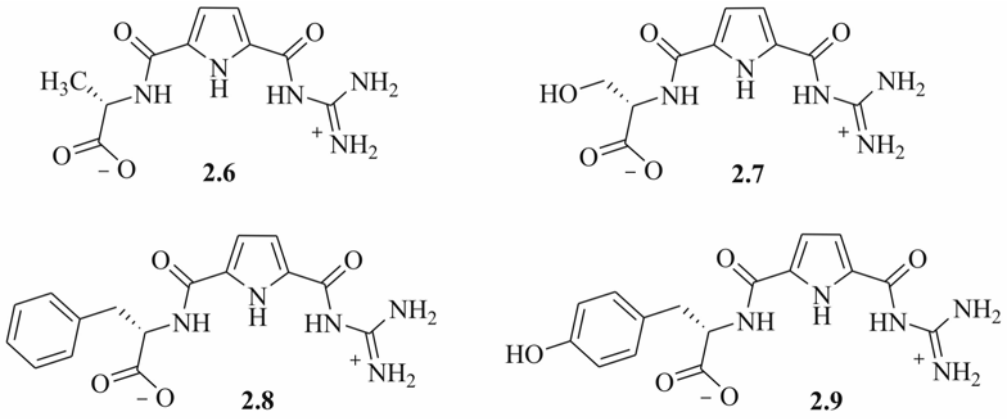

Fig. 5.6 *Increased flexibility of the α-amino acid derived zwitterions leads to the formation of vesicular structures.*

AFM experiments with freshly prepared solutions of all four compounds suggest the formation of vesicular structures. Although all four compounds show good solubility in DMSO, zwitterions **2.8** and **2.9** with aromatic amino acid side chains precipitated after some minutes. Therefore only the zwitterions derived from *L*-alanine and *L*-serine were analysed in more detail. ^{1}H-NMR dilution, COSY and NOESY experiments point to an unusual and weak bi-dentate binding mode between the carboxylate and the guanidinium group. This interaction results in extended and curved dimers. Beside the weaker ion pairing, hydrophobic or aromatic stacking interactions between the monomers are the dominant force for the formation of the vesicle membrane. The

amino acid side chains lead to a steric bulk in the middle of the membrane and introduce as consequence a curvature into the membrane as needed for the vesicle formation (Figure 5.7).

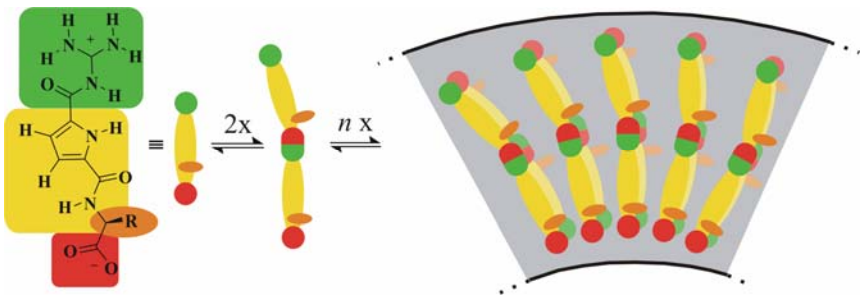

Fig. 5.7 *Schematic illustration of the membrane formation based on the self-assembly of α-amino acid derived zwitterionic monomers.*

In conclusion, the new building blocks derived from *α*-amino acids self-assemble into vesicular structures in solution which rank among the soft materials. It is surprising that small molecules like these zwitterions are able to form large structures like the observed vesicles.

5.3 Concepts for the syntheses of boxes, cages and new zwitterions

The last part of this thesis outlines three new projects for future work based on ideas obtained from molecular mechanics calculations. In the first project the synthesis of preorganized monomers with rigid linkers was introduced in order to form structurally very stable boxes with a defined internal volume. Therefore the *Bromide route* was developed: the guanidino group of the binding motive acts like a nucleophile and substitutes the bromides at the semi-flexible benzyl linker. In order to vary the spacer length the multi-purpose building block **2.10** was synthesized (Figure 5.8A). With its free amino group at the semi-flexible linker further reactions with different rigid spacers are possible. As first examples both naphthalene dianhydride and cyanuric acid chloride were used.

The second project presents a derivative of the primal zwitterion which introduces additional charges in the periphery of the pyrrole core. The key step is the nucleophilic substitution of the bromides by morpholine in the well-established precursor **4.32**. In the zwitterionic state the nitrogen atom of the morpholine substituents should be protonated (Figure 5.8B), leading to an increased solubility in water.

The last concept presents first results on the synthesis of a new zwitterionic binding motive which is capable of additional *π*-stacking. The charged end groups are separated by an aromatic subunit like benzene as most simple aromatic spacer or naphthalene as example for an extended aromatic unit. Synthetically the fully protected zwitterion with the benzene spacer (**4.43**) was

available in three steps. Theoretical evaluations on DFT level were performed for both compounds. The obtained geometry of the naphthalene derivative shows the possibility of aromatic stacking interactions (Figure 5.8C), although the necessary conformational change of the monomers from planarity to a tilted structure during the dimerization process might compensate the additional dimerization energy.

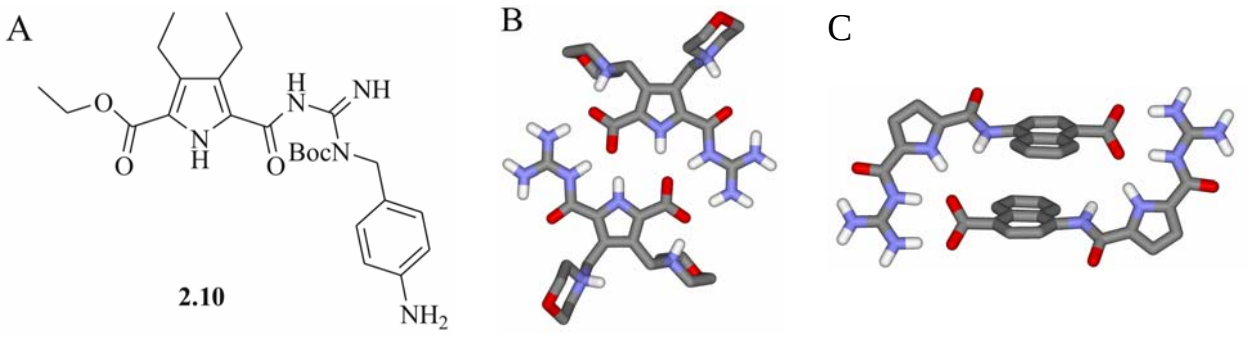

Fig. 5.8 *A) Multi-purpose building block **2.10**; B) dimerized morpholine zwitterion; C) naphthalene derived zwitterion capable of stacking interactions.*

5.4 Conclusion

This PhD thesis introduced several concepts for the construction of new supramolecular assemblies in polar solvents. Although the building blocks differ in their binding mode and association strength they follow the same principle: one main driving force for the self-assembly in polar solutions in combination with one texturing force. The main self-assembly process is based on the mutual interaction of hydrogen-bond enforced ion pairs which deliver the association energy needed for stable, supramolecular structures even in polar solvents. The texturing force itself is represented by the linkers between the zwitterionic building blocks or parts of them. The different length and functionalization of the linkers have a tremendous influence on the mode of self-assembly leading to cyclic dimers, vesicles, layers or solid spheres. Hence, this principle is suitable for the construction of programmable monomers. Since the derivatisation of the main binding motive is rather simple it offers a great number of new and undoubtedly fascinating structures with potential applications in material and biomimetic science.

6 Zusammenfassung

Der Schwerpunkt dieser Doktorarbeit liegt auf der Synthese und Analyse von supramolekularen Verbindungen, deren Grundbaustein das Guanidiniocarbonylpyrrolcarboxylat-Zwitterion darstellt (Abbildung 6.1). Auf Grund der Selbstkomplementarität dieses Bausteins und seiner außergewöhnlich stabilen Selbstassoziation in polaren Solventien wurde er für die Synthese von supramolekularen Monomeren eingesetzt. Die sich an die Synthese anschließende Analyse der erhaltenen Aggregate erlaubte es, einen faszinierenden Einblick in den Selbstassoziationsprozess dieser neuen Verbindungsklasse zu erlangen.

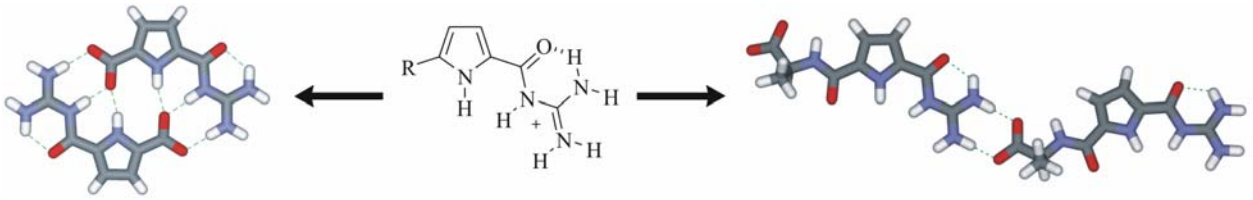

Abb. 6.1 *Guanidiniocarbonylpyrrole als Rezeptoren für Carboxylate: selbstkomplementäre Grundbausteine für supramolekulare Verbindungen (Wasserstoffbrückenbindungen sind als grüne, gestrichelte Linien dargestellt).*

6.1 Supramolekulare Strukturen auf Basis der Selbstassoziation von Bis- oder Triple-Zwitterionen

Es wurden drei Bis-Zwitterionen und ein Triple-Zwitterion synthetisiert, deren Bindungsmotive über flexible Alkylketten kovalent miteinander verknüpft sind. Die Unterschiede zwischen den Linker-Molekülen liegen vor allem in ihrer Länge und chemischen Beschaffenheit. Die Analyse der entstandenen supramolekularen Verbindungen beweist den starken Einfluß des Linkers auf die Art der Selbstassoziation. Obwohl die Ionenpaarbildung die treibende Kraft ist, führen erst die zusätzlichen Wechselwirkungen, entweder zwischen dem Linker und dem Solvens oder zwischen den Linkerketten selbst, zu der charakteristischen Struktur der supramolekularen Verbindung. Das erste Beispiel ist das Bis-Zwitterion **2.2**, in dem zwei zwitterionische Bindungsmotive über einen langen und hydrophilen Triethylenglykol-Linker verbunden sind (Abbildung 6.2). Die Selbstassoziation von **2.2** führt zur Ausbildung von zyklischen Dimeren, deren Größe sich auf wenige Nanometer beschränkt. Gelöst in DMSO liegt **2.2** in einem konzentrationsabhängigen Monomer-Dimer-Gleichgewicht vor, wobei in höher konzentrierten Lösungen das Dimer die dominante Spezies ist. DOSY NMR, dynamische Lichtstreuung und Kleinwinkelneutronenstreuung zeigen einen hydrodynamischen Radius von r_H = 2.0 nm für das Dimer von **2.2**. Desweiteren

konnte unter den gegebenen Bedingungen die Ausbildung größerer Aggregate zumindest im detektierbaren Meßbereich ausgeschlossen werden.

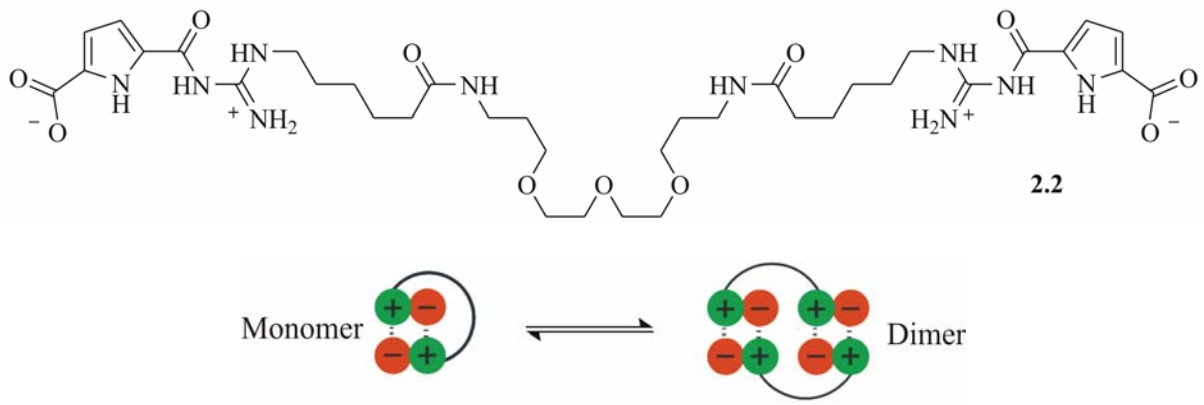

Abb. 6.2 *Bis-Zwitterion **2.2** dimerisiert unter Ausbildung einer zyklischen Struktur.*

Das zweite Bis-Zwitterion **2.3** verknüpft zwei Bindungsmotive mit einem kurzen und hydrophoben Linker (Abbildung 6.3). In Lösung liegt **2.3** ebenfalls in einem konzentrationsabhängigen Monomer-Dimer-Gleichgewicht vor. Jedoch führt der Selbstassoziationsprozess von **2.3** auch zur Ausbildung von größeren Strukturen in Form von wohl definierten Vesikeln. Dieser neue Aspekt der Selbstassoziation wurde mit DLS untersucht, wobei für die Vesikel ein Durchmesser von 140 nm ermittelt wurde. Mit Hilfe der Ergebnisse von AFM- und SANS-Experimente konnte ein Strukturmodel für die Membran entwickelt werden. Im Vergleich zu **2.2** verhält sich **2.3** wie ein Bolaamphiphil. Das unpolare Mittelstück der Monomere ist wahrscheinlich maßgeblich für die Ausbildung der Vesikel verantwortlich.

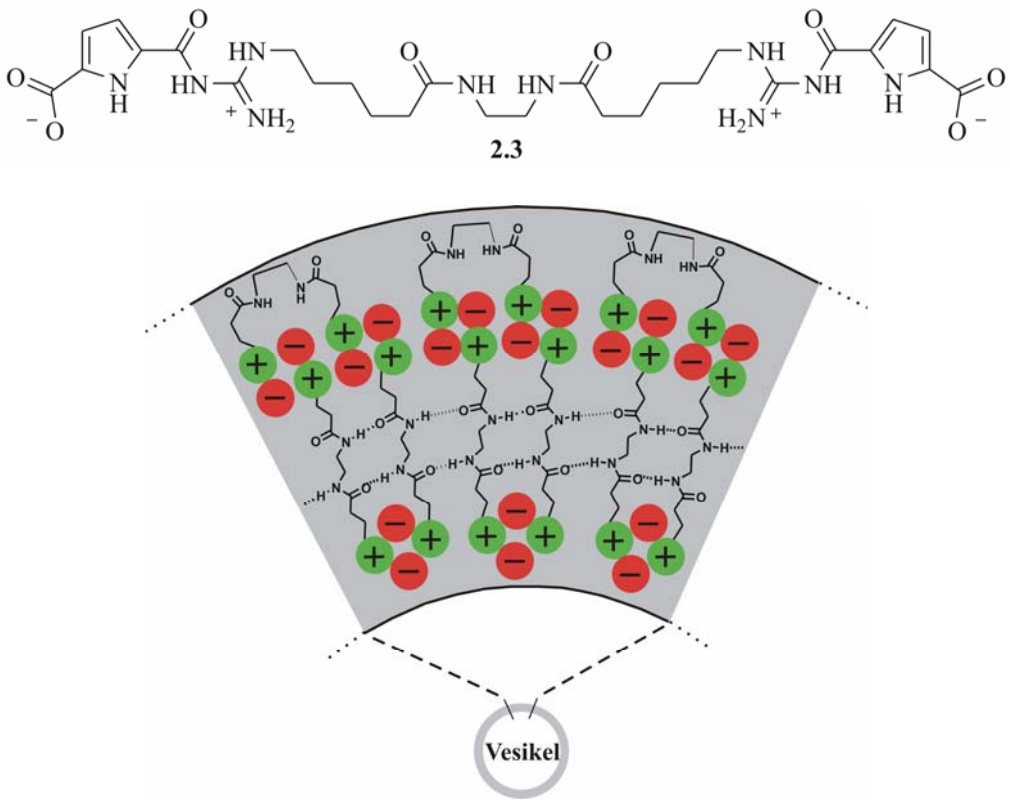

Abb. 6.3 *Die Selbstassoziation des Bis-Zwitterions* ***2.3*** *führt zur Ausbildung von großen Vesikeln auf Basis der bolaamphiphilen Struktur des Monomers.*

Das dritte Beispiel, Bis-Zwitterion **2.4**, unterscheidet sich nur in der Länge des unpolaren Linkers, der über zehn CH_2 Einheiten verfügt, anstelle von zwei, wie es in **2.3** der Fall ist (Abbildung 6.4). Analog zu **2.3** liegt **2.4** in Lösung auch in einem konzentrationsabhängigen Monomer-Dimer-Gleichgewicht vor und bildet Vesikel mit einem Durchmesser von 140 nm aus. Im Fall einer Wechselwirkung mit einer festen Oberfläche scheiden sich diese Vesikel unter Ausbildung von schichtartigen Strukturen ab. AFM-Experimente haben gezeigt, dass sich aus stark verdünnten Lösungen Monolagen abscheiden, wohingegen konzentrierte Lösungen zu mehrschichtigen Strukturen führen. Alle experimentellen Daten deuten bei diesem System auf den starken Einfluß des Linkers als treibende Kraft zur Schichtbildung hin. Im Vergleich zu **2.3** führen wahrscheinlich die längeren Alkylketten des Linkers zu wesentlich stärkeren *van der Waals*-Wechselwirkungen innerhalb der unpolaren Region.

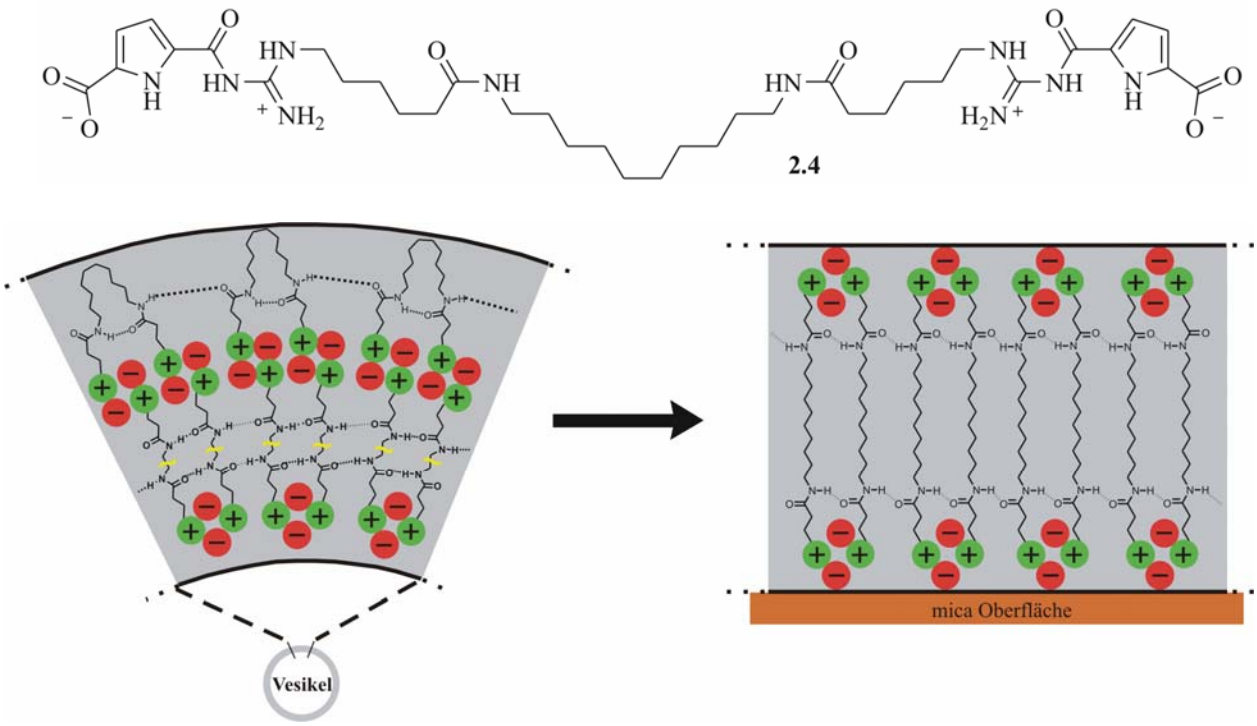

Abb. 6.4 *Die Selbstassoziation des Bis-Zwitterions* ***2.4*** *führt zur Ausildung von Vesikeln, die sich auf einer Oberfläche in Form von großflächigen Schichten umorientieren (Die Alkylketten innerhalb der Vesikelmembran sind verkürzt als gelbe Wellenlinie dargestellt.).*

Das letzte Beispiel in diesem Projekt ist das Triple-Zwitterion **2.5**. Dieser Baustein ist bisher der einzige, der drei zwitterionische Bindungsmotive in einem Molekül vereint (Abbildung 6.5). Dieser bedeutende Unterschied spiegelt sich auch in einem veränderten Selbstassoziationsverhalten wider. In Lösung ist das Dimer die kleinste supramolekulare Einheit von **2.5**, das im Gleichgewicht mit zylinderförmigen Oligomeren vorliegt. Diese wurmartigen Strukturen knäulen sich zusammen und bilden, im Gegensatz zu den Vesikeln der Zwitterionen **2.3** und **2.4**, Vollkugeln mit einem gemittelten Durchmesser von 90 nm und einem inhomogenen Inneren. Im Zuge der Probenpräparation für die AFM-Experimente lagern sich die sphärischen Partikel auf mica ab und bilden dabei runde, plattenförmige Strukturen aus. Die innere Struktur dieser Platten zeigt ein Netzwerk auf, das auf kleinen runden Partikeln bzw. Platten basiert. Diese kleinen Strukturen werden wahrscheinlich durch die wurmartigen Oligomere, wie sie in Lösung vorliegen, gebildet. Konzentrationsabhängige AFM-Experimente zeigten große, einzelne Platten, die sich mit zunehmender Konzentration in eine weitläufige netzwerkartige Struktur umwandeln. Dieses Verhalten ist aller Wahrscheinlichkeit nach auf das Verschmelzen einer großen Anzahl von Vollkugeln während der Probenpräparation zurückzuführen. Dieser hierarchische Prozess der Selbstassoziation von **2.5** steht damit im klaren Gegensatz zu den zuvor vorgestellten Bis-Zwitterionen.

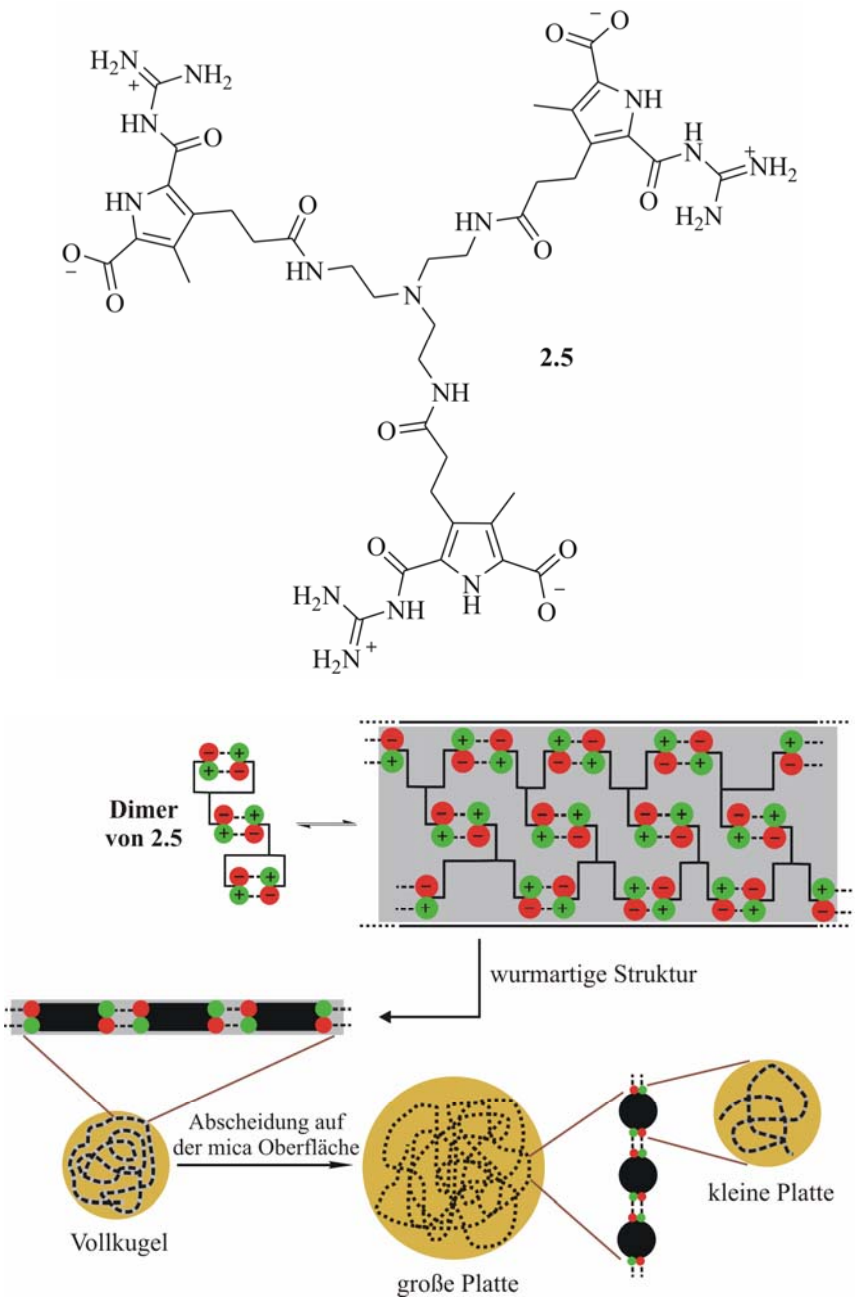

Abb. 6.5 *Das Triple-Zwitterion* **2.5** *bildet in einem hierarchischen Selbstassoziationsprozess Vollkugeln mit einer netzwerkartigen Struktur aus.*

Als Fazit kann festgehalten werden, dass die strukturellen und chemischen Eigenschaften der Linkermoleküle einen sehr großen Einfluss auf die Selbstassoziation der vier vorgestellten Monomere hat. Die Kombination einer starken Triebkraft in Form von selbstassoziierenden Ionenpaaren zusammen mit einer strukturgebenden Kraft, eingeführt durch die Linkermoleküle, eröffnet die Möglichkeit, unterschiedliche Nanostrukturen aufzubauen.

6.2 Änderung des Bindungsmodus: vesikulare Strukturen basierend auf α-Aminosäure-abgeleiteten Zwitterionen

Der zweite Teil dieser Doktorarbeit beschreibt die Synthese und Analyse von vier neuen, zwitterionischen Bausteinen. Die Idee dieses Konzeptes ist es, die geladenen Endgruppen durch die Einführung von α-Aminosäuren räumliche stärker zu trennen. Abbildung 6.6 zeigt die hergestellten Verbindungen, die von *L*-Alanin, *L*-Serin, *L*-Phenylalanin und *L*-Tyrosin abgeleitet wurden.

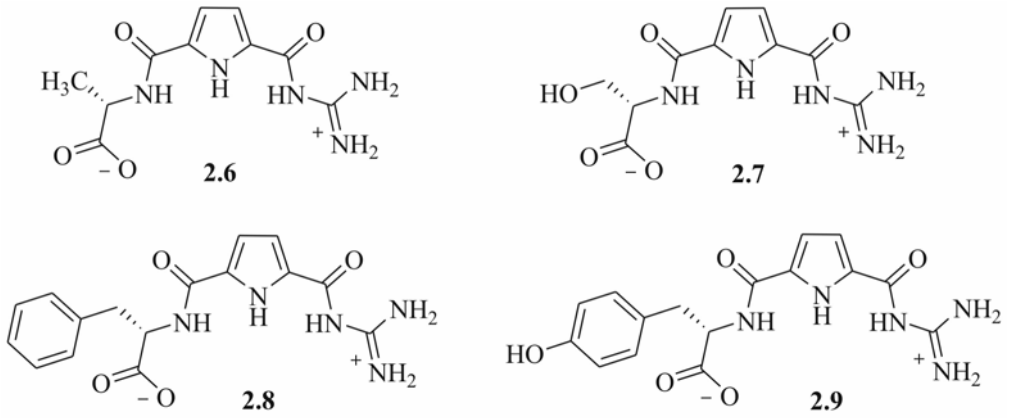

Abb. 6.6 *Vier neue zwitterionische Bausteine auf Basis von vier verschiedenen α-Aminosäuren.*

AFM-Experimente mit frisch hergestellten Proben aller vier Verbindungen lassen die die Ausbildung von vesikularen Strukturen vermuten. Alle vier Verbindungen sind in DMSO sehr gut löslich, wobei sich aber die Zwitterionen **2.8** und **2.9** mit aromatischen Aminosäureseitenketten nach wenigen Minuten als Feststoffe niederschlugen. Aus diesem Grund konnten nur die Zwitterionen basierend auf *L*-Alanin und *L*-Serin detaillierter untersucht werden. ^{1}H-NMR-Verdünnungsreihen, COSY- und NOESY-Experimente deuten auf einen ungewöhnlichen und schwachen bi-dentaten Bindungsmodus zwischen der Carboxylat- und Guanidiniumgruppe hin, der zur Ausbildung gestreckter, aber leicht abgewinkelter Dimere führt. Neben der schwächeren Ionenpaarwechselwirkung finden zusätzliche hydrophobe beziehungsweise aromatische Stapelwechselwirkungen zwischen den Monomeren statt, welche die eigentliche Triebkraft für die Membranbildung der Vesikel darstellen. Die Seitenketten der Aminosäuren bedingen eine große sterischen Raumbeanspruchung in der Mitte der Membran und führen dadurch zu einer Krümmung der Membran wie es für die Ausbildung von Vesikeln nötig ist (Abbildung 6.7).

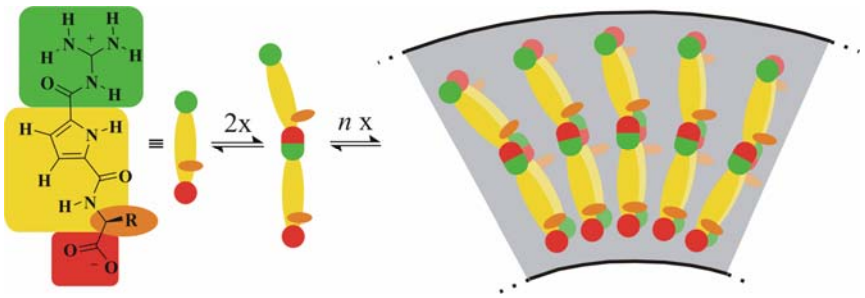

Fig. 6.7 *Schematische Darstellung der Membranbildung auf Basis der Selbstassoziation von a-Aminosäure-abgeleiteten, zwitterionischen Monomeren.*

Es ist festzuhalten, dass die neuen zwitterionischen Bausteine, basierend auf *α*-Aminosäuren, in Lösung Vesikel ausbilden. Auf Basis der experimentellen Daten müssen diese Strukturen auf jeden Fall zu der Klasse der *soft materials* gezählt werden. Dabei ist es erstaunlich, dass Moleküle selbst von so geringer Größe Vesikel ausbilden, wie sie hier vorgestellt wurden.

6.3 Konzepte für die Synthese von Schachteln, Käfigen und neuen zwitterionischen Bindungsmotiven

Der letzte Teil dieser Doktorarbeit umreißt drei zukünftige Projekte, die auf den Ergebnissen computergestützter Vorarbeiten beruhen. Das erste Projekt beschreibt die Synthese von vororganisierten Monomeren, die durch gezielte Selbstassoziation stabile Dimere mit wohl definiertem Innenvolumen formen sollen. Hierfür wurde die *Bromid-Route* entwickelt: die Guanidinogruppe des Bindungsmotivs führt dabei eine nukleophile Substitution der Bromide an den benzylischen Positionen der semi-flexiblen Linkermoleküle durch. Um jedoch auch die Länge des Abstandshalters vernünftig variieren zu können, wurde der Multifunktionsbaustein **2.10** entwickelt (Abbildung 6.8A). Mit Hilfe seiner freien Aminogruppe am Linkerbaustein konnte er mit verschiedenen, starren Molekülen verknüpft werden. Dabei wurden in den ersten Beispielen Naphthalintetracarbonsäuredianhydrid beziehungsweise Cyanursäurechlorid verwendet.

Das zweite Projekt behandelt die Synthese eines positiv geladenen Derivats des ursprünglichen Zwitterions. Der Schlüsselschritt ist dabei die nukleophile Substitution der Bromide im Vorläufermolekül **4.32** durch Morpholin. Im zwitterionischen Zustand sollten die Stickstoffatome der Morpholin-Substituenten protoniert sein (Abbildung 6.8B) und somit zu einer besseren Löslichkeit in Wasser führen.

Das letzte Konzept präsentiert die ersten Ergebnisse der Synthese eines neuen zwitterionischen Bindungsmotivs, das zusätzlich über die Möglichkeit von aromatischen Wechselwirkungen verfügt. Die geladenen Endgruppen wurden durch aromatische Untereinheiten wie zum Beispiel

einen Benzolring als einfachsten Linker oder einem Naphthalinring als nächst größere, aromatische Einheit getrennt. Synthetisch ist das Benzolderivat in drei Schritten zugänglich. Theoretische Berechnungen auf DFT-Niveau wurden für beide Systeme durchgeführt. Die berechnete Geometrie des Naphthalinderivats weißt auf ein mögliches *π-stacking* hin (Abbildung 6.8C), jedoch könnte der notwendige Konformationswechsel von planar im Monomere zu verdrillt im Dimer die zusätzlich gewonnene Dimerisierungsenergie kompensieren.

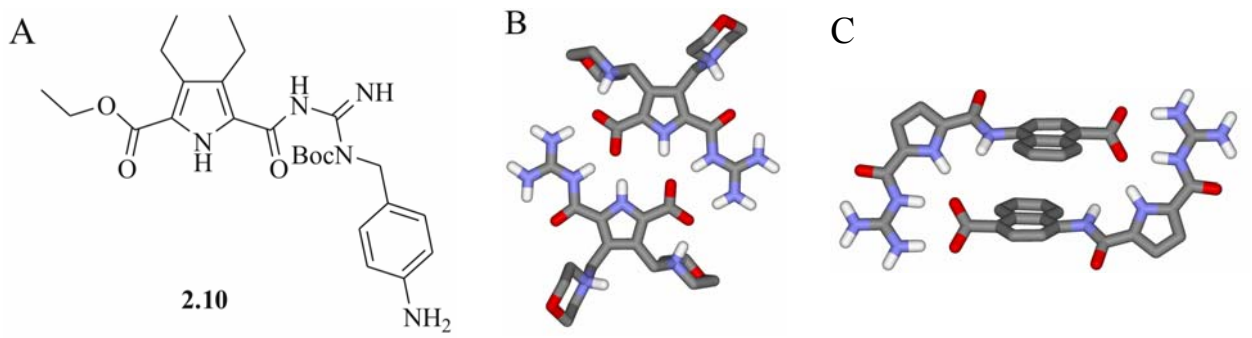

Abb. 6.8 *A) Multifunktionsbaustein* ***2.10****; B) dimerisiertes Zwitterion des Morpholin-Derivats; C) dimerisiertes Naphthalin-Derivat des ursprünglichen Zwitterions.*

6.4 Fazit

Diese Doktorarbeit stellte mehrere Konzept für den Aufbau von neuen supramolekularen Verbindungen in polaren Solventien vor. Obwohl sich die Bausteine bezüglich ihres Bindungsmodus und ihrer Assoziationsstärke unterscheiden, folgen sie alle dem gleichen Prinzip: eine Haupttriebkraft für den Selbstassoziationsprozess in polaren Lösemitteln in Kombination mit einer strukturgebenden Kraft. Die Haupttriebkraft stellen wasserstoffbrückenbindungsvermittelte Ionenpaare dar, die die nötige Assoziationsenergie für stabile, supramolekulare Strukturen auch in polaren Lösungen liefern. Die strukturierende Kraft selbst wird durch die Linkermoleküle zwischen den Zwitterionen oder Teilen von diesen vermittelt. Die unterschiedliche Länge und Funktionalisierung der Linker haben einen enormen Einfluss auf den Modus der Selbstassoziation, so dass die Bildung von zyklischen Dimeren, Vesikeln, Schichten oder Vollkugeln möglich war. Daher kann dieses Konzept für den Aufbau von programmierbaren Monomeren verwendet werden. Die Derivatisierung des zwitterionischen Bindungsmotivs gestaltet sich relativ einfach, so dass eine große Anzahl von neuen und zweifelsohne faszinierenden Nanostrukturen für zukünftige Anwendungen in der Materialwissenschaft und Biomimetik zur Verfügung steht.

7 Experimental section

7.1 General experimental methods

Solvents and chemicals

All solvents were dried according to literature procedures.[1] Dichloromethane and *N,N*-dimethyl formamide were dried by distillation from calcium hydride. Diethyl ether and tetrahydrofuran were distilled from sodium with benzophenone as indicator. Methanol was distilled from magnesium. All other commercial reagents were purchased and used as received unless otherwise specified.

Inert gas

Reactions with humidity-sensitive compounds were carried out under technical nitrogen (99.996 %, purchased from *Linde*), which was dried with blue gel and calcium chloride.

Vacuum pumps

Vacuubrand Diaphragm vacuum pump MZ C2

Vacuubrand Sliding vane rotary vacuum pump RD 8

Lyophilisation

Christ Alpha 1-4 LD plus

All lyophilisations were performed from salt-free water. If necessary, the substances were dissolved in a few millilitres of methanol.

Rotary evaporation

Büchi Rotavapor RE 111 and *Büchi* Water bath 461

Concentration under reduced pressure was performed by rotary evaporation at 40 °C at the appropriate pressure for the solvent used.

7.2 General analytical methods

Thin layer chromatography (TLC)

Machery-Nagel POLYGRAM SIL G/UV_{254} (40 × 80 mm plates, 0.25 mm)

Benda Nu-4 KL (short wavelength: 254 nm, long wavelength: 366 nm)

Reactions were monitored by TLC on silica gel 60 F254 precoated plates. Visualization of the spots was carried out by fluorescence quenching with 254 nm UV light. The TLC elution mixtures are reported in volume percent except otherwise stated.

Flash chromatography

Acros Organics, Silicagel for chromatography, 0.035-0.070, 60 Å

MP Biomedicals Company, MP Silica 32-63, 60 Å

Flash chromatography was performed on silica gel with the indicated solvent mixtures on columns of different diameter and length. Solvent mixtures used for flash chromatography are reported in volume percent. Yields refer to chromatographically purified and spectroscopical pure compounds, unless otherwise stated.

Nuclear magnetic resonance (NMR)

Bruker Avance 400 (^{1}H: 400 MHz; ^{13}C: 100 MHz)

Bruker DMX 600 (^{1}H: 600 MHz; ^{13}C: 150 MHz)

For standard analytical purpose ^{1}H-NMR spectra were recorded at 400 MHz and ^{13}C-NMR spectra at 100 MHz. All measurements were performed at room temperature, using DMSO-d_6 or $CDCl_3$ as solvents. The chemical shifts are reported in ppm from TMS (δ scale), but were measured against the solvent signal. All ^{1}H-DOSY NMR experiments were performed at 600 MHz, employing DMSO-d_6 as solvent. The chemical shifts are reported in ppm and measured against TMS (δ scale). The apparent coupling constants are given in Hertz. Their description of the fine structure means: s = singulett, br.s = broad singulett, d = dublett, t = triplett, dt = dublett of triplett, m = multiplett, br = broad signal. All assignments have been performed according to literature.[2]

Mass spectrometry (MS)

High resolution ESI and APCI: *Bruker Daltonik* MicrOTOF^{TM} focus

MALDI-TOF: *Bruker Daltonik* Autoflex$_{TOF}^{TM}$ II LRF 50

EI and FAB: *Finnigan* Mat 90

Fourier transform infrared spectrocopy (FT-IR)

Jasco FT-IR 410 Spectrophotometer

The maxima are classified in three intensities: s (strong), m (middle), w (weak) and are reported in cm^{-1}

Melting point

Büchi SMP-20 apparatus, according to *Dr. Tottoli*

All melting points were measured with open end glas capillary tubes and are not corrected.

7.3 Synthesis, deprotection and purification of bis-zwitterion 2.4 with the hydrophobic C10-spacer

7.3.1 Synthesis of the fully protected bis-zwitterion 4.11 [TR 243]

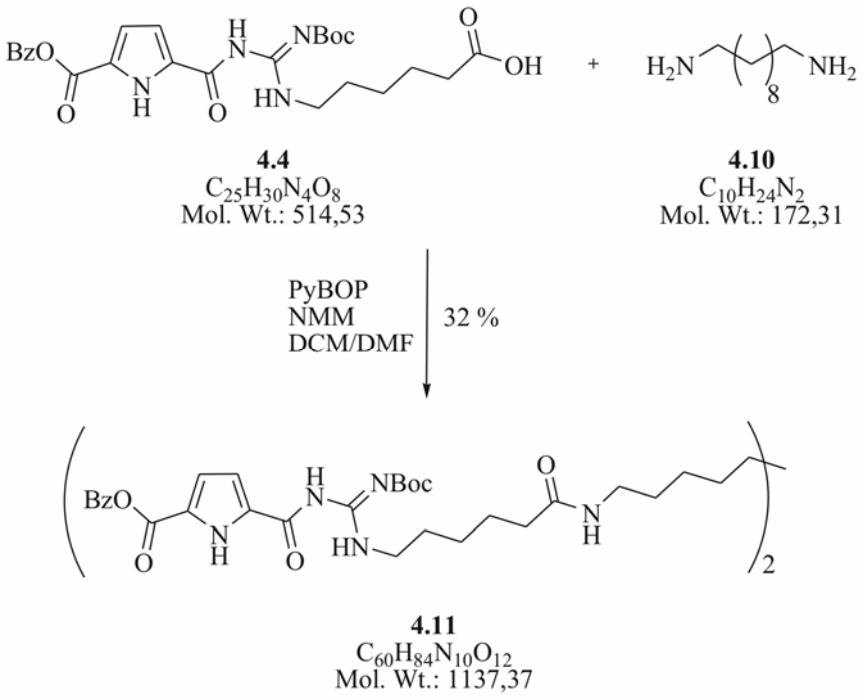

4.4
$C_{25}H_{30}N_4O_8$
Mol. Wt.: 514,53

4.10
$C_{10}H_{24}N_2$
Mol. Wt.: 172,31

4.11
$C_{60}H_{84}N_{10}O_{12}$
Mol. Wt.: 1137,37

A solution of **4.4** (1.03 g, 2.06 mmol, 2 eq) and PyBOP (1.29 g, 2.47 mmol, 2.4 eq) was stirred in DCM/DMF (50 ml, 4/1) and NMM (4 ml) for one hour at room temperature. After the addition of 1,10-diaminodecane **4.10** (160 mg, 0.93 mmol, 0.9 eq) the reaction mixture was stirred for 24 hours at room temperature. The slightly yellow solution was concentrated *in vacuo*, poured into water (50 ml), extracted with ethyl acetate (4 x 90 ml) and washed with a concentrated solution of sodium chloride (2 x 50 ml). The organic phase was dried with magnesium sulphate and concentrated *in vacuo*. The crude product was purified by column chromatography (SiO_2, ethyl acetate/cyclohexane/methanol = 8/1.5/0.5). For further purification the resulting oil was lyophilised from water/methanol (9/1) yielding **4.11** as a colourless solid.

$C_{60}H_{84}N_{10}O_{12}$	1137.37 g/mol
yield	340 mg (0.30 mmol, 32 %)
R_f	0.73 (SiO_2 with ethyl acetate/cyclohexane/methanol = 8/1.5/0.5)
melting point	66 °C

^{1}H-NMR (400 MHz, DMSO-d_6) δ = 1.26-1.33 (m, 16H, CH_2), 1.48 (s, 18H, CH_3), 1.43-1.58 (m, 12H, CH_2), 2.04 (t, 4H, $^{3}J_{CHCH}$ = 7.2 Hz, CH_2CONH), 2.98 (dt, 4H, $^{3}J_{CHCH}$ = 6.32 Hz, $^{3}J_{CHNH}$ = 6.08 Hz, NHCH_2CH$_2$), 3.50 (dt, 4H, $^{3}J_{CHCH}$ = 6.84 Hz, $^{3}J_{CHNH}$ = 5.92 Hz, NHCH_2CH$_2$), 5.29 (s, 4H, benzyl-CH_2), 6.77-6.78 (m, 2H, pyrrole-C*H*), 6.82-6.78 (m, 2H, pyrrole-C*H*) 7.31-7.45 (m, 10H, aryl-C*H*), 7.66 (t, 2H, $^{3}J_{NHCH}$ = 5.32 Hz, N*H*), 8.55 (t, 2H, $^{3}J_{NHCH}$ = 5.44 Hz, N*H*), 11.80 (br.s, 2H, N*H*), 12.35 (br.s, 2H, N*H*).

^{13}C-NMR (100 MHz, DMSO-d_6) δ = 25.0 (*C*H$_2$), 25.9 (*C*H$_2$), 26.4 (*C*H$_2$), 27.6 (*C*H$_3$), 28.5 (*C*H$_2$), 28.7 (*C*H$_2$), 28.9.6 (*C*H$_2$), 29.1 (*C*H$_2$), 35.3 (*C*H$_2$), 38.3 (*C*H$_2$), 40.6 (*C*H$_2$), 65.4 (benzyl-*C*H$_2$), 82.9 (C_q), 114.2 (pyrrole-*C*H), 115.7 (pyrrole-*C*H), 124.8 (C_q), 127.8, 128.0, 128.4 (aryl-*C*H), 135.5 (C_q), 136.3 (C_q), 152.1 (C_q), 155.5 (C_q), 159.8 (C_q), 169.9 (C_q), 171.7 (C_q).

HR-MS (ESI pos.) m/z = 1159.6137, calculated for $^{12}C_{60}H_{84}N_{10}O_{12} + Na^{+}$: 1159.6167

FT-IR (KBr) $\tilde{\nu}$ [cm^{-1}] = 3448 [w], 3323 [w], 2930 [w], 2935 [m], 2856 [w], 1717 [s], 1619 [s], 1583 [s], 1548 [s], 1409 [m], 1365 [s], 1276 [s], 1147 [s].

7.3.2 Deprotection of 4.11 and purification of bis-zwitterion 2.4 [TR 252]

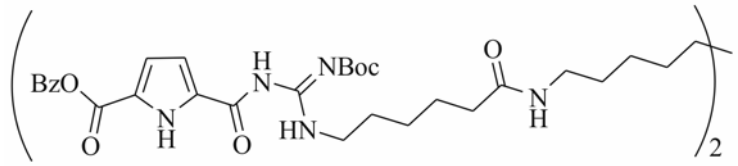

4.11
$C_{60}H_{84}N_{10}O_{12}$
Mol. Wt.: 1137,37

1) H_2/Pd/C
THF
2) TFA
3) $NaOH_{aq}$

90 %

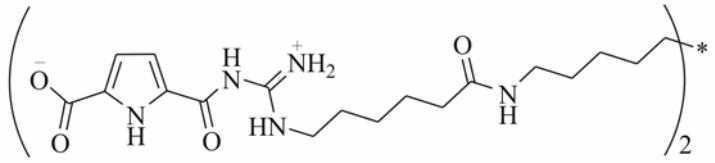

2.4
$C_{36}H_{56}N_{10}O_8$
Mol. Wt.: 756,89

A mixture of **4.11** (300 mg, 0.26 mmol, 1 eq) and palladium on activated charcoal (30 mg) in THF (30 ml) was stirred for four hours under hydrogen atmosphere. The reaction was controlled via TLC (ethyl acetate/cyclohexane/methanol = 8/1.5/0.5 + 1 % triethylamine). After complete conversion the mixture was filtered over a celite pad and washed several times with ethyl acetate. The solvent was evaporated and the resulting oil was dried in high vacuum. After the addition of TFA (4 ml) the reaction mixture was stirred for two hours at room temperature. After that the remaining TFA was removed in high vacuum. The resulting oil was dissolved in water and 0.5 N sodium hydroxide solution was added until a colourless solid precipitated (pH ~ 5-6). The crude product was filtered, washed several times with water and lyophilised from water resulting **2.4** as a colourless powder. For further purification **2.4** was suspended in water/dioxan (40 ml, 1/1, v/v) and refluxed for one hour. The colourless suspension was filtered and washed several times with pure water and diethyl ether. The resulting colourless solid (180 mg) was dried in high vacuum. For analytic purposes the picrate salt of **2.4** was produced by addition of aqueous picric acid to pure **2.4**. The suspension was refluxed until a clear deep yellow solution resulted. The picrate salt crystallized within 3 hours of cooling down the solution to room temperature.

$C_{36}H_{56}N_{10}O_8$	756.89 g/mol
yield	180 mg (0.24 mmol, 90 %)
melting point (picrate salt)	> 220 °C
^{1}H-NMR (picrate salt)	(400 MHz, DMSO-*d*$_6$) δ = 1.21-1.35 (m, 20H, C*H*$_2$), 1.51-1.55 (m, 8H, C*H*$_2$), 2.06 (t, 4H, $^3J_{CHCH}$ = 6.68 Hz, C*H*$_2$), 3.00 (dt, 4H, $^3J_{CHCH}$ = 5.52 Hz, $^3J_{CHNH}$ = 5.84 Hz, C*H*$_2$), 6.85 (br, 2H, pyrrole-C*H*), 7.01 (br, 2H, pyrrole-C*H*), 7.71 (br, 2H, N*H*), 8.58 (s, 4H, picrate-C*H*), 8.77 (br.s, 2H, N*H*), 10.77 (br.s, 2H, N*H*), 12.68 (br.s, 2H, N*H*), 13.12 (br.s, 2H, COO*H*); one CH_2 signal (4H) is superposed by water. The guanidinium-N*H*s (4H) are superposed by picrate-C*H*s and amide-N*H*s.
^{13}C-NMR (picrate salt)	(100 MHz, DMSO-*d*$_6$) δ = 24.8 (*C*H$_2$), 25.7 (*C*H$_2$), 26.4 (*C*H$_2$), 27.5 (*C*H$_2$), 28.7 (*C*H$_2$), 29.0 (*C*H$_2$), 29.2 (*C*H$_2$), 35.2 (*C*H$_2$), 38.4 (*C*H$_2$), 41.1 (*C*H$_2$), 115.2 (pyrrole-*C*H), 115.5 (pyrrole-*C*H), 124.2 (C_q), 125.2 (picrate-*C*H), 127.0 (C_q), 141.9 (C_q), 153.0 (C_q), 159.2 (C_q), 160.8 (C_q), 161.2 (C_q), 171.7 (C_q).
HR-MS (ESI pos.)	m/z = 757.4335, calculated for $^{12}C_{36}H_{56}N_{10}O_8 + H^+$: 757.4360
FT-IR (KBr)	$\tilde{\nu}$ [cm^{-1}] = 3323 [w], 3189 [w], 3097 [w], 2927 [m], 2856 [w], 1717 [m], 1646 [s], 1557 [m], 1485 [m], 1445 [m], 1348 [s], 1321 [s], 1218 [s].

7.4 Synthesis of the *α*-amino acid derived zwitterions

7.4.1 Synthesis of the *L*-alanine derived zwitterion 2.6

7.4.1.1 Synthesis of the *L*-alanine methyl ester hydrochloride 4.20a [TR 19]

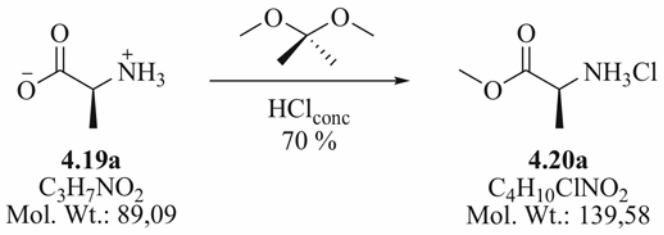

4.19a
$C_3H_7NO_2$
Mol. Wt.: 89,09

4.20a
$C_4H_{10}ClNO_2$
Mol. Wt.: 139,58

A suspension of *L*-alanine **4.19a** (3.00 g, 33.7 mmol, 1 eq) in 2,2-dimethoxypropane (87.7 g, 0.84 mol, 25 eq) was stirred vigorously while adding concentrated hydrochloric acid (17.2 ml). The solution was then stirred for 24 hours at room temperature. After that time the dark red solution was concentrated *in vacuo* and the resulting brown solid was dissolved in water (100 ml). The aqueous solution was washed three times with ethyl acetate (150 ml) and lyophilized providing a colourless oil, which crystallized in diethyl ether at 0 °C.

$C_4H_{10}ClNO_2$	139.58 g/mol
yield	3.29 g (23.6 mmol, 70 %)
melting point	180 °C
^{1}H-NMR	(400 MHz, DMSO-d_6) δ = 1.42 (d, $^3J_{CHCH}$ = 7.2, 3H, CH_3), 3.73 (s, 3H, CH_3), 4.02-4.08 (m, 1H, CH), 8.54 (br.s, 3H, NH_3^+).
^{13}C-NMR	(100 MHz, DMSO-d_6) δ = 15.6 (CH$_3$), 47.8 (CH), 52.7 (CH$_3$), 170.4 (C_q).
FT-IR (KBr)	$\tilde{\nu}$ [cm^{-1}] = 3006 [s], 2932 [s], 1725 [s], 1606 [m], 1495 [m], 1238 [m], 812 [w], 612 [w], 518 [w].

7.4.1.2 Synthesis of the fully protected *L*-alanine derived zwitterion 4.21a [TR 28]

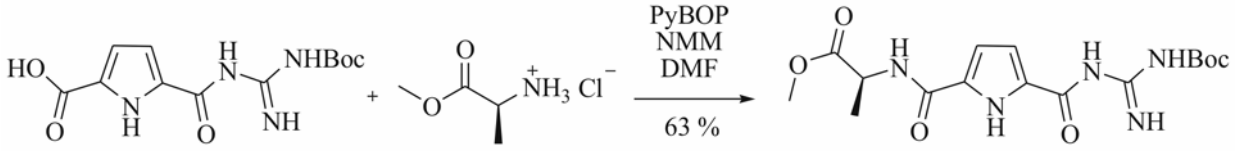

4.18
$C_{12}H_{16}N_4O_5$
Mol. Wt.: 296,28

4.20a
$C_4H_{10}ClNO_2$
Mol. Wt.: 139,58

4.21a
$C_{16}H_{23}N_5O_6$
Mol. Wt.: 381,38

A mixture of the *N*-boc-protected guanidinocarbonylpyrrole compound **4.18** (1.00 g, 3.38 mmol, 1 eq), PyBOP (1.76 mg, 3.38 mmol, 1 eq) and NMM (5.00 ml) was stirred in DMF (50 ml) at room temperature for one hour. The methyl ester **4.20a** (282 mg, 3.38 mmol, 1 eq) was added to the solution and then stirred for 24 h at room temperature. The resulting yellow solution was hydrolized with water (100 ml). The suspension was then extracted with diethyl ether (3 x 120 ml), the organic phases were combined, dried with magnesium sulphate and evaporated. The resulting orange oil was purified by column chromatography (SiO_2, ethyl acetate/cyclo-hexane/isopropanol = 6/3.5/0.5) yielding a colourless oil which was dissolved in a mixture of methanol and water. After lyophilisation the pure product was a slightly yellow powder.

$C_{16}H_{23}N_5O_6$	381.38 g/mol
yield	820 mg (2.15 mmol, 63 %)
R_f	0.71 (SiO_2 with ethyl acetate/cyclohexane/isopropanol = 6/3.5/0.5)
melting point	141 °C
^{1}H-NMR	(400 MHz, DMSO-d_6) δ = 1.38 (d, 3H, $^3J_{CHCH}$ = 7.2 Hz, CH_3), 1.46 (s, 9H, CH_3), 3.64 (s, 3H, CH_3), 4.42-4.49 (m, 1H, CH), 6.83 (br, 2H, pyr-role-CH), 8.57 (br.s, 1H, NH), 8.66 (d, $^3J_{NHCH}$ = 6.96 Hz, 1H, NH), 9.32 (br.s, 1H, NH), 10.86 (br.s, 1H, NH), 11.46 (br.s, 1H, NH).
^{13}C-NMR	(100 MHz, DMSO-d_6) δ = 16.8 (CH_3), 27.7 (CH_3), 47.8 (CH_3), 51.9 (CH), 112.7 (pyrrole-CH), 158.4 (C_q), 159.4 (C_q), 173.1 (C_q).
HR-MS (ESI pos.)	m/z = 404.1549, calculated for $^{12}C_{16}H_{23}N_5O_6 + Na^+$: 404.1546
FT-IR (KBr)	$\tilde{\nu}$ [cm^{-1}] = 3386 [m], 3274 [w], 2981 [w], 2954 [w], 2949 [w], 2937 [w],

1731 [s], 1634 [s], 1550 [s], 1471 [m], 1305 [m], 1241 [s], 842 [w], 755 [w], 600 [w].

7.4.1.3 Deprotection of 4.21a and purification of the *L*-alanine derived zwitterion 2.6 [TR 376]

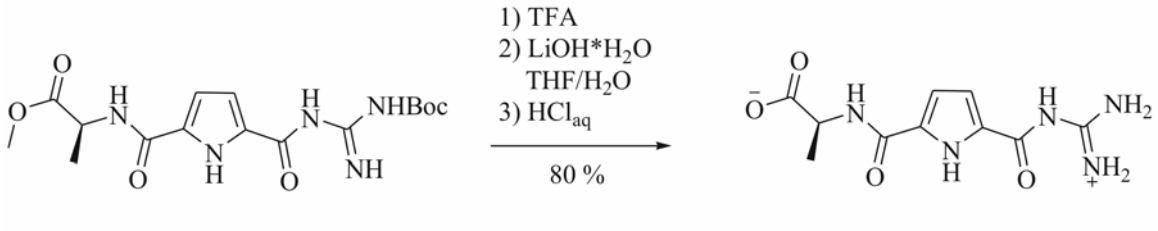

4.21a
$C_{16}H_{23}N_5O_6$
Mol. Wt.: 381,38

2.6
$C_{10}H_{13}N_5O_4$
Mol. Wt.: 267,24

A solution of fully protected **4.21a** (100 mg, 0.26 mmol, 1 eq) in TFA (5 ml) was stirred for 30 minutes at room temperature. The TFA was evaporated *in vacuo* to give a slightly brown oil, which was dissolved in a mixture of THF and water (20 ml, 4/1). After addition of lithium hydroxide monohydrate (54 mg, 1.31 mmol, 5 eq), the reaction mixture was stirred until TLC control (ethyl acetate/cyclohexane/isopropanol = 6/3.5/0.5 + 1 % triethylamine) showed no more starting material. After evaporation of the organic solvent, water (20 ml) was added. The zwitterion was produced by adjusting the pH to a value of 5-6 with 1 N aqueous hydrochloric acid. The colourless precipitate was filtered and washed several times with pure water and diethyl ether. After recrystallisation from water and dioxan, the analytical pure zwitterionic product was dried over phosphorous pentoxid in the desiccator.
The picrate salt of **2.6** was produced by suspending zwitterionic **2.6** in a few drops of methanol and addition of aqueous picric acid yielding the yellow picrate salt, which was filtered and dried over phosphorous pentoxid in the desiccator.

$C_{10}H_{13}N_5O_4$	267.24 g/mol
yield	56 mg (0.21 mmol, 80 %)
melting point (picrate salt)	194 °C (decompostition)
^{1}H-NMR (picrate salt)	(400 MHz, DMSO-d_6) δ = 1.38 (d, 3H, $^3J_{CHCH}$ = 7.3, CH_3), 4.37-4.44 (m, 1H, C*H*), 6.93-6.95 (m, 1H, pyrrole-C*H*), 7.03-7.05 (m, 1H, pyrrole-C*H*),

8.17 (br.s, 4H, guanidinium-N*H*$_2$), 8.57 (s, 2H, picrate-C*H*), 8.66 (d, $^3J_{NHCH}$ = 7.2, 1H, N*H*), 10.95 (br.s, 1H, N*H*), 12.49 (br.s, 1H, N*H*); the signal for the free acid is not detected due to the exchange with the solvent.

^{13}C-NMR (picrate salt) (100 MHz, DMSO-d_6) δ = 17.0 (*C*H$_3$), 47.8 (*C*H), 113.1 (pyrrole-*C*H), 115.3 (pyrrole-*C*H), 124.1 (C_q), 125.2 (picrate-*C*H), 132.2 (C_q), 141.9 (C_q), 154.8 (C_q), 158.8 (C_q), 159.4 (C_q), 160.8 (C_q), 174.3 (C_q).

HR-MS (ESI pos.) m/z = 290.0866, calculated for $^{12}C_{10}H_{13}N_5O_4 + Na^+$: 290.0865

FT-IR (KBr) $\tilde{\nu}$ [cm^{-1}] = 3385 [m], 3328 [m], 3199 [w], 3131 [w], 2990 [w], 1702 [s], 1638 [s], 1612 [s], 1559 [s], 1480 [m], 1433 [m], 1365 [m], 1335 [s], 1081 [w], 711 [w], 608 [w].

7.4.2 Synthesis of the *L*-serine derived zwitterion 2.7

7.4.2.1 Synthesis of the *L*-serine methyl ester hydrochloride 4.20b [TR 90]

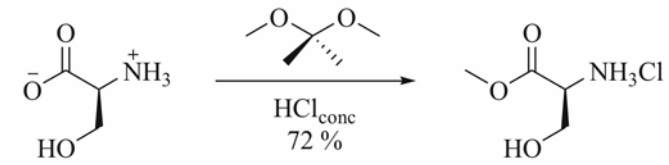

4.19b
$C_3H_7NO_3$
Mol. Wt.: 105,09

4.20b
$C_4H_{10}ClNO_3$
Mol. Wt.: 155,58

A suspension of *L*-serine **4.19b** (2.00 g, 19.0 mmol, 1 eq) in 2,2-dimethoxypropane (93.3 g, 0.76 mol, 40 eq) was stirred vigorously while adding concentrated hydrochloric acid (9.53 ml). The solution was then stirred for 24 hours at room temperature. After that time the dark red solution was concentrated *in vacuo* and the resulting brown solid was elutriated with diethyl ether. After filtration the crude product was recrystallized from isopropanol. The colourless solid was filtrated, washed with cold diethyl ether and dried in high vacuum.

$C_4H_{10}ClNO_3$ 155.58 g/mol

yield 2.14 g (13.8 mmol, 72 %)

melting point 179 °C

^{1}H-NMR (400 MHz, DMSO-d_6) δ = 3.74 (s, 3H, CH_3), 3.78-3.87 (m, 2H, CH_2), 4.09-4.11 (m, 1H, CH), 5.60 (br.s, 1H, OH), 8.54 (br.s, 3H, NH_3^+).

^{13}C-NMR (100 MHz, DMSO-d_6) δ = 52.7 (CH$_3$), 54.3 (CH), 59.4 (CH$_2$), 168.5 (C_q).

FT-IR (KBr) $\tilde{\nu}$ [cm^{-1}] = 3350 [s], 2943 [s], 1748 [s], 1594 [m], 1512 [s], 1472 [m], 1257 [s], 900 [w], 794 [w], 581 [w].

7.4.2.2 Synthesis of the fully protected *L*-serine derived zwitterion 4.21b [TR 104]

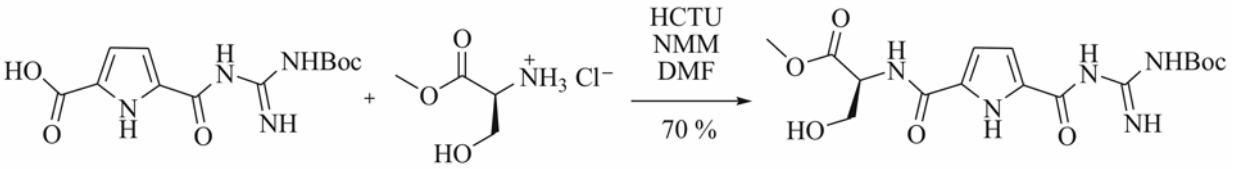

4.18
$C_{12}H_{16}N_4O_5$
Mol. Wt.: 296,28

4.20b
$C_4H_{10}ClNO_3$
Mol. Wt.: 155,58

4.21b
$C_{16}H_{23}N_5O_7$
Mol. Wt.: 397,38

A mixture of the *N*-boc-protected guanidinocarbonylpyrrole compound **4.18** (750 mg, 2.53 mmol, 1 eq), HCTU (1.05 g, 2.53 mmol, 1 eq) and NMM (2.00 ml) was stirred in DMF (20 ml) at room temperature for one hour. The methyl ester **4.20b** (394 mg, 2.53 mmol, 1 eq) was added to the solution and then stirred for 24 h at room temperature. The resulting yellow solution was hydrolized with water (100 ml). The suspension was then extracted with diethyl ether (3 x 120 ml), the organic phases were combined, dried with magnesium sulphate and evaporated. The resulting orange oil was purified by column chromatography (SiO_2, ethyl acetate/cyclohexane/isopropanol = 6/3.5/0.5 + 1 % triethylamine) yielding a colourless oil which was dissolved in a mixture of methanol and water. After lyophilisation the pure product was a colourless powder.

$C_{16}H_{23}N_5O_7$ 397.38 g/mol

yield 710 mg (1.79 mmol, 70 %)

R_f 0.35 (SiO_2 with ethyl acetate/cyclohexane/isopropanol = 6/3.5/0.5 + 1 % triethylamine)

melting point 125 °C

^{1}H-NMR (400 MHz, DMSO-d_6) δ = 1.46 (s, 9H, CH_3), 3.65 (s, 3H, CH_3), 3.70-3.80

(m, 2H, CH_2), 4.51-4.59 (m, 1H, C*H*), 5.09 (t, $^3J_{OHCH}$ = 5.68, 1H, OH), 6.83 (br, 2H, pyrrole-C*H*), 8.56 (br.s, 1H, N*H*), 8.63 (d, $^3J_{NHCH}$ = 7.56 Hz, 1H, N*H*), 9.31 (br.s, 1H, N*H*), 10.84 (br.s, 1H, N*H*), 11.59 (br.s, 1H, N*H*).

^{13}C-NMR (100 MHz, DMSO-d_6) δ = 27.8 (CH_3), 51.9 (CH_3), 55.0 (*C*H), 61.1 (CH_2), 113.0 (pyrrole-*C*H), 159.6 (C_q), 171.0 (C_q).

HR-MS (ESI pos.) m/z = 420.1496, calculated for $^{12}C_{16}H_{23}N_5O_7 + Na^+$: 420.1495

FT-IR (KBr) $\tilde{\nu}$ [cm^{-1}] = 3386 [m], 3279 [w], 2981 [w], 2954 [w], 2932 [w], 1732 [s], 1637 [s], 1549 [s], 1467 [m], 1298 [s], 1240 [s], 842 [w], 782 [w], 755 [w].

7.4.2.3 Deprotection of 4.21b and purification of the *L*-serine derived zwitterion 2.7 [TR 112]

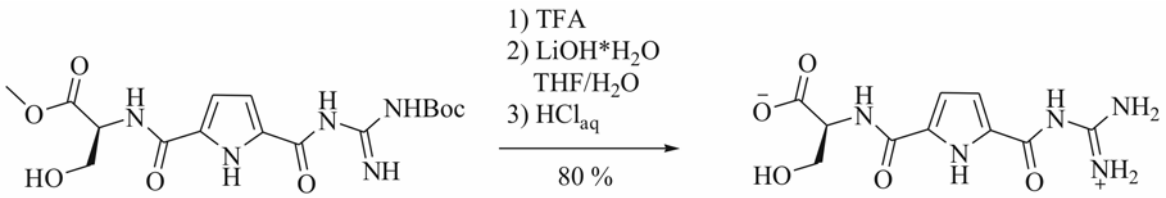

4.21b
$C_{16}H_{23}N_5O_7$
Mol. Wt.: 397,38

2.7
$C_{10}H_{13}N_5O_5$
Mol. Wt.: 283,24

A solution of fully protected **4.21b** (0.70 g, 1.76 mmol, 1 eq) in TFA (3 ml) was stirred for 30 minutes at room temperature. The TFA was evaporated *in vacuo* to give a slightly brown oil, which was dissolved in a mixture of THF and water (20 ml, 4/1). After addition of lithium hydroxide monohydrate (738 mg, 17.6 mmol, 10 eq), the reaction mixture was stirred until TLC control (ethyl acetate/cyclohexane/isopropanol = 6/3.5/0.5 + 1 % triethylamine) showed no more starting material. After evaporation of the organic solvent, water (20 ml) was added. The zwitterion was produced by adjusting the pH to a value of 5-6 with 1 N aqueous hydrochloric acid. The colourless precipitate was filtered and washed several times with pure water and diethyl ether. After recrystallization from water and dioxan, the analytically pure zwitterionic product was dried over phosphorous pentoxid in the desiccator.

The picrate salt of **2.7** was produced by suspending zwitterionic **2.7** in a few drops of methanol and addition of aqueous picric acid yielding the yellow picrate salt, which was filtered and dried over phosphorous pentoxid in the desiccator.

$C_{10}H_{13}N_5O_5$	283.24 g/mol
yield	399 mg (1.41 mmol, 80 %)
melting point (picrate salt)	195 °C (decomposition)
^{1}H-NMR (picrate salt)	(400 MHz, DMSO-d_6) δ = 3.76 (br, 2H, CH_2), 4.49 (br, 1H, C*H*), 5.06 (br, 1H, OH), 6.94 (br, 1H, pyrrole-C*H*), 7.04 (br, 1H, pyrrole-C*H*), 8.15 (br.s, 4H, guanidinium-NH_2), 8.58 (s, 2H, picrate-C*H*), 8.64 (d, $^3J_{NHCH}$ = 7.44, 1H, N*H*), 10.96 (br.s, 1H, N*H*), 12.65 (br.s, 1H, N*H*); the signal for the free acid is not detected due to the exchange with the solvent.
^{13}C-NMR (picrate salt)	(100 MHz, DMSO-d_6) δ = 55.1 (*C*H), 61.2 (*C*H_2), 113.5 (pyrrole-*C*H), 115.1 (pyrrole-*C*H), 124.2 (aryl-*C*H), 125.2 (picrate-*C*H), 125.7 (aryl-*C*H), 132.3 (C_q), 141.9 (C_q), 154.9 (C_q), 159.0 (C_q), 159.6 (C_q), 160.8 (C_q), 171.2 (C_q).
HR-MS (ESI pos.)	m/z = 284.0990, calculated for $^{12}C_{10}H_{13}N_5O_5 + H^+$: 284.0995
FT-IR (KBr)	$\tilde{\nu}$ [cm^{-1}] = 3358 [m], 3178 [w], 3078 [w], 2963 [w], 1716 [s], 1638 [s], 1555 [s], 1477 [w], 1431 [w], 1364 [m], 1321 [s], 1274 [s], 852 [w], 742 [w], 615 [w].

7.4.3 Synthesis of the *L*-phenylalanine derived zwitterion 2.8

7.4.3.1 Synthesis of the *L*-phenylalanine methyl ester hydrochloride 4.20c [TR 19]

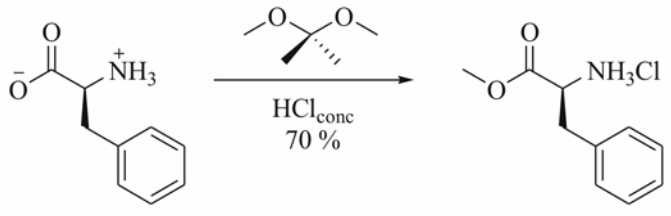

4.19c
$C_9H_{11}NO_2$
Mol. Wt.: 165,19

4.20c
$C_{10}H_{14}ClNO_2$
Mol. Wt.: 215,68

A suspension of *L*-phenylalanine **4.19c** (5.00 g, 30.3 mmol, 1 eq) in 2,2-dimethoxypropane (78.8 g, 0.76 mol, 25 eq) was stirred vigorously while adding concentrated hydrochloric acid (15.2

ml). The solution was then stirred for 24 hours at room temperature. After that time the dark red solution was concentrated *in vacuo* and the resulting brown solid was elutriated with diethyl ether. After filtration the crude product was recrystallized from ethanol/ethyl acetate (40 ml, v/v 95/5). The colourless solid was filtrated, washed with cold diethyl ether and dried in high vacuum.

$C_{10}H_{14}ClNO_2$	215.68 g/mol
yield	4.54 g (21.1 mmol, 70 %)
melting point	180 °C
^{1}H-NMR	(400 MHz, DMSO-d_6) δ = 3.08-3.26 (m, 2H, CH_2), 3.64 (s, 3H, CH_3), 4.19-4.22 (m, 1H, C*H*), 7.23-7.34 (m, 5H, aryl-C*H*), 8.83 (br.s, 3H, NH_3^+).
^{13}C-NMR	(100 MHz, DMSO-d_6) δ = 35.8 (*C*H$_2$), 52.5 (*C*H$_3$), 53.3 (*C*H), 127.2 (aryl-*C*H), 128.6 (aryl-*C*H), 129.4 (aryl-*C*H), 134.8 (*C*q), 169.3 (*C*q).
FT-IR (KBr)	$\tilde{\nu}$ [cm^{-1}] = 3092 [m], 2945 [s], 2846 [s], 2696[m], 2623 [m], 1747 [s], 1584 [s], 1496 [s], 1447 [m], 1292 [m], 1241 [s], 741 [s], 701 [s].

7.4.3.2 Synthesis of the fully protected *L*-phenylalanine derived zwitterion [TR 27] 4.21c

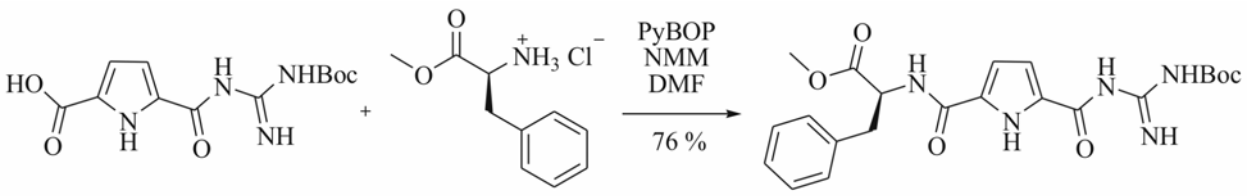

4.18
$C_{12}H_{16}N_4O_5$
Mol. Wt.: 296,28

4.20c
$C_{10}H_{14}ClNO_2$
Mol. Wt.: 215,68

4.21c
$C_{22}H_{27}N_5O_6$
Mol. Wt.: 457,48

A mixture of the *N*-boc-protected guanidinocarbonylpyrrole compound **4.18** (1.00 g, 3.38 mmol, 1 eq), PyBOP (1.76 mg, 3.38 mmol, 1 eq) and NMM (5.00 ml) was stirred in DMF (50 ml) at room temperature for one hour. The methyl ester **4.20c** (728 mg, 3.38 mmol, 1 eq) was added to the solution and then stirred for 24 h at room temperature. The resulting yellow solution was hydrolized with water (100 ml). The suspension was then extracted with diethyl ether (3 x

120 ml), the organic phases were combined, dried with magnesium sulphate and evaporated. The resulting orange oil was purified by column chromatography (SiO_2, ethyl acetate/cyclohexane/isopropanol = 6/3.5/0.5 + 1 % triethylamine) yielding a colourless oil which was dissolved in a mixture of methanol and water. After lyophilisation the pure product was a colourless powder.

$C_{22}H_{27}N_5O_6$	457.48 g/mol
yield	1.18 g (2.15 mmol, 76 %)
R_f	0.79 (SiO_2 with ethyl acetate/cyclohexane/isopropanol = 6/3.5/0.5 + 1 % triethylamine)
melting point	121 °C
^{1}H-NMR	(400 MHz, DMSO-d_6) δ = 1.46 (s, 9H, CH_3), 3.00-3.17 (m, 2H, CH_2), 3.62 (s, 3H, CH_3), 4.64-4.70 (m, 1H, C*H*), 6.80 (br, 2H, pyrrole-C*H*), 7.17-7.30 (m, 5H, aryl-C*H*), 8.56 (br.s, 1H, N*H*), 8.75 (d, $^3J_{NHCH}$ = 7.72 Hz, 1H, N*H*), 9.32 (br.s, 1H, N*H*), 10.82 (br.s, 1H, N*H*), 11.42 (br.s, 1H, N*H*).
^{13}C-NMR	(100 MHz, DMSO-d_6) δ = 27.7 (*C*H_3), 36.5 (*C*H_2), 51.9 (*C*H_3), 53.7 (*C*H), 112.7 (pyrrole-*C*H), 126.5 (aryl-*C*H), 128.2 (aryl-*C*H), 129.0 (aryl-*C*H), 137.3 (C_q), 158.4 (C_q), 159.5 (C_q), 172.1 (C_q).
HR-MS (ESI pos.)	m/z = 458.2036, calculated for $^{12}C_{22}H_{27}N_5O_6 + H^+$: 458.2039
FT-IR (KBr)	$\tilde{\nu}$ [cm^{-1}] = 3388 [m], 3270 [w], 2976 [w], 2954 [w], 2932 [w], 1731 [s], 1637 [s], 1544 [s], 1476 [m], 1398 [s], 1240 [s], 840 [w], 782 [w], 751 [w], 698 [w].

7.4.3.3 Deprotection of 4.21c and purification of the *L*-phenylalanine derived zwitterion 2.8 [TR 376]

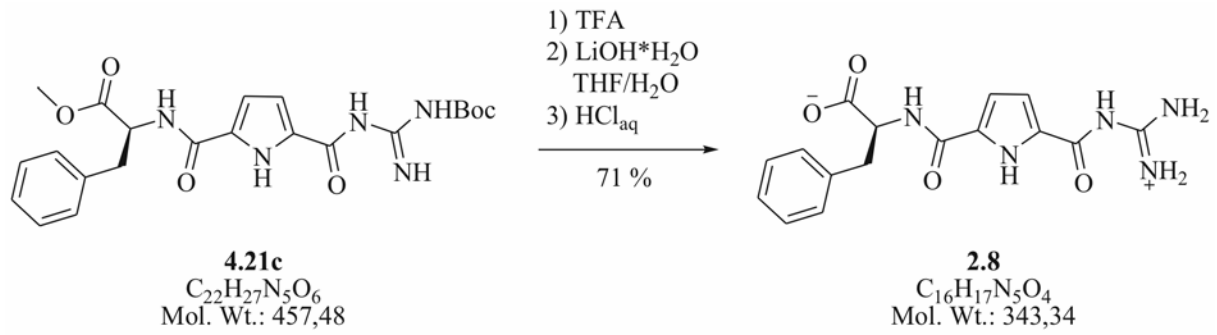

4.21c
$C_{22}H_{27}N_5O_6$
Mol. Wt.: 457,48

2.8
$C_{16}H_{17}N_5O_4$
Mol. Wt.: 343,34

A solution of fully protected **4.21c** (100 mg, 0.22 mmol, 1 eq) in TFA (5 ml) was stirred for 30 minutes at room temperature. The TFA was evaporated *in vacuo* to give a slightly brown oil, which was dissolved in a mixture of THF and water (20 ml, 4/1). After addition of lithium hydroxide monohydrate (45 mg, 1.09 mmol, 5 eq), the reaction mixture was stirred until TLC control (ethyl acetate/cyclohexane/isopropanol = 6/3.5/0.5 + 1 % triethylamine) showed no more starting material. After evaporation of the organic solvent, water (20 ml) was added. The zwitterion was produced by adjusting the pH to a value of 5-6 with 1 N aqueous hydrochloric acid. The colourless precipitate was filtered and washed several times with pure water and diethyl ether. After recrystallization from water and dioxan, the analytical pure zwitterionic product was dried over phosphorous pentoxid in the desiccator.

The picrate salt of **2.8** was produced by suspending zwitterionic **2.8** in a few drops of methanol and addition of aqueous picric acid yielding the yellow picrate salt, which was filtered and dried over phosphorous pentoxid in the desiccator.

$C_{16}H_{17}N_5O_4$	343.34 g/mol
yield	53 mg (1.55 mmol, 71 %)
melting point (picrate salt)	149 °C (decomposition)
^{1}H-NMR (picrate salt)	(400 MHz, DMSO-d_6) δ = 2.96-3.21 (m, 2H, CH_2) 4.62-4.68 (m, 1H, C*H*), 6.88 (br, 1H, pyrrole-C*H*), 6.99 (br, 1H, pyrrole-C*H*), 7.16-7.29 (m, 5H, aryl-C*H*), 8.11 (br.s, 4H, guanidinium-NH_2), 8.58 (s, 2H, picrate-C*H*), 8.72 (d, $^3J_{NHCH}$ = 8.2, 1H, N*H*), 11.00 (br.s, 1H, N*H*), 12.38 (br.s,

1H, N*H*); the signal for the free acid is not detected due to the exchange with the solvent.

^{13}C-NMR (picrate salt) (100 MHz, DMSO-d_6) δ = 36.6 (CH_2), 53.7 (*C*H), 113. (pyrrole-*C*H), 125.2 (picrate-*C*H), 126.4 (aryl-*C*H), 128.1 (aryl-*C*H), 129.0 (aryl-*C*H), 137.7 (C_q), 141.9 (C_q), 159.0 (C_q), 160.8 (C_q), 172.9 (C_q).

HR-MS (ESI pos.) m/z = 344.1350, calculated for $^{12}C_{16}H_{17}N_5O_4 + H^+$: 344.1358

FT-IR (KBr) $\tilde{\nu}$ [cm^{-1}] = 3381 [m], 3208 [w], 3087 [w], 2927 [w], 1702 [s], 1637 [s], 1610 [s], 1553 [s], 1477 [m], 1436 [m], 1365 [m], 1317 [s], 1272 [s], 912 [w], 755 [w], 702 [w].

7.4.4 Synthesis of the *L*-tyrosine derived zwitterion 2.9

7.4.4.1 Synthesis of the *L*-tyrosine methyl ester hydrochloride 4.20d [TR 91]

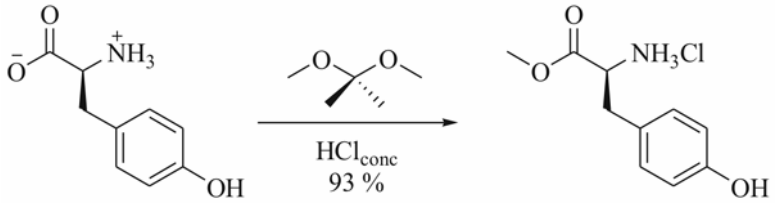

4.19d
$C_9H_{11}NO_3$
Mol. Wt.: 181,19

4.20d
$C_{10}H_{14}ClNO_3$
Mol. Wt.: 231,68

A suspension of *L*-tyrosine **4.19d** (4.00 g, 22.1 mmol, 1 eq) in 2,2-dimethoxypropane (87.7 g, 0.88 mol, 40 eq) was stirred vigorously while adding concentrated hydrochloric acid (11.0 ml). The solution was then stirred for 24 hours at room temperature. After that time the dark red solution was concentrated *in vacuo* and the resulting brown solid was dissolved in water (100 ml). The aqueous solution was washed three times with diethyl ether (150 ml) and lyophilized providing a colourless solid.

$C_4H_{14}ClNO_3$ 231.68 g/mol

yield 4.73 g (20.4 mmol, 93 %)

melting point 182 °C

^{1}H-NMR (400 MHz, DMSO-d_6) δ = 2.96-3.09 (m, 2H, CH_2), 3.66 (s, 3H, CH_3), 4.12-4.16 (m, 1H, C*H*), 6.73 (d, 2H, $^3J_{CHCH}$ = 8.44, aryl-CH), 7.00 (d, 2H,

$^3J_{CHCH}$ = 8.44, aryl-CH), 8.54 (br.s, 3H, NH_3^+), 9.46 (s, 1H, O*H*).

^{13}C-NMR (100 MHz, DMSO-d_6) δ = 35.1 (CH_2), 52.5 (CH_3), 53.4 (*C*H), 115.4 (aryl-*C*H), 124.3 (C_q), 130.3 (aryl-*C*H), 156.7 (C_q), 169.4 (C_q).

FT-IR (KBr) $\tilde{\nu}$ [cm^{-1}] = 3324 [m], 3072 [w], 3007 [w], 2880 [m], 1744 [s], 1615 [w], 1591 [w], 1514 [s], 1448 [w], 1225 [m], 838 [w], 733 [w], 595 [w], 512 [w].

7.4.4.2 Synthesis of the fully protected *L*-tyrosine derived zwitterion 4.21d [TR 105]

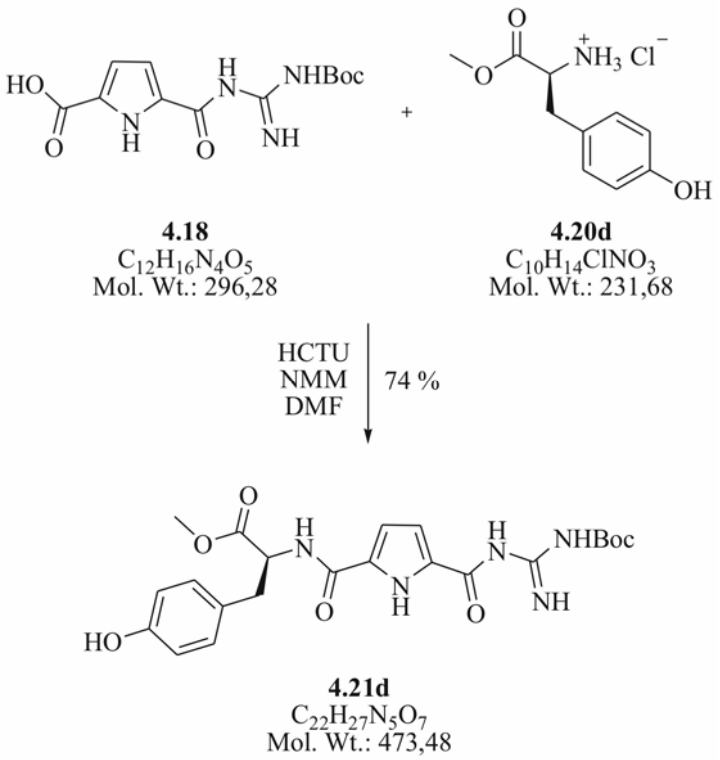

4.18
$C_{12}H_{16}N_4O_5$
Mol. Wt.: 296,28

4.20d
$C_{10}H_{14}ClNO_3$
Mol. Wt.: 231,68

4.21d
$C_{22}H_{27}N_5O_7$
Mol. Wt.: 473,48

A mixture of the *N*-boc-protected guanidinocarbonylpyrrole compound **4.18** (750 mg, 2.53 mmol, 1 eq), HCTU (1.05 g, 2.53 mmol, 1 eq) and NMM (2.00 ml) was stirred in DMF (20 ml) at room temperature for one hour. The methyl ester **4.20d** (587 mg, 3.38 mmol, 1 eq) was added to the solution and then stirred for 24 h at room temperature. The resulting yellow solution was hydrolized with water (100 ml). The suspension was then extracted with diethyl ether (3 x 120 ml), the organic phases were combined, dried with magnesium sulphate and evaporated. The resulting orange oil was purified by column chromatography (SiO_2, ethyl acetate/cyclohexane/isopropanol = 6/3.5/0.5 + 1 % triethylamine) yielding a colourless oil which was dissolved in a mixture of methanol and water. After lyophilisation the pure product was a

colourless powder.

$C_{22}H_{27}N_5O_7$	473.48 g/mol
yield	890 mg (2.15 mmol, 74 %)
R_f	0.51 (SiO_2 with ethyl acetate/cyclohexane/isopropanol = 6/3.5/0.5 + 1 % triethylamine)
melting point	155 °C
^{1}H-NMR	(400 MHz, DMSO-d_6) δ = 1.46 (s, 9H, CH_3), 2.88-3.03 (m, 2H, CH_2), 3.62 (s, 3H, CH_3), 4.54-4.60 (m, 1H, CH), 6.64 (d, $^3J_{CHCH}$ = 8.56, 2H, aryl-CH), 6.80 (br, 2H, pyrrole-CH), 7.04 (d, $^3J_{CHCH}$ = 8.6, 2H, aryl-CH), 8.55 (br.s, 1H, NH), 8.68 (d, $^3J_{NHCH}$ = 7.84, 1H, NH), 9.19 (br.s, 1H, OH), 9.31 (br.s, 1H, NH), 10.80 (br.s, 1H, NH), 11.40 (br.s, 1H, NH).
^{13}C-NMR	(100 MHz, DMSO-d_6) δ = 27.7 (CH$_3$), 35.8 (CH$_2$), 51.9 (CH$_3$), 54.1 (CH), 112.7 (pyrrole-CH), 115.0 (aryl-CH), 127.3 (C_q), 129.9 (aryl-CH), 156.0 (C_q), 158.4 (C_q), 159.4 (C_q), 172.2 (C_q).
HR-MS (ESI pos.)	m/z = 474.1991, calculated for $^{12}C_{22}H_{27}N_5O_7 + H^+$: 474.1989
FT-IR (KBr)	$\tilde{\nu}$ [cm^{-1}] = 3384 [m], 3279 [w], 2981 [w], 2954 [w], 2949 [w], 2932 [w], 1732 [s], 1635 [s], 1544 [s], 1467 [m], 1298 [m], 1240 [s], 1148 [s], 840 [w], 782 [w], 755 [w].

7.4.4.3 Deprotection of 4.21d and purification of the *L*-tyrosine derived zwitterion 2.9 [TR 116]

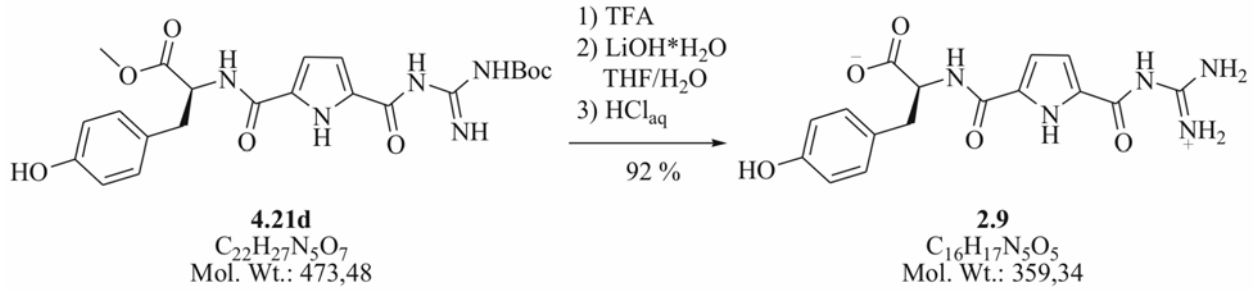

4.21d
$C_{22}H_{27}N_5O_7$
Mol. Wt.: 473,48

2.9
$C_{16}H_{17}N_5O_5$
Mol. Wt.: 359,34

A solution of fully protected **4.21d** (800 mg, 1.69 mmol, 1eq) in TFA (5 ml) was stirred for 30 minutes at room temperature. The TFA was evaporated *in vacuo* to give a slightly brown oil,

which was dissolved in a mixture of THF and water (20 ml, 4/1). After addition of lithium hydroxide monohydrate (346 mg, 8.44 mmol, 5 eq), the reaction mixture was stirred until TLC control (ethyl acetate/cyclohexane/isopropanol = 6/3.5/0.5 + 1 % triethylamine) showed no more starting material. After evaporation of the organic solvent, water (20 ml) was added. The zwitterion was produced by adjusting the pH to a value of 5-6 with 1 N aqueous hydrochloric acid. The colourless precipitate was filtered and washed several times with pure water and diethyl ether. After recrystallization from water and dioxan, the analytically pure zwitterionic product was dried over phosphorous pentoxid in the desiccator.

The picrate salt of **2.9** was produced by suspending zwitterionic **2.9** in a few drops of methanol and addition of aqueous picric acid yielding the yellow picrate salt, which was filtered and dried over phosphorous pentoxid in the desiccator.

$C_{16}H_{17}N_5O_5$	359.34 g/mol
yield	607 mg (1.69 mmol, 92 %)
melting point (picrate salt)	162 °C (decomposition)
^{1}H-NMR (picrate salt)	(400 MHz, DMSO-d_6) δ = 2.80-3.12 (m, 2H, CH_2), 4.56 (br, 1H, C*H*), 6.63 (d, $^3J_{CHCH}$ = 7.96, 2H, aryl-C*H*), 6.89 (br, 1H, pyrrole-C*H*), 6.98 (br, 1H, pyrrole-C*H*), 7.05 (d, $^3J_{CHCH}$ = 7.96, 2H, aryl-C*H*), 8.09 (br.s, 4H, guanidinium-NH_2), 8.58 (s, 2H, picrate-C*H*), 8.65 (d, $^3J_{NHCH}$ = 7.72, 1H, N*H*), 9.17 (s, 1H, O*H*), 10.94 (br.s, 1H, N*H*), 12.38 (br.s, 1H, N*H*), 12.77 (br.s, 1H, COO*H*).
^{13}C-NMR (picrate salt)	(100 MHz, DMSO-d_6) δ = 35.6 (*C*H$_2$), 54.0 (*C*H), 113.1 (pyrrole-*C*H), 115.0 (aryl-*C*H), 125.1 (picrate-*C*H), 127.6 (C_q), 128.1 (C_q), 129.9 (aryl-*C*H), 141.8 (C_q), 155.9 (C_q), 173.0 (C_q).
HR-MS (ESI pos.)	m/z = 360.1299, calculated for $^{12}C_{16}H_{17}N_5O_5 + Na^+$: 360.1307
FT-IR (KBr)	$\tilde{\nu}$ [cm^{-1}] = 3393 [m], 3332 [m], 3203 [w], 3127 [w], 2963 [w], 1702 [s], 1650 [s], 1610 [s], 1558 [s], 1512 [m], 1329 [m], 1248 [s], 760 [w], 712 [w].

7.5 Concepts for the synthesis of boxes, cages and new zwitterions

7.5.1 Synthesis of boxes and cages

7.5.1.1 Synthesis of the fully protected zwitterion 4.23 [TR 406]

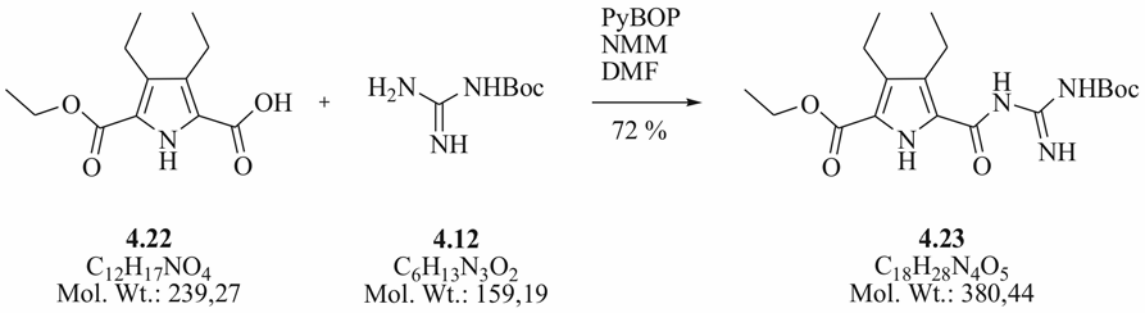

4.22
$C_{12}H_{17}NO_4$
Mol. Wt.: 239,27

4.12
$C_6H_{13}N_3O_2$
Mol. Wt.: 159,19

4.23
$C_{18}H_{28}N_4O_5$
Mol. Wt.: 380,44

A mixture of ethylester **4.22** (5.0 g, 20.9 mmol, 1 eq), PyBOP (10.9 g, 20.9 mmol, 1 eq) and NMM (5 ml) was stirred in DMF (50 ml) at room temperature for 30 minutes. *N*-Boc-guanidine **4.12** (4.99 g, 31.4 mmol, 1.5 eq) was added and the resulting solution was stirred for 12 hours at room temperature. The orange solution was mixed with water (150 ml), causing a slightly brown solid to precipitate. After extraction of the suspension with diethyl ether (3 x 100 ml), the organic phase was washed with a concentrated sodium chloride solution (2 x 50 ml), dried with magnesium sulphate and concentrated *in vacuo*. The crude product was purified by column chromatography (SiO_2, hexane/ethyl acetate = 7/3 + 1 % triethylamine) yielding a brown crystalline powder.

$C_{18}H_{28}N_4O_5$	380.44 g/mol
yield	5.74 g (15.1 mmol, 72 %)
R_f	0.52 (SiO_2 with hexane/ethyl acetate = 7/3)
melting point	121 °C
^{1}H-NMR	(400 MHz, DMSO-d_6) δ = 1.06 (t, $^3J_{CHCH}$ = 7.32, 3H, CH_3), 1.07 (t, $^3J_{CHCH}$ = 7.32, 3H, CH_3), 1.31 (t, $^3J_{CHCH}$ = 7.08, 3H, CH_3), 1.48 (s, 9H, CH_3), 2.65 (q, $^3J_{CHCH}$ = 7.48, 2H, CH_2), 2.74 (q, $^3J_{CHCH}$ = 7.44, 2H, CH_2), 4.28 (q, $^3J_{CHCH}$ = 7.08, 2H, CH_2), 8.43 (br.s, 1H, N*H*), 9.45 (br.s, 1H, N*H*), 10.14 (br.s, 1H, N*H*), 10.61 (br.s, 1H, N*H*).
^{13}C-NMR	(100 MHz, DMSO-d_6) δ = 14.2 (*C*H_3), 15.9 (*C*H_3), 17.1 (*C*H_2), 17.3 (*C*H_2), 27.7 (*C*H_3), 59.9 (*C*H_2), 132.5 (C_q), 160.3 (C_q).

HR-MS (ESI pos.) m/z = 381.2134, calculated for $^{12}C_{18}H_{28}N_4O_5 + H^+$: 381.2137

FT-IR (KBr) $\tilde{\nu}$ [cm^{-1}] = 3458 [w], 3395 [m], 3286 [w], 2972 [w], 2932 [w], 2874 [w], 1732 [s], 1637 [s], 1546 [s], 1241 [s], 855 [w], 754 [w], 609 [w].

7.5.1.2 Synthesis of the fully protected monomer 4.25 [TR 462]

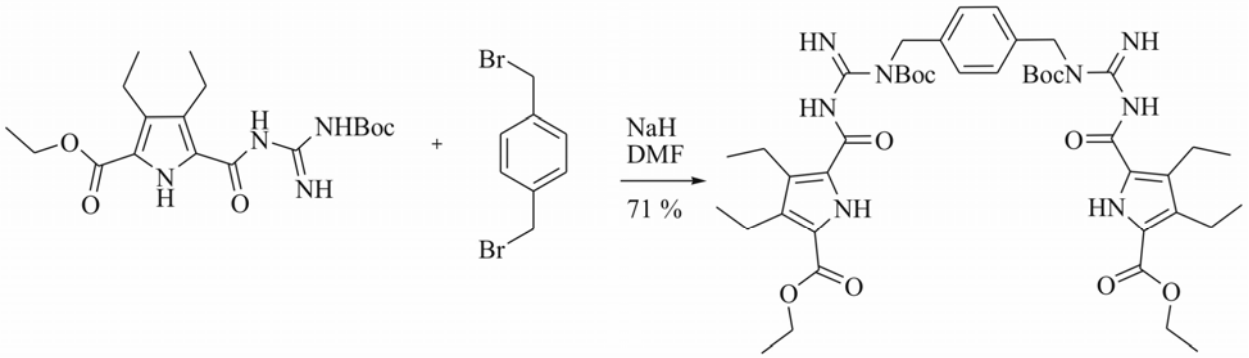

4.23
$C_{18}H_{28}N_4O_5$
Mol. Wt.: 380,44

4.24
$C_8H_8Br_2$
Mol. Wt.: 263,96

4.25
$C_{44}H_{62}N_8O_{10}$
Mol. Wt.: 863,01

Sodium hydride (63 mg, 1.58 mmol, 2.4 eq) was suspended in DMF (20 ml) and stirred for 5 minutes at room temperature. After addition of the pyrrole compound **4.23** (500 mg, 1.31 mmol, 2 eq) the suspension was stirred until it resulted in a clear slightly yellow solution. The addition of dibromide **4.24** (173 mg, 0.66 mmol, 1 eq) resulted in a darkening of the solution, which was stirred over night. After that the solution was mixed with water (60 ml) and extracted with ethyl acetate (3 x 100). The organic phase was dried with magnesium sulphate and concentrated *in vacuo*. The crude product was purified by column chromatography (SiO_2, cyclohexane/ethyl acetate = 8/2) yielding a fluffy colourless powder.

$C_{44}H_{62}N_8O_{10}$ 863,01 g/mol

yield 400 mg (0.46 mmol, 71 %)

R_f 0.20 (SiO_2 with cyclohexane/ethyl acetate = 8/2)

melting point 165 °C

^{1}H-NMR (400 MHz, DMSO-d_6/$CDCl_3$ = 5/3) δ = 0.89 (t, $^3J_{CHCH}$ = 7.32, 6H, CH_3), 1.00 (t, $^3J_{CHCH}$ = 7.44, 6H, CH_3), 1.24 (t, $^3J_{CHCH}$ = 7.20, 6H, CH_3), 1.28 (s, 18H, CH_3), 2.56 (q, $^3J_{CHCH}$ = 7.44, 4H, CH_2), 2.58 (q, $^3J_{CHCH}$ = 7.20, 4H,

CH_2), 4.17 (q, $^3J_{CHCH}$ = 7.08, 4H, CH_2), 5.19 (s, 4H, CH_2), 7.21 (s, 4H, aryl-C*H*), 9.32 (br.s, 2H, N*H*), 9.82 (br.s, 2H, N*H*), 10.44 (br.s, 2H, N*H*).

^{13}C-NMR (100 MHz, DMSO-d_6/$CDCl_3$ = 5/3) δ = 13.9 (*C*H_3), 15.5 (*C*H_3), 15.7 (*C*H_3), 17.0 (*C*H_2), 27.1 (*C*H_3), 47.5 (*C*H_2), 59.4 (*C*H_2), 83.6 (C_q), 118.8 (C_q), 125.7 (aryl-*C*H), 128.5 (C_q), 129.9 (C_q), 132.3 (C_q), 136.9 (C_q), 154.0 (C_q), 159.6 (C_q), 159.9 (C_q), 170.8 (C_q).

HR-MS (ESI pos.) m/z = 863.4666, calculated for $^{12}C_{44}H_{62}N_8O_{10} + H^+$: 863.4666

FT-IR (KBr) $\tilde{\nu}$ [cm^{-1}] = 3456 [m], 3369 [m], 2974 [w], 2930 [w], 2869 [w], 1714 [s], 1605 [s], 1552 [w], 1491 [m], 1463 [m], 1369 [m], 1290 [s], 1240 [s], 949 [w], 851 [w], 831 [w], 781 [w], 757 [w].

7.5.1.3 Synthesis of the fully protected zwitterion 4.27 [TR 468]

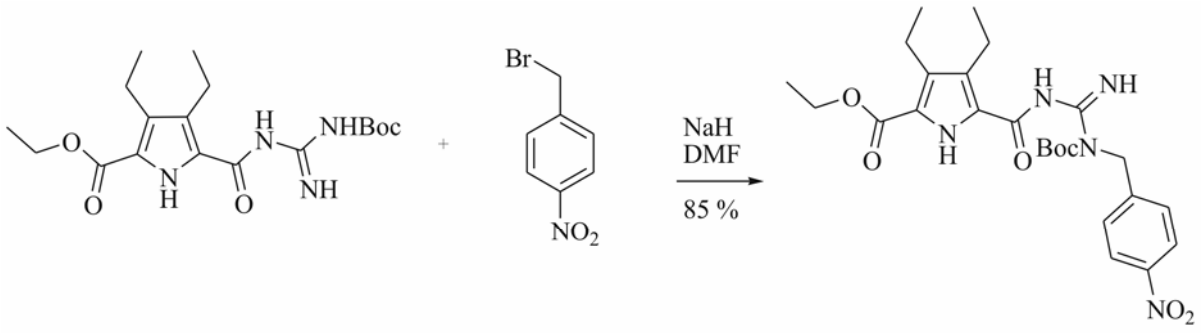

4.23
$C_{18}H_{28}N_4O_5$
Mol. Wt.: 380,44

4.26
$C_7H_6BrNO_2$
Mol. Wt.: 216,03

4.27
$C_{25}H_{33}N_5O_7$
Mol. Wt.: 515,56

Sodium hydride (328 mg, 8.20 mmol, 1.2 eq) was suspended in DMF (80 ml) and stirred for 5 minutes at room temperature. After addition of the pyrrole compound **4.23** (2.60 g, 6.83 mmol, 1 eq) the suspension was stirred until a clear yellow solution was obtained. With addition of p-nitro-benzylbromid **4.26** (1.48 g, 6.83 mmol, 1 eq) the colour of the solution changed from deep yellow over purple to finally deep red. After stirring the solution over night at room temperature it was poured into water (70 ml) and extracted with diethyl ether (3 x 150). After that the organic phase was dried with magnesium sulphate and concentrated *in vacuo*. The main part of the pure product was isolated by crystallization from methanol yielding a colourless crystalline solid. The remaining crude product was purified by column chromatography (SiO_2, dichloro-methane/hexane/ethyl acetate = 7/2.6/0.4) yielding a fluffy colourless powder.

$C_{25}H_{33}N_5O_7$	515.56 g/mol
yield	crystallization: 2.63 g (5.10 mmol, 75 %)
	column chromatography: 360 mg (0.70 mmol, 10 %)
R_f	0.57 (SiO_2 with dichloromethane/hexane/ethyl acetate = 7/2.6/0.4)
melting point	111 °C
^{1}H-NMR	(400 MHz, DMSO-d_6) δ = 0.92 (t, $^3J_{CHCH}$ = 7.32, 3H, CH_3), 1.02 (t, $^3J_{CHCH}$ = 7.32, 3H, CH_3), 1.22 (t, $^3J_{CHCH}$ = 7.08, 3H, CH_3), 1.35 (s, 9H, CH_3), 2.59 (q, $^3J_{CHCH}$ = 7.32, 2H, CH_2), 2.61 (q, $^3J_{CHCH}$ = 7.32, 2H, CH_2), 4.20 (q, $^3J_{CHCH}$ = 7.08, 2H, CH_2), 5.35 (s, 2H, CH_2), 7.55 (d, $^3J_{CHCH}$ = 9.00, 2H, aryl-C*H*), 8.23 (d, $^3J_{CHCH}$ = 8.84, 2H, aryl-C*H*), 9.29 (br.s, 1H, N*H*), 10.11 (br.s, 1H, N*H*), 10.37 (br.s, 1H, N*H*).
^{13}C-NMR	(100 MHz, DMSO-d_6) δ = 14.1 (*C*H_3), 15.8 (*C*H_3), 16.0 (*C*H_3), 17.2 (*C*H_2), 27.3 (*C*H_3), 47.8 (*C*H_2), 59.8 (*C*H_2), 84.3 (C_q), 119.2 (C_q), 123.7 (aryl-*C*H), 127.0 (aryl-*C*H), 128.7 (C_q), 130.1 (C_q), 132.4 (C_q), 146.4 (C_q), 146.9 (C_q), 153.7 (C_q), 159.4 (C_q), 160.1 (C_q), 170.9 (C_q).
HR-MS (ESI pos.)	m/z = 516.2449, calculated for $^{12}C_{25}H_{33}N_5O_7 + H^+$: 516.2458
FT-IR (KBr)	$\tilde{\nu}$ [cm^{-1}] = 3432 [m], 3385 [m], 2967 [w], 2932 [w], 2869 [w], 1715 [m], 1607 [m], 1522 [m], 1459 [m], 1420 [m], 1369 [m], 1348 [m], 1279 [s], 1243 [s], 941 [w], 826 [w], 759 [w], 598 [w].

7.5.1.4 Synthesis of the fully protected, multi-purpose zwitterion 2.10 [TR 475]

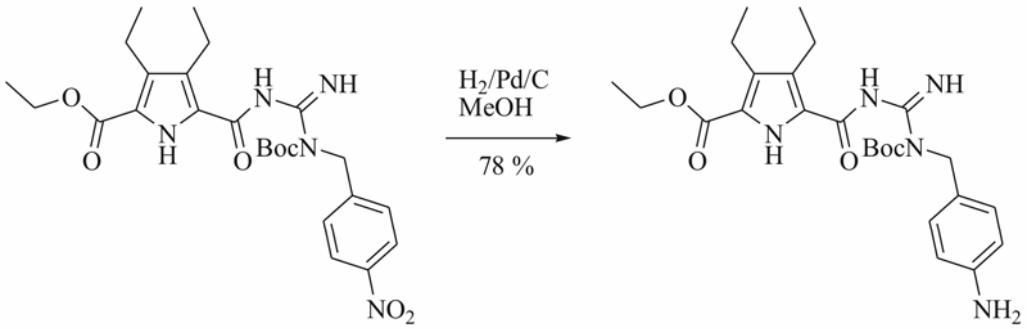

4.27
$C_{25}H_{33}N_5O_7$
Mol. Wt.: 515,56

2.10
$C_{25}H_{35}N_5O_5$
Mol. Wt.: 485,58

A mixture of **4.27** (200 mg, 0.239 mmol, 1 eq) and palladium on activated charcoal (20 mg) in methanol (20 ml) was stirred for 30 minutes under hydrogen atmosphere. The reaction was controlled via TLC (dichloromethane/hexane/ethyl acetate = 7/2.6/0.4 + 1 % triethylamine). After complete conversion the mixture was filtered over a celite pad and washed several times with ethyl acetate. The solvent was evaporated and the resulting oil was purified by column chromatography (SiO_2, dichloromethane/hexane/ethyl acetate = 7/2.6/0.4) yielding a slightly yellow powder.

$C_{25}H_{35}N_5O_5$	485.58 g/mol
yield	146 mg (0.30 mmol, 78 %)
R_f	0.20 (SiO_2 with dichloromethane/hexane/ethyl acetate = 7/2.6/0.4)
melting point	151 °C
^{1}H-NMR	(400 MHz, DMSO-d_6) δ = 1.00 (t, $^3J_{CHCH}$ = 7.32, 3H, CH_3), 1.05 (t, $^3J_{CHCH}$ = 7.32, 3H, CH_3), 1.27 (t, $^3J_{CHCH}$ = 7.04, 3H, CH_3), 1.41 (s, 9H, CH_3), 2.63 (q, $^3J_{CHCH}$ = 7.48, 2H, CH_2), 2.70 (q, $^3J_{CHCH}$ = 7.48, 2H, CH_2), 4.24 (q, $^3J_{CHCH}$ = 7.08, 2H, CH_2), 4.96 (s, 2H, NH_2), 5.04 (s, 2H, CH_2), 6.51 (d, $^3J_{CHCH}$ = 8.48, 2H, aryl-C*H*), 6.96 (d, $^3J_{CHCH}$ = 8.84, 2H, aryl-C*H*), 9.24 (br.s, 1H, N*H*), 10.14 (br.s, 1H, N*H*), 10.35 (br.s, 1H, N*H*).
^{13}C-NMR	(100 MHz, DMSO-d_6) δ = 14.1 (*C*H$_3$), 15.9 (*C*H$_3$), 16.1 (*C*H$_3$), 17.2 (*C*H$_2$), 27.4 (*C*H$_3$), 47.5 (*C*H$_2$), 59.8 (*C*H$_2$), 83.7 (C_q), 113.8 (aryl-*C*H), 118.9 (C_q), 125.4 (C_q), 127.3 (aryl-*C*H), 128.6 (C_q), 130.0 (C_q), 132.5

(C_q), 147.5 (C_q), 154.3 (C_q), 159.7 (C_q), 160.1 (C_q), 170.8 (C_q).

HR-MS (ESI pos.) m/z = 486.2713, calculated for $^{12}C_{25}H_{35}N_5O_5 + H^+$: 486.2716

FT-IR (KBr) $\tilde{\nu}$ [cm^{-1}] = 3443 [w], 3351 [m], 3016 [w], 2975 [w], 2927 [w], 2869 [w], 17014 [s], 1604 [m], 1466 [m], 1358 [s], 1273 [s], 1238 [s], 830 [w], 656 [w].

7.5.1.5 Synthesis of the fully protected monomer 4.29 [TR 513]

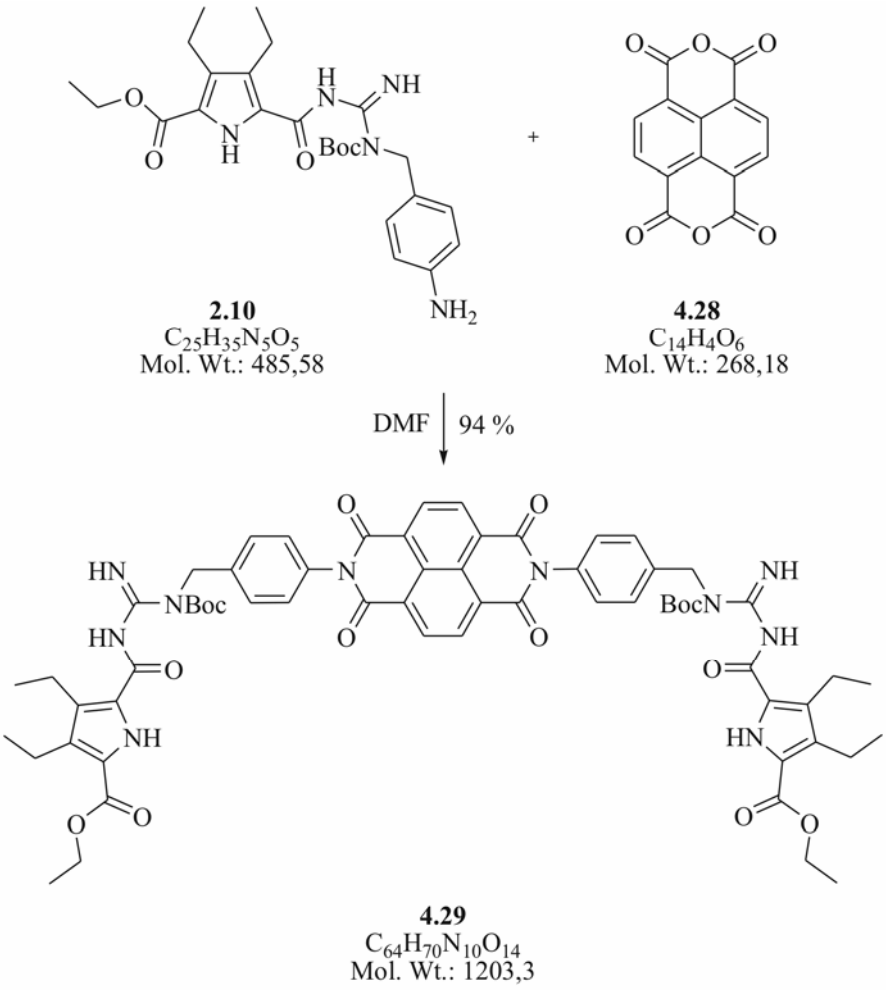

A slurry of amine **2.10** (80 mg, 0.17 mmol, 2 eq) and NDA **4.28** (22 mg, 0.08 mmol, 1 eq) in DMF (1 ml) was stirred at 80 °C for 12 hours. After cooling down to room temperature the clear brown solution was poured into water (10 ml) and extracted with ethyl acetate (3 x 10 ml). The organic phase was dried with magnesium sulphate and concentrated *in vacuo*. The resulting brown oil was dissolved in chloroform and the crude product was precipitated with methanol. The brown flaky solid was recrystallized from methanol/chloroform yielding a light brown fluffy

powder.

$C_{64}H_{70}N_{10}O_{14}$	1203.30 g/mol
yield	80 mg (0.07 mmol, 94 %)
R_f	0.88 (SiO_2 with ethyl acetate/hexane = 9/1 + 1 % triethylamine)
melting point	189 °C
^{1}H-NMR	(400 MHz, $CDCl_3$) δ = 1.10 (t, $^3J_{CHCH}$ = 7.56, 6H, CH_3), 1.14 (t, $^3J_{CHCH}$ = 7.36, 6H, CH_3), 1.32 (t, $^3J_{CHCH}$ = 7.2, 6H, CH_3), 1.46 (s, 18H, CH_3), 2.72 (q, $^3J_{CHCH}$ = 7.68, 4H, CH_2), 2.79 (q, $^3J_{CHCH}$ = 7.44, 4H, CH_2), 4.30 (q, $^3J_{CHCH}$ = 7.20, 4H, CH_2), 5.39 (s, 4H, CH_2), 7.30 (d, $^3J_{CHCH}$ = 8.32, 4H, aryl-C*H*), 7.51 (d, $^3J_{CHCH}$ = 8.32, 4H, aryl-C*H*), 8.82 (s, 4H, aryl-C*H*), 9.48 (d, $^4J_{NHNH}$ = 6.16, 2H, N*H*), 9.54 (s, 2H, N*H*), 10.65 (d, $^4J_{NHNH}$ = 5.44, 2H, N*H*).
^{13}C-NMR	(100 MHz, $CDCl_3$) δ = 14.5 (*C*H_3), 16.0 (*C*H_3), 16.2 (*C*H_3), 18.0 (*C*H_2), 18.1 (*C*H_2), 28.1 (*C*H_3), 47.9 (*C*H_2), 60.3 (*C*H_2), 85.2 (C_q), 119.8 (C_q), 127.2 (C_q), 127.4 (C_q), 127.9 (aryl-*C*H), 128.8 (aryl-*C*H), 129.0 (C_q), 131.5 (aryl-*C*H), 133.6 (C_q), 133.7 (C_q), 139.8 (C_q), 155.0 (C_q), 160.7 (C_q), 161.1 (C_q), 163.0 (C_q), 172.2 (C_q).
HR-MS (ESI pos.)	m/z = 1203.5131, calculated for $^{12}C_{64}H_{70}N_{10}O_{14} + H^+$: 1203.5150
FT-IR (KBr)	$\tilde{\nu}$ [cm^{-1}] = 3438 [w], 3385 [w], 2972 [w], 2929 [w], 2869 [w], 1715 [s], 1678 [s], 1599 [m], 1465 [m], 1347 [m], 769 [w].

7.5.1.6 Synthesis of the fully protected monomer 4.31 [TR 514]

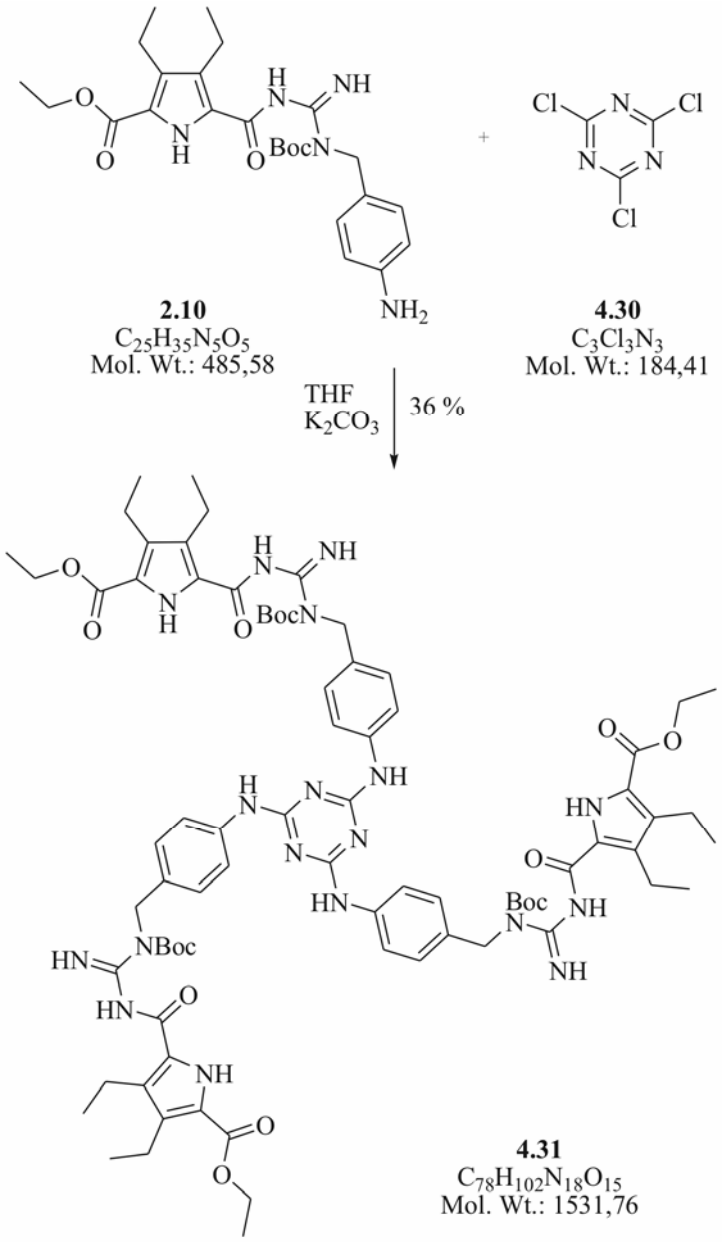

Triturated potassium carbonate (68 mg, 0.49 mmol, 9 eq) was added to a solution of amine **2.10** (80 mg, 0.17, 3 eq) in THF (2 ml). The suspension was stirred at room temperature while a solution of cyanuric acid chloride **4.30** (10 mg, 0.06 mmol, 1 eq) in THF (1 ml) was added dropwise. After stirring the resulting slightly yellow suspension over night at room temperature the fine precipitate was filtrated and washed several times with abs THF. The clear yellow solution was then concentrated *in vacuo* yielding a yellow oil, which was purified by column chromatography (SiO_2, hexane/ethyl acetate = 7/3 + 1 % triethylamine). The pure product was obtained as a slightly green-yellow solid.

$C_{78}H_{102}N_{18}O_{15}$	1531.76 g/mol
yield	30 mg (0.02 mmol, 36 %)
R_f	0.81 (SiO_2 with hexane/ethyl acetate = 7/3 + 1 % triethylamine)
melting point	80 °C
^{1}H-NMR	(400 MHz, $CDCl_3$) δ = 1.07 (t, $^3J_{CHCH}$ = 7.48, 9H, C*H*$_3$), 1.11 (t, $^3J_{CHCH}$ = 7.32, 9H, C*H*$_3$), 1.32 (t, $^3J_{CHCH}$ = 7.04, 9H, C*H*$_3$), 1.44 (s, 27H, C*H*$_3$), 2.69 (q, $^3J_{CHCH}$ = 7.48, 6H, C*H*$_2$), 2.74 (q, $^3J_{CHCH}$ = 7.44, 6H, C*H*$_2$), 4.30 (q, $^3J_{CHCH}$ = 7.20, 6H, C*H*$_2$), 5.25 (s, 6H, C*H*$_2$), 7.34 (d, $^3J_{CHCH}$ = 8.56, 6H, aryl-C*H*), 7.51 (br.s, 3H, N*H*), 7.53 (d, $^3J_{CHCH}$ = 8.60, 6H, aryl-C*H*), 9.43 (br.s, 6H, N*H*), 10.58 (br.s, 3H, N*H*).
^{13}C-NMR	(100 MHz, $CDCl_3$) δ = 14.9 (*C*H$_3$), 16.0 (*C*H$_3$), 16.1 (*C*H$_3$), 18.0 (*C*H$_2$), 28.1 (*C*H$_3$), 47.9 (*C*H$_2$), 60.3 (*C*H$_2$), 85.0 (C_q), 121.5 (aryl-*C*H), 127.4 (aryl-*C*H), 128.9 (C_q), 131.6 (C_q), 133.6 (C_q), 134.9 (C_q), 136.2 (C_q), 155.0 (C_q), 160.5 (C_q), 161.2 (C_q), 164.2 (C_q), 172.0 (C_q).
HR-MS	Data not available; see chapter 4.4.1 for detailed information.
FT-IR (KBr)	$\tilde{\nu}$ [cm^{-1}] = 3452 [w], 3369 [w], 2971 [w], 2932 [w], 2868 [w], 1715 [m], 1608 [m], 1548[s], 1511 [m], 1458 [m], 1279 [m], 1240 [s], 832 [w], 600 [w].

7.5.2 Synthesis of the fully protected morpholine derivative

7.5.2.1 Synthesis of the morpholine substituted, fully protected pyrrole dicarboxylic acid 4.34 [TR 489]

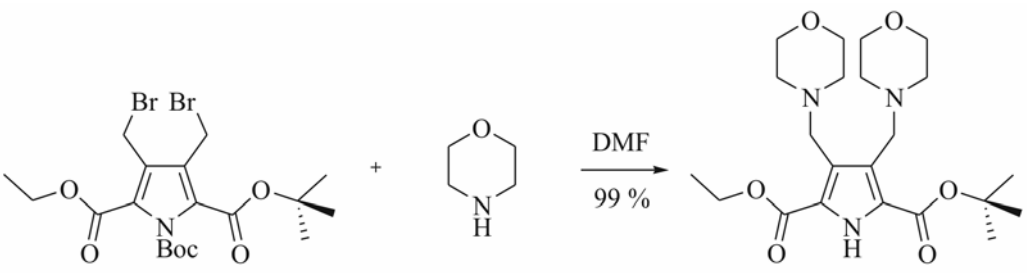

4.32
$C_{19}H_{27}Br_2NO_6$
Mol. Wt.: 525,23

4.33
C_4H_9NO
Mol. Wt.: 87,12

4.34
$C_{22}H_{35}N_3O_6$
Mol. Wt.: 437,53

To a solution of dibromide **4.32** (1.00 g, 1.90 mmol, 1 eq) in DMF (20 ml) morpholine **4.33** (1.00 g, 11.4 mmol, 6 eq) was added. The solution was stirred over night at room temperature. The resulting yellow solution was poured into water and extracted with diethyl ether (2 x 100 ml). The organic phase was dried with magnesium sulphate and concentrated *in vacuo*. The resulting deep orange oil was purified by column chromatography (SiO_2, ethyl acetate/hexane = 8/2 + 1 % triethylamine) yielding a clear colourless oil which crystallized within two days at room temperature.

$C_{22}H_{35}N_3O_6$	437.53 g/mol
yield	830 mg (1.89 mmol, 99 %)
R_f	0.37 (SiO_2 with ethyl acetate/hexane = 8/2 + 1 % triethylamine)
melting point	104 °C
^{1}H-NMR	(400 MHz, DMSO-d_6) δ = 1.30 (t, $^3J_{CHCH}$ = 7.04, 3H, CH_3), 1.53 (s, 9H, CH_3), 2.28-2.37 (br, 8H, CH_2), 3.48-3.53 (br, 8H, CH_2), 3.70 (s, 2H, CH_2), 3.72 (s, 2H, CH_2), 4.25 (q, $^3J_{CHCH}$ = 7.04, 2H, CH_2), 11.67 (s, 1H, N*H*).
^{13}C-NMR	(100 MHz, DMSO-d_6) δ = 14.1 (*C*H_3), 28.0 (*C*H_3), 51.2 (*C*H_2), 53.3 (*C*H_2), 59.7 (*C*H_2), 60.1 (*C*H_2), 81.2 (C_q), 123.0 (C_q), 124.9 (C_q), 126.8 (C_q), 160.0 (C_q), 160.4 (C_q), 170.3 (C_q).
HR-MS (ESI pos.)	m/z = 438.2599, calculated for $^{12}C_{22}H_{35}N_3O_6 + H^+$: 438.2604
FT-IR (KBr)	$\tilde{\nu}$ [cm^{-1}] = 3452 [w], 3386 [w], 3234 [w], 2958 [w], 2928 [w], 2858 [w], 2802 [w], 2762 [w], 1697 [s], 1561 [w], 1456 [m], 1368 [m], 1350 [w], 1282 [s], 864 [w], 784 [w], 619 [w].

7.5.2.2 Synthesis of the mono-protected pyrrole dicarboxylic acid 4.35 [TR 490]

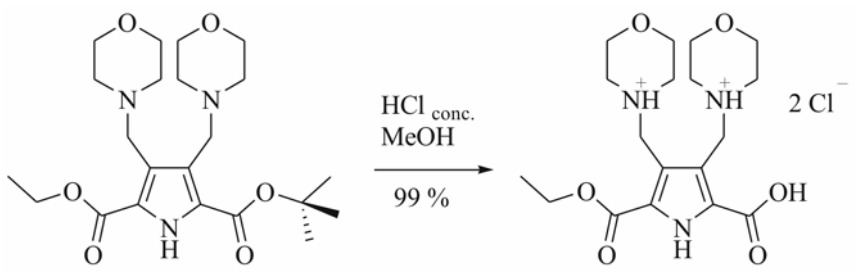

4.34
$C_{22}H_{35}N_3O_6$
Mol. Wt.: 437,53

4.35
$C_{18}H_{29}Cl_2N_3O_6$
Mol. Wt.: 454,35

To a solution of pyrrole compound **4.34** (100 mg, 0.23 mmol, 1 eq) in methanol (10 ml) concentrated hydrochloric acid (0.5 ml) was added. The clear light green solution was stirred over night and then concentrated *in vacuo*. The resulting green-yellow solid was diluted in water and lyophilized yielding a light yellow solid.

$C_{18}H_{29}Cl_2N_3O_6$	454.35 g/mol
yield	103 mg (0.23 mmol, 99 %)
melting point	> 220 °C
^{1}H-NMR	(400 MHz, DMSO-d_6) δ = 1.35 (t, $^3J_{CHCH}$ = 7.20, 3H, CH_3), 3.28 (br, 8H, CH_2), 3.88 (br, 8H, CH_2), 4.33 (q, $^3J_{CHCH}$ = 7.20, 2H, CH_2), 4.67 (br, 4H, CH_2), 13.11 (s, 1H, NH).
^{13}C-NMR	(100 MHz, DMSO-d_6) δ = 14.0 (CH_3), 42.6 (CH_2), 49.9 (CH_2), 51.0 (CH_2), 61.1 (CH_2), 63.1 (C_q), 118.9 (C_q), 125.2 (C_q), 126.8 (C_q), 159.7 (C_q), 161.2 (C_q).
HR-MS (ESI pos.)	m/z = 382.1973, calculated for $^{12}C_{18}H_{27}N_3O_6 + H^+$: 382.1978
FT-IR (KBr)	$\tilde{\nu}$ [cm^{-1}] = 3429 [m], 3154 [w], 3010 [w], 2927 [w], 2745 [w], 1735 [s], 1710 [s], 1677 [s], 1455 [w], 1281 [m], 1205 [s], 865 [w], 797 [w], 727 [w].

7.5.2.3 Synthesis of the fully protected zwitterion 4.36 [TR 492]

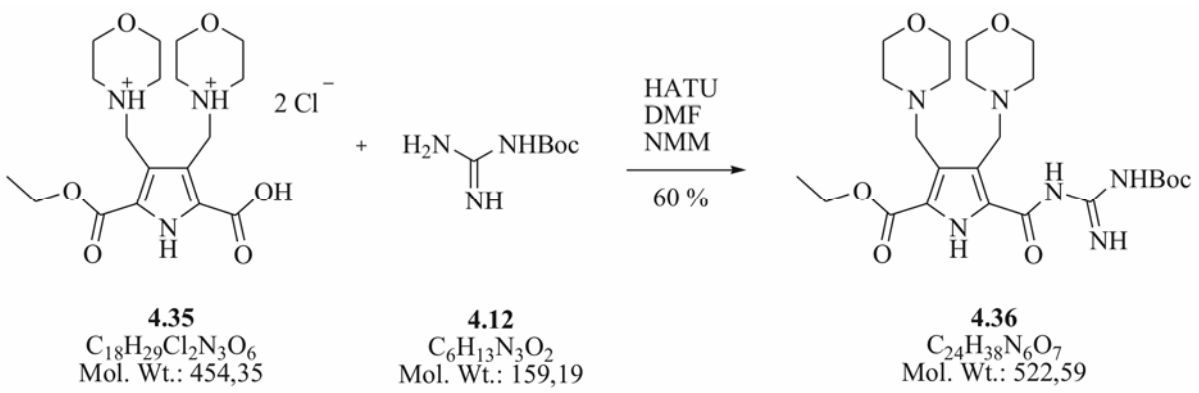

4.35
$C_{18}H_{29}Cl_2N_3O_6$
Mol. Wt.: 454,35

4.12
$C_6H_{13}N_3O_2$
Mol. Wt.: 159,19

4.36
$C_{24}H_{38}N_6O_7$
Mol. Wt.: 522,59

A mixture of the acid **4.35** (320 mg, 0.70 mmol, 1 eq), HATU (295 mg, 0.78 mmol, 1.1 eq) and triethylamine (4 ml) was stirred in DMF (10 ml) at room temperature for 30 minutes. *N*-Boc-guanidine **4.12** (224 g, 1.41 mmol, 2 eq) was added and the resulting solution was stirred over night at room temperature. The yellow solution was mixed with water (30 ml), whereas a slightly yellow solid precipitated. After extraction of the suspension with ethyl acetate (3 x 25 ml), the organic phase was dried with magnesium sulphate. While concentrating the solution *in vacuo* urchin-like colourless crystals precipitated which were filtrated after cooling the mother liquor. The remaining crude product was purified by column chromatography (SiO_2, ethyl acetate/hexane/methanol/triethylamine = 5/4/0.5/0.5) yielding a colourless powder.

$C_{24}H_{38}N_6O_7$	522.59 g/mol
yield	crystallization: 200 mg (0.38 mmol, 54 %)
	column chromatography: 20 mg (0.04 mmol, 6 %)
R_f	0.46 (SiO_2 with ethyl acetate/hexane/methanol/triethylamine = 5/4/0.5/0.5)
melting point	204 °C
^{1}H-NMR	(400 MHz, $CDCl_3$) δ = 1.39 (t, $^3J_{CHCH}$ = 7.08, 3H, C*H*$_3$), 1.48 (s, 9H, C*H*$_3$), 2.45 (br, 4H, C*H*$_2$), 2.62 (br, 4H, C*H*$_2$), 3.64 (br, 4H, C*H*$_2$), 3.67 (s, 2H, C*H*$_2$), 3.69 (s, 2H, C*H*$_2$), 3.92 (br, 4H, C*H*$_2$), 4.37 (q, $^3J_{CHCH}$ = 7.20, 2H, C*H*$_2$), 8.95 (s, 2H, N*H*), 9.82 (s, 1H, N*H*), 14.07 (br.s, 1H, N*H*).
^{13}C-NMR	(100 MHz, DMSO-d_6) δ = 14.5 (*C*H$_3$), 28.3 (*C*H$_3$), 51.4 (*C*H$_2$), 52.1 (*C*H$_2$), 52.9 (*C*H$_2$), 53.4 (*C*H$_2$), 61.3 (*C*H$_2$), 66.1 (*C*H$_2$), 67.2 (*C*H$_2$), 123.6

(C_q), 127.6 (C_q), 154.0 (C_q), 159.9 (C_q), 160.3 (C_q).

HR-MS (ESI pos.) m/z = 523.2875, calculated for $^{12}C_{24}H_{38}N_6O_7 + H^+$: 523.2880

FT-IR (KBr) $\tilde{\nu}$ [cm^{-1}] = 3411 [m], 3326 [m], 2971 [w], 2932 [w], 2852 [w], 2811 [w], 1708 [m], 1666 [s], 1625 [m], 1560 [m], 1457 [m], 1366 [m], 1266 [s], 863 [w], 779 [w], 615 [w].

7.5.3 Synthesis of the fully protected zwitterion capable of π-stacking

7.5.3.1 Synthesis of *p*-amino benzoic acid methyl ester 4.40 [TR 525]

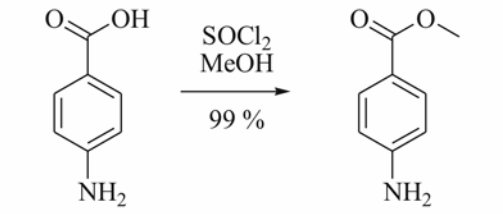

4.39
$C_7H_7NO_2$
Mol. Wt.: 137,14

4.40
$C_8H_9NO_2$
Mol. Wt.: 151,16

p-Amino benzoic acid **4.39** (2.00 g, 14.6 mmol, 1 eq) was dissolved in methanol (22 ml). After cooling down the solution to *ca.* 0 °C thionyl chloride (1.59 ml, 21.9 mmol, 1.5 eq) was added slowly. The resulting colourless suspension was stirred for 48 hours at room temperature. After evaporation of the solvent and the excess of thionyl chloride water (30 ml) was added. The clear colourless solution was extracted with ethyl acetate (3 x 100 ml). The organic phase was washed with a saturated sodium hydrogen carbonate solution and dried with magnesium sulphate. During the evaporation of the solvent the product precipitated as a colourless solid.

$C_8H_9NO_2$ 151.16 g/mol

yield 2.19 g (14.5 mmol, 99 %)

R_f 0.59 (SiO_2 with ethyl acetate/hexane = 6/4 + 1 % triethylamine)

melting point 110 °C

^{1}H-NMR (400 MHz, $CDCl_3$) δ = 3.85 (s, 3H, CH_3), 4.07 (br.s, 2H, NH_2), 6.63 (d, $^3J_{CHCH}$ = 8.72, 2H, aryl-C*H*), 7.84 (d, $^3J_{CHCH}$ = 8.68, 2H, aryl-C*H*).

^{13}C-NMR (100 MHz, $CDCl_3$) δ = 51.7 (*C*H_3), 113.9 (aryl-*C*H), 119.9 (*C*q), 131.7

(aryl-*C*H), 151.0 (C_q), 167.3 (C_q).

MS (EI) m/z = 151.0, calculated for $^{12}C_8H_9NO_2$: 151.1

FT-IR (KBr) $\tilde{\nu}$ [cm^{-1}] = 3466 [w], 3410 [w], 3340 [m], 3230 [w], 3070 [w], 3031 [w], 2990 [w], 2943 [w], 2845 [w], 1685 [s], 1637 [m], 1598 [s], 1515 [m], 1434 [m], 1314 [s], 1287 [s], 964 [w], 839 [w], 771 [w], 699 [w], 617 [w].

7.5.3.2 Synthesis of the benzylic ester 4.42 [TR 526]

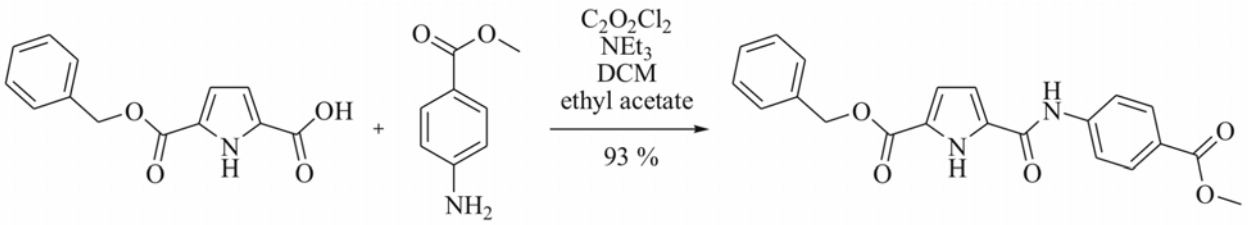

4.41
$C_{13}H_{11}NO_4$
Mol. Wt.: 245,23

4.40
$C_8H_9NO_2$
Mol. Wt.: 151,16

4.42
$C_{21}H_{18}N_2O_5$
Mol. Wt.: 378,38

The pyrrole carboxylic acid **4.41** (100 mg, 0.43 mmol, 1 eq) was suspended in a mixture of dichloromethane (20 ml) and ten drops of dimethyl formamide. After addition of oxalyl chloride (109 µl, 1.29 mmol, 3 eq) the solution was refluxed for 90 minutes. Evaporation of the solvent and the remaining oxalyl chloride resulted in a yellow solid which was dissolved in dichloromethane (20 ml). The solution was cooled to *ca.* 0 °C and methyl ester **4.40** (194 mg, 1.29 mmol, 3 eq) was added. The suspension was stirred for 30 minutes at 0 °C and then two hours at room temperature. Afterwards a solution of triethylamine (180 µl, 1.29 mmol, 3 eq) in ethyl acetate (10 ml) was added and the resulting clear yellow reaction mixture was stirred for 30 minutes at room temperature. Finally the resulting suspension was washed with 0.5 N hydrochloric acid. The organic phase was dried with magnesium sulphate and concentrated *in vacuo*. The crude product was purified by column chromatography (SiO_2, ethyl acetate/hexane = 6/4 + 1 % triethylamine) yielding a colourless solid. For further purification the solid was suspended in diethyl ether, stirred for 15 minutes and then filtrated over a G4 frit yielding the analytical pure product as colourless solid.

$C_{21}H_{18}N_2O_5$ 378.38 g/mol

yield 150 mg (0.40 mmol, 93 %)

R_f	0.76 (SiO_2 with ethyl acetate/hexane = 6/4 + 1 % triethylamine)
melting point	191 °C
^{1}H-NMR	(400 MHz, $CDCl_3$) δ = 3.91 (s, 3H, C*H*$_3$), 5.34 (s, 2H, C*H*$_2$), 6.72-6.73 (m, 1H, pyrrole-C*H*), 6.96-6.97 (m, 1H, pyrrole-C*H*), 7.33-7.44 (m, 5H, aryl-C*H*), 7.68 (d, $^3J_{CHCH}$ = 8.84, 2H, aryl-C*H*), 7.85 (s, 1H, N*H*), 8.03 (d, $^3J_{CHCH}$ = 8.84, 2H, aryl-C*H*), 10.09 (br.s, 1H, N*H*).
^{13}C-NMR	(100 MHz, $CDCl_3$) δ = 52.2 (*C*H$_3$), 66.9 (*C*H$_2$), 110.7 (aryl-*C*H), 116.2 (aryl-*C*H), 119.3 (aryl-*C*H), 126.2 (C_q), 126.3 (C_q), 128.6 (aryl-*C*H), 128.7 (aryl-*C*H), 128.8 (aryl-*C*H), 129.2 (C_q), 131.1 (aryl-*C*H), 135.6 (C_q), 141.6 (C_q), 158.0 (C_q), 160.1 (C_q), 166.7 (C_q).
HR-MS (ESI pos.)	m/z = 401.1107, calculated for $^{12}C_{21}H_{18}N_2O_5 + Na^+$: 401.1113
FT-IR (KBr)	$\tilde{\nu}$ [cm^{-1}] = 3362 [w], 3291 [w], 3070 [w], 2949 [w], 1716 [s], 1654 [m], 1594 [m], 1535 [m], 1405 [m], 1313 [m], 1258 [s], 764 [m], 748 [w], 695 [w].

7.5.3.3 Synthesis of the fully protected zwitterion 4.43 [TR 527]

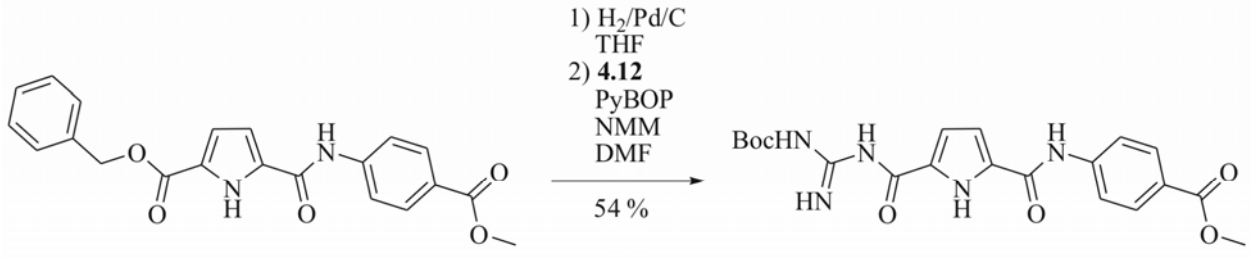

4.42
$C_{21}H_{18}N_2O_5$
Mol. Wt.: 378,38

4.43
$C_{20}H_{23}N_5O_6$
Mol. Wt.: 429,43

Benzyl ester **4.42** (130 mg, 0.34 mmol, 1 eq) and palladium on activated charcoal (20 mg) were suspended in THF and stirred under hydrogen atmosphere at room temperature until TLC control (ethyl acetate/hexane = 6/4 + 1 % triethylamine) indicated no more starting material. The solution was filtered over a celite pad, which was washed several times with ethyl acetate. Then the solution was concentrated *in vacuo*. The resulting colourless solid was dissolved in a mixture of DMF (2 ml) and NMM (0.5 ml). After addition of PyBOP (197 mg, 0.38 mmol, 1.1 eq) the slightly yellow solution was stirred for 20 minutes at room temperature. Finally *N*-boc-guanidin

4.12 (109 mg, 0.69 mmol, 2 eq) was added and the reaction solution was stirred over night at room temperature. The solution was mixed with water and extracted twice with diethyl ether (2 x 20 ml). The organic phase was dried with magnesium sulphate and concentrated *in vacuo*. The crude product was purified by column chromatography (SiO_2, ethyl acetate/hexane = 6/4 + 1 % triethylamine) yielding a colourless solid.

$C_{20}H_{23}N_5O_6$	429.43 g/mol
yield	80 mg (0.19 mmol, 54 %)
R_f	0.61 (SiO_2 with ethyl acetate/hexane = 6/4 + 1 % triethylamine)
melting point	> 220 °C
^{1}H-NMR	(400 MHz, $CDCl_3$ + 5% DMSO-d_6) δ = 1.38 (s, 9H, CH_3), 3.77 (s, 3H, CH_3), 6.77 (d, $^3J_{CHCH}$ = 4.04, 1H, pyrrole-C*H*), 6.92 (d, $^3J_{CHCH}$ = 4.04, 1H, pyrrole-C*H*), 7.72 (d, $^3J_{CHCH}$ = 8.84, 2H, aryl-C*H*), 7.87 (d, $^3J_{CHCH}$ = 8.84, 2H, aryl-C*H*), 8.38 (br.s, 1H, N*H*), 9.01 (br.s, 1H, N*H*), 9.64 (s, 1H, N*H*), 10.98 (br.s, 1H, N*H*).
^{13}C-NMR	(100 MHz, $CDCl_3$ + 5% DMSO-d_6) δ = 27.9 (*C*H_3), 51.7 (*C*H_3), 82.4 (C_q), 113.7 (pyrrole-*C*H), 113.8 (pyrrole-*C*H), 119.1 (aryl-*C*H), 124.7 (C_q), 130.4 (aryl-*C*H), 143.1 (C_q), 158.7 (C_q), 166.6 (C_q).
HR-MS (ESI pos.)	m/z = 452.1541, calculated for $^{12}C_{20}H_{23}N_5O_6 + Na^+$: 452.1546
FT-IR (KBr)	$\tilde{\nu}$ [cm^{-1}] = 3373 [w], 3235 [w], 2981 [w], 1735 [m], 1628 [m], 1589 [m], 1540 [s], 1314 [s], 1278 [s], 1240 [s], 844 [w], 769 [w], 609 [w].

7.6 Sample preparation for the NMR studies

NMR dilution studies

Solutions of the appropriate compound were obtained with varying concentrations by diluting aliquots of concentrated stock solutions in DMSO-*d6* to a total volume of 600 µl. The chemical shifts were recorded for each sample relative to the deuterated solvent.

DOSY NMR studies

Solutions of the appropriate compounds were obtained by diluting aliquots of concentrated stock solutions in DMSO-*d6* to a total volume of 600 µl. TMS was used as internal reference. For each sample the chemical shifts and diffusion coefficients were recorded on a *Bruker* DMX 600 spectrometer equipped with a gradient unit and a conventional 5 mm broadband (^{15}N-^{31}P)/^{1}H probe with automatic tune/match accessory and z axis gradient coil capable of producing pulsed magnetic field gradients in z direction of 52 G cm^{-1}. The longitudinal eddy current delay sequence with bipolar gradient pulse pairs for diffusion (BPP-LED)[3] and additional sinusoidal spoil gradients after the second and fourth 90° pulses was used with the following acquisition parameters (Tab. 7.1). Spoiler gradient strengths: 17.13 and 13.17 % of maximum gradient strength in 32 linear steps. Signal averaging from 16 to 288 scans per increment as required for adequate signal-to-noise ratio. Data were acquired and processed using the software XWIN-NMR 3.5, patch level 6.

Tab. 7.1 *Acquisition parameters for the DOSY NMR studies*

	2.2	**2.3**	**2.4**	**2.5**
Duration δ of bipolar gradient pulse	5-8 ms	5-8 ms	5-8 ms	5-8 ms
Diffusion time Δ	50 ms	50 ms	50 ms	50 ms
Spoiler gradient time	5 ms	5 ms	5 ms	5.4 ms

The hydrodynamic radii of the appropriate structures were calculated via the *Stokes-Einstein* equation with $k_{Boltzmann} = 1.38066 \cdot 10^{-23}$ N·m/K and $\eta_{DMSO} = 1.987 \cdot 10^{-3}$ N·s/m^2 (see Chapter 3.4.1 for detailed information).[4]

1 J. Leonard, B. Lygo, J. Procter, *Praxis der Organischen Chemie*, **1996**, Wiley-VCH.
2 M. Hesse, H. Meier, B. Zeeh, *Spektroskopische Methoden in der organischen Chemie*, **2005**, Thieme.
3 D. Wu, A. Chen, C. Johnson, Jr., *J. Magn. Reson. A* **1995**, *115*, 260-264.
4 a) H.-G. Elias, *Polymere: Von Monomeren und Makromolekülen zu Werkstoffen*, **1996** Hüthig & Wepf Verlag, Heidelberg; b) D. Lide, *CRC Handbook of Chemistry and Physics 1995-1996, 76th Edition*, **1996**, CRC Press, Boca Raton.

8 Appendix

8.1 Experimental data of the NMR dilution studies

8.1.1 Bis-zwitterion 2.2

Tab. 8.1 *Relative intensity of the guanidinio amide NH signal in dependency to the solution concentration of* ***2.2****.*

concentration [mM]	monomer signal set [%]	dimer signal set [%]
50	0.28	0.7
40	0.35	0.62
30	0.40	0.58
20	0.43	0.55
15	0.49	0.49
10	0.53	0.46
7.5	0.59	0.40
5.0	0.68	0.30
2.5	0.75	0.20
1.0	0.86	0.11
0.5	0.91	0.08

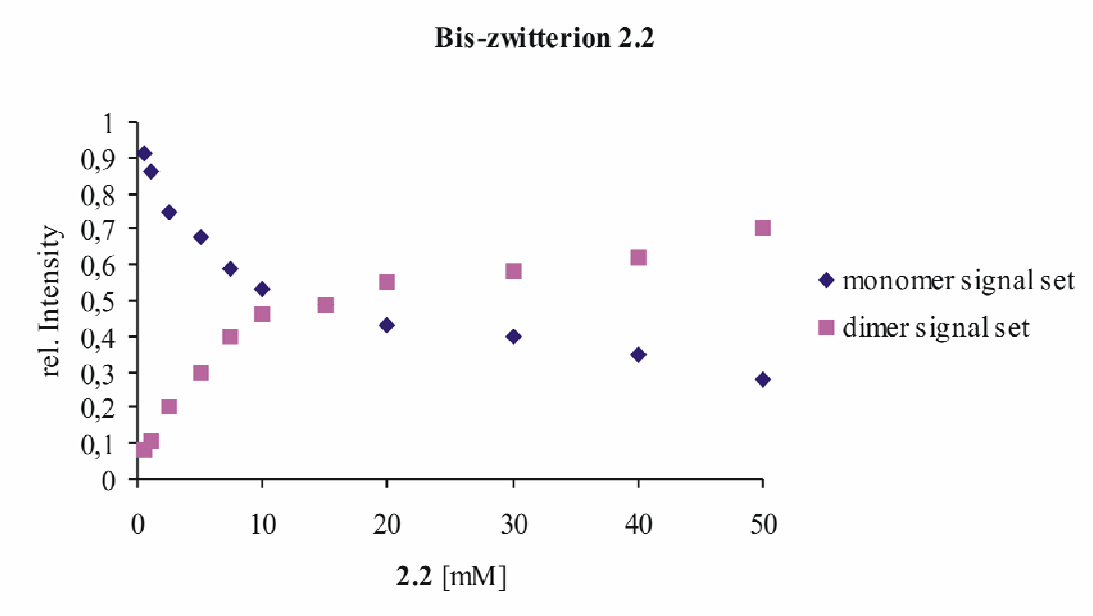

Fig. 8.1 *Concentration dependent monomer-dimer equilibrium of bis-zwitterion* ***2.2****.*

8.1.2 Bis-zwitterion 2.3

Tab. 8.2 *Relative intensity of the pyrrole NH signal in dependency to the solution concentration of **2.3**.*

concentration [mM]	monomer signal set [%]	dimer signal set [%]
50	0.23	0.77
40	0.29	0.71
30	0.33	0.66
20	0.38	0.62
15	0.40	0.60
10	0.45	0.55
7.5	0.51	0.48
5.0	0.57	0.44
2.5	0.66	0.33
1.0	0.80	0.20
0.5	0.84	0.16

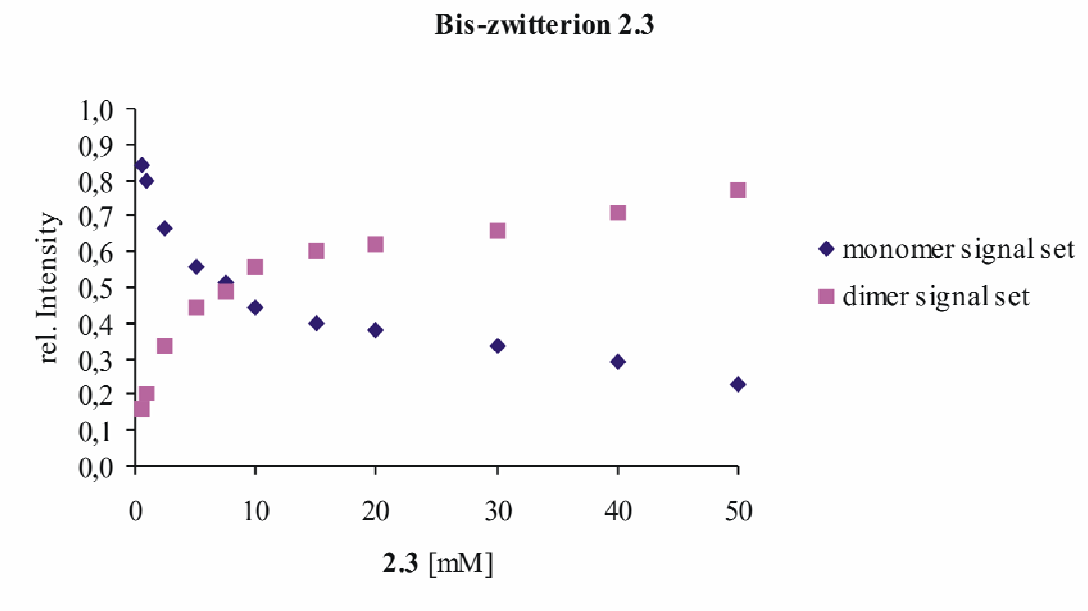

Fig. 8.2 *Concentration dependent monomer-dimer equilibrium of bis-zwitterion **2.3**.*

8.1.3 Bis-zwitterion 2.4

Tab. 8.3 *Relative intensity of the pyrrole NH signal in dependency to the solution concentration of **2.4**.*

concentration [mM]	monomer signal set [%]	dimer signal set [%]
50	0.30	0.70
45	0.31	0.69
40	0.34	0.66
35	0.38	0.62
30	0.42	0.58
25	0.46	0.54
20	0.50	0.50
17.5	0.55	0.45
15	0.57	0.43
12.5	0.59	0.41
10	0.62	0.38
7.5	0.67	0.33
5.0	0.74	0.26
2.5	0.83	0.17
1.0	0.89	0.11
0.5	0.94	0.06

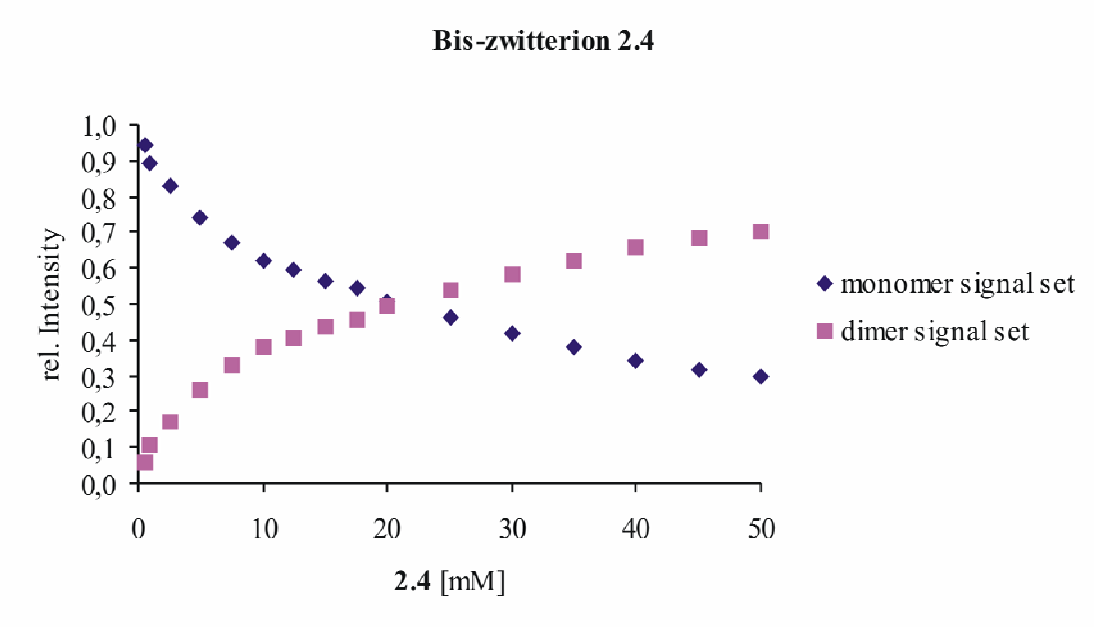

Fig. 8.3 *Concentration dependent monomer-dimer equilibrium of bis-zwitterion **2.4**.*

8.1.4 Zwitterion 2.6

Tab. 8.4 *Concentration dependent signal shift of the guanidinio amide NH proton in bis-zwitterion **2.6**.*

concentration [mM]	δ
100	11.5292
90	11.5011
80	11.4768
70	11.4455
60	11.4159
50	11.3754
40	11.3347
30	11.2924
25	11.2665
20	11.2473
17.5	11.2324
15	11.2189
12.5	11.2050
10	11.1949
7.5	11.1718
5	11.1475
2.5	11.1160
1	11.0863
0.5	11.0572

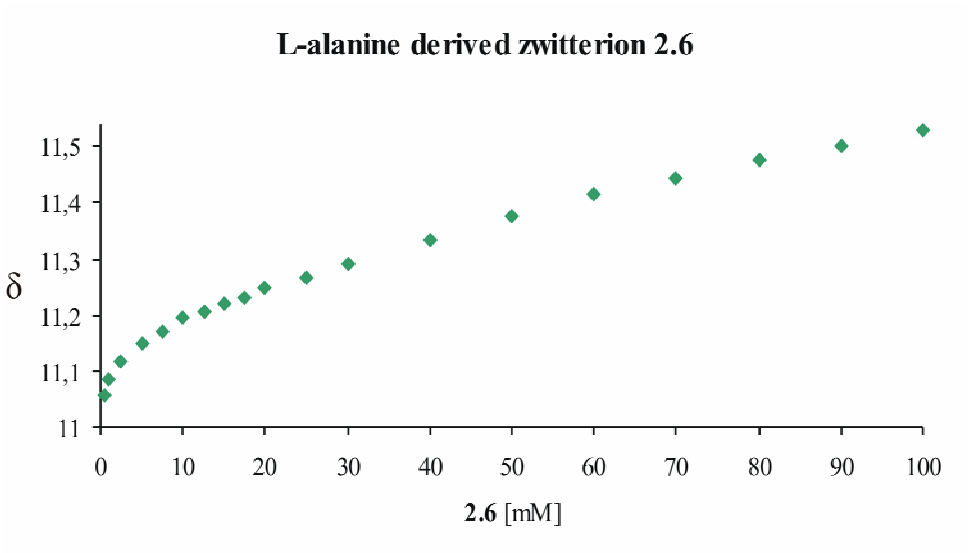

Fig. 8.4 *Concentration dependent signal shift of the guanidinio amide NH proton in zwitterion **2.6**.*

8.1.5 Zwitterion 2.7

Tab. 8.5 *Concentration dependent signal shift of the guanidinio amide NH proton in zwitterion **2.7**.*

concentration [mM]	δ
100	11.6791
90	11.6450
80	11.6198
70	11.5879
60	11.5519
50	11.5099
40	11.4638
30	11.4095
25	11.3852
20	11.3540
17.5	11.3388
15	11.3252
12.5	11.3088
10	11.2940
7.5	11.2741
5	11.2460
2.5	11.2305
1	11.2062
0.5	11.2012

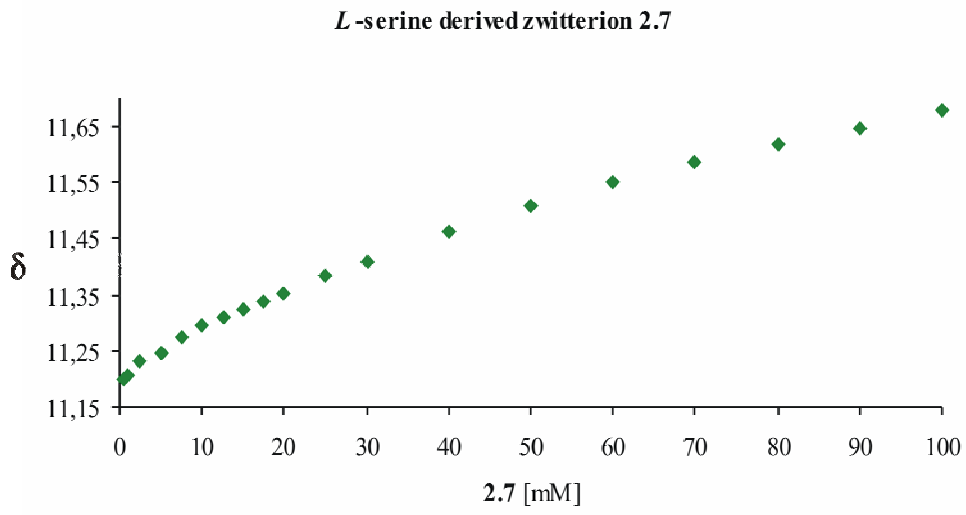

Fig. 8.5 *Concentration dependent signal shift of the guanidinio amide NH proton in zwitterion **2.7**.*

8.2 Experimental data of the DOSY NMR studies

8.2.1 Bis-zwitterion 2.2

Tab. 8.6 *Signal dependent diffusion coefficients D of bis-zwitterion **2.2** (**1 mM**, monomer signal set, T = 299.9 K).*

δ [ppm]	$\boldsymbol{D \cdot 10^{10}}$ **[m²/s]**	
7.725	1.479	
7.003	1.502	
6.643	1.496	
3.319	8.691	water
3.209	1.570	
2.991	1.541	
2.501	6.719	DMSO
2.054	1.477	
1.501	1.508	
1.302	1.491	

Tab. 8.7 *Signal dependent diffusion coefficients D of bis-zwitterion **2.2** (**30 mM**, dimer signal set, T = 299.0 K).*

δ [ppm]	$\boldsymbol{D \cdot 10^{11}}$ **[m²/s]**	
7.749	5.502	
6.982	4.809	
6.636	4.751	
3.476	5.020	
3.438	5.000	
3.338	5.814	
3.314	$7.459 \cdot 10^{10}$	water
3.071	5.333	
2.511	$6.170 \cdot 10^{10}$	DMSO
2.071	5.820	
1.605	5.943	
1.542	5.994	
1.315	6.606	
0.007	$5.418 \cdot 10^{10}$	TMS

Tab. 8.8 *Signal dependent diffusion coefficients D of the fully protected precursor **4.6** (**4 mM**, T = 299.6 K).*

δ [ppm]	$\boldsymbol{D \cdot 10^{10}}$ **[m²/s]**	
12.391	1.188	
11.354	1.233	
8.909	1.097	
8.547	1.056	
7.734	1.062	

6.744	1.075	
6.644	1.176	
3.493	1.050	
3.06o	1.020	
2.506	6.412	DMSO
2.051	1.036	
1.589	1.051	
1.491	1.076	
0.002	6.100	TMS

Tab. 8.9 *Mean diffusion coefficients and hydrodynamic radii of **2.2** and **4.6**.*

	Ø D [m^2/s]	$r_H \cdot 10^{-9}$ [m]
2.2 (1 mM)	$1.51 \cdot 10^{-10}$	0.73
2.2 (30 mM)	$5.51 \cdot 10^{-11}$	2.00
4.6 (4 mM)	$1.07 \cdot 10^{-10}$	1.03

8.2.2 Bis-zwitterion 2.3

Tab. 8.10 *Signal dependent diffusion coefficients D of bis-zwitterion **2.3** (**1 mM**, monomer signal set, T = 299.1 K).*

δ [ppm]	$\boldsymbol{D \cdot 10^{10}}$ **[m^2/s]**	
7.723	1.150	
6.864	1.161	
6.531	1.143	
3.321	8.616	water
3.262	1.188	
3.106	1.135	
2.501	6.791	DMSO
2.063	1.114	
1.591	1.107	
1.533	1.109	
1.311	1.153	
0.000	6.266	TMS

Tab. 8.11 *Signal dependent diffusion coefficients D of bis-zwitterion **2.3** (**30 mM**, dimer signal set, T = 299.1 K).*

δ [ppm]	$\boldsymbol{D \cdot 10^{11}}$ **[m^2/s]**	
7.844	6.527	
6.966	$1.196 \cdot 10^{10}$	
6.621	6.506	
3.340	$8.430 \cdot 10^{10}$	water
3.296	7.171	

3.110	9.473	
3.072	6.789	
2.505	$6.387 \cdot 10^{10}$	DMSO
2.071	7.779	
1.595	7.579	
1.536	7.450	
1.314	7.671	
0.000	$6.356 \cdot 10^{10}$	TMS

Tab. 8.12 *Signal dependent diffusion coefficients D of the fully protected precursor **4.9** (**1 mM**, T = 300.1 K).*

δ [ppm]	$\boldsymbol{D \cdot 10^{10}}$ **[m²/s]**	
12.350	1.400	
11.851	1.438	
8.560	1.397	
7.761	1.409	
7.386	1.398	
6.824	1.396	
6.772	1.410	
5.289	1.397	
3.499	1.457	
3.322	8.717	water
3.047	1.411	
2.502	6.793	DMSO
2.039	1.397	
1.482	1.395	
1.273	1.458	
0.000	6.417	TMS

Tab. 8.13 *Mean diffusion coefficients and hydrodynamic radii of **2.3** and **4.9**.*

	Ø *D* [m²/s]	$r_H \cdot 10^{-9}$ [m]
2.3 (1 mM)	$1.124 \cdot 10^{-10}$	0.98
2.3 (30 mM)	$7.759 \cdot 10^{-11}$	1.42
4.9 (1 mM)	$1.413 \cdot 10^{-10}$	0.78

8.2.3 Bis-zwitterion 2.4

Tab. 8.14 *Signal dependent diffusion coefficients D of bis-zwitterion **2.4** (**2.5 mM**, monomer signal set, T = 303.0 K).*

δ [ppm]	$\boldsymbol{D \cdot 10^{10}}$ **[m²/s]**	
8.504	1,372	
7,715	1,364	

6,989	1,410	
6,632	1,391	
3,325	8,259	water
2,902	1,431	
2,502	6,382	DMSO
2,054	1,341	
1,575	1,414	
1,211	1,193	
0,971	1,382	
0,904	1,397	
0,000	6,329	TMS

Tab. 8.15 *Signal dependent diffusion coefficients D of bis-zwitterion **2.4** (**30 mM**, dimer signal set, T = 299.1 K).*

δ [ppm]	$\boldsymbol{D \cdot 10^{11}}$ **[m²/s]**	
7,717	8.210	
6,987	9.780	
6,630	9.260	
3,335	$7.379 \cdot 10^{10}$	water
2,978	5.820	
2,502	$6.011 \cdot 10^{10}$	DMSO
2,053	7.930	
1,304	7.340	

Tab. 8.16 *Signal dependent diffusion coefficients D of the fully protected precursor **4.11** (**5 mM**, T = 303.0 K).*

δ [ppm]	$\boldsymbol{D \cdot 10^{10}}$ **[m²/s]**	
11,859	1,078	
11,724	1,028	
8,559	1,081	
7,679	1,081	
7,441	1,078	
7,384	1,088	
7,332	1,091	
6,819	1,078	
6,768	1,078	
5,289	1,069	
3,502	1,188	
3,320	8,184	water
2,979	1,069	
2,500	6,295	DMSO
2,031	1,088	
1,326	1,078	
0.001	5.984	TMS

Tab. 8.17 *Mean diffusion coefficients and hydrodynamic radii of **2.4** and **4.11**.*

	$Ø\ D$ [m^2/s]	$r_H \cdot 10^{-9}$ [m]
2.4 (2.5 mM)	$1.387 \cdot 10^{-10}$	0.81
2.4 (25 mM)	$8.892 \cdot 10^{-11}$	1.33
4.11 (5 mM)	$1.079 \cdot 10^{-10}$	1.04

8.2.4 Bis-zwitterion 2.5

Tab. 8.18 *Signal dependent diffusion coefficients D of bis-zwitterion **2.5** (**2 mM**, T = 303.4 K).*

δ [ppm]	$\boldsymbol{D \cdot 10^{11}}$ **[m^2/s]**	
14,673	8,905	
12,628	9,131	
12,371	9,042	
11,069	7,150	
3,758	7,937	
3,326	$8{,}068 \cdot 10^{-10}$	water
2,868	7,643	
2,503	$6{,}196 \cdot 10^{-10}$	DMSO
2,188	7,847	
2,096	7,725	
0,000	$6{,}029 \cdot 10^{-10}$	TMS

Tab. 8.19 *Signal dependent diffusion coefficients D of bis-zwitterion **2.5** (**20 mM**, dimer signal set, T = 303.4 K).*

δ [ppm]	$\boldsymbol{D \cdot 10^{11}}$ **[m^2/s]**	
14.627	8.688	
12.625	6.185	
12.383	8.470	
11.069	7.150	
7.998	6.817	
3.760	6.650	
3.339	$7.820 \cdot 10^{-10}$	water
2.870	6.320	
2.504	$6.083 \cdot 10^{-10}$	DMSO
2.179	6.050	
0.000	$5.735 \cdot 10^{-10}$	TMS

Tab. 8.20 *Signal dependent diffusion coefficients D of the fully protected precursor **4.17** (**2 mM**, T = 303.4 K).*

δ [ppm]	$\boldsymbol{D \cdot 10^{10}}$ **[m^2/s]**	
7.691	1.154	

4.246	1.096	
3.326	8.417	water
3.057	1.098	
2.924	1.082	
2.505	6.535	DMSO
2.432	1.112	
2.262	1.089	
2.160	1.093	
1.469	1.091	
1.290	1.105	
0.003	6.213	TMS

Tab. 8.21 *Mean diffusion coefficients and hydrodynamic radii of* ***2.5*** *and* ***4.17****.*

	Ø D [m^2/s]	$r_H \cdot 10^{-9}$ [m]
2.5 (2 mM)	$8.15 \cdot 10^{-11}$	1.37
2.5 (20 mM)	$6.98 \cdot 10^{-11}$	1.60
4.17 (2 mM)	$1.59 \cdot 10^{-10}$	0.70

8.3 Abbreviations

AFM	atomic force microscopy
° C	degree celcius
Å	Ångström
Abb.	Abbildung
abs.	absolute
Ala	alanine
aq.	aqueous
boc	tert-butoxycarbonyl
c	centi
c	concentration
ca.	circa
CD	circular dichroism
$CDCl_3$	deuterated chloroform
cm	centimetre
COSY	correlated spectroscopy
d	thickness
D	diffusion coefficient
DAN	dialkoxy naphthalene
DCM	dichloromethane
δ	chemical shift
λ	wavelength
DFT	density functional theory
DLS	dynamic light scattering
DMF	*N*,*N*-dimethyl formamide
DMSO	dimethyl sulfoxide

DMSO-*d6*	deuterated dimethyl sulfoxide
DNA	deoxyribonucleic acid
DOSY	diffusion ordered spectroscopy
E	energy
EI	electron ionisation
en	ethylenediamine
eq	equivalent(s)
Eq.	equation
ESI	electrospray ionisation
et al.	et alii
η	viscosity
eV	electronvolt
f	friction
FAB	fast atom bombardment
FT-IR	Fourier-transform infrared
g	gram
h	height
h	Planck's constant
HATU	O-(7-Azabenzotriazol-1-yl)-*N*,*N*,*N*',*N*'-tetramethyluronium-hexafluoro-phosphate
HB denpols	hydrogen-bonded dendronized polymers
HCTU	1-[Bis-(dimethylamino)-methylen]-5-chlor-benztriazolium-3-oxid-hexafluorophosphate
HPLC	high performance liquid chromatography
HR-MS	high resolution mass spectrometry
Hz	Hertz
I	intensity
ITC	isothermal titration calorimetry
K	Kelvin
K_{ass}	association constant
k_B	Boltzmann constant
kHz	kilo Hertz
kJ	kilo Joule
l	litre
m	milli
m	mass
m/z	mass per charge
MALDI-TOF	matrix-assisted laser desorption/ionisation time of flight
MHz	Mega Hertz
M	micro
µM	micromolar
mM	millimolar
MS	mass spectrometry
N	Normal
n	fraction index
NDA	naphthalene dianhydride
NDI	naphthalene diimide
neg.	negative
nm	nanometre
NMM	*N*-methyl morpholine

NMR	nuclear magnetic resonance
NOE	nuclear Overhauser effect
NOESY	nuclear Overhauser spectroscopy
p	para
p	impulse
Pd	palladium
Pd/C	palladium on charcoal
PGSE	pulsed gradient spin echo
pH	pondus hydrogenii
Phe	phenylalanine
pm	pico meter
pos.	positive
ppm	parts per million
PVP	poly-(4-vinylpyridine)
PyBOP	(Benzotriazol-1-yloxy)-tripyrrolidinophosphonium-hexafluorophosphate
R	rest
r	radius
R_f	retention factor
r_H	hydrodynamic radius
rpm	rounds per minute
SANS	small angle neutron scattering
SEM	scanning electron microscopy
Ser	serine
sin	sinus
SiO2	silicagel
T	temperature
t	time
TEM	transmission electron microscopy
TFA	trifluoroacetic acid
THF	tetrahydrofuran
TLC	thin layer chromatography
TMS	tetramethylsilane
Tyr	tyrosine
U	voltage
UV	ultraviolett
vol%	volume percentage

8.4 List of publications

1 C. Schmuck, Th. Rehm, F. Gröhn, K. Klein, F. Reinhold: "Ion Pair Driven Self-Assembly of a Flexible Bis-Zwitterion in Polar Solution: Formation of Discrete Nanometer-Sized Cyclic Dimers" *J. Am. Chem. Soc.* **2006**, *128*, 1430-1431.

2 C. Schmuck, Th. Rehm, K. Klein, F. Gröhn: "Formation of Vesicular Structures through the Self-Assembly of a Flexible Bis-Zwitterion in Dimethyl Sulfoxide" *Angew. Chem. Int. Ed.* **2007**, *46*, 1723-1727.

3 C. Schmuck, Th. Rehm: "Foldamer Hybrids: Defined Supramolecular Structures from Flexible Molecules" in *Foldamers – Structure, Properties, and Application*, Editors: S. Hecht, I. Huc; **2007**, Wiley-VCH, Weinheim.

4 C. Schmuck, Th. Rehm, L. Geiger, M. Schäfer: "Synthesis and Self-Association of Flexible Guaniniocarbonylpyrrole–Carboxylate Zwitterions in DMSO: Intra- versus Intermolecular Ion Pairing" *J. Org. Chem.* **2007**, *72*, 6162-6170.

5 C. Schmuck, V. Bickert, M. Merschky, L. Geiger, D. Rupprecht, J. Dudaczek, P. Wich, Th. Rehm, U. Machon: "A Facile and Efficient Multi-Gram Synthesis of *N*-Protected 5-(Guanidinocarbonyl)-1*H*-pyrrole-2-carboxylic Acids" *Eur. J. Org. Chem.* **2008**, 324-329.

6 Th. Rehm, C. Schmuck: "How to achieve self-assembly in polar solutions based on specific interactions? Some general guidelines" *Chem. Commun.* **2008**, 801-813.

7 Th. Rehm, V. Stepanenko, X. Zhang, F. Würthner, F. Gröhn, K. Klein, C. Schmuck: "A new type of soft vesicle forming molecule: an amino acid derived guanidiniocarbonyl pyrrole carboxylate zwitterion" *Org. Lett.* **2008**, *10*, 1469-1472.

Erklärung

Hiermit erkläre ich an Eides statt, dass ich die Dissertation

„A Guide to Supramolecular Assemblies in Polar Solutions

From Nanometre-sized Cyclic Dimers to Large Vesicular Structures"

selbständig angefertigt und keine anderen als die von mir angegebenen Quellen und Hilfsmittel benutzt habe.

Ich erkläre außerdem, dass diese Dissertation weder in gleicher oder anderer Form bereits in einem anderen Prüfungsverfahren vorgelegen hat.

Ich habe früher außer den mit dem Zulassungsgesuch urkundlich vorgelegten Graden keine weiteren akademischen Grade erworben oder zu erwerben versucht.

Würzburg, den 23.05.2008